Bioremediation of Ethanol in Air Using a Gas-Fluidized Bioreactor

A Thesis Submitted to the

College of Graduate Studies and Research in
Partial Fulfillment of the Requirements for the Degree of
Doctor of Philosophy (Ph.D.)

In the
Division of Environmental Engineering
University of Saskatchewan

By
Kyla Clarke

Permission to Use

In presenting this thesis in partial fulfillment of the requirements for a doctorate of philosophy from the University of Saskatchewan, I agree that the Libraries of this University may make it freely available for inspection. I further agree that permission to copy this thesis in any manner, in whole or in part, for scholarly purposes may be granted by Dr. Gordon Hill or Dr. Todd Pugsley who supervised my thesis work or, in their absence, by the Dean of the College of Engineering. It is understood that any copying, publication, or use of this thesis or parts thereof for financial gain shall not be allowed without my written permission. It is also understood that due recognition shall be given to me and to the University of Saskatchewan in any scholarly use which may be made of the material in my thesis. Requests for permission to copy or to make other use of material in this thesis in whole or part should be addressed to:

Chair of the Division of Environmental Engineering

University of Saskatchewan

Saskatoon, Saskatchewan

Canada S7N 5A9

Abstract

A gas-fluidized bed bioreactor was developed in this research as a new method for treating polluted air. The fluidization characteristics of selected packing materials were investigated. Then, bioremediation was tested using two types of packing in a fluidized bioreactor, as well as in a comparable packed bed. Microorganisms on the particles biodegrade contaminants in the polluted air, which flows up through the bed. At high flowrates, the polluted air fluidizes the particles, while at low velocities the operation is in packed bed mode.

Initially, sawdust was selected for use as a packing material. Due to the poor fluidization properties of sawdust, glass spheres were added. A mixture of sawdust and glass spheres remained well mixed during fluidization. In the mixture, interparticle forces increased with increasing moisture in the sawdust, eventually causing defluidization of the bed. In the absence of bioremediation, mass transfer was studied between ethanol-contaminated air and sawdust/glass sphere packing, and found to be higher in the fluidized versus packed mode. In bioremediation experiments, ethanol removal efficiencies were as high as 95% in both operating modes. The maximum elimination capacities (EC) of ethanol were 75 and 225 g m^{-3} sawdust h^{-1} in the fluidized and packed beds respectively.

The packing of the fluidized bed bioreactor was optimized in order to boost bioremediation rates. Experiments showed that peat granules fluidized well in a bubbling regime, likely due to their relatively high density and sphericity. In peat bioremediation trials, the fluidized mode outperformed the packed bed; the maximum ECs were 1520 and 530 g m^{-3}

peat h^{-1}, respectively. Removal efficiency in the fluidized mode decreased with velocity, because the size and amount of large bubbles increased.

A steady-state model of the fluidized bioreactor was developed. By taking account of bubble properties during fluidization, the model helps to explain how bubble size, microbial properties and bioreactor residence time affect removal efficiency and elimination capacity of the bioreactor.

A peat gas-fluidized bioreactor shows promise as an efficient, low-cost technology for air treatment. Particle mixing in the fluidized bed may prevent operating problems associated with the packed bed bioreactor. Fluidized bioreactors are ideal for the treatment of high volume, low concentration air emissions.

Acknowledgements

I would like to thank my supervisors Dr. G.A. Hill and Dr. T. Pugsley of the Department of Chemical Engineering. I was very fortunate to have supervisors with successful professional careers, who provided excellent guidance and mentorship throughout my research.

The expertise of Richard Blondin, Dragan Čekić and Tivadar Wallentiny is much appreciated for countless hours of assistance with analytical work, the construction of the experimental apparatus, and the maintenance of equipment. As well, thank you to Jan Compain for ensuring that my degree requirements were always in order.

The University of Saskatchewan and the Natural Sciences and Engineering Research Council of Canada are thanked for their financial support.

Thanks to my friends, laboratory colleagues and office mates for your help, friendship and moral support: Elizabet, Erin, Ruihong, Danmei, Jason, Reza, Erica, Hossain, Janice, Mike, Gareth, Venkat, Santosh, Pankej, Atreyee, and others. You have helped to make the challenges of grad studies a memorable experience and will be missed.

Finally, special, heartfelt thanks to Myles, Cole, and my family for all of their care and support.

Table of Contents

List of Tables

List of Figures

CHAPTER 1 – Introduction

1.1 Motivation

Emissions of volatile organic compounds (VOCs) are a cause of respiratory and health problems, and they are harmful to the environment. VOCs are termed secondary pollutants, because in the atmosphere they contribute to the formation of other contaminants, including ground-level ozone, which in turn leads to smog. In addition, VOC emissions may cause nuisance odours and they are implicated as a contributor to climate change. VOCs have high vapour pressures, and thus liquid VOCs at ambient temperatures will vaporize easily. Sources of VOCs are emissions from transportation, industrial processes, municipal wastewater treatment, and solvents in consumer products such as paint, inks and degreasing agents. Environment Canada estimates that annual VOC emissions in Canada were 2531 kilotonnes in 2005 and they predict that annual emissions will be as high as 2864 in 2015 (Environment Canada, 2007).

In general, pollution reduction and controls cost money to industry and provide no increase in corporate revenue. Society on the other hand, achieves benefits from the reduction of air pollution. Public pressure has motivated governments in Canada and elsewhere to establish environmental regulations on air pollution. Once regulations are in place, industrial emitters usually seek the most cost-effective methods of reducing their air emissions. If a pollution control method is selected, it ideally must be efficient, inexpensive, and easy to operate.

1.2 Treatment of VOC Emissions

When VOC emissions are continuously generated by a facility, an air pollution treatment system can be installed. For example, emissions may be collected from the vapour space over

industrial and municipal wastewater ponds, or from the vents of hydrocarbon storage tanks. Conventional methods for treating VOC emissions are physical and chemical processes. These include incineration, chemical scrubbers, and adsorption beds. High energy costs are associated with incineration, while chemical scrubbers have high maintenance requirements (Burgess et al., 2001). Adsorption processes require frequent replacement or regeneration of adsorption material, resulting in increased operating costs (Burgess et al., 2001).

Bioremediation is an inexpensive and environmentally-friendly method of treating waste gases and liquids, and contaminated soils. It involves the use of biological processes rather than chemical or physical processes to eliminate contaminants. Pollutants are decomposed in often complex reactions by bacteria, fungi and other microorganisms. Typically these reactions occur at atmospheric pressure and ambient temperatures. The raw materials of bioremediation processes are simple and inexpensive. The requirements of the microorganisms are a small supply of nutrients and water. The contaminant(s) which are bioremediated are usually the principle energy source of the microorganisms. Bioremediation has been used extensively for treating a wide range of both organic and inorganic air pollutants including VOCs (both aliphatic and aromatic compounds), sulphide compounds, and ammonia (Kennes and Thalasso, 1998). Typically in the bioremediation of VOCs, the contaminant is completely transformed into more benign products, including biomass, carbon dioxide and water. In contrast, physical and chemical air pollution treatment methods often transfer contaminants from one phase to another, or generate other waste products.

1.3 Methods for Bioremediating Polluted Air Emissions

Waste gases have been treated by biological methods for over seventy years (Kennes and Thalasso, 1998). Until several decades ago, the development of bioremediation methods took place mostly in Europe, but bioremediation of air pollution is now frequently used commercially in North America and Japan (Kennes and Thalasso, 1998). For the treatment of VOC emissions, bioremediation typically takes place in a bioreactor. In bioreactors, microorganisms may be free-floating in liquid solution, or attached to solid surfaces. The selection of a type of bioreactor largely depends on the solubility and volatility of the contaminant which is being treated. The

bioreactor may be dominated by a liquid phase, gas phase, or both. In the following discussion, bioreactors for treating VOC emissions are categorized by the dominant fluid phase into three groups: bioscrubbers and external loop airlift bioreactors, trickling biofilters and membrane bioreactors, and bulk media biofiltration.

1.3.1 Bioscrubbers and External Loop Airlift Bioreactors

In bioscrubbers and external loop airlift bioreactors, microorganisms are often suspended in aqueous solution. In some designs they are immobilized onto solid supporting material that is completely immersed in the solution. In bioscrubbers (Figure 1.1), contaminants in waste gases are first dissolved into the aqueous solution and the solution is then pumped to the bioreactor, where microorganisms decompose the contaminants. Bioscrubbing is suitable for contaminants that are very water soluble and have a low volatility, such that there is sufficient residence time to absorb the contaminants into the liquid solution (Kennes and Thalasso, 1998). A unique advantage of bioscrubbers is that they can also be used for anaerobic biodegradation processes (Burgess et al., 2001).

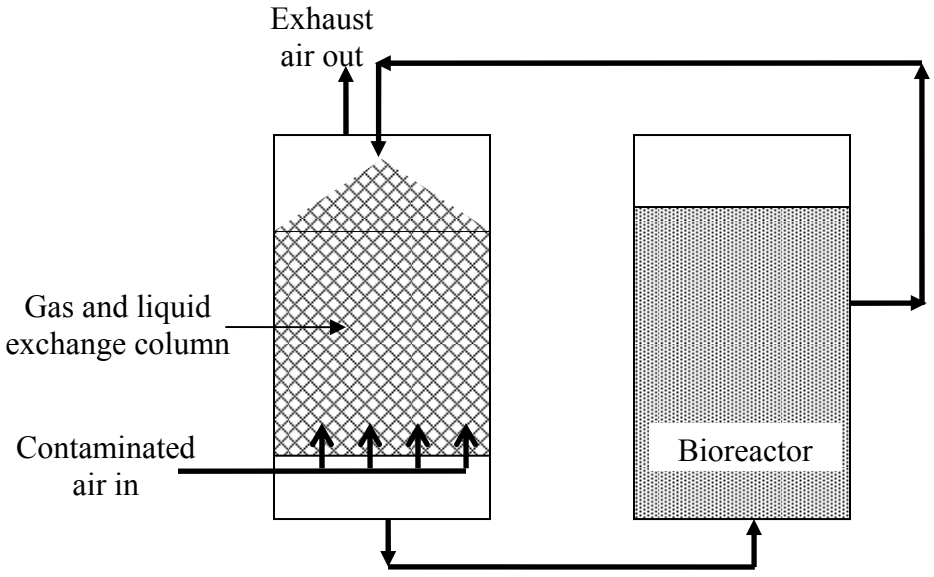

Figure 1.1 Bioscrubber design.

External loop airlift bioreactors (ELAB) have been studied during the past few decades as a new type of bioscrubber. An ELAB is a single vessel where the liquid solution recirculates through an external loop (Figure 1.2). ELABs have been used to treat toluene which is hydrophobic and highly volatile (Harding et al., 2003), as well as hydrophilic compounds (Nikakhtari and Hill, 2006). Nikakhtari and Hill (2006) designed an ELAB which contains a submerged solid support, on which microorganisms are grown.

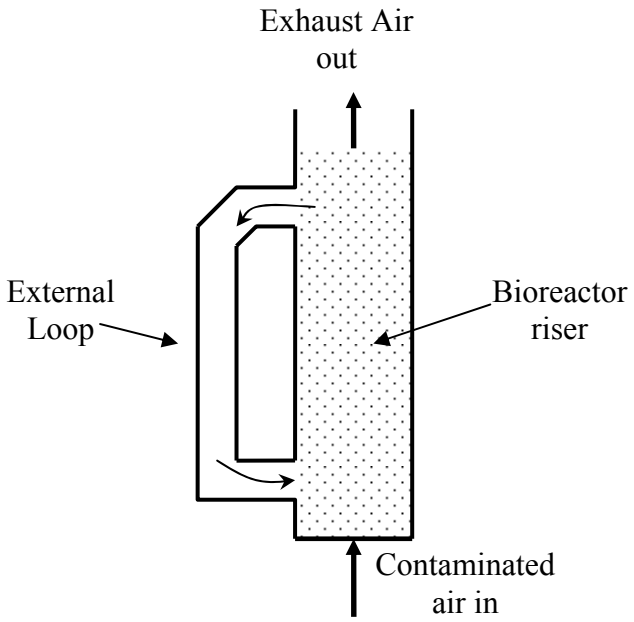

Figure 1.2 External loop airlift bioreactor (adapted from Harding et al., 2003).

1.3.2 Trickling Biofilters and Membrane Bioreactors

Trickling biofilters and membrane bioreactors involve both gas and liquid phases. Trickling biofilters (Figure 1.3) are generally counter-current contacting beds. These bioreactors contain a solid bed of packing material, on which microorganisms grow. A constant flow of re-circulating liquid is sprayed over the top of the bed, and the polluted gas stream is injected at the base of the bioreactor vessel. The pollutants transfer from the gas phase to the liquid stream, and then transfer through the liquid to the microorganisms on the surface of the solid packing.

Trickling biofilters are more effective for contaminants which have lower solubilities in water and higher volatilities than those treated in bioscrubbers.

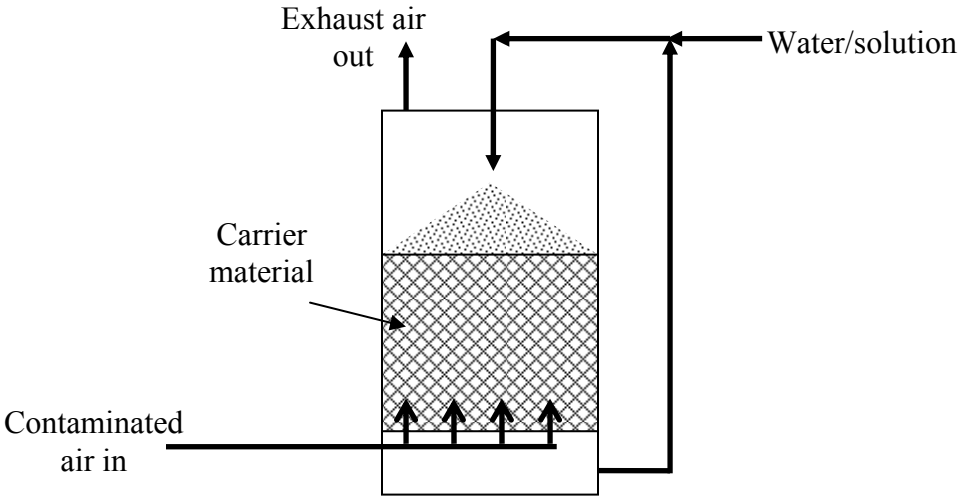

Figure 1.3 Trickling biofilter.

Membrane bioreactors are a more recent technology for the treatment of waste gases. In these bioreactors, a porous membrane creates an interface between the waste gas stream and a liquid (Burgess et al., 2001). The contaminant in the polluted air is transferred through the membrane to the liquid phase. Microorganisms in the liquid phase biodegrade the contaminant. The membrane allows for selectivity so that only certain components can pass through the membrane and it also prevents microorganisms from contaminating the outlet gas stream.

1.3.3 Bulk Media Biofiltration

In bulk media biofiltration, waste gases come into direct contact with wet, solid material, on which microorganisms are supported. Biofilters (Figure 1.4) are a popular, commercial biotreatment method. The packing of biofilters is often organic material with a high surface area such as wood products, peat, compost, and soil. Waste gas flows upwards through the packed

bed. If the bulk media is organic, it can supply additional nutrients to the microbial cultures supported upon it (Kennes and Thalasso, 1998). Although the bulk media may be periodically moistened with water or a solution of nutrients, there is no mobile liquid phase. As a result, biofilters can be used for treating contaminants with a low solubility in water (Kennes and Thalasso, 1998).

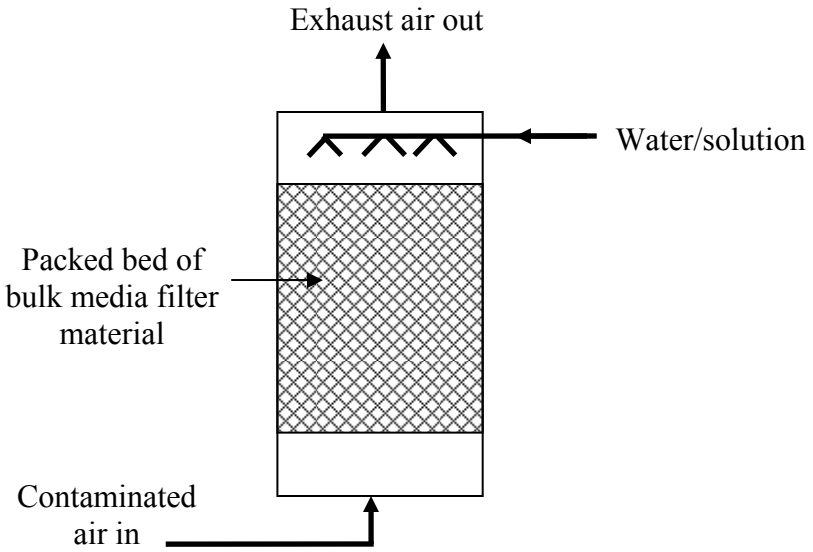

Figure 1.4 Biofilter.

A biofilter at a BP Amoco refinery in Whiting, Indiana, successfully treated VOC emissions from an industrial wastewater treatment facility (Morrison et al., 2003). A dissolved air flotation unit at the refinery was covered in order to capture up to 2.93 m^3 s^{-1} of air contaminated with benzene, toluene, xylene, and ethyl benzene. These emissions were then passed through a biofilter. The biofilter was installed to reduce the high operating costs of an existing carbon adsorption unit that had originally been used to treat these VOC emissions.

Operability problems can occur with biofilters; it is difficult to control humidity, temperature and pH in the packing (Jorio and Heitz, 1999), resulting in gas channelling and lower biodegradation efficiencies (Leslous et al., 2004). Moisture content, especially, must be carefully controlled to maintain the efficiency of the biofilter. Too much moisture can cause stagnant, anaerobic areas within the biofilter (Kennes and Thalasso, 1998), while too little moisture slows down or stops microbial growth (Burgess, 2001).

A few authors have recently investigated a variation of the conventional packed bed biofilters which involves using gas-solid fluidized and three-phase spouted beds for treating waste gases (Leslous et al., 2004; Wright and Raper, 1998). Incentives behind developing fluidized bioremediation of air pollution include improving upon the reaction rates of other types of bioreactors and increasing runtimes by reducing operating problems such as bed clogging. Fluidized bioreactors are discussed in the following section.

1.4 Fluidized Bioreactor for Treating VOC Emissions

1.4.1 Introduction to Fluidization

In fluidization, gas or liquid is directed into a bed of particles at a sufficiently high velocity to cause the bed of particles to behave with fluid-like properties. As the velocity of a fluid flowing up through a packed bed of particles is increased from zero, the pressure drop of the fluid across the bed will also increase. The pressure drop is caused by drag force as the fluid flows through the particles. The bed will begin to fluidize when the drag force induced by the upwardly moving fluid counterbalances the buoyant weight of the particles. The advantages of fluidization include more homogeneous conditions in the bed due to the rapid mixing of the solids, and high heat and mass transfer between the fluid and the particles (Kunii and Levenspiel, 1991). A disadvantage is that solids can be broken down in the bed and carried out with the fluid flow, causing problems downstream. Agglomeration of fine or cohesive particles within the bed may also occur.

The superficial gas velocity at which fluidization occurs is known as the minimum fluidization velocity, u_{mf}. Below u_{mf}, the fluid flows through the void space between adjacent particles. The particles do not move, and are in a fixed bed state. Above u_{mf}, a gas-solid fluidized bed may exhibit several types of hydrodynamic regimes, including smooth fluidization (delayed bubbling), bubbling, slugging, turbulent fluidization, fast fluidization, and pneumatic conveying (Figure 1.5). Depending upon the fluidization regime, the fluid flows up through the interparticle spaces, and also as bubbles or slugs (large bubbles).

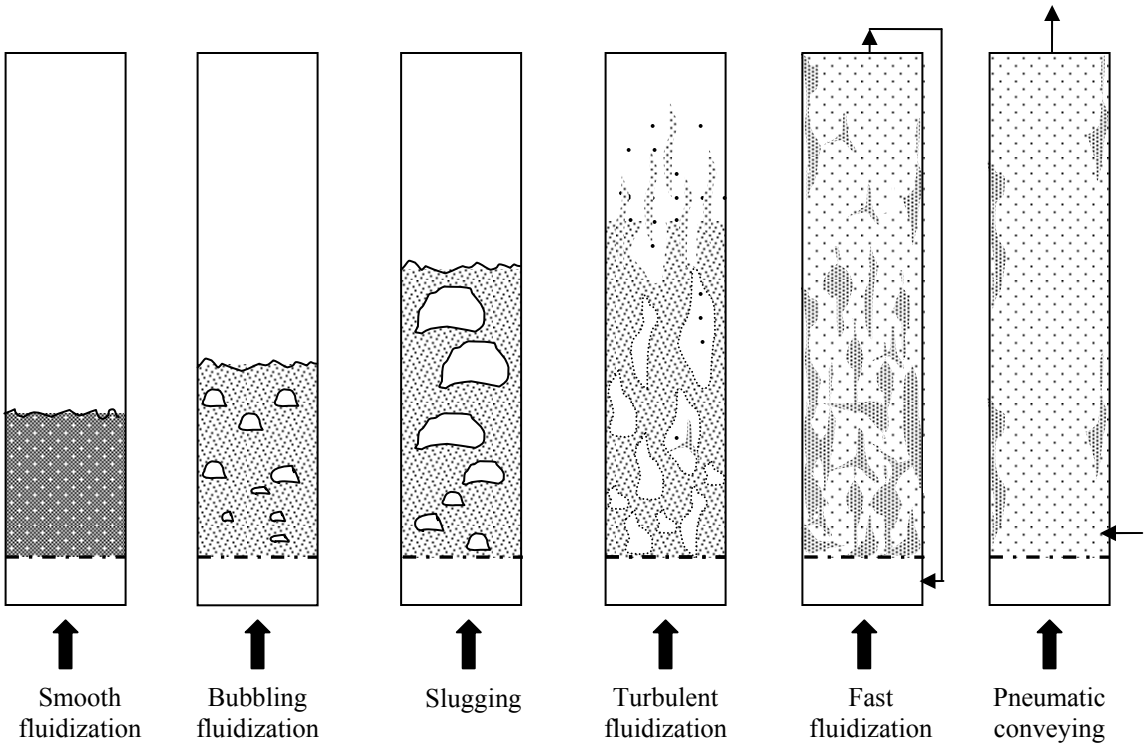

Figure 1.5 Fluidization regimes at increasing gas velocity (modified from Lim et al., 1995).

Geldart (1973) grouped the behaviour of fluidized particles into four classes based on the Sauter mean particle diameter (d_p) and particle density (ρ_p). Sauter mean particle diameter is defined as the diameter of a sphere with the same ratio of volume to surface area as the particle of interest. The boundaries between groups are empirically derived. Class A powders fluidize easily. In a bed of Class A powders, the bed expands as superficial gas velocity increases above u_{mf}. Then at a certain velocity, the onset of bubbling occurs. Class B particle beds also fluidize well and begin to bubble at u_{mf}. Class C particles are very difficult to fluidize, as the particles are cohesive. Fluidized beds of Class C particles tend to have severe channelling and low particle mixing. Class D particles are large and tend to spout when fluidized (spouted beds). Table 1.1 shows the size range of particles in each Geldart class at two examples of (ρ_p - ρ_f) values.

Table 1.1 Geldart classification of fluidized particles (Geldart, 1973).

Geldart Class	$(\rho_p - \rho_f)$ kg m^{-3}	d_p 10^{-6} m
C	500	< 33
Cohesive powders, difficult to fluidize	1000	< 21
A	500	33 to 400
Powders, easiest to fluidize, aeratable bed	1000	21 to 220
B	500	400 to 1300
Sand-like particles, easy to fluidize, bubbling bed	1000	220 to 1000
D	500	> 1300
Coarse particles, spoutable bed	1000	> 1000

1.4.2 Effect of Liquid on Fluidization

Interparticle forces can have a considerable effect on fluidization hydrodynamics. When liquid is present in a fluidized bed, liquid bridge forces are a type of interparticle force that is significant for particle sizes less than 5000 μm. Liquid forms a bridge between adjacent particles (Figure 1.6). In extreme cases liquid may entirely fill the interstitial spaces. Liquid bridging forces are affected by liquid loading, viscosity and surface tension of the liquid, and surface porosity, shape and surface roughness of the particles (Seville et al., 2000; Wright and Raper, 1999). Seville et al. (2000) describe liquid bridging forces as having both static ($F_{IP,S}$) and dynamic ($F_{IP,D}$) components which are defined as:

$$F_{IP,S} = 2\pi r_2 \gamma + \pi r_2^2 \Delta P \tag{1.1}$$

$$F_{IP,D} = 6\pi \mu_f R^2 v / a \tag{1.2}$$

where ΔP is the difference between the lower pressure within the liquid bridge and the pressure of the surroundings.

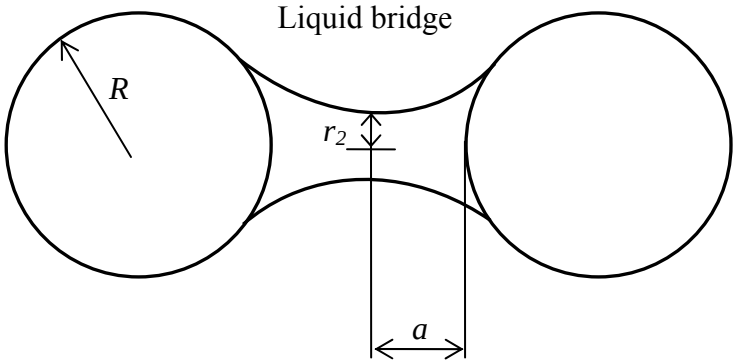

Figure 1.6 Diagram of a liquid bridge.

Interparticle forces such as liquid bridging can cause particles to become more cohesive, which can lead to defluidization (McLaughlin and Rhodes, 2001). Defluidization refers to a diminished quality of fluidization. In a bubbling bed, this includes particle agglomeration, channelling of the fluid stream, and reduced bubbling behaviour. The effect of liquid on fluidization can be described as changes in the Geldart classification of the particles (Seville and Clift, 1984). Particles can transition from Geldart class A, B or D to class C as a result of addition of a liquid (Seville et al., 2000; Wright and Raper, 1999). Several studies indicate that the characteristics of particles of different Geldart classes are actually determined by the ratio of the interparticle force (F_{IP}) to the fluid drag force (or buoyant particle weight) (Seville and Clift, 1984; Molerus, 1983; McLaughlin and Rhodes, 2001). These studies attempt to define the ratios of forces at which fluidization behaviour shifts between Geldart classifications, and they are summarized in Table 1.2. Buoyant particle weight (F_B) is calculated as follows:

$$F_B = \left(\rho_p - \rho_f\right)\frac{\pi d^2}{6} g \tag{1.3}$$

Table 1.2 Force ratio at boundaries between Geldart classes.

Boundary	F_{IP}/F_B	Reference
Geldart class B-A	6.25	Molerus, 1982
Geldart class A-C	1900	Molerus, 1982
Geldart class B-A	0.44	Seville and Clift, 1984
Geldart class B-A	0.06	McLaughlin and Rhodes, 2001
Geldart class A-C	1.07	McLaughlin and Rhodes, 2001

In Table 1.2, the ratios of interparticle force to buoyant weight at the class B-A and A-C boundaries depend upon how the authors determine interparticle forces. Molerus (1982) calculated interparticle force based on Van der Waals forces, while Seville and Clift (1984) and McLaughlin and Rhodes (2001) calculated interparticle force based on liquid bridging forces. Table 1.2 indicates that the force ratio (F_{IP}/F_B) is much higher for the A-C boundary than for the B-A boundary. As a result, the force ratio may account for the differences observed in the fluidization behaviour of the different Geldart classes. Furthermore, in the fluidization of moist particles, high interparticle forces are responsible for cohesion, moving Class B or D particles to Class A or C and causing poor fluidization characteristics.

1.4.3 Bioremediation in Fluidized Beds

Liquid-solid and three-phase (gas-liquid-solid) fluidized bioreactors are used for the treatment of wastewater (Schügerl, 1997; Rabah and Dahab, 2004). In these fluidized bioreactors, the wastewater is the fluidization stream. Chung et al. (2001) investigated a three-phase fluidized bioreactor for treating air emissions. Air contaminated with ammonia and hydrogen sulphide was bubbled into the base of a bioreactor. The bioreactor was filled with liquid solution and a bed of calcium-alginate beads containing immobilized microbial cells.

On the other hand, the use of gas-fluidized bioreactors is rare. In these bioreactors, gas is the fluidization stream and the spaces between the particles of the bed are primarily occupied by a gas phase. The particles of the bioreactor bed must be moist in order to support microbial life. As discussed in the previous section, this moisture can lead to defluidization. When designing a

gas-fluidized bioreactor it is desirable to select particles that when moist have a minimal ratio of interparticle forces to buoyant particle weight. This ratio can be minimized by choosing particles with higher densities, larger sizes, less moisture, or lower surface roughness.

Wright and Raper (1998) studied the biodegradation of ammonia using a three-phase spouted bed. The contaminated gas was the fluidization stream, while the liquid phase consisted of a nutrient solution which was continuously supplied to the top of the bed. A variety of particles were evaluated for use in either a bubbling fluidized bed or a spouted bed, including glass ballotini, rice hulls, plastic discs and granules, silica gel, molecular sieves, vermiculite, perlite, activated carbon, cork, polystyrene, and expanded clay. The particles conformed to Geldart classes B and D. In general due to the addition of the liquid stream, there was high wall adhesion and high particle aggregation during fluidization. In some cases, gas channelling through the bed was observed. The authors found that the Geldart D particles in spouted beds exhibited better fluidization qualities. Geldart D, expanded clay particles showed the most promise for use in a bioreactor. In a bioremediation experiment the clay particles were inoculated with a microbial culture. Then the clay was mobilized in a vessel with a conical base. The inlet air stream contained 20 to 40 g m^{-3} of ammonia. The highest ammonia elimination capacity achieved in the study was approximately 330 g m^{-3} h^{-1}, where the ammonia percentage removal was approximately 50%. There was high attrition of the clay, producing very fine particles. Elimination capacity is defined as the mass of pollutant consumed per packed particle bed volume per unit time, and removal efficiency is defined as the difference between the inlet and outlet concentration as a percentage of the inlet concentration.

Leslous et al. (2004) proposed the biodegradation of ethanol and toluene-contaminated air using a gas-solid fluidized bed of sawdust, and their bioremediation results are reported in Delebarre et al. (2007). In this design there is no separate liquid stream, unlike the spouted bed bioreactor of Wright and Raper (1998). Nevertheless, water is an essential requirement for the growth and maintenance of microorganisms in two-phase gas-solid fluidized bioreactors, and water must be introduced to moisten the particles. Leslous et al. (2004) concluded that the ideal moisture content is 45 wt% (wet basis) for sawdust particles. In a gas-solid fluidized bioreactor of sawdust the ethanol elimination capacity ranged between 600 and 1000 g m^{-3} h^{-1}, at a removal efficiency of 80% (Delebarre et al., 2007). For the removal of toluene, an elimination capacity of approximately 18 g m^{-3} h^{-1} was achieved at a removal efficiency of 70%. Bioremediation

rates were found to vary with the type of microorganisms in the bioreactor. As well, they reported that the moisture content in the sawdust bed was difficult to control. The concentration of microbial cells was directly dependent on the moisture content of the sawdust and therefore hard to control.

1.5 Fundamentals of Modelling Fluidized Bioreactors

1.5.1 Microbial growth

Bioremediation rates in a bioreactor depend in part on the types of microbial species present and their respective growth kinetics on the pollutant substrate. Simple batch reactors, often consisting of shake flasks, are used to determine the kinetics of microbial growth. A culture of a pure species or a mixture of different species is grown in a liquid nutrient solution containing a known initial substrate concentration. The growth of the culture and depletion of the substrate are then monitored over time. Microbial growth is inferred by measuring the concentration of biomass (X), which is proportional to the number of microbial cells, at various time intervals.

Microbial growth typically follows first order kinetics in terms of biomass, and zero order in terms of substrate concentration. The growth rate is:

$$r_x = \frac{dX}{dt} = \mu X \tag{1.4}$$

where μ is the specific growth rate of the culture.

The specific growth rate depends on the concentration of substrate(s) supplying the energy and nutrient requirements of the microorganism. In terms of a bioreactor for treating polluted air, the substrate is the contaminant in the air stream. The Monod model assumes that there is only one substrate which limits growth:

$$\mu = \frac{\mu_m S}{K_s + S} \tag{1.5}$$

Certain substrates will also inhibit growth because they affect the catalytic activity of the enzymes of the microbes. The Haldane model for substrate-inhibited enzyme reactions is converted to a microbial growth model in a similar form to the Monod model:

$$\mu = \frac{\mu_m S}{K_s + S + \frac{S^2}{K_I}} \tag{1.6}$$

Another important biokinetic parameter is biomass yield, Y_{xs}, which is defined as the rate of biomass production per the consumption rate of the substrate.

$$Y_{xs} = \frac{\frac{dX}{dt}}{-\frac{dS}{dt}} \tag{1.7}$$

For the Monod and Haldane growth models, growth rate is calculated by equations 1.8 and 1.9 respectively:

$$\left[\frac{dX}{dt}\right] = \left(\frac{\mu_m SX}{K_s + S}\right) \tag{1.8}$$

$$\left[\frac{dX}{dt}\right] = \left(\frac{\mu_m SX}{K_s + S + \frac{S^2}{K_I}}\right) \tag{1.9}$$

The rate of utilization of the substrate is calculated for the Monod and Haldane models with equations 1.10 and 1.11, respectively:

$$-\left[\frac{dS}{dt}\right] = \left(\frac{\mu_m SX}{K_s + S}\right)\frac{1}{Y_{XS}} \tag{1.10}$$

$$-\left[\frac{dS}{dt}\right] = \left(\frac{\mu_m SX}{K_s + S + \frac{S^2}{K_I}}\right)\frac{1}{Y_{XS}} \tag{1.11}$$

In any type of bioreactor, the material balance for the biomass and substrate is:

[Accumulation rate] = [Rate of addition] – [Rate of removal] + [Rate of formation] (1.12)

For batch reactor experiments, assuming a constant value for the biomass yield, the biomass concentration at any time can be calculated from a rearrangement of Equation 1.7, using the initial biomass and substrate concentrations (X_0, S_0):

$$X = X_0 + Y_{XS}\left(S_0 - S\right) \tag{1.13}$$

In an ideal batch reactor, after inoculation, cells are neither added nor removed. If there is negligible gas stripping from the reactor and the reactor volume is constant, then equations 1.8 to 1.11 represent the mass balances for biomass and substrate.

1.5.2 Biofilms

In a fluidized bioreactor, the microorganisms will likely exist as part of a biofilm on the surface and in the pores of particles in the fluidized bed. The term biofilm refers to microbial cells, both living and dead, in a fluid-like matrix. A biofilm may contain multiple layers of one or many types of microorganisms. Biofilms can float as "slime" in liquid or attach to surfaces. A surface biofilm is formed when individual cells land on the surface, cluster together and then stick to the surface in a certain pattern (Costerton and Stewart, 2001). The cells group together in small micro-colonies. Cells in the colony then start producing a slimy, fluid matrix containing extracellular polymer substances (EPS) that completely engulfs them. Approximately one third of the biofilm is comprised of cells and the remainder is the liquid matrix. The biofilm has the ability to absorb water, dissolved substances and trap small suspended particles. The cells also send out signals to other cells to produce EPS material, resulting in many micro-colonies growing together. Chemical gradients exist in the biofilm which results in diffusional flow of substances, including food sources, through the biofilm.

1.5.3 Modelling bubbling fluidized beds

Bubbling fluidized bed reactor models should consider the mechanics of the bubbles, in order to better predict reactor performance (Kunii and Levenspiel, 1990). An important bubble

property to determine is rise velocity during fluidization. Davidson and Harrison (1963) show that bubbles rise at a finite velocity. The rise of a bubble in a fluidized bed of particles is similar to the rise of a large bubble in liquid, although the presence of other bubbles in a fluidized bed significantly impacts rise velocity. For a single bubble, rise velocity in a liquid mainly depends on inertial forces. A combination of a theoretical force balance and experiments demonstrate that rise velocity of a single bubble (u_{br}) is function of bubble diameter (d_b) (Davidson and Harrison, 1963):

$$u_{br} = 0.711(d_b g)^{0.5} \tag{1.14}$$

In a bubbling fluidized bed, the gas between the particles moves upwards. As a result the absolute rise velocity of the bubble relative to the height of the bed, u_b is greater than u_{br}, and it is calculated base on the difference between the total superficial velocity of the gas (u_o) and the minimum fluidization velocity:

$$u_b = u_o - u_{mf} + u_{br} \tag{1.15}$$

1.6 Research Objectives

The overall purpose of this research project is to design and test a gas-solid fluidized bed bioreactor for treating VOC emissions, with the intent of improving upon existing bioremediation methods such as biofiltration.

Specific objectives of the research included the following:

1. Find an effective method of fluidizing microorganisms, immobilized on particles.
2. Determine mass transfer rates of ethanol from a waste gas stream to particles in a fluidized and a packed bed, in the absence of bioremediation.
3. Measure ethanol bioremediation performance in a gas-fluidized bioreactor and compare to that of a packed bed bioreactor for the treatment of ethanol emissions.
4. Optimize the type of particles used in the gas-fluidized bioreactor, based on the bioremediation results of objective 3, and then compare bioremediation performance in a fluidized bed to a packed bed bioreactor using the new type of bed material.

5. Model the fluidized and packed bed bioreactors to understand the parameters that affect bioreactor performance.

1.7 Reproducibility

In the experiments conducted for Chapters 2 and 5, triplicate pressure drop *versus* velocity profiles were obtained at each particle bed composition and moisture content, demonstrating that these profiles were repeatable. As an example, Figure A.13 (Appendix A) shows triplicate pressure drop versus velocity profiles for material 3 peat at 40 wt% moisture. Only one profile at each experimental condition is represented in Figures 2.2, 2.3, 2.4, 5.3, 5.4, and 5.5.

Reproducibility of the experimental results was an important consideration in the bioremediation experiments presented in Chapters 3 and 4. In bioremediation using the sawdust and glass sphere packing, reproducibility was demonstrated initially by the bioremediation trials reported in Figure 3.5. Bioremediation trials were repeated at various inlet ethanol loadings, with different sawdust moisture contents. Not only does Figure 3.5 show that these variations in moisture content had little influence on bioremediation, this figure illustrates that the bioremediation experiments were reproducible. In addition, section 3.3.2 describes the reproducibility of the gas chromatograph analysis methods of Chapters 3 and 4.

In bioremediation experiments using the peat bed bioreactor described in Chapter 4, additional sampling was used to demonstrate reproducibility. At each inlet ethanol loading, at least three samples of inlet and outlet air from the bioreactor were taken for ethanol analysis in glass sampling bulbs. The mean concentration of the outlet ethanol concentration was used in the calculation of elimination capacity and removal capacity. Error bars on Figures 4.5 and 4.6 represent two standard deviations on either side of the mean value of the elimination capacity.

1.8 Nomenclature

a	Half of the separation distance between particles (m)
d, d_p	Particle diameter, Sauter mean particle diameter (m)
d_b	Bubble diameter (m)
F_B	Buoyant particle weight (N)
F_{IP}	Interparticle force (N)
$F_{IP,S}$, $F_{IP,D}$	Static and dynamic components of the liquid bridging force (N)
g	Gravitational acceleration
K_I	Inhibition constant (g m^{-3})
K_s	Saturation constant (g m^{-3})
r_2	Radius of the liquid bridge at the thinnest point (m)
r_x	Rate of formation of biomass in liquid (g m^{-3} h^{-1})
R	Particle radius (m)
S	Growth limiting substrate concentration in liquid (g m^{-3})
t	Time (h)
u_{br}, $u_{b,}$	Bubble rise velocity in a stagnant liquid and in a fluidized bed (m s^{-1})
u_{mf} ,u_o	Minimum fluidization velocity and superficial gas velocity (m s^{-1})
v	Relative velocity between two particles connected by a liquid bridge (m s^{-1})
X	Biomass concentration in liquid (g m^{-3})

Greek Letters

ΔP	Difference between pressure in liquid bridge and surroundings (Pa)
γ	Surface tension of the liquid (N/m)
μ	Specific growth rate of biomass (h^{-1})
μ_f	Viscosity of the fluidizing stream (kg m^{-1} s^{-1})
μ_m	Maximum specific growth rate of biomass (h^{-1})
ρ_p	Particle density (kg m^{-3})
ρ_f	Density of the fluidizing stream (kg m^{-3})

1.9 References

Burgess, J.E.; Parsons, S.A.; Stuetz, R.M. Developments in odour control and waste gas treatment biotechnology: a review, *Biotech. Adv.* **2001**, *19*, 35-63.

Costerton, J.W.; Stewart, P.S. Battling Biofilms. *Sci. Am.* **2001**, *285,* 74-81.

Chung, Y.; Huang, C.; Liu, C.; Bai, H. Biotreatment of hydrogen sulphide- and ammonia-containing waste gases by fluidized bed bioreactor. *J. Air Waste Manage. Assoc*. **2001**, *51* (2), 163-172.

Davidson, J.F.; Harrison, D. Fluidised Particles; Cambridge University Press: Cambridge, United Kingdom, 1963, pp 21-41.

Environment Canada website, Criteria Air Contaminants (CAC) Emission summaries, VOCs: **www.ec.gc.ca/pdb/cac/Emissions1990-2015/EmissionsSummaries/VOC,** 2007.

Geldart, D. Types of gas fluidization. *Powder Tech.* **1973**, *7*, 285-292.

Harding, R.C.; Hill, G.A.; Lin, Y.H. Bioremediation of Toluene-contaminated Air using an External Loop Airlift Bioreactor. *J. Chem. Technol. Biotechnol.* **2003**, *78*, 406-411.

Jorio, H.; Heitz, M. Traitement de l'air par biofiltration. *Can. J. Civ. Eng*. **1999**, *26*, 402-424.

Kennes, C., Thalasso, F. Waste Gas Biotreatment Technology. *J. Chem. Technol. Biotechnol.* **1998**, *72*, 303-319.

Kunii, D.; Levenspiel, O. Fluidized reactor models. 1. For bubbling beds of fine, intermediate, and large particles. 2. For the lean phase. Freeboard and fast fluidization. *Ind. Eng. Chem. Res.* **1990**, *29*, 1226-1234.

Kunii, D.; Levenspiel, O. Fluidization Engineering, Second Ed.; Butterworth-Heinemann: Newton, MA, 1991, pp 7-11; 146-150.

Leslous, A.; Delebarre, A.; Pre, P.; Warlus, S.; Zhang, N. Characterization and selection of materials for air biofiltration in fluidized beds. *Int. J. Chem. Reactor Eng*. **2004**, *2*(Article A20), 1-19.

Lim, K.S.; Zhu, J.X.; Grace J.R. Hydrodynamics of gas-solid fluidization. *Int. J. Multiphase Flow.* **1995**, *21(Suppl.),* 141-193.

Molerus, O. Interpretation of Geldart's type A, B, C and D Powders by Taking into Account Interparticle Cohesion Forces. *Powder Tech.* **1982**, *33*, 81-87.

Morrison, J.; Schowengerdt, M.; Vernengo, S. Apply biofiltration methods to manage VOC emissions. *Hydrocarb. Process.* **2003**, *82*(10), 91-94.

McLaughlin, L.J.; Rhodes, M.J. Prediction of fluidized bed behaviour in the presence of liquid bridges. *Powder Tech.* **2001**, *114*, 213-223.

Nikakhtari, H.; Hill, G.A. Continuous bioremediation of phenol polluted air in an external loop airlift bioreactor with a packed bed. *J. Chem. Technol. Biotechnol*. **2006**, *81*, 1029-1038.

Rabah, F. K. J.; Dahab, M. F. Biofilm and Biomass Characteristics in High-performance Fluidized-bed Biofilm Reactors. *Water Res.* **2004**, *38*, 4262-4270.

Schügerl, K. Three-phase-biofluidization: application of three-phase fluidization in biotechnology, a review. *Chem. Eng. Sci*. **1997**, *52*, 3661-3668.

Seville, J.P.K.; Clift, R.. The effect of thin liquid layers on fluidisation characteristics. *Powder Tech.* **1984**, *37*, 117-129.

Seville, J.P.K.; Willet, C.D.; Knight, P.C. Interparticle forces in fluidisation: a review. *Powder Tech.* **2000**, *113*, 261-268.

Wright, P.C.; Raper, J.A. Investigation into the viability of a liquid-film three-phase spouted bed biofilter. *J. Chem. Technol. Biotechnol*. **1998**, *73*, 281-291.

Wright, P.C.; Raper, J. A. Examination of dispersed liquid-phase three-phase fluidized beds Part 2: Porous, and non-spherical particle systems. *Powder Tech.* **1999**, *102*, 37-51.

CHAPTER 2 – Fluidization of Moist Sawdust in Binary Particle Systems in a Gas-solid Fluidized Bed

A similar version of this chapter has been copyrighted and published in the journal **Chemical Engineering Science**:

Clarke, K.L.; Pugsley, T.; Hill, G.A. Fluidization of moist sawdust in binary particle systems in a gas-solid fluidized bed. *Chem. Eng. Sci.* **2005**, *60*, 6909-6918.

Contribution of Ph.D. candidate

Experiments were planned and performed by Kyla Clarke. In addition, Todd Pugsley and Gordon Hill provided guidance in preparing the experimental plan. The submitted manuscript was written by Kyla Clarke, while Todd Pugsley and Gordon Hill provided editorial input.

Contribution of this paper to the overall study

The primary objective of the Ph.D. research is to develop a gas-solid fluidized bioreactor for treating contaminated air. This paper describes the experimental development of a suitable packing material for a fluidized bioreactor. The two main requirements of the bed particles are that they are able to be fluidized, and they are able to retain moisture. Moisture is required for growth and maintenance of microorganisms which are supported on the particles. Sawdust particles were selected as a potential packing material of the fluidized bioreactor. However, the poor fluidization properties of moist sawdust particles needed to be addressed. The following chapter describes the addition of a second, inert particle to enhance the fluidization of moist sawdust. Experiments demonstrated the affect of variables such as sawdust moisture content, glass sphere size and amount of glass spheres on the fluidization of binary mixtures.

Additional experimental details not in the manuscript

Preliminary work for this chapter involved selection of a type of packing for a fluidized bioreactor. Celite® (diatomaceous earth) particles were first considered for the fluidized bioreactor but were subsequently ruled out because Celite is a suspected carcinogen. Dust control to mitigate the risk of Celite to human health would be difficult both in the bench-scale fluidization experiments planned for this Ph.D. project and in an industrial-scale fluidized bioreactor. It was also desirable to avoid using the various types of inorganic and organic particles which were trialed in a study of a three-phase spouted bed bioreactor by Wright and Raper (1998), as none of those particles showed promise. Wright and Raper (1998) found that fluidization of certain particle types was nearly impossible because the particles stuck together due to the addition of water, while other particle types were unable to hold moisture and dried out.

The sawdust particles and specification A-55 glass spheres (Potters Canada, Moose Jaw, SK, Canada) used in this study are shown in Figure 2.01 (a) and (b). Waste white spruce wood chips were obtained from the NorSask Forest Products Ltd. Sawmill in Meadow Lake, SK, Canada and ground into smaller sawdust particles. The results of a Tyler series sieve analysis of the sawdust particles is presented in Table A.1 in Appendix A. Sample particle size distributions of the glass spheres are shown in Figure A.12. Figure 2.02 is a photograph of the Wiley mill used to grind wood chips into sawdust particles. Figure 2.03 shows a mixture of sawdust and glass spheres during fluidization.

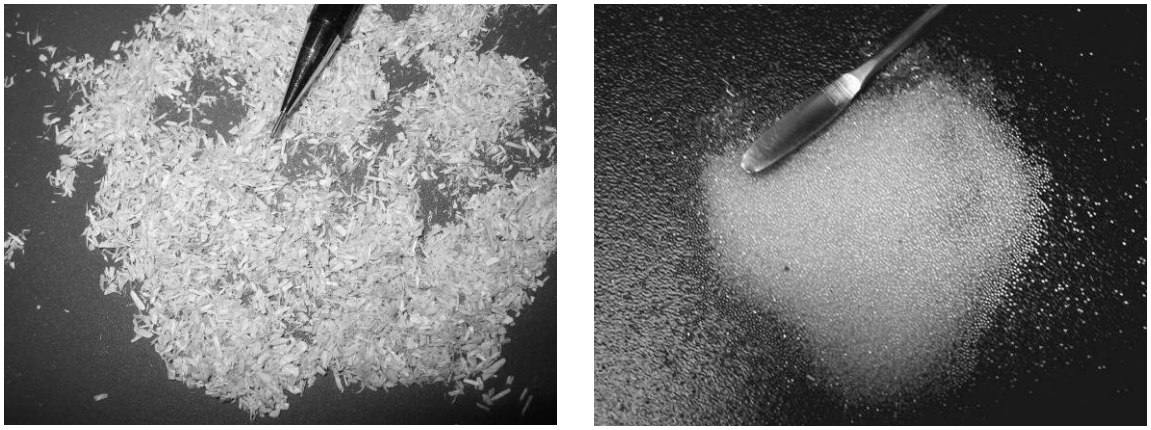

(a) (b)

Figure 2.01 (a) Sawdust particles (Sauter mean diameter of 0.625 mm), (b) Glass spheres, specification A-055 (Sauter mean diameter of 0.516 mm).

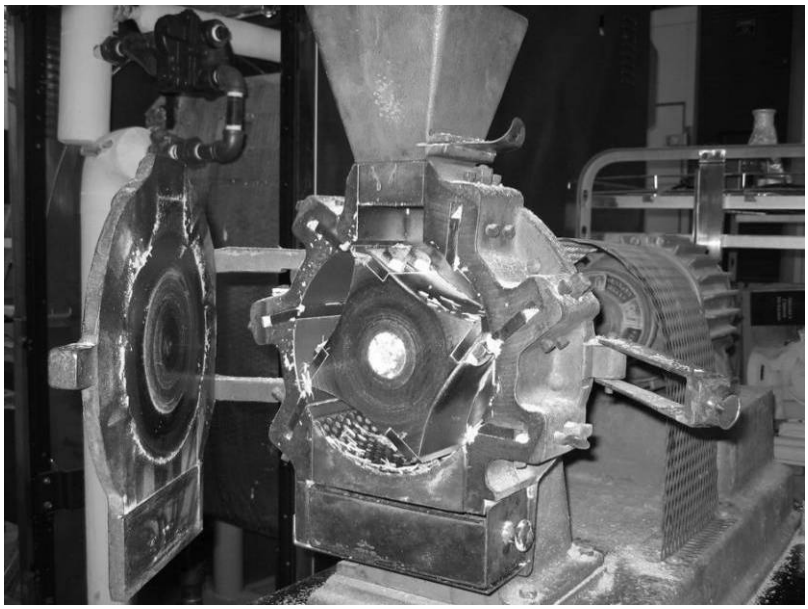

Figure 2.02 Wiley mill used to grind wood chips into sawdust particles.

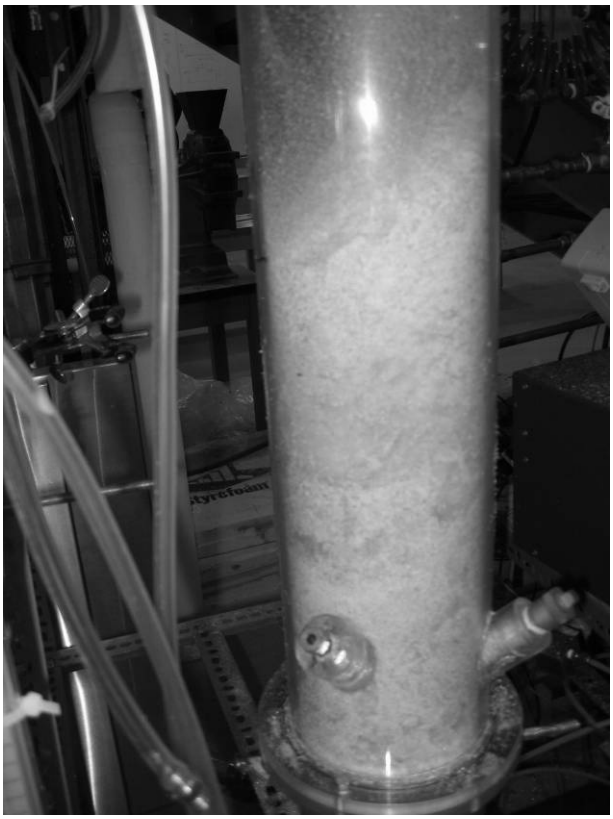

Figure 2.03 Binary mixture of sawdust (0.625 mm) and glass spheres (0.516mm) during fluidization.

The perforated distributor plate of the fluidized bed apparatus was designed according to the rules of thumb in Kunii and Levenspiel (1991). The distributor was constructed using a clear, acrylic plate. Holes were machine drilled to be 1.0 mm in diameter on a square pitch with 3.5 mm between the centre of each hole.

The flowrate of air to the fluidized bed was metered with a flow orifice plate with a 12.7 mm (0.5 inch opening). The orifice plate was designed according to ASME standards for fluid flow in closed conduits (Miller et al., 1990). It was bolted between pipe flanges in a horizontal section of 2 inch diameter pipe. Figure 2.04 shows a schematic of the orifice plate. Pressure taps on the upstream and downstream side of the orifice plate were connected to a differential pressure transmitter in order to measure the pressure drop across the orifice. The pressure drop was then correlated to flowrate through the orifice based on orifice flowmeter theory. Refer to Appendix A (Figure A.8) for a calibration curve providing superficial gas velocity in the bioreactor as a function of pressure drop across the flow orifice plate.

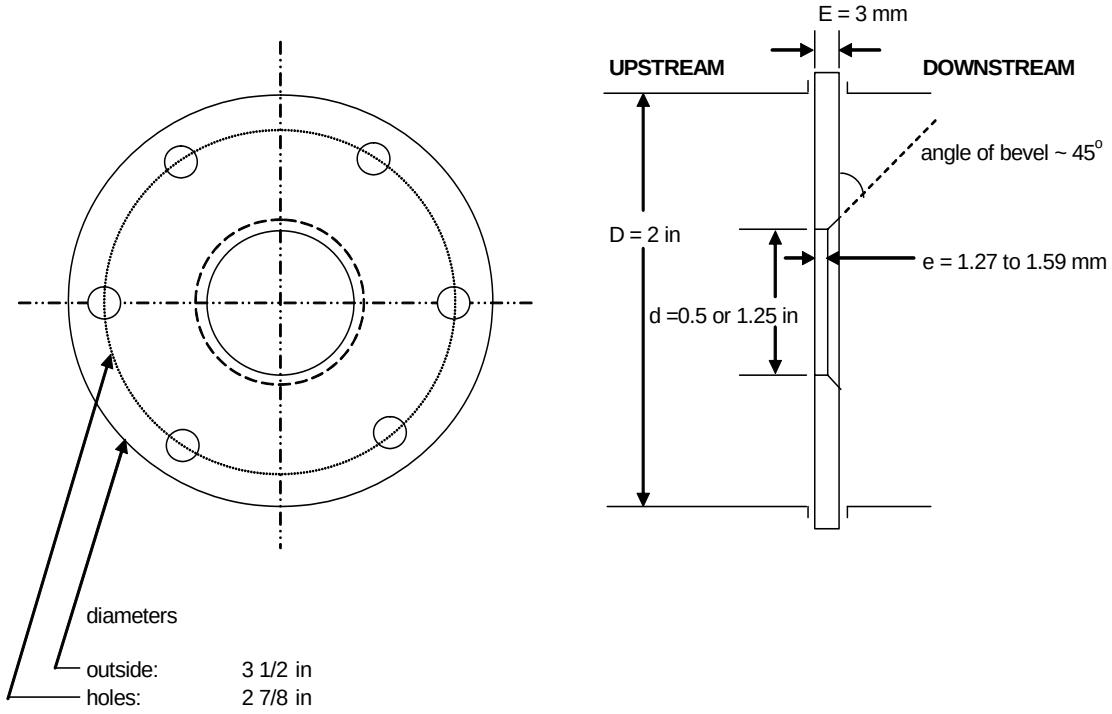

Figure 2.04 Schematic of 12.7 mm (0.5 inch) and 31.8 mm (1.25 inch) orifice plates.

Manuscript

2.1 Abstract

The fluidized behaviour of binary mixtures of moist sawdust and glass spheres has been investigated. The sawdust alone was observed to fluidize poorly, with extensive channelling occurring. The addition of 0.322 mm and 0.516 mm glass spheres to the fluidized bed of sawdust improved the fluidization characteristics. The mixtures of sawdust and 0.322 mm spheres were completely mixed when fluidized. Mixtures of sawdust and 0.516 mm spheres were either partially or completely mixed, depending upon gas velocity in the fluidized bed. As the moisture content of the sawdust was increased, the minimum fluidization velocity of the binary mixture also increased. There was an upper limit to the moisture content of the sawdust at which fluidization could be achieved. When the moisture content of the sawdust exceeded 33 wt% and 54 wt% on a dry basis, agglomeration and channelling occurred in the mixtures of sawdust and glass spheres, with sizes 0.322 mm and 0.516 mm, respectively. The moisture likely contributes to interparticle liquid bridging forces. Binary mixtures of larger 0.777 mm and 1.042 mm glass spheres and up to 82% moisture sawdust did not readily agglomerate, but the two components completely segregated during fluidization.

2.2 Introduction

Biomass such as sawdust can be processed by gasification or pyrolysis in gas-solid fluidized beds yielding fuel gases (Aznar et al., 1992a). A new fluidization application for sawdust is as a support for microorganisms in gas-solid fluidized bioreactors (Leslous et al., 2004). By itself, sawdust does not fluidize well and it exhibits channelling and Geldart C fluidization behaviour (Aznar et al., 1992a, Reina et al., 2000). Reina et al. (2000) theorize that aggregation of the sawdust occurs due to interlacing between unattached fibres, forming nets that retain other finer particles. Agglomeration of particles is a well known cause of poor fluidization performance. One means of enhancing sawdust fluidization is by adding a second, inert

component to the fluidized bed, such as sand (Aznar et al, 1992a). A similar approach was used for wheat straw by Bilbao et al. (1987).

In gas-solid fluidized bed bioreactors, microorganisms are immobilized onto particles which are fluidized by a gas stream. Moisture must be introduced to the bioreactor as it is an essential requirement for growth and maintenance of the microorganisms. For sawdust particles, Leslous et al. (2004) suggest that the ideal moisture content is 82 wt%, on a dry basis, in a gas-solid fluidized bioreactor. Previous studies (Bilbao et al., 1987; Aznar et al., 1992a, 1992b) have investigated the fluidization of binary mixtures of sand and dry biomass (Table 2.1). However, if sawdust is to be used to immobilize active microorganisms in a bioreactor, it must be wet. The presence of moisture affects fluidization behaviour by introducing interparticle liquid bridge forces (Seville and Clift, 1984; Seville et al., 2000). The effect of liquid on fluidization can be described as changes in the Geldart classification of the particles (Seville and Clift, 1984). The fluidized behaviour of particles can shift from Geldart class A or D to class C as a result of addition of a liquid; as well, either increasing viscosity or surface tension of the liquid, results in a shift from Geldart B class to class C (McLaughlin and Rhodes, 2001). An understanding of the fluidized behaviour of wet sawdust is necessary if the fluidized bed bioreactor technology is to be developed further. Therefore, in the current study we investigate the fluidization of binary mixtures of moist sawdust and glass spheres and the interrelationship between moisture content, composition of the binary mixture, and fluidization properties.

Table 2.1 Minimum fluidization velocity of binary mixtures.

	u_{vf} ($m\ s^{-1}$)		u_{mf} ($m\ s^{-1}$)	
	0.794 mm straw and sand (Bilbao et al., 1987)		***0.507 mm sawdust and sand (Aznar et al., 1992a)***	
Volume fraction of sand	***0.158 mm sand***	***0.346 mm sand***	***0.16 mm sand***	***0.34 mm sand***
0.5	0.13	0.20	0.05	0.155
0.7	0.07	0.150	0.045	0.15

2.3 Binary Particle Mixtures

2.3.1 Mixing and Segregation in Fluidized Binary Mixtures

Segregation of particles can occur in fluidized beds of binary mixtures. Segregation is a function of the differences in density and size of the components, and gas velocity in the bed (Chiba et al., 1979). Components with different densities, but the same size will segregate to a greater extent than components of different sizes and similar densities (Kunii and Levenspiel, 1991). The component with the larger density, termed jetsam, has a tendency to sink, and the lighter component, termed flotsam, will float. In cases where there is no difference in density, the larger particle is termed jetsam (Chiba et al., 1979). The amount of segregation varies with gas flowrate in the bed. A binary system with severe segregation at the minimum fluidization velocity, will exhibit decreasing segregation when velocity is increased (Kunii and Levenspiel, 1991).

Chiba et al. (1979) define three mixing states of binary systems in fluidized beds: completely mixed, completely segregated and partially mixed. In a completely segregated system the top and bottom of the fluidized bed consist of pure flotsam and pure jetsam particles, respectively. In a completely mixed system there is no variation in the concentration of the jetsam and flotsam components throughout the bed. In a partially mixed fluidized bed, there will be a high concentration of jetsam at the bottom and a high concentration of flotsam at the top, while the middle of the bed may be completely mixed. Rowe and Nienow (1976) define the degree of mixing, M, as:

$$M = \frac{x_{j,top}}{x_{j,bed}} \tag{2.1}$$

where $x_{j,top\ and}\ x_{j,bed}$ are the mass fractions of jetsam particles in the top of the bed and in the whole bed, respectively. The bed is thus perfectly mixed when M is equal to one.

2.3.2 Minimum Fluidization Velocity of Binary Mixtures

The minimum fluidization velocity, u_{mf}, of a binary mixture of particles is a function of the two types of particles and their relative concentrations (Aznar et al., 1992a). The component

with the lower minimum fluidization velocity is termed the fluid component, and other is termed the packed component (Rowe and Nienow, 1976). In the case of sawdust particles in a single component system, the minimum fluidization velocity may not exist at all because sawdust may not fluidize (Aznar et al., 1992a). Chiba et al. (1979) demonstrate that u_{mf} is also a function of the amount of segregation or mixing in the bed. A completely mixed binary system will start to fluidize at a single velocity $u_{mf,}$ between the minimum fluidization velocities of the fluid and packed components by themselves, called u_f and u_{pk} respectively. In a completely segregated binary system, fluidization begins near u_f but the bed is not completely fluidized until the velocity approaches u_{pk}. A partially mixed system is intermediate between these two extremes.

There are various techniques presented in the literature to define and determine the minimum fluidization velocity of binary mixtures, by using pressure drop *versus* velocity profiles. Chiba et al. (1979) obtained pressure drop *versus* velocity curves using fast and slow defluidization methods, while decreasing bed velocity. Noda et al. (1986) defluidized the bed quickly, and then obtained pressure drop *versus* velocity data while increasing velocity to complete fluidization and then decreasing velocity. Aznar et al. (1992a) obtained u_{mf} while increasing velocity from a well-mixed, packed bed. The minimum fluidization velocity can be defined as the point of intersection of the lines of pressure drop *versus* velocity at complete fluidization (horizontal line) and during the packed bed state (Chiba et al., 1979 and Aznar et al., 1992a). Kunii and Levenspiel (1991) define u_{mf} for a fluidized bed containing a wide size distribution as the intersection of the fixed bed pressure drop *versus* velocity line, and the line of bed weight divided by cross sectional area *versus* velocity (horizontal line). Alternatively minimum fluidization velocity is defined as the point where both components are fluidized, and it is determined visually (Noda et al, 1986 and Bilbao et al., 1987). Bilbao et al. (1987) denote this point as u_{vf}. Many of the studies on binary particle mixtures have developed equations for calculating the minimum fluidization velocity. These equations are summarized in Table 2.2.

Table 2.2 Modeling minimum fluidization velocities of binary mixtures.

Reference	Correlations for u_{mf} *and* u_{vf} of binary mixtures	Supplemental equations
Rowe and Nienow (1976)	$u_{mf} = u_s \left(\frac{u_b}{u_s} \right)^{x_b^2}$ (2.2)	
Chiba et al. (1979)	For a completely mixed bed:	$\overline{\rho} = V_f \rho_f + (1 - V_f)\rho_{pk}$ (2.5)
	$u_{mf} = u_f \frac{\overline{\rho}}{\rho_f} \left(\frac{\overline{d}}{d_f} \right)^2$ (2.3)	$\overline{d} = \left[N_f d_f^3 + (1 - N_f) d_{pk}^3 \right]^{1/3}$ (2.6)
	For a completely segregated bed:	$N_f = \frac{1}{1 + \left(\frac{1}{V_f} - 1 \right) \left(\frac{d_f}{d_{pk}} \right)^3}$ (2.7)
	$u_{mf} = \frac{u_f}{\left(1 - \frac{u_f}{u_{pk}} \right) x_f + \frac{u_f}{u_{pk}}}$ (2.4)	
Noda et al. (1986)	$Ar = A\mathrm{Re}_{p,mf}^2 + B\mathrm{Re}_{p,mf}$ (2.8)	$\frac{1}{\overline{\rho_p}} = \frac{x_f}{\rho_f} + \frac{x_{pk}}{\rho_{pk}}$ (2.11)
		$\frac{1}{\overline{d_p}\,\overline{\rho_p}} = \frac{x_f}{d_f \rho_f} + \frac{x_{pk}}{d_{pk} \rho_{pk}}$ (2.12)
	$\mathrm{Ar} = \frac{\left(\overline{d_p} \right)^3 \rho_g (\overline{\rho_p} - \rho_g) g}{\mu^2}$ (2.9)	$A = 36.2 \left(\frac{d_{pk} \rho_f}{d_f \rho_{pk}} \right)^{-0.196}$ (2.13)
	$\mathrm{Re}_{p,mf} = \frac{\overline{d_p} u_{mf} \rho_g}{\mu}$ (2.10)	For a completely mixed bed:
		$B = 1397 \left(\frac{d_{pk} \rho_f}{d_f \rho_{pk}} \right)^{0.296}$ (2.14)
		For a partially mixed bed where $d_{pk}/d_f > 3$, and $\rho_p/\rho_f \sim 1$:
		$B = 6443 \left(\frac{d_{pk} \rho_f}{d_f \rho_{pk}} \right)^{-1.86}$ (2.15)
Bilbao et al.(1987)	$u_{vf} = u_{pk} - (u_{pk} - u_f) X_f$ (2.16)	$u_{pk} = 50 d_{pk}^{0.84}$ (2.17)
		$X_f = \frac{x_f}{x_f + \frac{\rho_f}{\rho_{pk}} (1 - x_f)}$ (2.18)

2.4 Experimental

An acrylic, bench-scale fluidized bed, illustrated in Figure 2.1 was used for this study. The vessel is cylindrical, with an inner diameter of 0.139 m and a height above the distributor plate of 1.81 m. Below the distributor, there is a windbox, 0.162 m in height. The perforated-plate distributor has 1.0 mm holes on a square pitch, with 6.4 % open area. A 100 mesh size wire screen covers the distributor to prevent material from plugging the holes. Ambient air is supplied with a blower. Any entrained fines in the outlet air of the fluidized bed were collected in a cyclone.

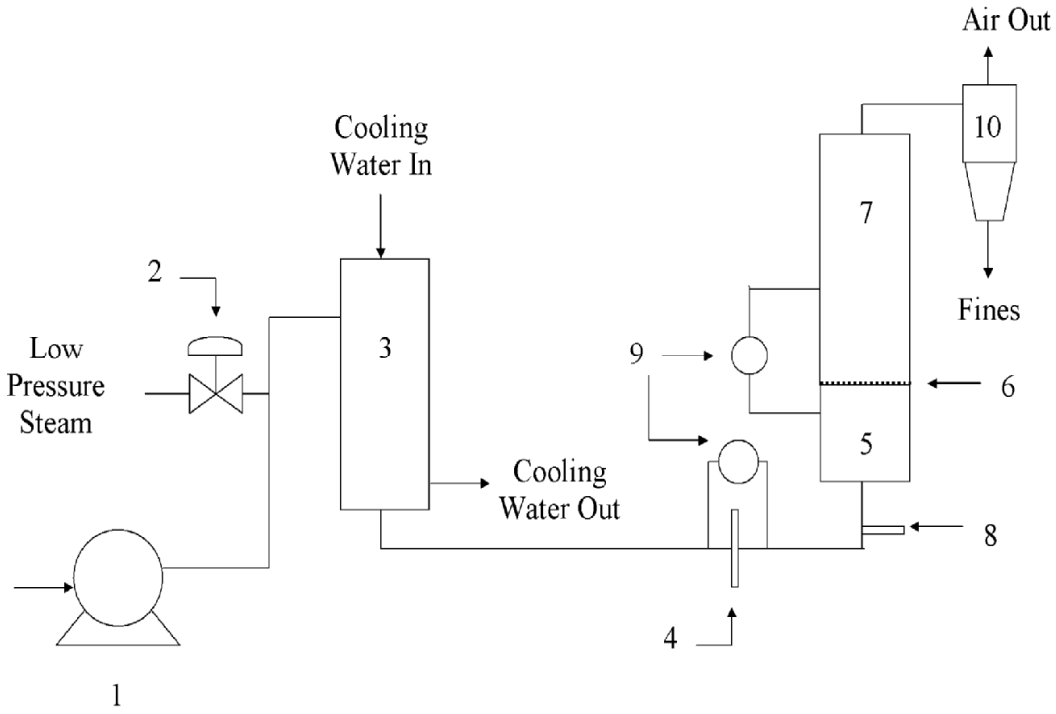

Figure 2.1 Experimental apparatus: (1) blower; (2) steam control valve; (3) heat exchanger; (4) orifice plate; (5) windbox; (6) distributor and wire screen; (7) fluidized bed; (8) humidity and temperature probe; (9) differential pressure transducers; (10) cyclone.

Flow of air to the fluidized bed was metered with a flow orifice plate, which was designed according to ASME standards for fluid flow in closed conduits (Miller et al., 1990). The pressure drop across the orifice plate and the combined pressure drop across the distributor

and fluidized bed were measured with differential pressure transducers. The transducers were calibrated with a DPI 610 pressure calibrator by Druck (New Fairfield, CT). The pressure drop through the distributor and wire screen was separately measured at all air velocities used in the experiments, so that pressure drop across the fluidized bed by itself could be calculated from:

$$\Delta p_{bed} = \Delta p_{tot} - \Delta p_d \tag{2.19}$$

The inlet air was cooled to 20 ºC +/- 1 ºC with a heat exchanger, supplied with cooling water at 5 to 15 ºC. Relative humidity of the inlet air was adjusted between 90 to 100% by injecting low pressure steam into the inlet air. For the experiments involving 8% moisture sawdust, relative humidity of the air was adjusted to be less than 30%. Both humidity and temperature of the inlet air were measured with a HMP 230 Series probe by Vaisala (Helsinki, Finland). A model MC1-333 data acquisition board by Validyne Engineering (Northridge, CA) was used for data collection from the differential pressure transducers and the humidity and temperature probe. Continuous data logging was carried out using LabVIEW™ software, created by National Instruments (Austin, TX).

The particles used in the fluidization experiments included sawdust and glass spheres. Waste white spruce wood chips were obtained from the NorSask Forest Products Ltd. Sawmill in Meadow Lake, SK, Canada. The wood chips were ground in a #1 Wiley mill, fitted with a 1 mm screen, manufactured by Arthur H. Thomas Co., Philadelphia, PA. The sawdust was then sieved in Tyler Series sieves in a Ro-Tap sieve shaker for 20 minutes. Particles between 0.354 and 1.00 mm were retained for fluidization experiments. Four sizes of glass spheres, technical specifications A-055, A-070 and A-100, and industrial specification #5 were obtained from Potters Canada, Moose Jaw, SK, Canada. The properties of the sawdust and glass spheres are summarized in Table 2.3.

A Mastersizer S-Series Long Bench particle size analyzer by Malvern Instruments Inc. (Malvern, Worcestershire, UK) was used to determine the number volume mean diameter of the glass spheres. The Sauter mean diameter, d_p, is calculated from the number volume mean by the Malvern software. The mean particle diameter of dry, 8% moisture, sawdust was determined by hand sieving a representative sample and recording the weight fraction retained on each sieve, using the method outlined by Allen (1997). The Sauter mean diameter is then calculated by the following equation:

$$d_p = \frac{1}{\sum_i \left(x_i / d_{p,i} \right)} \tag{2.20}$$

Table 2.3 Properties of particles.

	Particle size, d_p (mm)	Skeletal density, ρ_s (kg m^{-3})	Particle density, ρ_p (kg m^{-3})	Bulk density, ρ_b (kg m^{-3})	Sphericity, ϕ_S	Bed voidage, ε_m	Minimum fluidization velocity[a], u_{mf} (m s^{-1})
Sawdust (82% Moist.)	0.625		510	213	0.44		0.41
Sawdust (54% Moist.)	0.625		469	195	0.44		0.43
Sawdust (45% Moist.)	0.625		453	175	0.44		0.32
Sawdust (33% Moist.)	0.625		433	171	0.44		0.32
Sawdust (26% Moist.)	0.625		419	171	0.44		0.27
Sawdust (8% Moist.)	0.625	1543	364	170	0.44	0.50	0.25
#5 specification glass spheres	0.322	2483	2483	1470	1.0	0.41	0.051
A-055 specification glass spheres	0.516	2481	2481	1460	1.0	0.41	0.29
A-070 specification glass spheres	0.777	2484	2484	1460	1.0	0.41	0.42
A-100 specification glass spheres	1.042	2495	2495	1490	1.0	0.40	0.63

[a]Sawdust particles at all moisture contents are poorly fluidized in a single component system.

Bulk densities, ρ_b, were determined by measuring the mass of a known volume of particles placed inside a graduated cylinder, without packing down the particles. Helium

intrusion, with an Ultrapycnometer 1000, by Quantachrome Instruments, (Boynton Beach, FL) was used to measure the skeletal density, ρ_s, of the sawdust and glass spheres. A Ruska (Houston, TX) mercury pycnometer, operated at pressures of 0.048 to 1520 kPa, was used to measure the fixed bed interparticle voidage, ε_m, of dry sawdust. The particle density of the sawdust, ρ_p, was calculated as follows:

$$\rho_p = \frac{\rho_b}{1-\varepsilon_m} \tag{2.21}$$

The glass spheres are non-porous. As a result the interparticle voidage of the spheres was determined by Equation 2.21 where $\rho_p = \rho_s$. The particle density of moist sawdust was calculated from Equation 2.22 proposed by Wright and Raper (1999).

$$\rho_{p,wet} = \frac{m_p + \frac{(\%moist)m_p}{100}}{\frac{m_p}{\rho_p} + \frac{(\%moist)m_p}{\rho_L}} \tag{2.22}$$

where m_p is the mass of the particles, and ρ_L is the density of the liquid.

The sphericity of the glass spheres was assumed to be 1.0. The effective sphericity $\phi_{s,eff}$ of dry sawdust was established from packed bed data of pressure drop *versus* velocity, by the method outlined in Kunii and Levenspiel (1991), using the Ergun equation (Equation 2.23):

$$\Delta p_{bed} = L_m \left[\frac{150\mu(u_o)(1-\varepsilon_m)^2}{\varepsilon_m^3(\phi_{s,eff} d_p)^2} + 1.75\frac{1-\varepsilon_m}{\varepsilon_m^3}\frac{\rho_g u_o^2}{\phi_{s,eff} d_p} \right] \tag{2.23}$$

where $\phi_{s,eff} \sim \phi_s$.

Fluidization experiments were conducted by adjusting the moisture content of the sawdust and the composition of the binary mixture of sawdust and glass spheres. These experiments included the fluidization of sawdust by itself at different moisture contents ranging between 8 and 82 wt% (Table 2.3). Moisture analysis of the sawdust before and after fluidization was performed with a Mettler Toledo (Columbus, OH) HB43 Halogen Moisture analyzer, with the samples heated to 160 ºC. The total bed height was 0.13 to 0.14 m, except for the fluidization of glass spheres by themselves, as insufficient material was available. The

spheres were placed in the bed first, followed by the sawdust. The air velocity was rapidly increased, until slugging or turbulent flow was observed. Then the flow was stopped quickly, to obtain a well-mixed, packed bed as per the approach of Noda et al. (1986). The bed pressure drop and superficial velocity through the bed were recorded as flowrate was gradually increased and then decreased. The minimum fluidization velocity was determined as the point of intersection of the fixed bed line and the initial bed weight divided by bed cross sectional area (horizontal line), at increasing air velocities from the well-mixed, packed bed, similar to the approach of Kunii and Levenspiel (1991). For this study, fluidization is designated as either adequate or poor by visual observation. In adequate fluidization a bubbling regime is observed, without the formation of channels at increasing gas velocities. The formation of a solid plug which collapses, followed by bubbling as velocity is increased, is also considered to be adequate fluidization. Fluidization is considered to be poor if channels form while increasing gas velocity or if agglomeration of the particles occurs in the bed at any gas velocity. As well, complete segregation of the particles constitutes poor fluidization.

2.5 Results and Discussion

Sawdust by itself does not achieve adequate fluidization at moisture contents of 8 to 82 wt% on a dry basis. For two of these moisture contents (33 and 54 wt%), Figures 2.2 and 2.3 show the pressure drop *versus* velocity profiles for sawdust by itself. After minimum fluidization velocity u_{mf} is reached there is a peak in the pressure drop curve due to a brief period of plug formation. Then there is a trough in the pressure drop curve due to the formation of channels in the bed. As gas velocity is further increased, a slug flow regime occurs. In the case of pure sawdust, fluidization was poor at all moisture contents.

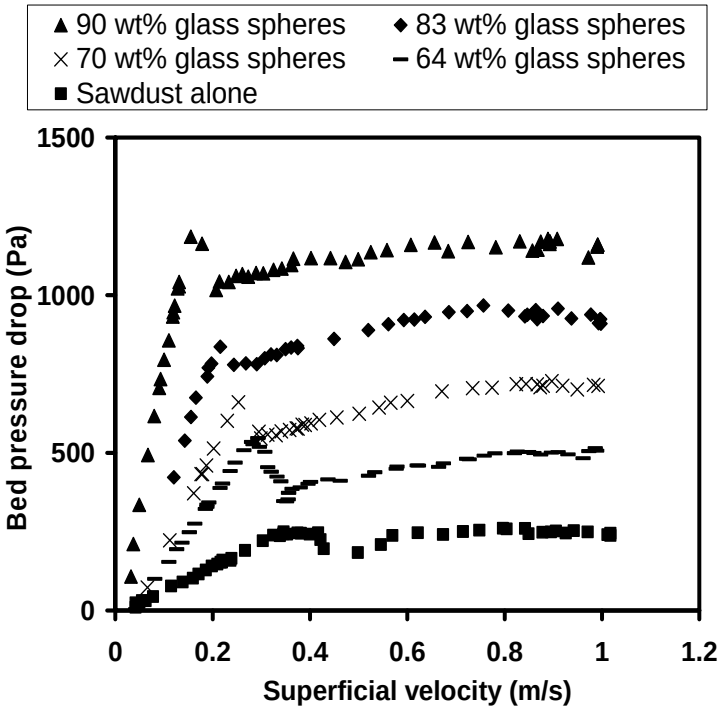

Figure 2.2 Binary mixtures of sawdust (33% moisture) and 0.322 mm glass spheres at increasing gas velocity.

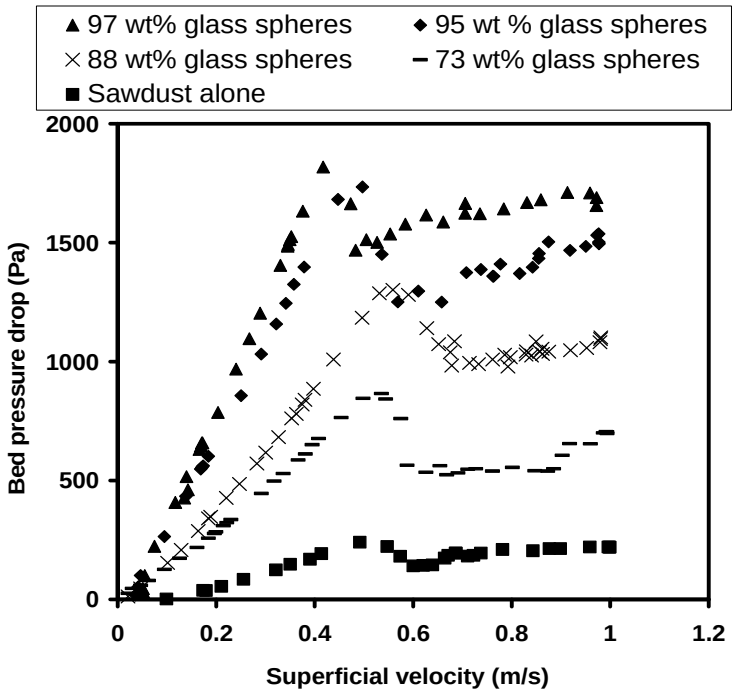

Figure 2.3 Binary mixtures of sawdust (54% moisture) and 0.516 mm glass spheres at increasing gas velocity.

In order to compare the fluidization behaviour of pure sawdust to mixtures of sawdust and glass spheres, the point at which a bed of pure sawdust transitions from a packed bed state to a poorly fluidized state was approximated by the method described in section 2.4. On the plot of bed pressure drop *versus* gas velocity, the intersection of the fixed bed line with the horizontal line representing initial bed weight divided by bed cross sectional area was taken as the minimum fluidization velocity of pure sawdust. It should be noted that the fixed bed pressure drop data obtained as the gas velocity was increased was used for this determination. For decreasing gas velocities, the bed often does not return to a packed bed state, and continues to exhibit channelling until the velocity is zero.

Figures 2.2 and 2.3 also show examples of pressure drop *versus* velocity curves of binary mixtures of sawdust and glass spheres, at various mass fractions of spheres. With increasing mass fraction of spheres, the region of channelling disappears and bubbling flow takes place. Mass fractions of 70% (mass of spheres to total mass of spheres and moist sawdust) and greater of 0.322 mm glass spheres result in adequate fluidization with 33 % moisture sawdust. Mass fractions of 88% and greater of 0.516 mm glass spheres produce adequate fluidization with 54% moisture sawdust. Visually, mixtures of sawdust and 0.322 mm glass spheres appear to be well mixed at moisture contents of 33% or less. The mixtures of 54% moisture sawdust and 0.516 mm glass spheres are partially to completely mixed slightly above u_{mf} of the mixture, and become completely mixed as velocity is increased above u_{mf}. Figures 2.2 and 2.3 also show that as the mass fraction of glass spheres increases at a constant bed height, the pressure drop across the fluidized bed at fluidization increases, because the total weight of fluidized mass has increased.

As an example of the influence of sawdust moisture on the fluidized bed behaviour, the pressure drop *versus* velocity curve for 50 vol% mixtures of 0.322 mm glass spheres and sawdust at varying moisture contents is shown in Figure 2.4. These correspond to mass fractions of glass spheres ranging from 88% to 90%, depending on the moisture content of the sawdust. At 8 and 26% moisture, fluidization is adequate. After u_{mf} is reached, bubbling commences, followed by slugging. At 33% moisture, a brief period of plug formation occurs at u_{mf}, followed by bubbling and then slugging. At 45% moisture, there is significant plug formation as indicated by the large peak at u_{mf}. Then there is channelling, signified by a trough in the pressure drop curve. At 82% moisture there is severe agglomeration of the particles, resulting in channelling at almost all

velocities. Agglomeration occurs between all adjacent particles, both sawdust and spheres. In addition, there was significant adherence of particles to the sides of the vessel, which greatly decreased the maximum pressure drop in the bed.

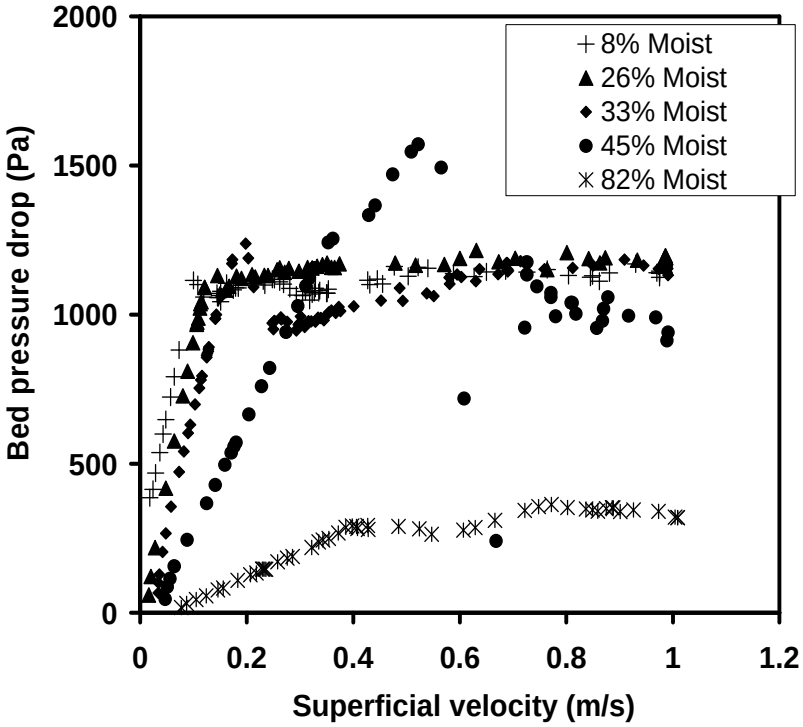

Figure 2.4 50:50 by bulk volume binary mixtures of sawdust and 0.322 mm glass spheres at increasing gas velocity.

Figure 2.5 illustrates the relationship between moisture content and the minimum fluidization velocity of binary mixtures of sawdust and 0.322 or 0.516 mm glass spheres. An S-shaped curve such as this one is indicative of a critical value of moisture content beyond which fluidization of the binary mixture is not possible. The maximum moisture contents for adequate fluidization occur in the transition region prior to the higher velocities in the S-shaped curve. In mixtures of sawdust and 0.322 mm or 0.516 mm glass spheres, when the moisture content of the sawdust exceeds 33% or 54% respectively, agglomeration occurs between both sawdust particles and the glass spheres, resulting in channelling. The bed shifts from Geldart B fluidization behaviour to Geldart C, likely due to liquid bridge forces between adjacent particles becoming significant compared to buoyant weight of the particles. The ratio of liquid bridge forces to buoyant weight is lower for the 0.516 mm *versus* the 0.322 mm spheres. As a result, the upper

limit to the moisture content of the sawdust at which adequate fluidization can be achieved in binary mixtures is higher in 0.516 mm *versus* 0.322 mm spheres. As moisture content increases, the minimum fluidization velocity of the binary mixture also increases. In part, the increased values of u_{mf} are caused by the increase in particle density of the sawdust at increasing moisture content. The increase in particle density by itself does not account for the S-curve relationship between u_{mf} and moisture content shown in Figure 2.5.

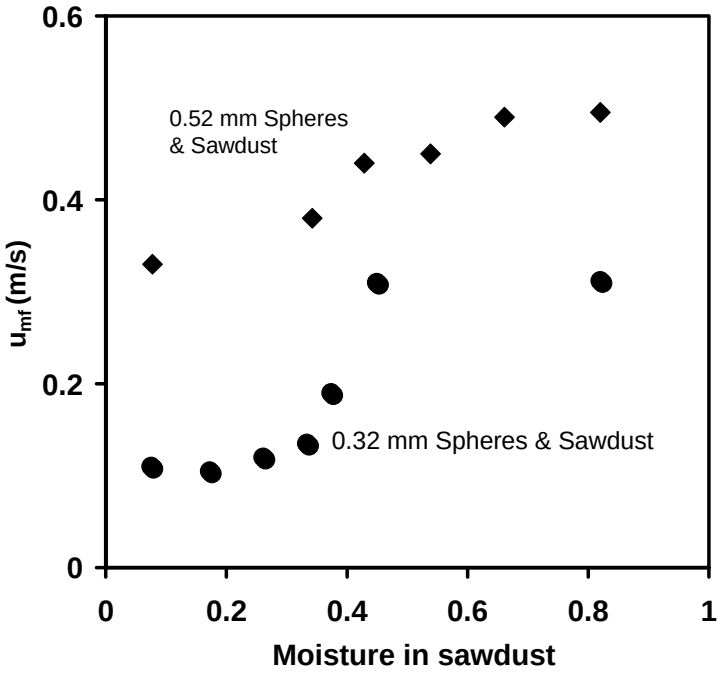

Figure 2.5 Minimum fluidization velocity of 50:50 by bulk volume binary mixtures of glass spheres and sawdust.

With increasing mass fraction of glass spheres, the minimum fluidization velocity of binary mixtures of 0.322 mm glass spheres decreases, as shown in Figure 2.6. The u_{mf} of the binary mixture is above the u_{mf} of the glass spheres alone (0.051 m s^{-1}) and is below the u_{mf} of sawdust alone (0.25 and 0.32 m s^{-1} for 8% and 33% moisture respectively). Comparatively in Figure 2.7, the u_{mf} of the binary mixture was observed again to be above that of the glass spheres alone (0.29 m s^{-1}), but now is seen to sometimes surpass the u_{mf} of sawdust alone (0.25 and 0.43 m s^{-1} for 8% and 54% moisture respectively). Pressure drop *versus* velocity data and visual

observations demonstrated that fluidization is poor for binary mixtures with low concentrations of glass spheres, and therefore u_{mf} is not shown on Figure 2.7 for these conditions.

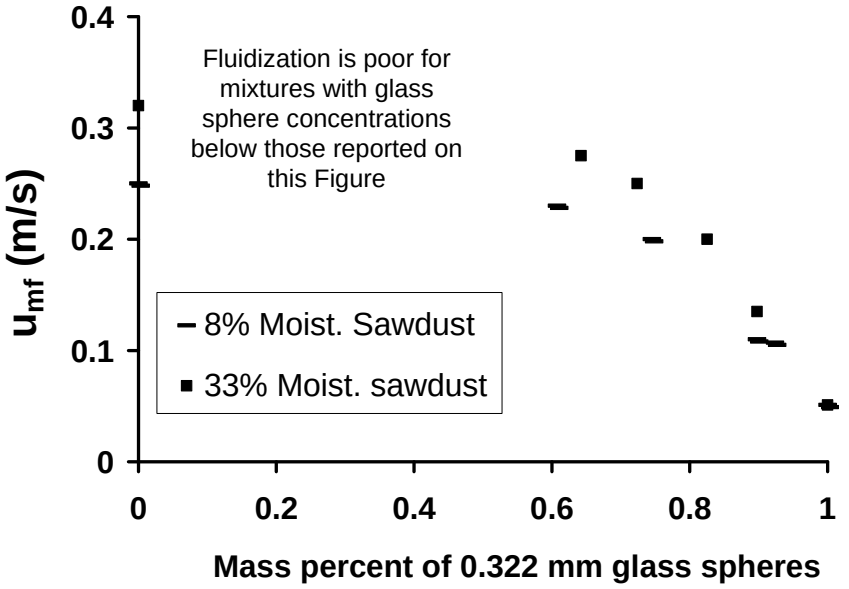

Figure 2.6 Minimum Fluidization velocities of binary mixtures of 0.322 mm glass spheres and sawdust.

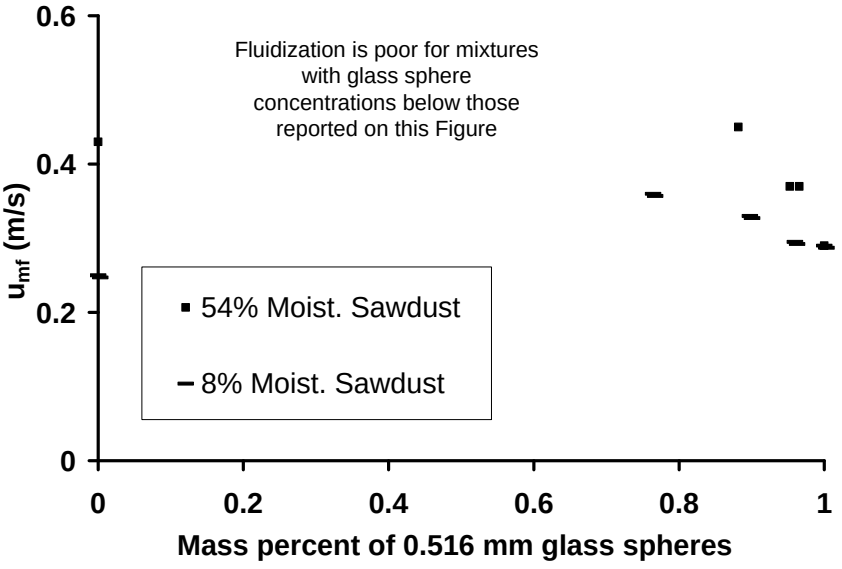

Figure 2.7 Minimum Fluidization velocities of binary mixtures of 0.516 mm glass spheres and sawdust.

Figures 2.8 and 2.9 compare the actual u_{mf} of binary mixtures of 33% moisture sawdust and 0.322 mm spheres, and 54% moisture sawdust and 0.516 mm spheres to predicted values of u_{mf} based on the correlations presented in Table 2.2. Equations 2.3 and 2.10 significantly underestimate the contribution to u_{mf} by the sawdust. Equation 2.16 is most successful at estimating u_{mf} of the binary mixture. But using Equation 2.17 to determine u_{pk} as a function of d_{pk} alone for use in Equation 2.16 is not appropriate. Figure 2.5 illustrates that u_{mf} of the mixture changes with the moisture content of the sawdust, partially due to the change in the particle density of the sawdust. For sawdust alone, u_{pk} is more likely a function of both d_{pk} and ρ_{pk}. Although sawdust by itself exhibits poor fluidization, a value of u_{mf} can be estimated experimentally (see the last column of Table 2.3). If the experimental value of u_{mf} for pure sawdust is substituted for u_{pk} in Equation 2.16, a more accurate prediction of u_{mf} of the binary mixture is possible. For mixtures of 33 and 54% moisture sawdust respectively, Equation 2.16 becomes:

$$u_{vf} = 0.32 - (0.32 - u_f)X_f \tag{2.24}$$

$$u_{vf} = 0.43 - (0.43 - u_f)X_f \tag{2.25}$$

However, in Figure 2.9, at 54% moisture, Equation 2.25 fails to predict that the u_{mf} of the mixtures is greater than the u_{mf} of 0.516 mm spheres and 54% moisture sawdust by themselves. By defining a higher value of u_{pk} of 0.71 m s^{-1}, Equation (2.25) for 54 wt% moisture sawdust becomes:

$$u_{vf} = 0.71 - (0.71 - u_f)X_f \tag{2.26}$$

It can then be seen that the modified versions of Equation 2.16 (i.e. Equations 2.24 and 2.26) follow the experimental minimum fluidization velocities in Figures 2.8 and 2.9, respectively. It should be pointed out that in Figures 2.8 and 2.9, it is assumed that u_{vf} is equal to u_{mf}.

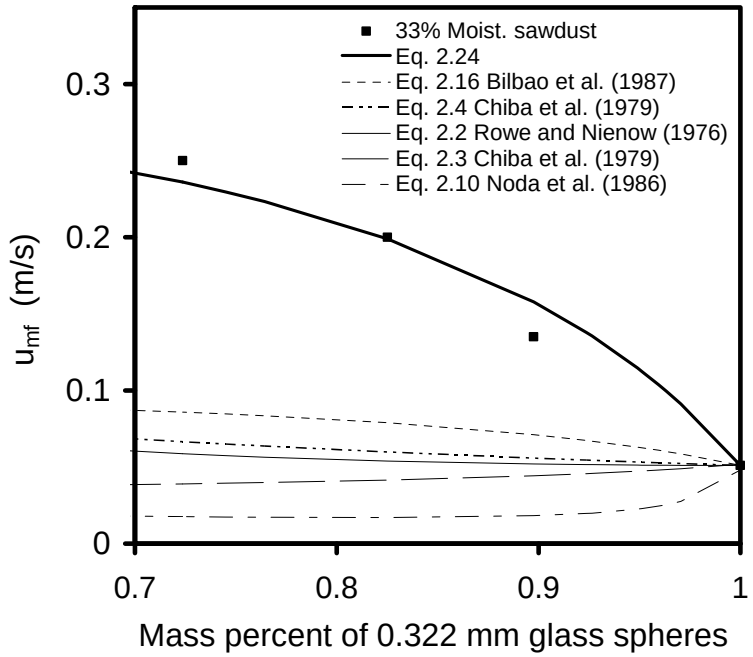

Figure 2.8 Predictions of u_{mf} of binary mixtures of sawdust (33% moisture) and 0.322 mm glass spheres.

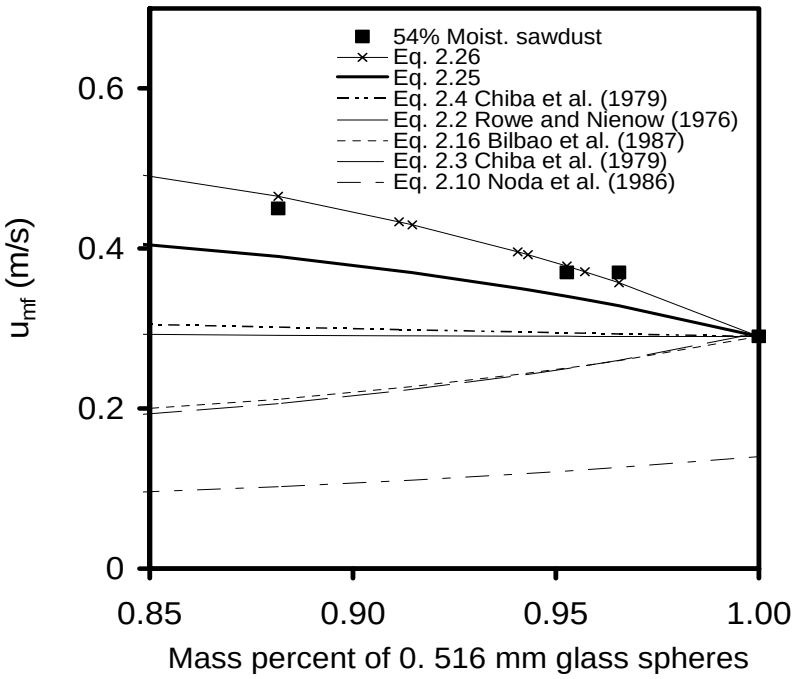

Figure 2.9 Predictions of u_{mf} of binary mixtures of sawdust (54% moisture) and 0.516 mm glass spheres.

Binary mixtures of 0.777 and 1.042 mm glass spheres with 82% moisture sawdust did not fluidize at either 88 or 94 wt% glass spheres. The spheres and the sawdust remained completely segregated at all velocities. As gas velocity was increased, the sawdust at the surface of the bed began to channel first, and continued to channel as the glass spheres in the bottom of the bed began to fluidize. In addition, the sawdust was quickly elutriated from the fluidized bed when the velocity was sufficient for fluidization of the spheres. Agglomeration was not observed in the mixture. Elutriation of the sawdust likely occurred when the gas velocity exceeded the terminal velocity of the sawdust. The terminal velocity, u_t, of 82% moisture, 0.354 mm (the smallest size in appreciable quantity) sawdust particles was estimated to be 0.56 m s^{-1} using the graphical method of Haider and Levenspiel (Kunii and Levenspiel, 1991). The minimum fluidization velocities of the binary mixtures of 82% moisture sawdust and spheres were 0.49 and 1.4 m s^{-1} for 0.777 and 1.042 mm spheres respectively.

2.6 Conclusions

The addition of 0.322 mm and 0.516 mm glass spheres to a fluidized bed of 0.625 mm sawdust improves the fluidization characteristics. In binary mixtures of sawdust and glass spheres, the upper limit of the moisture content of the sawdust at which fluidization can be achieved is 33% and 54% with 0.322 mm and 0.516 mm spheres, respectively.

The larger 0.777 and 1.042 mm spheres likely do not agglomerate in mixtures with 82% moisture sawdust as a result of the lower ratio of liquid interparticle forces to buoyant weight of the particles. The large differences in density and size between the sawdust and spheres result in the complete segregation of the components. In addition, if the gas velocity exceeds the terminal velocity of the sawdust, the sawdust will be elutriated from the vessel. Thus, in binary mixtures of moist sawdust, there is a very narrow range of sphere sizes for which bubbling fluidization is possible. The minimum size of the second inert particle is limited by the ratio of interparticle liquid bridging forces to buoyant weight, and the maximum size is limited by the degree of segregation of the binary mixture.

Existing correlations are unsuccessful at predicting the minimum fluidization velocity of the binary mixtures of glass spheres and sawdust. The correlations of Noda et al. (1986) and Bilbao et al. (1987) are based on different definitions of minimum fluidization velocity. In addition, the correlations of Rowe and Nienow (1976), Noda et al. (1986), Bilbao et al. (1987), and Chiba et al (1979) may be strongly dependent on the types of particles used in their experiments.

For mixtures of 0.322 mm spheres and sawdust, u_{mf} of the mixture appears intermediate between the u_{mf} of the individual components, and for 0.516 mm spheres and sawdust, the mixture u_{mf} appears higher than the u_{mf} of the components. It is noteworthy that the u_{mf} of 0.322 mm spheres is significantly lower than the u_{mf} of the sawdust, while the u_{mf} of 0.516 mm spheres is very similar to that of sawdust. More research is needed to improve the fundamental understanding of why binary mixtures of glass spheres and sawdust can improve the fluidization quality. Studies published to date using sand and sawdust have presented only experimental results without a discussion of what the nature of interaction between the two types of particles may be. At this point we can only speculate on the mechanism of interaction. It seems plausible that interparticle capillary forces between the wet sawdust and the glass spheres create a situation whereby they do not behave as discrete particles. This postulated binary particle interaction is similar to the mechanism put forward by Nakagawa et al. (2002) for the fluidization of binary mixtures of very fine Geldart C powders with Geldart A or B powders. They propose that the formation of agglomerates of the fine and coarse powders occurs due to short-range interparticle forces. In our case, the interparticle force is due to moisture. The degree of mixing at u_{mf} may be a factor that influences this interaction, as it was observed that 0.322 mm spheres and 33% moisture sawdust were well mixed at all velocities, while 0.516 mm spheres and 54% moisture sawdust were partially mixed at u_{mf}. The interparticle forces will still exist, however, for those particles that are in contact.

2.7 Nomenclature

Ar	Archimedes number
d_f, d_{pk}	Particle size of fluid and packed component (m)
$\overline{d_p}, \overline{d}$	Mean particle size in a binary system, based on mass and volume fractions (m)
d_p	Sauter mean particle diameter (m)
$d_{p,i}$	Average diameter of particles in size range "i" (m)
g_c	Dimensionless constant
L_m	Height of packed bed of particles (m)
m_p	Mass of particle, dry (kg)
M	Degree of mixing in a binary component fluidized bed
N_f	Number fraction of fluid component in binary mixture
$Re_{p,mf}$	Particle Reynolds number at minimum fluidization
u_b, u_s	Minimum fluidization velocity of larger and smaller components in single component fluidized beds (m s^{-1})
u_f, u_{pk}	Minimum fluidization velocity of fluid and packed components in single component fluidized beds (m s^{-1})
u_o	Superficial velocity of gas through bed of particles (m s^{-1})
u_{mf}	Superficial velocity of gas at minimum fluidization (m s^{-1})
u_t	Terminal velocity of particles (m s^{-1})
u_{vf}	Superficial velocity of gas where both components in a binary mixture are fluidized (m s^{-1})
V_f	Volume fraction of fluid component in binary mixture
x_f, x_{pk}	Weight fraction of fluid and packed component in binary mixture
x_b	Mass fraction of larger particle in a binary mixture
x_i	Mass fraction of particles in size range "i"
X_f, X_{pk}	Real volume fractions of fluid and packed components defined by Equation 2.18

Greek symbols

ε_m	Fraction of voids in a packed bed of particles

ϕ_S, $\phi_{S,eff}$	Sphericity and effective sphericity of a particle
μ	Viscosity of gas stream (kg m^{-1} s^{-1})
Δp_{bed}	Pressure drop across fluidized bed (Pa)
Δp_d	Pressure drop across distributor and wire screen (Pa)
Δp_{tot}	Pressure drop across distributor, wire screen and fluidized bed (Pa)
ρ_b	Bulk density of particles (kg m^{-3})
ρ_f, ρ_{pk}	Particle density of fluid and packed components in binary mixture (kg m^{-3})
ρ_L	Density of water (kg m^{-3})
ρ_p	Particle or envelope density (including particle pore volume) (kg m^{-3})
$\rho_{p,wet}$	Particle density of moist particles (kg m^{-3})
$\overline{\rho_p}$, $\overline{\rho}$	Mean particle density in a binary system based on mass and volume fractions (kg m^{-3})
ρ_s	Skeletal density (excluding particle pore volume) (kg m^{-3})
ρ_g	Density of gas stream (kg m^{-3})

2.8 References

Allen, T. Particle Size Measurement Volume 1; Chapman and Hall: London, 1997, pp 256-276.

Aznar, M.P.; Gracia-Gorria, F.A.; Corella, J. Minimum and maximum velocities for fluidization for mixtures of agricultural and forest residues with a second fluidized solid. I. Preliminary data and results with sand-sawdust mixtures. *Int. Chem. Eng.* **1992**, *32* (1), 95-102.

Aznar, M.P.; Gracia-Gorria, F.A.; Corella, J. Minimum and maximum velocities for fluidization for mixtures of agricultural and forest residues with a second fluidized solid. II. Experimental results for different mixtures. *Int. Chem. Eng.* **1992**, *32* (1), 103-113.

Bilbao, R.; Lezaun, J.; Abanades, J.C. Fluidization velocities of sand/straw binary Mixtures. *Powder Tech.* **1987**, *52*, 1-6.

Chiba, S.; Chiba, T.; Nienow, A.W.; Kobayashi, H. The minimum fluidisation velocity, bed expansion and pressure-drop profile of binary particle mixtures. *Powder Tech.* **1979**, *22*, 255-269.

Kunii, D.; Levenspiel, O. Fluidization Engineering, Second Ed.; Butterworth-Heinemann: Newton, MA, 1991, pp 71-75; 95-108.

Leslous, A.; Delebarre, A.; Pre, P.; Warlus, S.; Zhang, N. Characterization and selection of materials for air biofiltration in fluidized beds. *Int. J. Chem. Reactor Eng*. **2004**, *2* (Article A20), 1-19.

McLaughlin, L.J.; Rhodes, M.J. Prediction of fluidized bed behaviour in the presence of liquid bridges. *Powder Tech.* **2001**, 114, 213-223.

Miller, R.W.; Lee, W.F.Z.; Gomez, C.J. Measurement of Fluid Flow in Pipes using Orifice, Nozzle, and Venturi, ASME-MFC-3M-1989; ASME American Society of Mechanical Engineers: New York, 1990.

Nakagawa, N.; Suzuki, R.; Toda, K.; Kato, K. Minimum fluidization velocity of binary particle mixtures with adhesive fine powder. *J. Chem. Eng. Jpn.* **2002**, *35*(7), 595-603.

Noda, K.; Uchida, S.; Makino, T.; Kamo, H. Minimum fluidization velocity of binary mixture of particles with large size ratio. *Powder Tech.* **1986**, *46*, 149-154.

Reina, J.; Velo, E.; Puigjaner, L. Predicting the minimum fluidization velocity of polydisperse mixtures of scrap-wood particles. *Powder Tech.* **2000**, *111*, 245-251.

Rowe, P.N.; Nienow, A.W. Particle mixing and segregation in gas fluidised beds: a review. *Powder Tech.* **1976**, *15*, 141-147.

Seville, J.P.K.; Clift, R. The effect of thin liquid layers on fluidisation characteristics. *Powder Tech.* **1984**, *37*, 117-129.

Seville, J.P.K.; Willet, C.D.; Knight, P.C. Interparticle forces in fluidisation: a review. *Powder Tech.* **2000**, *113*, 261-268.

Wright, P.C.; Raper, J.A. Examination of dispersed liquid-phase three-phase fluidized beds Part 2: Porous and non-spherical particle systems. *Powder Tech.* **1999**, *102*, 37-51.

Wright, P.C.; Raper, J.A. Investigation into the viability of a liquid-film three-phase spouted bed biofilter. *J. Chem. Technol. Biotechnol.* **1998**, *73*, 281-291.

CHAPTER 3 – Direct Comparison of Fluidized and Packed Bed Bioreactors for Bioremediation of an Air Pollutant

A condensed version of this chapter was published in the proceedings of the **12th International Fluidization Conference** and a similar version of this chapter has been copyrighted and published in the **International Journal of Chemical Reactor Engineering**:

Clarke, K.L.; Hill, G.A.; Pugsley, T. Treatment of VOC emissions in a gas-solid fluidized bioreactor. Proceedings of the 12th International Fluidization Conference, Harrison Hot Springs, British Columbia, Canada, May 13-17, 2007.

Clarke, K.L.; Hill, G.A.; Pugsley, T. Direct comparison of fluidized and packed bed bioreactors for bioremediation of an air pollutant. *Int. J. Chem. Reactor Eng.* **2007**, *5*(Article A11), 1-12.

Contribution of Ph.D. candidate

Experiments were planned and performed by Kyla Clarke. Todd Pugsley and Gordon Hill provided guidance in planning the experiments. The submitted manuscript was written by Kyla Clarke, while Gordon Hill and Todd Pugsley provided editorial assistance.

Contribution of this paper to the overall study

This paper presents experiments on the bioremediation of waste gas in a gas-solid fluidized bioreactor. This work involves the design and construction of a bench-scale fluidized bed vessel. The apparatus is tested for the treatment of ethanol-contaminated air. The packing of the bioreactor consists of a mixture of glass spheres and sawdust particles, which was described in Chapter 2 and shown to be a feasible packing option. The bioreactor was operated

in both packed and fluidized bed modes. The mass transfer from an ethanol- contaminated air stream to sawdust/glass sphere packing is compared for fluidized and packed bed operation modes. This chapter also provides details of the microbial growth kinetics of the predominant microorganism in the bioreactor.

Additional experimental details not in the manuscript

Apparatus

The apparatus which was used in the fluidization experiments presented in Chapter 2 was also used for the mass transfer and bioremediation experiments discussed in Chapter 3. The apparatus was modified so that a contaminated air stream could be injected into the inlet line to the bioreactor. Figures 3.01 and 3.02 are photographs of the experimental apparatus.

The flowrate of the contaminated air stream was measured with rotameters 1 or 2, or with mass flow meter 1, depending on the required inlet air flowrate to the vessel and the ethanol concentration. The calibration curves for the rotameters and mass flow meter are presented in Appendix A. For packed bed experiments involving a superficial gas velocity of 0.0024 m s^{-1}, the air to the bioreactor vessel was supplied by compressed laboratory air instead of from a blower, and air flow rate was measured with rotameter 3. The rotameters and mass flow meter were calibrated with a Precision wet test meter by Precision Scientific Co. (Chicago, IL).

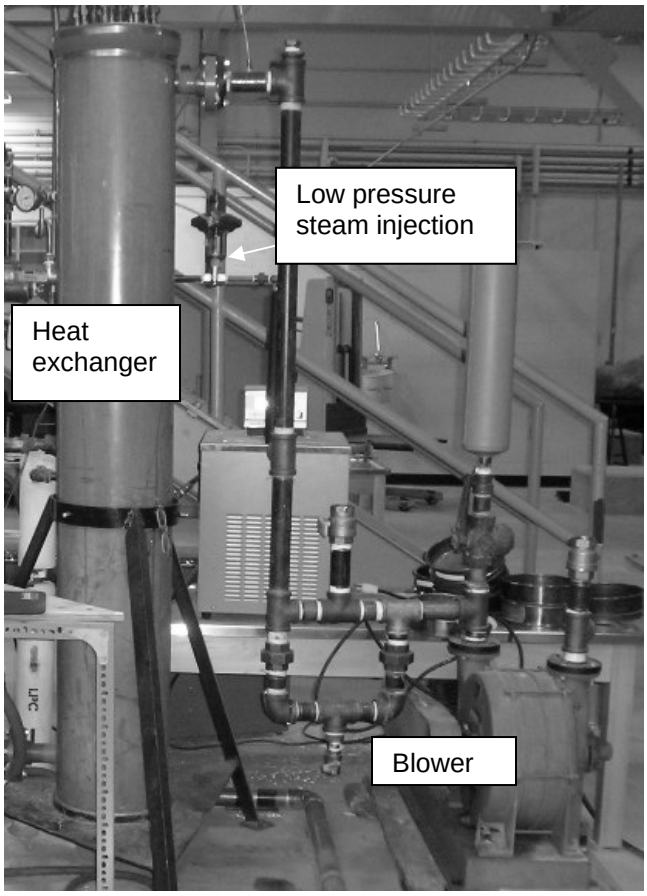

Figure 3.01 Apparatus set–up including steam injection, heat exchanger, air blower

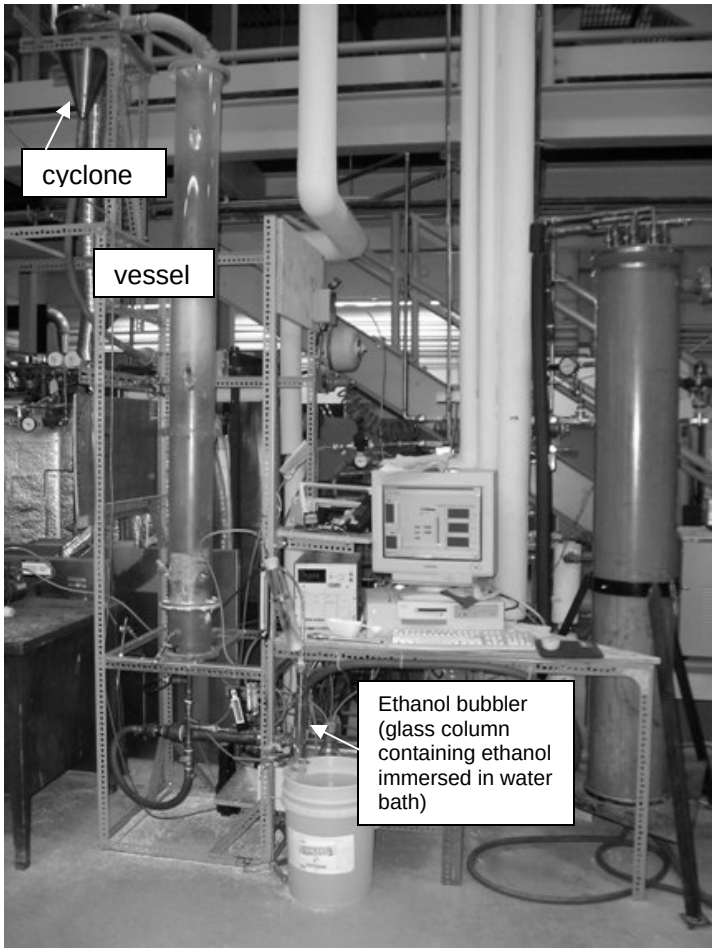

Figure 3.02 Apparatus during fluidized bioremediation experiments including vessel, cyclone, ethanol bubbler, computer for data logging.

Measurement of ethanol in gas

The experimental section reports the analysis of ethanol in samples of the inlet and outlet gas of the vessel, using a gas chromatograph. The GC calibration curve for ethanol in air was obtained with a series of standards containing a two-phase solution of ethanol in water. For each standard, 10.0 mL of solution containing a known concentration of ethanol in water was added to a 21.75 mL sample vial that was then sealed with a crimp cap containing a septum. The vials had 11.75 mL of vapour space above the liquid solution. The vials were held at room temperature to reach equilibrium. A 1.0 mL gas tight syringe was then used to withdraw 0.1 to 0.5 mL of the vapour space in the vials, via the septum. The aliquots were immediately injected into the GC. The GC peak area was then calibrated against the ethanol concentration in the vapour space. The concentration of ethanol in the vapour space was calculated from the liquid concentration of ethanol in the solution based on the Henry's law coefficient for ethanol in water (Cesario et al., 1997).

$$X_E H = P_E \tag{3.01}$$

where H for ethanol is 8.1038 x 10^{-6} atm*m^3 mol^{-1} at 25ºC. The Henry's law coefficient was also adjusted for the actual temperature of the laboratory, based on the van't Hoff equation:

$$\ln\left(\frac{1/H_{298^\circ K}}{1/H}\right) = \frac{-\Delta H_{sol}}{R}\left(1/T_{298^\circ K} - 1/T\right) \tag{3.02}$$

where -ΔH_{sol} is the standard enthalpy of solution of ethanol in water, 53,210 J mol^{-1}.

Figure A.1 (Appendix A) is an example of a GC calibration curve for ethanol concentrations in air. Table A.1 relates ethanol concentration in the liquid solution to the concentration in the vapour space for a set of calibration standards at 22 ^oC.

Adsorption isotherm

The equilibrium relationship (adsorption isotherm) between ethanol in the vapour and ethanol adsorbed on the sawdust/glass sphere packing is modelled by Equation 3.3 in this chapter. The adsorption isotherm was first determined by a static experiment. In this experiment, 3.7 g of a 26:74 vol% mixture of 71 wt% (dry basis) moist sawdust and glass spheres was added to each of seven 300 mL glass jars. Each jar was sealed with a septum and a known amount of ethanol (between 0 and 10 μL) was injected into each jar. The ethanol quickly

evaporated. The relative humidity in the laboratory was 42%. It was estimated that a portion of the moisture in the sawdust would evaporate, to create a situation of 100% relative humidity in the jar, reducing the sawdust moisture content to 67 wt%. After 96 hours, the vapour space in each jar was sampled by injecting a 1 mL gas-tight syringe into the septum and withdrawing a 1.0 mL sample. The samples were analyzed on the GC-FID. The amount of ethanol adsorbed onto the particles was calculated from the difference between the known amount of ethanol injected and the measured final concentration of ethanol in the vapour space. The final concentration of ethanol in the vapour space, and the amount of ethanol adsorbed on the particles is plotted in Figure 3.03. The experimental isotherm is fitted to Equation 3.3 using SPSS 14.0, with n=0.80 and k= 235.

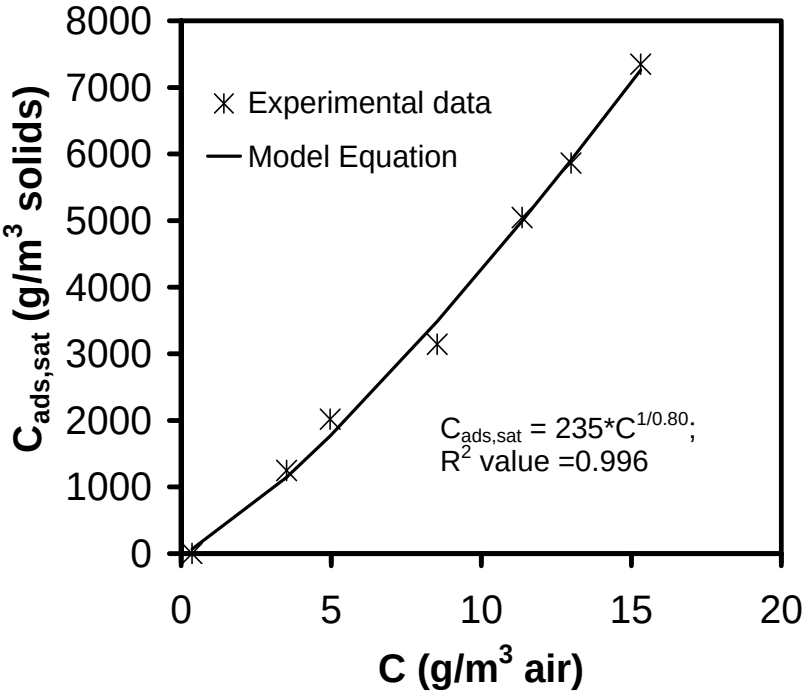

Figure 3.03 Adsorption isotherm of ethanol adsorbed on sawdust (67 wt% moisture) and glass sphere particles based on static equilibrium experiments.

The extremely small amounts of ethanol used in the glass jars of the static experiment were suspected to be a source of error. As a result, the adsorption isotherm was obtained again by a dynamic experimental method. The adsorption isotherm was determined from unsteady state mass transfer experiments by the dynamic method of frontal analysis (Lenz et al., 2002). This procedure involved the analysis of several packed bed breakthrough curves which recorded

outlet ethanol concentration versus time at 21 ºC. During these experiments, there is a net positive adsorption of ethanol onto the moist sawdust and glass sphere particles until steady state is reached, at which time $C_{out} = C_{in}$. The rate of adsorption of ethanol, N, to the particles is obtained from a mass balance across the vessel:

$$N = Q(C_{in} - C_{out}) \tag{3.03}$$

The concentration of ethanol adsorbed onto the packing at equilibrium, $C_{ads,sat}$, is found by integrating the rate of ethanol adsorption over time, and dividing by the volume occupied by the packing:

$$C_{ads,sat} = \frac{\int_{t} N dt}{V_B(1-\theta)} \tag{3.04}$$

where t is the time from the start of adsorption until $C_{out} = C_{in}$

For several packed bed trials at different inlet concentrations of ethanol, the rate of adsorption was integrated over time using Origin 6.0 software by Microcal Software, Inc. (Northampton, MA). Figure 3.04 shows the experimental adsorption isotherm (Equation 3.3) fit to experimental data using the statistical software SPSS 14.0 for Windows (SPSS Inc., Chicago, IL), where the parameters of the equation are: n=0.74 and k= 189:

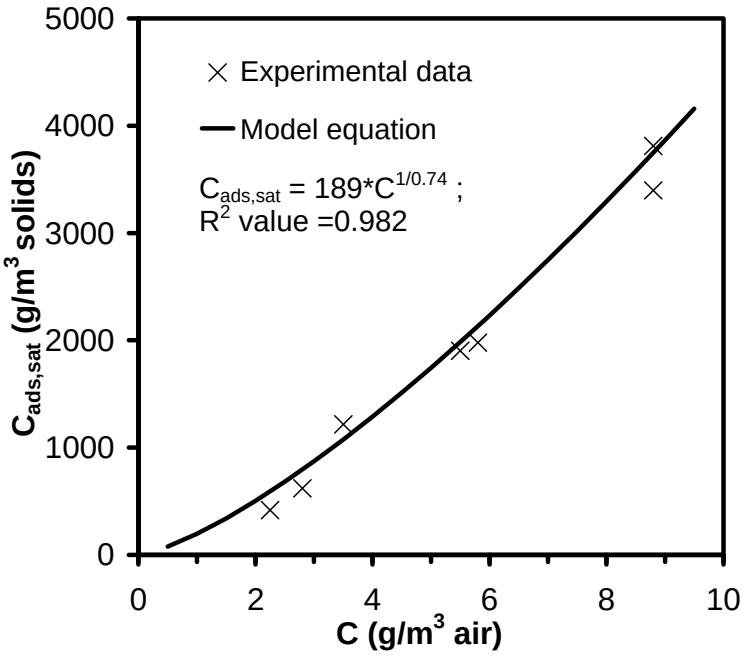

Figure 3.04 Adsorption isotherm of ethanol adsorbed on sawdust (67 wt% moisture) and glass sphere particles based on packed bed breakthrough curves, at 21 ^{o}C.

The adsorption isotherm relationship shown in Figure 3.04 agrees well with the results of the static equilibrium experiment that was conducted earlier.

Mass Transfer Coefficients

This chapter reports the bulk mass transfer coefficients of ethanol from the gas stream to the sawdust/glass sphere packing. For the packed bed cases and the fluidized bed plug flow case, mass transfer coefficients were found by comparing ethanol breakthrough experiments to values predicted from a model. The bed was modelled with non-dispersed plug flow of the gas stream, without bioremediation, using the partial differential Equations 3.1 and 3.2 in the following manuscript. A program was written in Matlab to solve these equations by a fully implicit finite difference method. The numerical method and the Matlab code are in Appendix B. For each experimental breakthrough trial (note that trials were completed at various inlet ethanol concentrations), Matlab was used to predict the breakthrough curve. For each trial, the value of the mass transfer coefficient (K) used in the Matlab program was adjusted by trial and error until the breakthrough curve predicted by the model matched the experimental breakthrough curve. At a given superficial gas velocity, the predicted values of K from the various trials were averaged, and the average value is reported in Table 3.1 in the manuscript. Figures 3.05, 3.06 and 3.07 show comparisons between experimental breakthrough curves and model-predicted breakthrough curves at certain inlet ethanol concentrations.

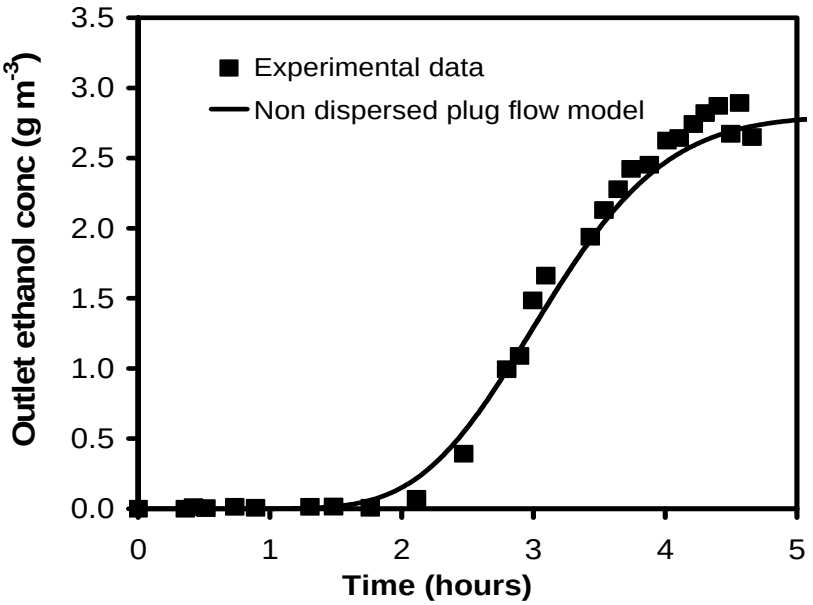

Figure 3.05 Breakthrough curve of packed bed adsorption run (superficial gas velocity = 0.0024 m s^{-1}, C_{in} = 2.9 g m^{-3}, mass transfer coefficient of model = 13 h^{-1}).

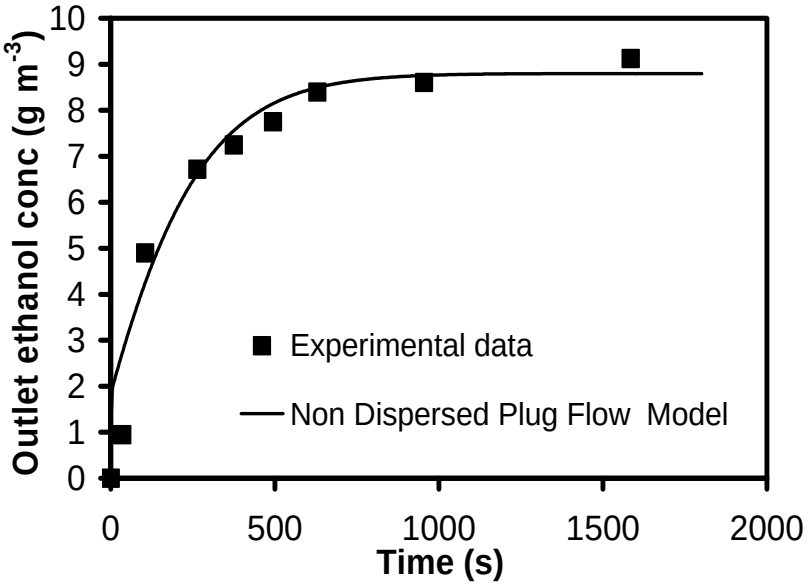

Figure 3.06 Breakthrough curve of packed bed adsorption run (superficial gas velocity = 0.16 m s^{-1}, C_{in} = 8.8 g m^{-3}, mass transfer coefficient of model = 32 h^{-1}).

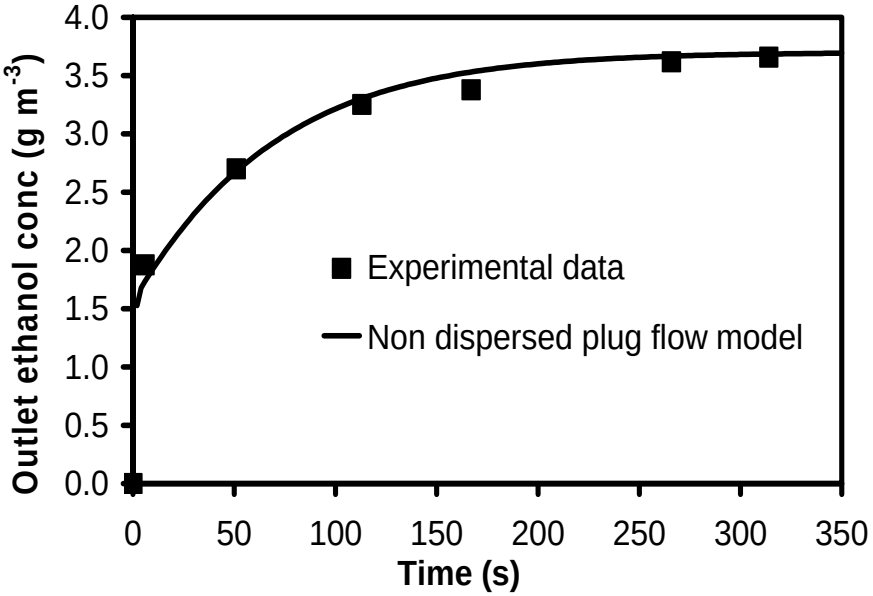

Figure 3.07 Breakthrough curve of fluidized bed adsorption run (non-dispersed plug flow model, superficial gas velocity = 0.7 m s^{-1}, C_{in} = 3.7 g m^{-3}, mass transfer coefficient of model = 81 h^{-1}).

Equation 3.4 (manuscript) was used to calculate the mass transfer coefficient for the completely mixed fluidized bed case. For each trial, $\ln(C_{in}–C)$ versus time was plotted, and K was the slope of this linear relationship. The predicted values of K from the various trials were averaged, and the average value is reported in Table 3.1 (manuscript). Figure 3.08 shows a comparison between an experimental breakthrough curve and the model-predicted breakthrough curve at C_{in} = 3.7 g m^{-3}.

Inoculation of bioreactor packing

A microbial culture was established in the bioreactor packing by first growing the bacteria species *Pseudomonas putida* in 1.0 L of nutrient solution, containing 1000 g m^{-3} of ethanol, under sterile conditions. When growth was well-established in the solution (between 24 and 48 hours), the solution was mixed with 3.1 L of dry sawdust and glass sphere packing. The packing was then added to the empty bioreactor vessel. Dry air was passed through the packing for approximately 2 hours until the moisture content of the sawdust was approximately 67 wt% (dry basis). Then saturated air (100% humidity), contaminated with ethanol, was directed through the bioreactor vessel.

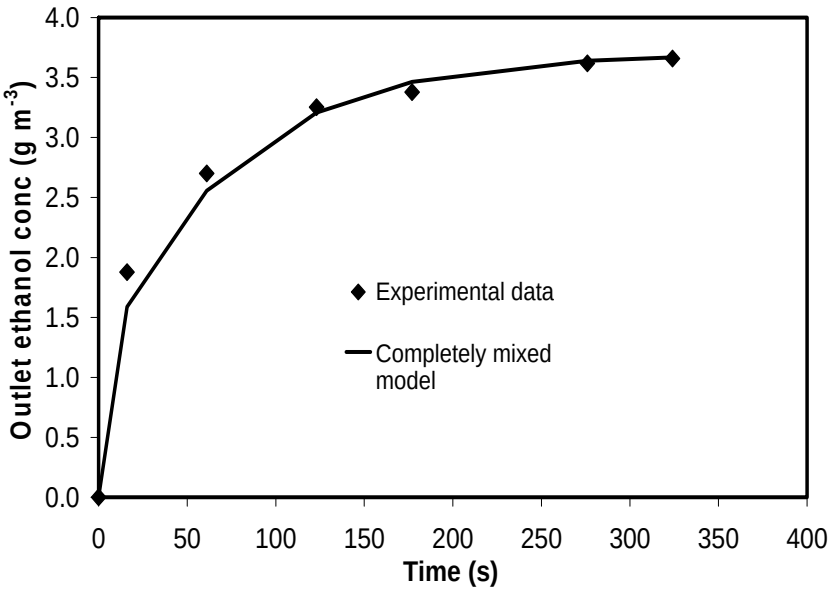

Figure 3.08 Breakthrough curve of fluidized bed adsorption run (completely mixed model, superficial gas velocity = 0.7 m s^{-1}, C_{in} = 3.7 g m^{-3}, mass transfer coefficient of model = 49 h^{-1}).

Batch shake flask experiments

The experimental section of this chapter briefly discusses the determination of biokinetic growth parameters of the predominant cell line (*Hansenula anomala).* These parameters were found using batch shake flask cultures. At various intervals over 48 hours, a 2 mL liquid sample from the batch culture was aseptically withdrawn through a syringe needle immersed in the shake flask. Ethanol and biomass concentrations in the samples were determined. Ethanol concentration was measured using the GC-FID apparatus described in the experimental section. 0.5 μL of each liquid sample was injected into the GC using an auto-sampler. The temperatures of the injector and detector were 150 ºC and 200 ºC respectively. The oven temperature was held at 40 ºC for 1.9 minutes, and then ramped up to 115 ºC at 50ºC/min. The column inlet pressure was 90 kPa gauge, and helium was used as the carrier gas at a linear velocity of 30 cm s^{-1}. The GC-FID was calibrated using a set of standard solutions containing known concentrations of ethanol in water. Figure A.2 in Appendix A is an example of a calibration curve for liquid ethanol samples. Biomass concentration in the samples was determined using an optical density technique. The optical density of the sample was measured on a spectrophotometer at a wavelength of 620 nm. The optical density was correlated to biomass concentration based on a calibration discussed in the following section.

Biomass calibration

A separate biomass calibration culture of the predominant cell line, *Hansenula anomala*, which is a yeast species, was grown in 250 mL of nutrient medium using ethanol as the only carbon source. After the exponential growth phase of the culture was completed, 100 mL of the culture was divided into four centrifuge vials. The culture was centrifuged three times for five minutes at 5000 RPM. After the first two centrifuge steps, the liquid in the vials was decanted off, 15 mL of deionised water was added to each vial, and the vials were mixed on a vortex mixer. Then the contents of every two vials were combined into a single vial, such that half the number of vials remained. After the third centrifuge step, the liquid in the final vial was decanted off, and the contents of the vial were quantitatively transferred into a pre-weighed aluminum dish using 4.0 mL of deionised water. The dish was dried in a vacuum oven at 65ºC at 22 inches Hg vacuum pressure for 24 hours. The difference between the initial and final mass of the dish was equal to the dry weight of biomass in 100 mL of culture. This mass was corrected with the dry mass of solids in 4 mL of deionised water. The biomass concentration of the culture was calculated to be 109 g dry weight/m^3.

Serial dilutions of a 1 ml sample of the biomass calibration culture were made in sterile 0.85 wt% saline solution and plated onto Difco Plate Count agar plates. After four days of growth at ambient laboratory temperature, colonies on the agar plates were counted. The concentration of cells in the calibration culture was estimated to be 5.5×10^{9} CFU/L. Based on the biomass concentration of the culture (109 g dry weight/m^3), the mass of each cell is 2.0×10^{-11} g (DW). This approximation is reasonable considering that the diameter of a typical yeast cell ranges from 5 to 10 μm. Assuming that the cell is spherical, cell density is identical to that of water and 30% of the yeast cell is dry mass, the mass of a typical yeast cell would range from 2.0×10^{-11} g (DW) to 1.6×10^{-10} g (DW).

The remainder of the 250 mL biomass calibration culture (biomass concentration of 109 g DW/m^3) was used to make various dilutions in nutrient medium. The optical density of each dilution was measured on the spectrophotometer at a wavelength of 620 nm. The biomass concentration of the dilutions was plotted against optical density readings to serve as the biomass calibration curve, as shown in Figure A.10 (Appendix A).

Biokinetic growth parameters

Biokinetic parameters were determined from the batch shake flask cultures. Yield, Y_{xs}, is calculated from Equation 1.13. The remaining biokinetic parameters were determined by a best fit of the experimental growth data to a Monod growth model (Equations 1.8 and 1.10) and the Haldane growth model (Equations 1.9 and 1.11). These differential equations were solved numerically with a fourth order Runge-Kutta method. Then K_s, K_I, and μ_m are adjusted with a forward derivative, Newton method in the software Microsoft Excel, while using a sum of least squares method to fit the experimental data to the Monod and Haldane growth models. The growth parameters are summarized in Table 3.01, and Figures 3.09 and 3.010 compare the experimental data to the Monod and Haldane models respectively. The standard error of the estimate for biomass growth is +/-7.6 g m^{-3} and +/-12.2 g m^{-3} for the Monod and Haldane models respectively, using the parameters in Table 3.01.

Table 3.01 Biokinetic growth parameters.

Kinetic Parameter	Monod model	Haldane model
X_o (g m^{-3})	30	30
S_o (g m^{-3})	250	250
μ_m (h^{-1})	0.065	0.147
K_s (g m^{-3})	0.5	1.33
K_I (g m^{-3})	N/A	115
Y_{xs}	0.48	0.48

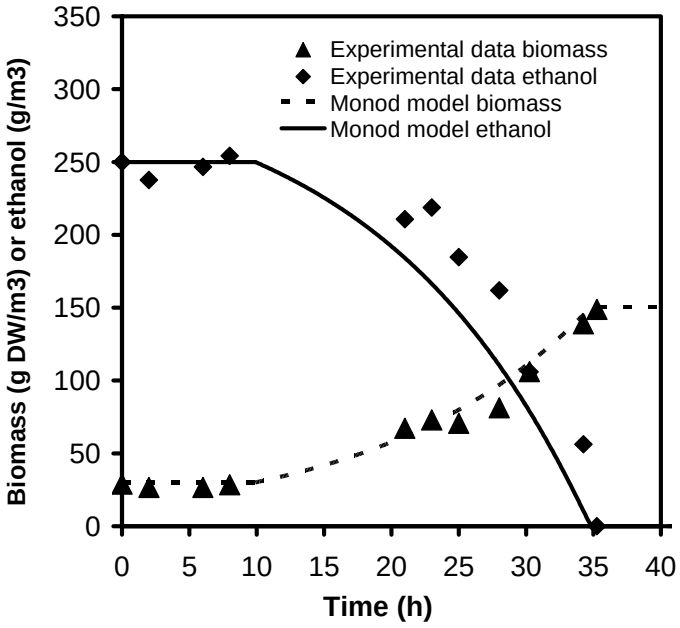

Figure 3.09 Comparison of experimental growth curve and substrate consumption to Monod model.

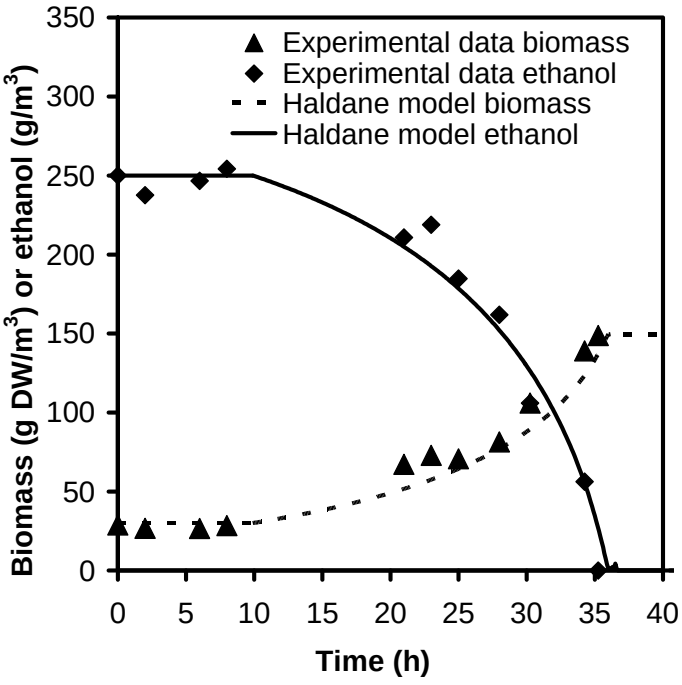

Figure 3.010 Comparison of experimental growth curve and substrate consumption to Haldane model.

Manuscript

3.1 Abstract

A gas-solid fluidized bed bioreactor has been successfully used for the bioremediation of ethanol (a model volatile organic compound, VOC) contaminated air. A key objective of this fluidized bioreactor study was to compare the performance of fluid bed operation to packed bed operation. A fluid bed system increased homogeneity and improved upon operating problems such as plugging and channelling normally associated with packed bed bioreactors. The bioreactor bed was comprised of a mixture of moist sawdust particles and glass spheres. Depending on the superficial velocity of the waste gas stream, the bioreactor could be operated in either packed or fluidized mode. During fluid bed operation, the sawdust and glass sphere mixture was maintained in a bubbling/slugging regime. As expected, fluid bed operation demonstrated significantly higher mass transfer rates but the maximum elimination capacity was 75 g m^{-3} sawdust h^{-1} as compared to 225 g m^{-3}sawdust h^{-1} for packed bed operation. In packed bed mode, higher ethanol concentrations were used in order to have comparable ethanol loadings and this may have contributed to faster growth rates and thus faster bioremediation rates.

3.2 Introduction

Emissions of volatile organic compounds (VOCs) can be harmful to human health and the environment. To mitigate these harmful effects, VOC emissions from point sources such as storage vessels or building ventilation ducting can be captured for treatment. Biological techniques can be highly effective for the treatment of VOC emissions, particularly for waste gas emissions with high volumetric rates and low contaminant concentrations (Le Cloirec et al., 2001). Biotreatment is often less expensive than physical and chemical treatment methods which include incineration, adsorption and scrubbing (Groenestijn and Kraakman, 2005). In addition, biotreatment processes offer superior environmental performance because they typically produce innocuous waste streams.

VOC emissions may include contaminants that are both soluble and insoluble in water. Biotrickling filters involve a continuous, recirculating stream of liquid that flows over packed bed media; these filters are very effective for treating waste gases that are water soluble and transfer easily from the waste gas to the liquid stream (Kennes and Thalasso, 1998). An external-loop airlift bioreactor was shown to be effective at treating the hydrophilic compounds ethanol and p-cresol (Wei et al., 1999). For treating air contaminated with both soluble and insoluble substances, biofilters (packed beds where microorganisms coat the packing) are already used in several industrial situations. Biofilters are normally designed to treat superficial gas velocities from 0.014 to 0.042 m s^{-1}, with contaminant concentrations less than 5 g m^{-3} (Le Cloirec et al., 2001). Le Cloirec et al. (2001) investigated a biofilter of moist wood chips to treat 0.06 to 1.3 g m^{-3} ethanol in air. They reported a decrease in biofilter performance with decreasing residence time of the polluted air. At a superficial gas velocity of 0.06 m s^{-1}, the removal efficiency was 98% at an ethanol loading of 143 g m^{-3} h^{-1}, while at 0.43 m s^{-1} the removal efficiency was 98% but the loading was limited to 101 g m^{-3} h^{-1}. Removal efficiency is defined as the difference between the inlet and outlet concentration as a percentage of the inlet concentration, and ethanol loading is calculated as the ethanol feed rate per packing bed volume of wood chips in the bioreactor.

Although biofilters have been used to treat waste gases, they have several operating problems. In particular, it is difficult to maintain uniform humidity, pH and cell growth across the bed, resulting in gas channelling and lower biodegradation efficiencies (Leslous et al., 2004a). A fluidized bed bioreactor may overcome the difficulties associated with biofilters. In gas-solid fluidized bioreactors, microorganisms are immobilized on solid particles and fluidized with a gas stream. The advantages of fluidization include homogeneous conditions in the bed due to the rapid and uniform mixing of particles and high rates of heat and mass transfer between the fluid and the particles (Kunii and Levenspiel, 1991).

There have been only two prior studies on the use of gas-fluidized bed bioreactors to treat contaminated air. The most comprehensive is that of Wright and Raper (1998) who used a three-phase spouted bed to treat ammonia-contaminated air. A spouted bed consists of particles which are larger than those used in traditional fluidized beds, so the particles are continuously spouted up the centre of the bed (Kunii and Levenspiel, 1991). A constant stream of mineral solution was directed onto the bed, and the liquid caused high wall adhesion and aggregation of particles

which interfered with spouting characteristics. The spouted bed achieved removal efficiencies from 0 to 40%, treating ammonia loadings of 500 to 650 g m^{-3} h^{-1}. The performance of the spouted bed exceeded that of a packed bed (Wright and Raper, 1998).

Leslous et al. (2004a and 2004b) carried out a detailed study of potential packing material for a fluidized bioreactor. The emphasis was on the fluidized characteristics of the materials. In the final paragraph of their conclusions section, Leslous et al. (2004a) report results from the biotreatment of ethanol-contaminated air in a fluidized bed bioreactor containing moist scrap wood particles to be 100% removal efficiencies for ethanol loadings less than 200 g m^{-3} h^{-1} and 80% for an ethanol loading of 1150 g m^{-3} h^{-1}. However no data or experimental details to support this conclusion was presented in the body of the paper.

The above-mentioned studies suggest that fluidized bed bioreactors show promise as an alternative for the treatment of VOC contaminated air. However, there is a limited amount of knowledge on the topic and further research is clearly needed. In the present study, we report on the development of a gas-solid fluidized bioreactor for the biotreatment of VOCs. The bioreactor packing consists of a binary mixture of moist sawdust and glass spheres, and ethanol was used as a candidate VOC. Previous studies of biotreatment of contaminated air found that moist biomass particles are difficult to fluidize because the particles tend to agglomerate (Wright and Raper, 1998; Leslous et al., 2004b). This problem has recently been overcome by mixing glass spheres with biomass (Clarke et al., 2005). While Leslous (2004a, 2004b) investigated only a fluidized bioreactor for treating contaminated air, this study compares fluidized bed performance to that of a packed bed (a biofilter).

3.3 Experimental

3.3.1 Apparatus

An acrylic, cylindrical, bench-scale bioreactor with an inside diameter of 0.14 m was used for this study (Figure 3.1). Further details of the vessel are described in Clarke et al. (2005). At superficial gas velocities greater than 0.0024 m s^{-1}, ambient air was supplied with a blower and the air was saturated by the injection of low pressure steam. Based on the measured

air humidity into the bioreactor bed, the steam flowrate was controlled by an automatic control valve which had a PI controller programmed in the instrumentation software LabVIEW™ (National Instruments, Austin, TX). The controller was set to maintain the humidity of the inlet air to the bioreactor at 100%. Air velocity was measured using an orifice plate. The inlet air was cooled to 20 to 25ºC with cooling water in a heat exchanger, such that the inlet air was maintained warmer than the ambient air. At a gas velocity of 0.0024 m s^{-1}, compressed laboratory air was used, and the air was humidified in two bubblers containing deionised water. The flowrate of air to the bubblers was metered with a rotameter. At all air flowrates, humidity and temperature of the inlet air were measured with a HMP 230 series probe by Vaisala (Helsinki, Finland). Ethanol contamination was introduced by directing a slip stream of the inlet air into an ethanol bubbler. The inlet air flowrate to the bubbler was metered using a rotameter.

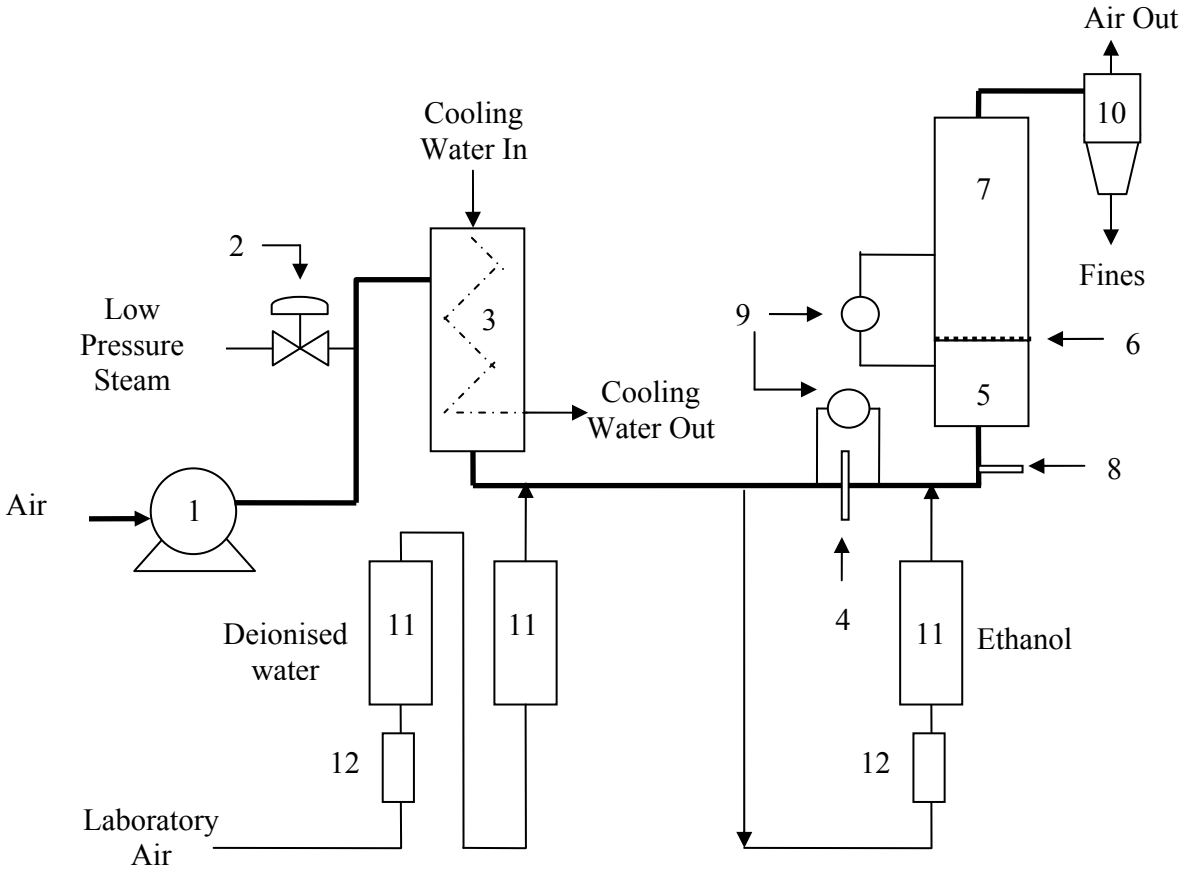

Figure 3.1 Experimental apparatus: (1) blower; (2) steam control valve; (3) heat exchanger; (4) orifice plate; (5) wind-box; (6) distributor and wire screen; (7) bioreactor; (8) humidity and temperature probe; (9) differential pressure transducers; (10) cyclone; (11) bubbler; (12) rotameter.

3.3.2 Analysis

Ethanol concentrations in the gas stream entering and exiting the bioreactor were determined using a Hewlett Packard 5890 series (Agilent Technologies, Palo Alto, CA) gas chromatograph fitted with a flame ionization detector and a Supelco (Bellefonte, PA) non-polar PTE-5^{TM} column. The injector and detector temperatures were 200 ºC, oven temperature was held at 40 ºC, column inlet pressure was 90 kPa, and helium was used as the carrier gas at a linear velocity of 30 cm s^{-1}. Samples were collected in glass sampling bulbs from ports on the bioreactor vessel, using vacuum to draw the contaminated air into the bulbs. A gas-tight syringe was used to withdraw 0.1 to 0.5 mL sub-samples from the bulbs which were manually injected into the GC. Reproducibility experiments were conducted to measure variation between sub-samples from three different sampling bulbs, as well as variation in the inlet ethanol loading to the bioreactor. The standard deviation between sub samples was less than eight percent of the average concentration of the sampling bulb. Ten samples were collected from the bioreactor inlet at steady state conditions, and the standard deviation of the samples was less than five percent of the average inlet concentration. Moisture content in the sawdust was measured with a Mettler Toledo (Columbus, OH) HB43 halogen moisture analyzer.

3.3.3 Particles

The bioreactor bed material consisted of 26 vol.% moist sawdust and 74 vol.% glass spheres. Sawdust with a Sauter mean diameter of 0.625 mm was produced by grinding waste spruce wood from the NorSask Forest Products Ltd. sawmill (Meadow Lake, SK, Canada). The sawdust was sieved in Tyler Series sieves, and particles between 0.354 and 1.00 mm were retained for this study. The moisture content of the sawdust was adjusted between 67 and 233 wt% (dry basis). A-070 specification, solid glass spheres, Sauter mean diameter of 0.516 mm, were obtained from Potters Canada (Moose Jaw, SK, Canada). A more detailed particle characterization is presented elsewhere (Clarke et al., 2005). Also, in previous work (Clarke et al., 2005), the fluidization behaviour, extent of mixing, and minimum fluidization velocity of mixtures of moist sawdust and glass spheres were studied. At conditions used in the current work, no segregation was observed between the sawdust particles and glass spheres. Bed

pressure drop profiles were obtained for sawdust (67 wt% moisture) and sphere mixtures, in order to determine fluidization regimes in the bed. The pressure profiles were measured in beds with heights of 14 cm, at increasing velocity, by the method described in Clarke et al. (2005).

3.3.4 Mass transfer

Transient mass transfer experiments were conducted in the bioreactor vessel in the absence of biodegradation, with fresh glass sphere and sawdust particles (67 wt% moisture) which were initially free of ethanol. Ethanol was introduced into the inlet air at time zero. Ethanol breakthrough curves were obtained for a packed and fluidized bed by measuring inlet and outlet concentrations of ethanol until steady state was reached. Superficial gas velocities were 0.0024 and 0.155 m s^{-1} in the packed bed trials and 0.7 m s^{-1} in the fluidized bed trials.

3.3.5 Bioremediation

The packing was inoculated with an active culture of *Pseudomonas putida* ATCC 23973 bacteria which can consume ethanol as its sole carbon source. Total packed bed volume was 3.1 L, resulting in a packed bed height of 20 cm. Ethanol-contaminated air was continuously fed into the vessel. Conditions in the system were not sterile, and after 30 days a mixed culture of microorganisms developed that could thrive on ethanol. Thus, at an industrial scale this process would not require costly sterilization equipment. A nutrient solution was periodically mixed into the packing in 50 to 125 mL batch additions every two to four days. The nutrient solution consisted of 0.84 g KH_2PO_4, 0.75 g K_2HPO_4 , 0.50 g $(NH_4)_2SO_4$, 0.06 g NaCl, 0.06 g $CaCl_2$, 0.06 g $MgSO_4$, 0.02g $Fe(NH_4)_2(SO_4)_2*6H_2O$, and 1 mL of trace mineral solution (per litre of deionized water: 0.20 g $ZnSO_4*7H_2O$, 0.06 g $MnCl_2*4H_2O$, 0.60 g H_3BO_3, 0.40 g $CoCl_2*6H_2O$, 0.02 g $CuCl_2*2H_2O$, 0.04 g $NiCl_2*6H_2O$, and 0.06 g $Na_2MoO_4*2H_2O$) in 1 litre deionized water. In industrial practice this nutrient solution could be replaced with low-cost, commercial fertilizer in liquid solution. Biodegradation was measured in packed bed experiments at various sawdust moisture contents, inlet ethanol concentrations, and superficial gas velocities. After four weeks of packed bed bioremediation, the two most abundant microbial species in the bed material were characterized by the EPCOR Water Laboratory (Edmonton, AB.), using the MIDI, Inc. (Newark,

DE) Sherlock microbial identification system, as *Hansenula anomala* and *Rhodotorula rubra*. The Sherlock system uses gas chromatographic analysis of cellular fatty acid methyl esters. These cell lines had overtaken *Pseudomonas putida* inocula in terms of cell count.

Biodegradation was then measured in fluidized bed trials at various ethanol concentrations with a superficial velocity of 0.7 m s^{-1} and sawdust moisture content of 67%. For both the packed and fluidized bed experiments, the bioreactor was allowed to reach steady state before biodegradation data was recorded. The bed was operated either in a packed or fluidized bed state continuously for seven months. A JEOL 840A scanning electron microscope (Tokyo, Japan) was used to observe sawdust which was not used in the bioreactor, and sawdust and glass spheres from the bioreactor. The particles were fixed in buffered glutaraldehyde prior to SEM measurements according to the procedure of Klainer and Betsch, 1970.

The pH of the cell packing was measured by mixing 4 g of packing in 20 mL of deionised water, and found to be slightly acidic at 5.7. Microbial cell counts in the bed material were determined every week during packed and fluidized bioremediation. Approximately 1 g of bed particles were sampled from close to the middle of the bed using a sample scoop. The sample was mixed with 10 mL of sterile 0.85% saline solution in a vortex mixer for 30 seconds. Then serial dilutions were plated onto Difco plate count agar. Total colony forming units per gram of material were determined after four days of growth. During bioremediation experiments, the cell concentration in the bioreactor ranged between 63 and 420 million cells/g dry sawdust. The total mass of moist packing in the bioreactor was approximately 3500 g. Over the course of the bioremediation experiment, approximately 30 g of packing was removed from the bioreactor for cell concentration analysis, accounting for less than 1% of the total packing mass.

Biokinetic parameters of the most dominant cell line were estimated from a batch, shake flask culture. The predominant cell line (*Hansenula anomala*) was removed from an agar plate and used to make an inoculant culture. A 4 mL aliquot of inoculant culture was added to a shake flask containing 250 g m^{-3} of ethanol in 125 mL of nutrient medium. For 48 hours, the mass concentration of cells (biomass) was determined by measuring optical density with a Shimadzu (Kyoto, Japan) UV-Vis Mini 1240 spectrophotometer at 620 nm, and ethanol concentrations in the solution were measured by gas chromatograph. From the batch growth curve, the maximum microbial growth rate was calculated to be 0.065 h^{-1} and biomass yield was 0.48 g dry weight biomass/g of ethanol.

3.4 Results and Discussion

3.4.1 Fluidization

Bed pressure drop profiles of two different compositions of sawdust and spheres are presented in Figure 3.2. At minimum fluidization there is the formation of a plug causing a peak in the pressure drop, which is followed by a decrease in pressure drop due to channelling. At higher gas velocities, this channelling gives way to a regime of bubbling/slugging fluidization that was deemed acceptable for these experiments. The slugging action causes particles to fly upwards and to settle down through the bed in a step-wise motion. Note that in fluidization pressure drop is 7.7 kPa/m bed, contributing to higher air compression costs than for a packed bed.

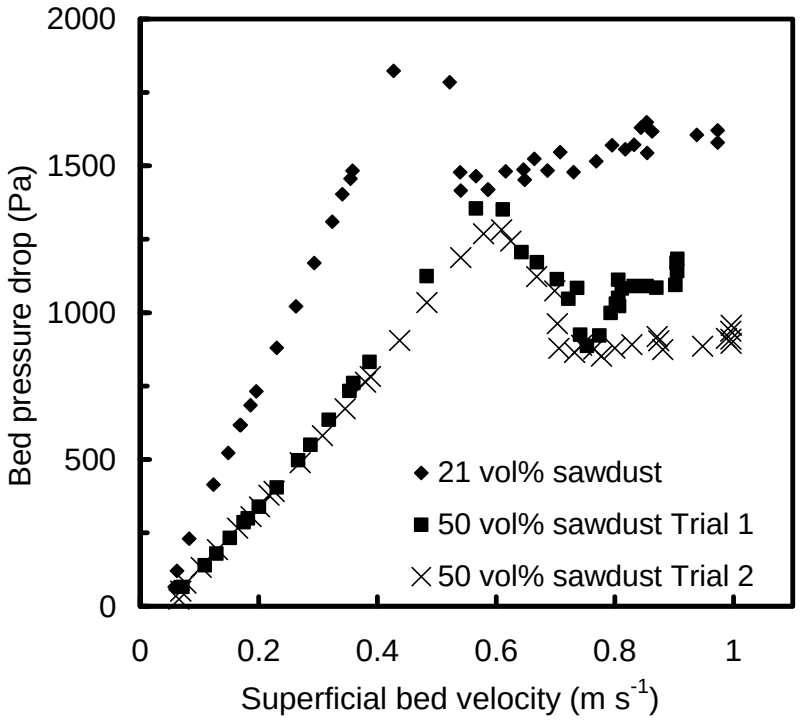

Figure 3.2 Pressure profiles of mixtures of glass spheres and sawdust at increasing gas velocity (sawdust moisture = 67 to 75 wt%).

3.4.2 Mass Transfer

Breakthrough curves obtained from mass transfer experiments on the packed and fluidized beds are shown in Figures 3.3 and 3.4. The bulk mass transfer coefficients determined from these experiments are summarized in Table 3.1. The mass transfer coefficient for the packed bed is calculated by modelling the gas phase as non-dispersed plug flow without bioremediation by the method in Hodge and Devinny (1997). The unsteady state mass balance of the ethanol in the gas phase in the vessel is described by the partial differential equations:

$$\frac{\partial C}{\partial t} = -V\frac{\partial C}{\partial z} - \left(\frac{1-\theta}{\theta}\right)\left[K\left(C_{ads,sat} - C_{ads}\right)\right] \tag{3.1}$$

and:

$$\frac{\partial C_{ads}}{\partial t} = K\left(C_{ads,sat} - C_{ads}\right) \tag{3.2}$$

In Equations 3.1 and 3.2, mass transfer between the gas phase and the moist sawdust and glass sphere packing is approximated with a linear driving force model, with a bulk mass transfer coefficient K. The saturation concentration of ethanol adsorbed in the solid at equilibrium, $C_{ads,sat}$, is a function of the gas phase ethanol concentration, and it is modelled by:

$$C_{ads,sat} = kC^{1/n} \tag{3.3}$$

$C_{ads,sat}$ is determined from the experimental breakthrough curves. The difference between the inlet and outlet flowrate of ethanol in the gas phase is integrated over time and divided by the volume occupied by the packing to obtain $C_{ads,sat}$. Then $C_{ads,sat}$ is plotted versus gas phase ethanol concentration C, for various mass transfer experiments, to find k and n. An implicit finite difference numerical method was used to solve Equations 3.1 and 3.2. The value of K was varied by trial and error until the predicted breakthrough curve matched the experimental breakthrough curve by the minimization of the sum of least squares method.

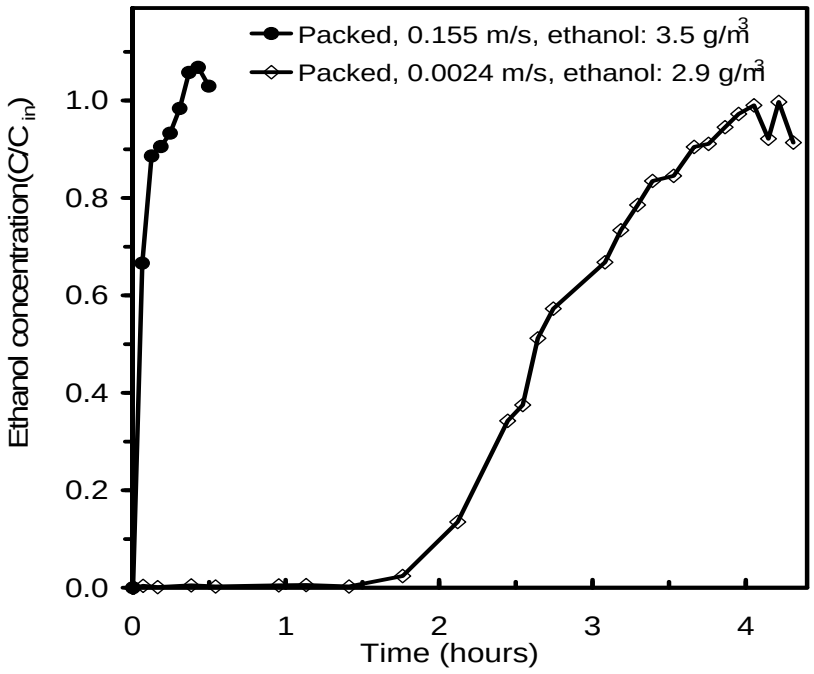

Figure 3.3 Breakthrough curves in packed beds (sawdust moisture 67 wt%).

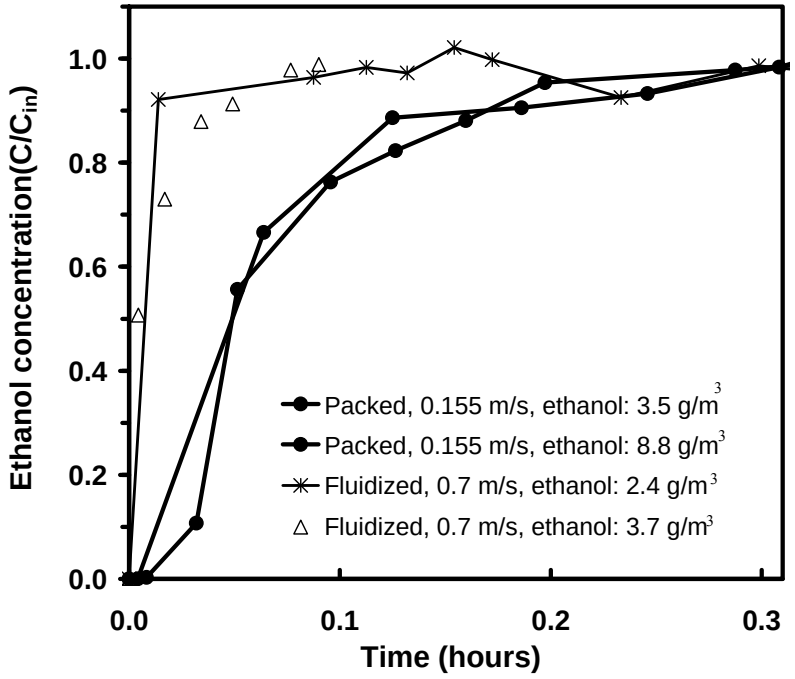

Figure 3.4 Breakthrough curves in fluidized and packed beds (sawdust moisture 67 wt%).

Table 3.1 Ethanol mass transfer from gas stream to particles in packed and fluidized beds.

Bioreactor	Superficial gas velocity (m s^{-1})	Mass transfer coefficient, K (h^{-1})
Packed	0.0024	13
Packed	0.155	32
Fluidized	0.70	81 (plug flow); 49 (mixed)

Two values are presented for the mass transfer coefficient in the fluidized bed, corresponding to the two ideal limits of non-dispersed plug flow (Hodge and Devinny, 1997) and perfect mixing of the gas (de Lasa et al., 1981). For perfect mixing of the gas, the convection term in Equation 3.1 is eliminated, and the mass flux of ethanol into the solids is equal to the mass flux from the gas phase:

$$\frac{\partial C_{ads}}{\partial t} = K\left(C_{ads,sat} - C_{ads}\right) = \left(\frac{\theta}{1-\theta}\right)K\left(C_{in} - C\right) \tag{3.4}$$

Equation 3.4 can be integrated directly. K is then determined from the experimental mass transfer data of concentration versus time. However, regardless of the hydrodynamic model, the mass transfer coefficient is significantly higher for the fluidized bed compared to the packed bed.

It is observed that the mass transfer coefficient increases with velocity in a packed bed, and is highest in a fluidized bed. Note that these experiments were conducted without biodegradation. Thus resistance across the gas and moist particle interface controls the mass transfer coefficient. The observation that the mass transfer coefficient increases with gas velocity is consistent with the Ranz correlation for mass transfer coefficient in a gas-solid fixed bed (Kunii and Levenspiel, 1991):

$$Sh = 2 + 1.8\left(\mathrm{Re}\right)^{1/2} Sc^{1/3} \tag{3.5}$$

Applying Equation 3.5, the mass transfer coefficient of the 0.7 m s^{-1} fluidized bed would be 2.1 times higher than that of the 0.155 m s^{-1} packed bed. This agrees with the information in Table 3.1 and falls in the middle of the plug flow and perfectly mixed models for the fluidized bed.

3.4.3 Bioremediation

The bioreactor with a mixed culture of microorganisms was successfully operated in both a fluidized and packed bed mode to treat ethanol-contaminated air. The sawdust and glass sphere mixture exhibited adequate fluidization at sawdust moisture contents of 67 to 75 wt% (dry basis) or less, and fluidization performance was poor at increasing moisture contents (Clarke et al., 2005). Packed bed bioremediation trials were conducted at several sawdust moisture contents to test whether a moisture content of 67 wt% reduced biodegradation performance. Figure 3.5 presents packed bed biodegradation at varying sawdust moisture concentrations, at a superficial gas velocity of 0.0024 m s^{-1}. Each data point represents the ethanol removal efficiency of the bioreactor in a steady state experiment at constant inlet ethanol concentration. Figure 3.5 illustrates that biodegradation is independent of sawdust moisture for the moisture range studied (67 to 233 wt%, dry basis). Therefore, a sawdust moisture content of 67 wt% was used in the remaining experiments, as it could be fluidized well. Although moisture is required for biodegradation, increasing sawdust moisture above 67 wt% in packed bed operation does not affect the biodegradation efficiency or capacity.

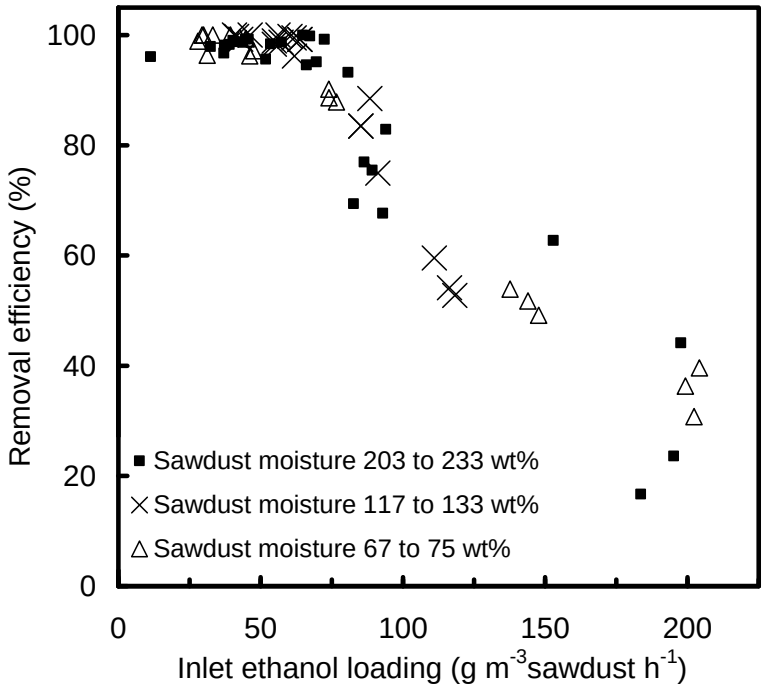

Figure 3.5 Effect of moisture on removal efficiency in a packed bed bioreactor (gas velocity =0.0024 m s^{-1}).

In the present study, ethanol loadings for both the packed and fluidized beds are reported in terms of packed bed volume of sawdust packing because the glass spheres contain very little microbial culture. However, the loading based on sawdust packed bed volume can be readily converted to a loading based on total packed bed volume by multiplying with a factor of 0.26. Figure 3.6 presents scanning electron microscope images of sawdust which was not used in the bioreactor, and sawdust and spheres which were removed from the bioreactor. There is a significant change in the microstructure of the sawdust surface after it was used for bioremediation. There are no microorganisms observed on the glass bead surface, suggesting that microbial growth primarily occurs on the sawdust.

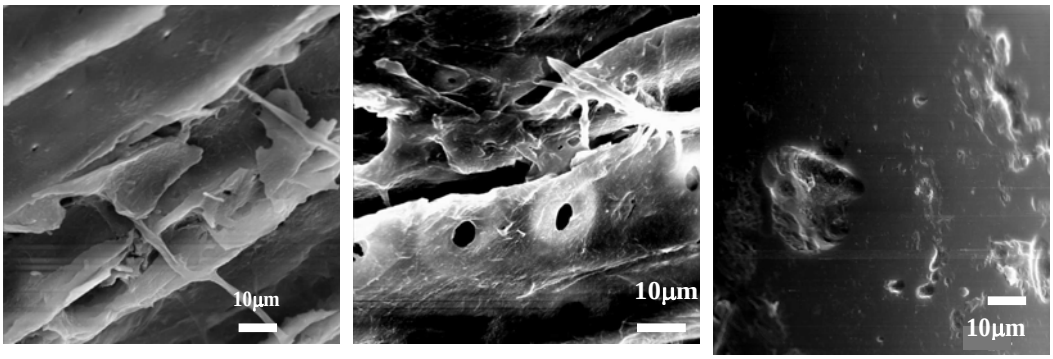

Figure 3.6 Scanning Electron microscope images a) Sawdust b) Sawdust from bioreactor c) Glass spheres from bioreactor.

Figure 3.7 illustrates the effect of superficial gas velocity on bioremediation in a packed bed. The results are shown in terms of elimination capacity (EC), which is defined for both the packed and fluidized bed modes as the mass of ethanol consumed per packed bed volume of sawdust per unit time. Note that during fluidization, interparticle space increases and as a result the volume of packing increases. For 100% removal efficiency, the elimination capacity is equal to the inlet ethanol loading. Hence, 100% removal efficiency can be represented by the straight line in Figure 3.7. EC reaches a maximum value of 225 g m^{-3}sawdust h^{-1} at velocities of 0.155 and 0.25 m s^{-1}, while the maximum is only 73 g m^{-3}sawdust h^{-1} at 0.0024 m s^{-1}.

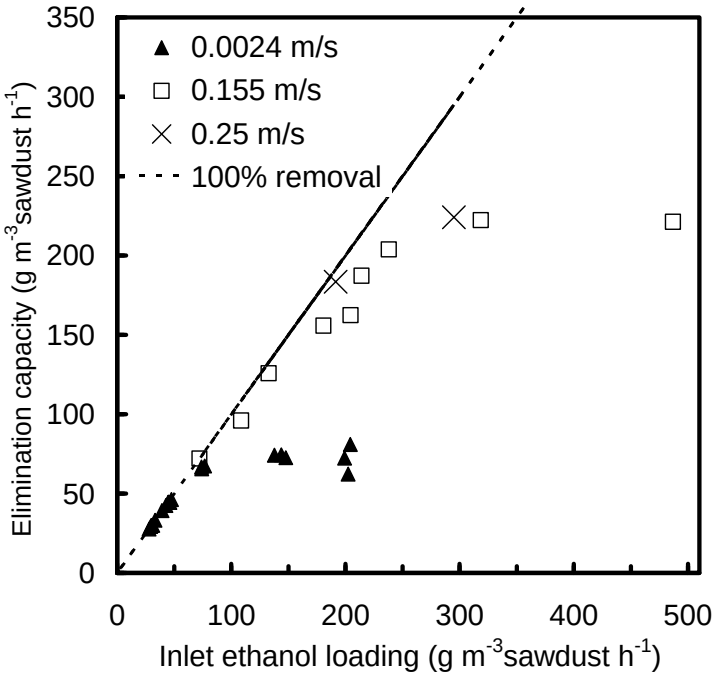

Figure 3.7 Effect of superficial gas velocity on EC in a packed bed (sawdust moisture = 67 wt%).

Biodegradation in the fluidized bed bioreactor is shown in Figure 3.8 where it is observed that the fluidized bed performance is comparable to that of the packed bed operated at the lowest velocity, 0.0024 m s^{-1}. The maximum EC for the fluidized bed is approximately 75 g m^{-3}sawdust h^{-1}. Over several months of operation, the sawdust particles appeared to age, as they changed color from white to dark brown. However, in spite of this color change, reproducibility experiments taken at different times demonstrated similar biodegradation performance. In addition, the fluidized bed remained well mixed during operation. Due to the high level of mixing, the fluidized bed did not exhibit plugging or uneven conditions which often occur in packed bed bioreactors.

In Figures 3.5, 3.7 and 3.8 it is observed that removal efficiency is greater than 95% at ethanol loadings up to maximum elimination capacity, after which removal efficiency steadily decreases. As loading to biofilters (packed beds) increases from zero, the removal efficiency is greater than 95%, until EC reaches a maximum (Deshusses and Johnson, 2000), and at higher loadings EC may decline (Delhoménie and Heitz, 2003). The shape of the EC curve is due to a shift in the overall rate-limiting mechanism. Delhoménie and Heitz (2003) and Ottengraf et al. (1986) suggest that below the maximum EC, diffusion in the biolayer limits the overall

biodegradation rate, and at loadings above the maximum EC, microbial growth kinetics are limiting. Therefore, although the mass transfer coefficient is higher in the fluidized bioreactor than the packed bed, it is of no value for bioremediation purposes once the overall rate in the bioreactor is controlled by the kinetics of growth.

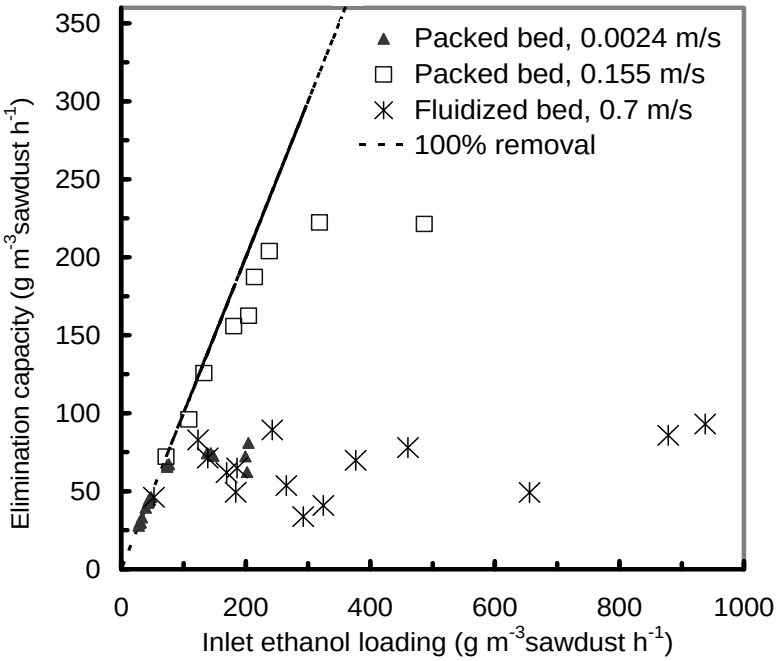

Figure 3.8 Effect of inlet ethanol loading on EC in a fluidized versus packed bed bioreactor (sawdust moisture = 67 wt%).

Deshusses and Johnson (2000) propose that biofilter performance generally depends on contaminant loading and not concentration, such that the EC curves will be the same for different combinations of inlet gas velocity and concentration. This explanation implies that growth kinetics are zero order with respect to the substrate concentration. However, (Deshusses and Johnson, 2000) also note that bioremediation performance may become dependent on both contaminant loading and concentration when the substrate concentration in the gas phase is very low (below 0.01 to 0.05 g/m^3) for contaminants with high Henry's law coefficients. In these cases, growth will be first order with respect to the substrate. In our case, because ethanol concentrations were low (less than 0.05 g m^{-3} in the gas phase) in both the fluidized and high velocity packed bed (superficial gas velocity 0.155 m s^{-1}) bioremediation trials, the kinetics were likely first order with respect to ethanol concentration. Since the high velocity packed bed was

operated at higher ethanol concentrations than the fluidized bed, the packed bed would have a greater microbial growth rate. Furthermore, if maximum elimination capacity is determined by microbial growth rate, maximum EC will be higher in the high velocity packed bed than the fluidized bed. Even if microbial kinetics were first order in the fluidized bed and zero order in the high velocity packed bed, the high velocity packed bed would again be operating at a higher microbial growth rate because ethanol concentrations were higher in the packed bed.

An additional explanation for the lower performance of the fluidized versus packed bed is that there may be fewer microbial cells available in a fluidized bed. The fluidization motion may reduce the steady state concentration of cells on the packing. The growth rate, and the overall biodegradation rate would be reduced at lower cell populations.

In the low velocity (0.0024 m s^{-1}) packed bed biodegradation trials, inlet ethanol was as high as 1.2 g m^{-3} in the gas phase. Growth kinetics were likely zero order with respect to ethanol concentration. Figure 3.7 shows that the maximum EC of the low velocity packed bed was much lower than that of the high velocity bed. Possibly, a process other than microbial kinetics limits the maximum EC of the low velocity bed. Kim and Deshusses (2005) propose that above the maximum EC of a biotrickling filter, biodegradation is limited by microbial growth kinetics, transport in the liquid, or diffusion in the biolayer. In addition, mass transfer of oxygen to the biomass was not measured. In the low velocity packed bed, the low mass transfer coefficient for ethanol from the gas phase to the particles suggests that the oxygen mass transfer coefficient may also be low. While ethanol mass transfer would increase with increased ethanol loading, oxygen mass transfer would not. As a result, oxygen mass transfer would limit the maximum EC of the low velocity packed bed. Another possible explanation is that in the low velocity packed bed, the gas stream may channel and bypass sections of the bed, a well-known phenomenon in packed beds operated at low velocities. As a result, a smaller portion of the microorganisms will come into contact with the contaminants, resulting in reduced microbial growth. Thus biodegradation rate and maximum EC are lower in the low velocity bed.

Table 3.2 summarizes the experimental results with the packed and fluidized bed bioreactors, with comparison to other packed bed (biofilter) studies.

Table 3.2 Maximum elimination capacity of fluidized and packed bed bioreactors.

Bioreactor	Bed Particles	Superficial gas velocity (m s^{-1})	Maximum elimination capacity (g m^{-3} h^{-1})
Packed bed current research	Sawdust & glass spheres	0.0024	73 based on sawdust 19 total bed volume
Packed bed current research	Sawdust & glass spheres	0.155	225 sawdust 59 total
Fluidized bed current research	Sawdust & glass spheres	0.70	75 sawdust 20 total
Packed bed (Le Cloirec et al., 2001)	Wood chips	0.06	227 total [a]
Packed bed (Le Cloirec et al., 2001)	Wood chips	0.43	175 total [a]
Packed bed (Arulneyam and Swaminathan, 2000)	Compost & polystyrene particles	0.0042	195 total
Packed bed (Arulneyam and Swaminathan, 2000)	Compost & polystyrene particles	0.013	195 total

[a] These are the highest elimination capacities reported in the study of Le Cloirec et al., 2001, while the maximum elimination capacity was not reported.

3.5 Conclusions

The application of gas-solid fluidized beds for the treatment of waste gases represents a promising new field of research. This study complements preliminary investigations of fluidized bioremediation, by providing a comprehensive comparison of a fluidized bed to a packed bed bioreactor. A binary mixture of moist sawdust and glass spheres has been shown to be a viable

packing for a fluidized bioreactor. Compared to a packed bed, fluid bed operation was shown to double the mass transfer rate of the pollutant from the gas phase to the solid particles.

In this study, classic bioremediation elimination capacity (EC) curves are obtained in both packed and fluidized modes which confirms that the bed is capable of supporting microorganisms, even when fluidized. The maximum elimination capacity was 75 g m^{-3} sawdust h^{-1} for the fluidized bed compared to 225 g m^{-3} in the high velocity packed bed (0.155 m s^{-1}), even though the fluidized bed has a higher mass transfer coefficient. At the maximum EC, it appears that the overall biotreatment rate is controlled by growth kinetics and since the packed bed is operated under higher ethanol concentrations, higher microbial growth rates result in higher EC values for packed bed operation.

A potential means to improve fluidization bioremediation performance is to recycle the outlet air from the fluidized bed back to the inlet, resulting in an increase in the concentration of ethanol to the bottom of the bed. In future studies it is planned to optimize the packing of the fluidized bioreactor. The glass spheres offer very little microbial growth support, which reduces the elimination capacity of the bioreactor in terms of total volume of the bed. A packing material which will support microorganisms and also fluidize adequately without glass spheres should improve the bioremediation performance. Also, the fluidized bioreactor should be tested for the treatment of a hydrophobic contaminant such as toluene. Visually, the fluidized bioreactor in this study was found to achieve a greater amount of particle mixing than the packed bed. It could be inferred that more mixing will result in more uniform bed conditions. As a result, gas-solid fluidized bioreactors may exhibit good operability in industrial settings.

3.6 Nomenclature

C Concentration of ethanol in gas phase (kg m^{-3} of gas phase)

C_{in} Concentration of ethanol in gas phase into vessel (kg m^{-3} of gas phase)

C_{ads} Concentration of ethanol in moist packing (kg m^{-3} of packing)

$C_{ads,sat}$ Saturation concentration of ethanol in moist packing (kg m^{-3} of packing)

H Henrys Law coefficient (atm*m^3 mol^{-1})

ΔH_{sol} Standard enthalpy of solution of ethanol in water (J mol^{-1})

k Constant in the equilibrium relationship between ethanol in the gas phase and in the packing (m^3 of gas phase m^{-3} of moist packing)

K Bulk mass transfer coefficient between gas and particles in Linear Driving Force model (h^{-1})

K_I Inhibition constant (g m^{-3})

K_s Saturation constant (g m^{-3})

n Constant in the equilibrium relationship between ethanol in the gas phase and in the packing

N Rate of adsorption of ethanol into particles (kg h^{-1})

Q Volumetric flowrate of ethanol contaminated air (m^3 h^{-1})

P_E Partial pressure of ethanol in air (atm)

R Gas constant

Re_p Particle Reynolds number

S Ethanol concentration in liquid (g m^{-3})

Sc Schmidt number

Sh Sherwood number

t Time (h)

T Temperature (K)

V Axial interstitial velocity of gas phase (m h^{-1})

V_B Bed volume, m^3

X Biomass concentration in liquid (g m^{-3})

X_E Concentration of ethanol in water (mol m^{-3})

z Axial coordinate in the fluidized or packed bed vessel (m)

Greek Letters

θ Porosity of the bed

μ_m Maximum growth rate (h^{-1})

3.7 References

Arulneyam, D.; Swaminathan, T. Biodegradation of ethanol vapour in a biofilter. *Bioproc. Eng.* **2000**, *22*, 63-67.

Clarke, K.L.; Pugsley, T.; Hill, G.A. Fluidization of moist sawdust in binary particle systems in a gas-solid fluidized bed. *Chem. Eng. Sci.* **2005**, *60*, 6909-6918.

De Lasa, H.I.; Errazu, A.; Barreiro, E.; Solioz, S. Analysis of fluidized bed catalytic cracking regenerator models in an industrial scale unit. *Can. J. Chem. Eng.* **1981**, *59*, 549-553.

Delhoménie, M.C.; Heitz, M. Elimination of chlorobenzene vapors from air in a compost-based biofilter. *J. Chem. Technol. Biotechnol.* **2003**, *78*, 588-595.

Deshusses, M.A.; Johnson, C.T. Development and validation of a simple protocol to rapidly determine the performance of biofilters for VOC treatment. *Environ. Sci. Technol.* **2000**, *34*(3), 461-467.

Groenestijn, J.W.; van Kraakman, N.J.R. Recent developments in biological waste gas purification in Europe. *Chem. Eng. J.* **2005**, *113*, 85-91.

Hodge, D.S.; Devinny, J.S. Determination of transfer rate constants and partition coefficients for air phase biofilters. *J. Environ. Eng*. **1997**, *123*, 577-585.

Kennes, C.; Thalasso, F. Waste Gas Biotreatment Technology. *J. Chem. Technol. Biotechnol.* **1998**, *72*, 303-319.

Kim, S.; Deshusses, M.A. Understanding the limits of H_2S degrading bio-trickling filters using a differential biotrickling filter. *Chem. Eng. J.* **2005**, *113*, 119-126.

Klainer, A.S.; Betsch, C.J. Scanning-beam electron microscopy of selected microorganisms. *J. Infect. Dis.* **1970**, *121*, 339-343.

Kunii, D.; Levenspiel, O. Fluidization Engineering, Second Ed.; Butterworth-Heinemann: Newton, MA, 1991, pp 71-75; 257-260.

Le Cloirec, P.; Humeau, P., Ramirez-Lopez, E.M. Biotreatments of odours: control and performances of a biofilter and a bioscrubber. *Wat. Sci. Tech.* **2001**, *44*(9), 219-226.

Lenz, K.; Beste, Y.A.; Arlt, W. Comparison of static and dynamic measurements of adsorption isotherms. *Separ. Sci. Tech*. **2002**, *37*, 1611-1629.

Leslous, A.; Delebarre, A.; Pre, P.; Warlus, S.; Zhang, N. Characterization and selection of materials for air biofiltration in fluidized beds. *Int. J. Chem. Reactor Eng.* **2004a**, *2*(Article A20), 1-19.

Leslous, A.; Pre, P.; Delebarre, A. Valorization of wood industry by-product for biological elimination of volatile organic compounds, REWAS'04. Global symposium on recycling, waste treatment and clean technology: proceedings, **2004b**, 351-359.

Ottengraf, S.P.P.; Meesters, J.J.P.; van den Oever, A.H.C.; Rozema, H.R. Biological elimination of volatile xenobiotic compounds in biofilters. *Bioproc. Eng.* **1986**, *1*, 61-69.

Wright, P.C.; Raper, J.A. Investigation into the viability of a liquid-film three-phase spouted bed biofilter. *J. Chem. Technol. Biotechnol.* **1998**, *73*, 281-291.

Wei, V.Q.; Hill, G.A.; MacDonald, D.G. Bioremediation of contaminated air using an external-loop airlift bioreactor. *Can. J. Chem. Eng.* **1999**, *77*, 955-962.

CHAPTER 4 – Improved VOC Bioremediation using a Fluidized Bed Peat Bioreactor

A similar version of this manuscript has been copyrighted and publsihed in ***Transactions of the Institute of Chemical Engineers, Part B: Process Safety and Environmental Protection***.

Clarke, K.L.; Hill, G.A.; Pugsley, T. Improved VOC bioremediation using a fluidized bed peat bioreactor. *Trans. I. Chem. E., Part B Process Saf. Environ. Protect*. **2008**, *86*, 283-290.

Contribution of Ph.D. candidate

Experiments were planned and performed by Kyla Clarke. Todd Pugsley and Gordon Hill provided guidance in planning the experiments. The submitted manuscript was written by Kyla Clarke, while Gordon Hill and Todd Pugsley provided editorial assistance.

Contribution of this paper to the overall study

Chapter 3 illustrated that a gas-solid fluidized bioreactor has the potential to bioremediate waste gas. However, the bioremediation performance of the fluidized sawdust/glass sphere bed was inferior to that of a comparable packed bed. Although glass spheres enabled the fluidization of sawdust particles, the spheres were found to be ill-suited for a bioreactor. There was very little microbial growth on the spheres. As a result, the spheres took up volume in the bioreactor bed, while contributing very little to the overall bioremediation rate. In this investigation, the bioreactor design has been improved with the selection of peat granules as an alternative packing material. Peat granules, by themselves, fluidized well in a bubbling bed regime, without the

addition of a second, inert particle. This paper presents a second set of bioremediation experiments using peat granules. The bench-scale bioreactor, developed in Chapter 3, is operated with both fluidized and packed beds of peat granules for the treatment of ethanol-contaminated air.

Additional experimental details not in the manuscript

The apparatus used in Chapter 3 was modified slightly for this study. The process of humidifying the inlet air to the bioreactor was altered. A humidification column was installed to replace the steam-injection method. The reason for the modification was that steam-injection required diligent supervision of the apparatus. The humidification column could be operated continuously for weeks at a time, with very little supervision. Deionised water supplied from a storage tank by a pneumatic pump was continuously sprayed into the humidifier at a flowrate between 0.9 and 2.8 mL s^{-1}. The temperature of the water to the humidifier was controlled at a temperature between 20 and 55 ^{o}C by a re-circulating hot water line which was immersed in the water tank. The water temperature was adjusted such that the inlet air to the bioreactor was several degrees warmer than ambient temperature.

Air flowrate through the ethanol bubbler was measured with rotameter 1 and mass flow meters 1 and 2. Rotameters 3 and 4 were used to measure inlet air flowrate to the apparatus at superficial gas velocities of 0.0024 and 0.082 m s^{-1} respectively. Rotameters 1 and 3 and mass flow meters 1 and 2 were calibrated with a Precision wet test meter by Precision Scientific Co. (Chicago, IL). Refer to the calibration curves in Appendix A. The flowrates measured by rotameter 4 were too large for it to be calibrated with the wet test meter.

At superficial gas velocities greater than 0.082 and less than 0.8 m s^{-1} in the bed, inlet air was metered with a flow orifice plate with a 12.7 mm (0.5 inch) opening, described in Chapter 2. For superficial velocities greater than 0.8 m s^{-1}, an orifice plate with a 31.8 mm (1.25 inch) opening was used. The orifice was designed and constructed to the same specifications as the 12.7 mm opening orifice. Refer to Figure 2.04 for a schematic of the orifice plate, and Appendix A (Figure A.9) for a calibration curve.

A different perforated distributor plate was used in the bench-scale vessel. It was designed specifically for a bed of moist peat granules, with a packed bed height of 0.14 m,

according to the rules of thumb in Kunii and Levenspiel (1991). The spacing between the centre of each hole was 4.0 mm, but was otherwise identical to the plate used in Chapters 2 and 3.

Figure 4.01 shows photographs of peat granules during fluidization.

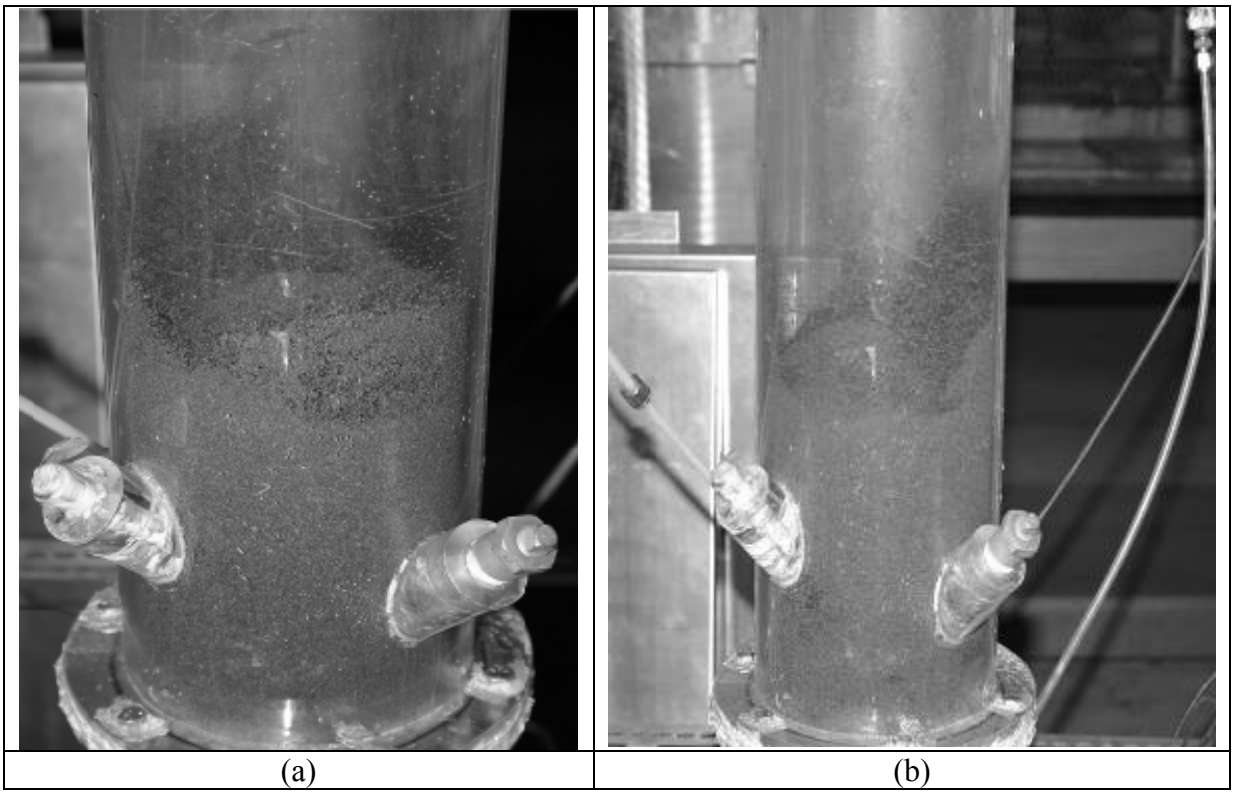

(a) (b)

Figure 4.01 Photographs of a fluidized bed of peat granules in the bioreactor vessel (superficial gas velocity = 0.5 m s^{-1}).

Manuscript

4.1 Abstract

A gas-solid fluidized bed bioreactor was successfully used to treat air contaminated with a volatile organic compound (VOC). A bioreactor containing both a fluidized and packed bed of moist peat granules removed ethanol, a representative VOC, from an air stream. The fluidized bed operation mode of the bioreactor outperformed the packed bed mode. The maximum elimination capacity (EC) of ethanol in the fluidized mode was 1520 g m^{-3} h^{-1}, with removal efficiencies ranging between 45 to 100%, at loadings up to 3400 g m^{-3} h^{-1}. Maximum EC was 530 g m^{-3} h^{-1} in the packed bed mode. Removal efficiency in the fluidized bioreactor was best at the lowest velocity, where the bubbling bed fluidization regime predominated. As gas velocity increased, the size and amount of large bubbles (slugs) increased and removal efficiency decreased while elimination capacity increased.

Keywords: gas-fluidized bioreactor, VOC contaminated air, bioremediation, peat granule.

4.2 Introduction

Synthetic crude oil is produced from vast oil sands deposits in Canada. Air emissions of contaminants such as volatile organic compounds (VOCs) are a side-effect of oil sands production. In Canada, VOCs are categorized as one of six criteria air contaminants, because they can be harmful to human health and contribute to air pollution problems. Environment Canada reports that 58,805 tonnes of VOCs were released from oil sands operations in the year 2005, and they project that these emissions will increase to 283,000 tonnes in 2010 as new oil sands projects are commissioned (Environment Canada, 2007). Sources of VOC emissions from oil sands operations include tailings ponds, extraction plant vents, tank farms, process tank areas, and exposed oil sands mines (National Energy Board, 2000).

Various technologies are used to treat volatile organic compound (VOC) emissions from industrial point sources such as oil sands operations, refineries, petrochemical plants, food processing plants, and power plants. The incentives behind air pollution treatment are usually to comply with government environmental regulations or to prevent nuisance odours. The novel method of a gas-solid fluidized bioreactor has recently been considered for treatment of VOC emissions in air (Clarke et al., 2007; Delebarre et al., 2007). In a gas-solid fluidized bioreactor, a bed of discrete particles are used to support microbial growth. The incoming polluted air stream fluidizes the bed, and microorganisms on the particles consume VOCs in the air. The VOCs provide the principal carbon and energy requirements of the microorganisms. In addition, microbial cells are nourished by moisture in the particles, and nutrients which are added to the bed.

Gas-solid fluidized bioreactors are a biological method of treating air pollution. In general, biological air treatment methods have the advantages of lower operating costs, and a lower environmental impact because they generate fewer waste products as compared to physical and chemical treatment methods (Groenestijn and Kraakman, 2005; Kennes and Thalasso, 1998). Gas-fluidized bioreactors are an attempt to improve upon the design of other biological treatment methods such as biofilters. Biofilters are packed bed bioreactors that have been used commercially for air treatment during the last several decades (Deshusses and Johnson, 2000). However biofilters have operating problems which reduce their efficiency. It is difficult to control bed temperature, pH and moisture content, and uneven conditions can develop throughout the bed (Jorio and Heitz, 1999), resulting in clogging of the bed and gas channelling (Leslous et al., 2004). In a fluidized bed on the other hand, fluidization promotes homogeneous conditions due to the rapid and uniform mixing of particles (Kunii and Levenspiel, 1991).

An important design consideration of a fluidized bioreactor is the type of particle used in the bed. As with biofilters, the particles must be able to hold moisture required for growth and maintenance of microbial cells which are supported on the particles. Biomass such as wood chips, peat, soil, and compost are often used in biofilters because these materials can hold high amounts of moisture. In biofilters, the recommended moisture content of peat, compost, and wood sub-products ranges from 43 to 400 wt% on a dry basis (Kennes and Thalasso, 1998). In addition, an obvious requirement of a fluidized bioreactor is that the particles can be fluidized. The fluidized state is influenced by the particle properties of size, size distribution, density,

shape, and moisture content. The fluidization state in turn influences mass and heat transfer characteristics, and the conversion in a fluidized reactor. For instance, poor fluidization behaviour such as gas channelling leads to poor VOC elimination.

Our group previously used a gas-solid fluidized bioreactor to remove VOC contamination from an air stream (Clarke et al., 2007). The particle bed consisted of a 26:74 v/v mixture of moist sawdust particles (d_p of 0.625 mm) and glass spheres (d_p of 0.516 mm). The glass spheres prevented agglomeration of sawdust particles during fluidization (Clarke et al., 2005), but also reduced the capacity of the fluidized bed for bioremediation activity. For comparison purposes, the bioreactor was operated in a packed bed mode using the same packing material. During fluidization mode, the sawdust and glass sphere mixture was maintained in a state that is best described as bubbling/slugging fluidization, in which large bubbles would periodically grow to form slugs that were nearly as large as the column diameter. Mass transfer experiments without bioremediation demonstrated that the fluidized bed had significantly higher mass transfer rates than the packed bed. The maximum bioremediation elimination capacity (EC) of the packed bed based on volume of sawdust (225 g m^{-3} sawdust h^{-1}) was comparable to those of other biofilter studies (Clarke et al., 2007). For both packed and fluidized bed modes, EC is defined as the mass of ethanol consumed in the bioreactor per total packed bed volume (or packed bed volume of sawdust) per unit time. Note that during fluidization, interparticle space increases and as a result the volume of packing increases. The maximum EC of the fluidized sawdust was only 75 g m^{-3} sawdust h^{-1}. One of the reasons for poorer performance in fluidized operation was speculated to be due to the inability of microbial cells to attach to the rigid sawdust particles during fluidization. It was clear that microbial cells did not attach in significant numbers to glass spheres even during packed bed operation, and that the majority of the bioremediation activity took place on the sawdust particles. There is therefore a need to find a particle bed for a gas-fluidized bioreactor which is capable of supporting more microorganisms, while also exhibiting good fluidization behaviour even when the particles are moist.

Delebarre et al. (2007) studied a gas-solid fluidized bed of sawdust to treat ethanol and toluene emissions. The removal efficiency of the bioreactor was approximately 80% at ethanol loadings (ethanol feedrate per total packed bed volume) between 750 and 1250 g m^{-3} h^{-1}. Bioremediation rates were found to vary with the type of microorganisms in the bioreactor. As well, moisture content in the sawdust bed was difficult to control. The concentration of

microbial cells in the bioreactor was directly dependent on the moisture content of the sawdust and therefore hard to control.

Several biofilter studies have shown that peat granules are effective as a packing for treatment of VOCs (Kiared et al., 1996; Bibeau et al., 2000; Chan and Lu, 2003). Kiared et al. (1996) found that a peat granule biofilter had a maximum elimination capacity of 120 g ethanol m^{-3} h^{-1}. Chan and Lu (2003) prepared 2.4 to 6 mm diameter composite particles of polyvinyl alcohol and peat, that were used in a biofilter for treating ethyl acetate. They observed poor initial performance of the biofilter, possibly due to a nitrogen deficiency. After soaking the peat particles in KNO_3 solution, the biofilter performance increased dramatically.

In the present work, a bed of peat granules was used in a gas-solid fluidized bioreactor. Moist peat granules fluidized well, without the occurrence of gas channelling. Peat granules, supporting a mixed culture of microorganisms, were used in a gas-fluidized bioreactor to treat ethanol, a candidate VOC. The bioremediation performance of the gas-fluidized bioreactor was then compared to that of a packed bed bioreactor (biofilter).

4.3 Materials and Methods

4.3.1 Apparatus

The bioreactor apparatus consists of an acrylic, cylindrical, bench-scale vessel, with an inside diameter of 0.14 m (Figure 4.1). The vessel height above the distributor plate is 1.81 m, and below the distributor there is a windbox, 0.162 m in height. The perforated-plate distributor has 1 mm holes on a square pitch, with a 5.1% open area. A 100-mesh size wire screen over the distributor prevents bed particles from plugging the distributor holes. At superficial gas velocities above 0.082 m s^{-1}, ambient air was supplied with a blower, and air velocity was measured using an orifice plate. At velocities of 0.082 m s^{-1} and lower, air was supplied by compressed laboratory air and measured with rotameters.

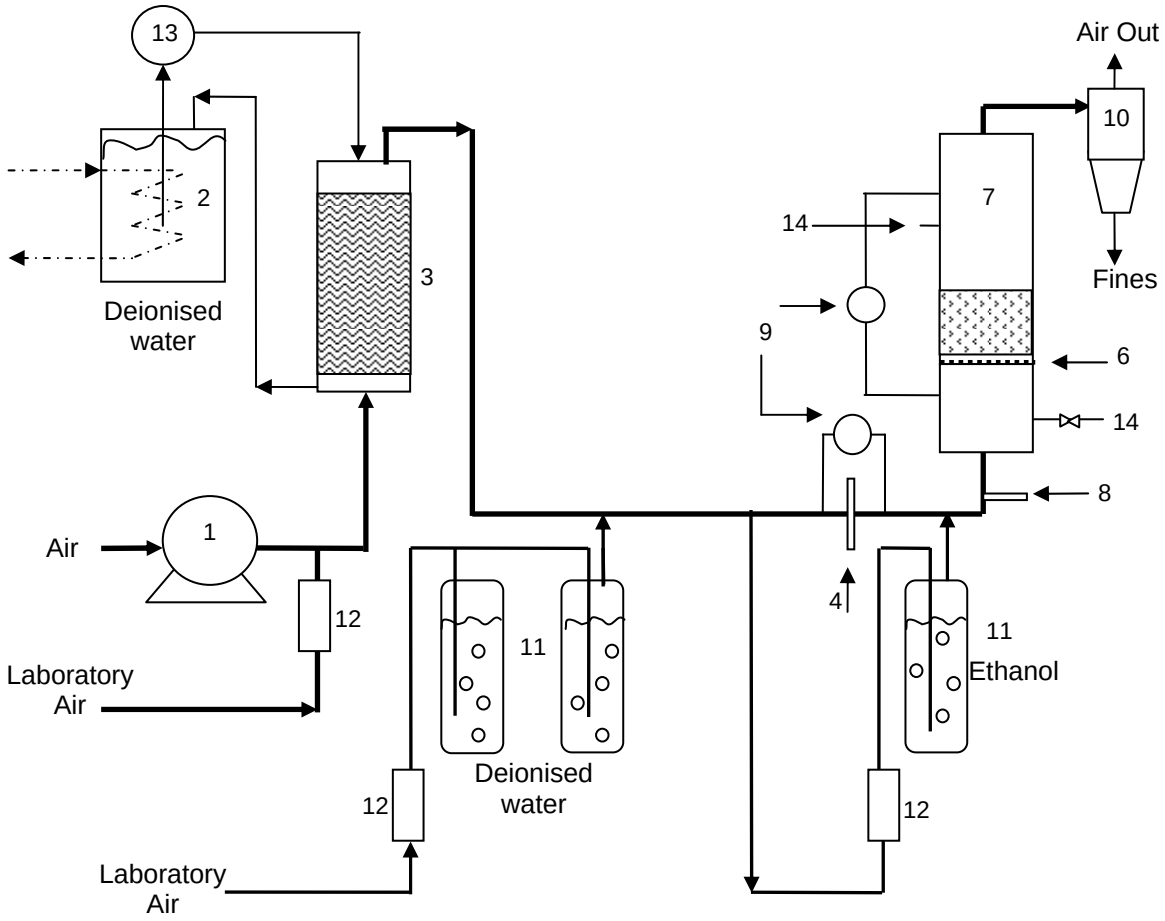

Figure 4.1 Experimental apparatus: (1) blower; (2) water storage (3) humidifier; (4) orifice plate; (5) wind-box; (6) distributor and wire screen; (7) bioreactor; (8) humidity and temperature probe; (9) differential pressure transducers; (10) cyclone; (11) bubbler; (12) rotameter; (13) pump; (14) sampling port.

The air entering the bioreactor was saturated with water. At velocities above 0.0024 m s^{-1}, the air was passed through a 0.24 m diameter counter-current humidification column. The humidifier contained a packed bed of rings (short segments of ¾ inch PVC pipe). The temperature of the water to the humidifier was controlled such that the inlet air to the bioreactor was 1 to 3 ^{o}C warmer than ambient temperature. This prevented the air stream from stripping moisture out of the bioreactor bed and drying out the particles. At a gas velocity of 0.0024 m s^{-1}, rather than passing the air through the humidification column, the air was saturated in two bubblers containing deionised water. At all air flowrates, humidity and temperature of the inlet air were continuously measured with a HMP 230 series probe by Vaisala (Helsinki, Finland).

Ethanol contamination was introduced by directing a slip stream of the inlet air into an ethanol bubbler. The inlet air flowrate to the ethanol bubbler was metered using a rotameter.

4.3.2 Particles

The packing of the bioreactor consisted of peat granules with a Sauter mean diameter initially of 680 μm. BioAPT peat granules (specification 10 to 42 mesh), manufactured from low-ash reed sedge peat were obtained from American Peat Technology LLC (Aitkin, MN). Peat granules with a narrower particle size distribution were created by sieving with Tyler Series equivalent sieves. The peat granules which were collected for use in bioremediation experiments passed through 24 mesh (710 μm) but were retained on 32 mesh (500 μm). Properties of the peat granules were further characterized both before and after use in bioremediation experiments. The particle characterization is summarized in Table 4.1. The particles are characterized by the same methods described in section 2.4.

Table 4.1 Particle characterization of peat granules.

Particles	d_p (μm)	ρ_b (kg m^{-3})	$\rho_{b,max}$ (kg m^{-3})	ρ_s (kg m^{-3})	ρ_p (kg m^{-3})	ε_m	ε_p	ϕ_s
Before bioremediation	680	680	740	1581	1240	0.45	0.22	0.87
After bioremediation	775	676	760	1541	1273	0.47	0.17	

4.3.3 Fluidization of Peat Granules

Initially, in the absence of microorganisms, peat granules were fluidized with air in the bioreactor vessel. Water was added to the peat to obtain a moisture content of 40 wt% (dry basis). The particle bed pressure drop and superficial gas velocity were recorded as flowrate to the vessel was gradually increased from the packed bed state. The minimum fluidization velocity was measured, and at the same time the quality of fluidization behaviour was assessed by observation. The minimum fluidization velocity was determined as the point of intersection

of the fixed bed pressure drop versus velocity line and the initial bed weight divided by bed cross-sectional area (horizontal line), similar to the approach of Kunii and Levenspiel (1991), and was found to be 0.21 m s^{-1}.

4.3.4 Analysis

Ethanol concentrations in the air entering and exiting the bioreactor were determined using a Hewlett Packard 5890 series (Agilent Technologies, Palo Alto, CA) gas chromatograph fitted with a flame ionization detector and a Supelco (Bellefonte, PA) non-polar PTE-5™ column. The injector and detector temperatures were 200 ºC, oven temperature was held at 40 ºC, column inlet pressure was 90 kPa, and helium was used as the carrier gas at a linear velocity of 30 cm s^{-1}. Samples were collected in glass sampling bulbs from ports on the bioreactor vessel, using vacuum to draw the contaminated air into the bulbs. A gas-tight syringe was used to withdraw 0.1 to 0.5 mL sub-samples from the bulbs which were manually injected into the GC. The standard deviation between sub-samples was determined to be less than eight percent of the average concentration of the sampling bulb, and the standard deviation of samples was less than five percent of the average inlet concentration. Moisture content in the peat particles was measured with a Mettler Toledo (Columbus, OH) HB43 halogen moisture analyzer.

4.3.5 Microorganism and Media

2.2 L of peat granules were inoculated with an active culture that had been growing for 24 hours on 0.6 g L^{-1} of ethanol. The inoculant culture, dominated by *Hansenula anomala* (also called *Pichia anomala*), originated from bioreactor bed particles used in previous experiments for the treatment of ethanol (Clarke et al. 2007). The peat granules were immediately placed in the bioreactor, and the packed height of the bed was 0.14 m. Ethanol-contaminated air, initially at a rate of 0.0024 m s^{-1}, was continuously fed into the vessel. Conditions in the system were not sterile. Throughout bioremediation experiments, a nutrient solution was periodically mixed into the packing in 50 to 125 mL batch additions every two to four days. The nutrient solution consisted of 0.84 g KH_2PO_4, 0.75 g K_2HPO_4, 0.50 g $(NH_4)_2SO_4$, 0.06 g NaCl, 0.06 g $CaCl_2$, 0.06 g $MgSO_4$, 0.02g $Fe(NH_4)_2(SO_4)_2*6H_2O$, and 1 mL of trace mineral solution (per litre of

deionised water: 0.20 g $ZnSO_4*7H_2O$, 0.06 g $MnCl_2*4H_2O$, 0.60 g H_3BO_3, 0.40 g $CoCl_2*6H_2O$, 0.02 g $CuCl_2*2H_2O$, 0.04 g $NiCl_2*6H_2O$, and 0.06 g $Na_2MoO_4*2H_2O$) in 1 litre deionised water.

Microbial cell counts in the peat granules bed were determined weekly during packed bed and fluidized bed bioremediation experiments by a plate count method. A 1 g sample of bed particles was taken from close to the middle of the bed using a sample scoop. The sample was mixed with 10 mL of sterile 0.85% saline solution in a vortex mixer for 30 seconds. Then serial dilutions were plated onto Difco plate count agar (Becton, Dickinson and Company, Franklin Lakes, NJ, USA). Total colony forming units (CFU) per dry gram of peat were determined after four days of growth at ambient laboratory temperature.

After nine weeks of bioreactor bioremediation operation, the most abundant microbial species in the bed material was characterized by the MIDI, Inc. (Newark, DE) Sherlock microbial identification system, as *Pichia* spp. The pH of the bioreactor packing was measured by mixing 1 g of packing in 10 mL of neutral, deionised water, and found to be acidic at 4.9.

4.3.6 Bioremediation

The bioreactor was operating continuously in either packed or fluidized mode for a total of 83 days. Similar to earlier studies (Clarke et al., 2007), packed bed bioremediation experiments were conducted at superficial gas velocities of 0.0024 and 0.082 m s^{-1}, while ethanol loading was varied. Ethanol concentrations in the inlet air ranged from 0.58 to 13.2 g m^{-3}, and from 0.04 to 0.58 g m^{-3} for each velocity respectively. Bioremediation performance and microbial counts indicated sluggish microbial growth for the first 21 days following inoculation of the packing in the bioreactor. A nutrient deficiency in the particle bed was suspected. Approximately 1 L of 3.8 wt% of $(NH_4)_2SO_4$ solution was mixed into the peat bed over several days. Bioremediation performance increased dramatically at constant ethanol loading. $(NH_4)_2SO_4$ supplementation was stopped when bioremediation performance reached a maximum at constant ethanol loading. During the bioremediation experiments moisture in the particles was maintained at 40 +/-4 wt% (dry basis) by humidification. The bed was allowed to reach stable conditions (constant elimination capacity) at a given ethanol loading, for at least 24 hours before collecting packed bed bioremediation data.

Fluidized bed bioremediation experiments were conducted at three different superficial gas velocities: 0.5, 0.75, and 1.0 m s^{-1} which correspond to approximately 2.5 to 5 times the minimum fluidization velocity. Ethanol concentrations in the inlet air ranged from 0.01 to 0.22 g m^{-3}. At each ethanol loading, the bioreactor was operated in fluidized mode for 6 to 7 hours, and it was observed that stable conditions were reached in less than two hours. Between fluidization trials, the bed was operated in packed bed mode at a velocity of 0.066 m s^{-1}, at the ethanol loading of the subsequent fluidization trial.

4.4 Results and Discussion

4.4.1 Fluidization of Peat Granules

Unlike a bed of moist sawdust (Clarke et al., 2005), the bed of peat granules exhibited favourable fluidization behaviour. It was possible to fluidize peat (d_p of 680 to 775 μm) with a moisture content of 40 wt% (dry basis) in a bubbling regime. The peat fluidized without channelling or the formation of a solid plug, which tends to greatly reduce bioremediation performance. As reported above, the minimum fluidization velocity (u_{mf}) was 0.21 m s^{-1}, and it is was noted that as superficial gas velocity increased above 0.55 m s^{-1} very large bubbles (slugs) began to appear in the fluidized bed.

In a fluidized bioreactor, peat granules have several advantages over the sawdust/glass sphere mixture used in our previous study (Clarke et al., 2007). The peat granules hold more moisture which helps to sustain microorganisms in the bioreactor, but can still be more effectively fluidized. The peat bed holds 200 kg m^{-3} moisture per bed volume *versus* 20 kg m^{-3} in the sawdust/glass sphere packing. Also, the u_{mf} of the peat (0.21 m s^{-1}) was much lower than that of the moist sawdust/glass sphere mixture (0.39 to 0.48 m s^{-1}) (Clarke et al., 2007). A lower u_{mf} is an advantage in a fluidized bioreactor because it allows a wider range of inlet gas flowrates and contaminant concentrations to be treated.

The same bed of peat particles was used for all bioremediation experiments. Particle size distributions of these granules before and after use are shown in Figure 4.2. Figure 4.3 shows the change in appearance of the peat granules. During bioremediation experiments, particles

increase in size with the Sauter mean diameter increasing from 680 to 775 μm. Figure 4.2 also indicates that the volume percentage of smaller particles decreased. The increase in particle size occurred in the first several days of the bioremediation experiments; when the peat bed was first put into operation. Very fine particles of peat in the initial mixture cohered to the larger particles, creating the larger agglomerates.

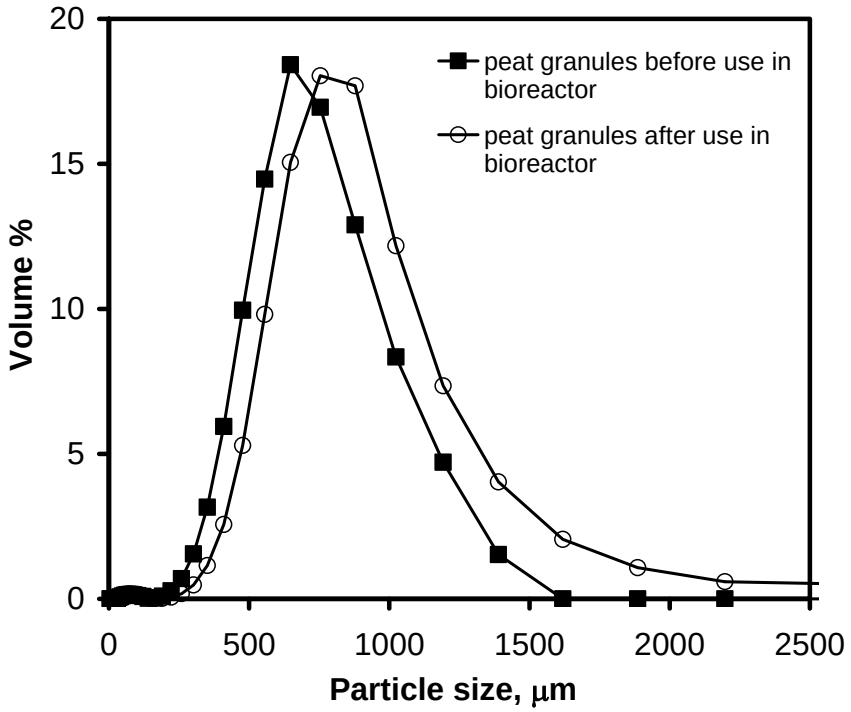

Figure 4.2 Particle size distribution of peat granules before and after use in bioremediation experiments.

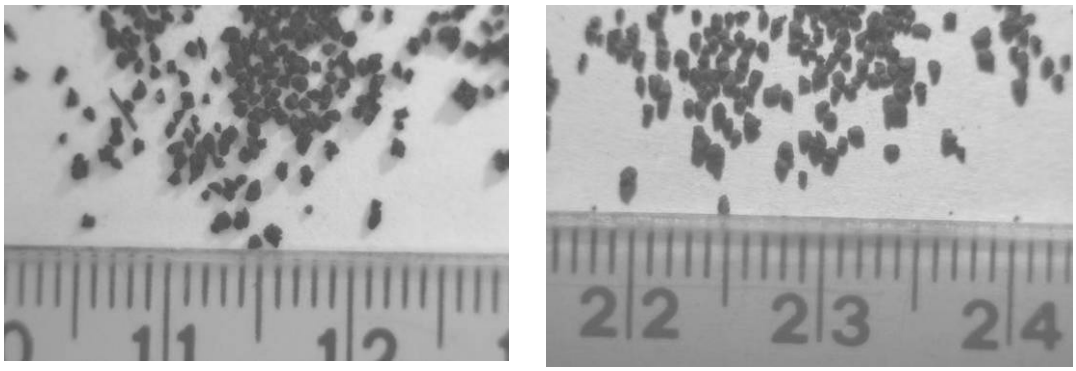

Figure 4.3 Peat granules before and after use in bioremediation experiments.

4.4.2 Bioremediation of an Air Pollutant

The peat bed bioreactor successfully treated ethanol-contaminated air in both packed and fluidized bed modes. A mixed culture of microorganisms flourished on the peat granule support. The cell concentration in the bioreactor ranged between 2.1 and 6.1 billion CFU g^{-1} dry peat. These results are comparable to those of Kiared et al. (1996), who found that bacterial count stabilized at 1 billion CFU g^{-1} of peat granules in a biofilter used to treat ethanol emissions. Figure 4.4 shows that for the current study, microbial cell count was directly related to ethanol loading in both the packed and fluidized modes of bioremediation. This is to be expected, since biomass is produced by consumption of ethanol.

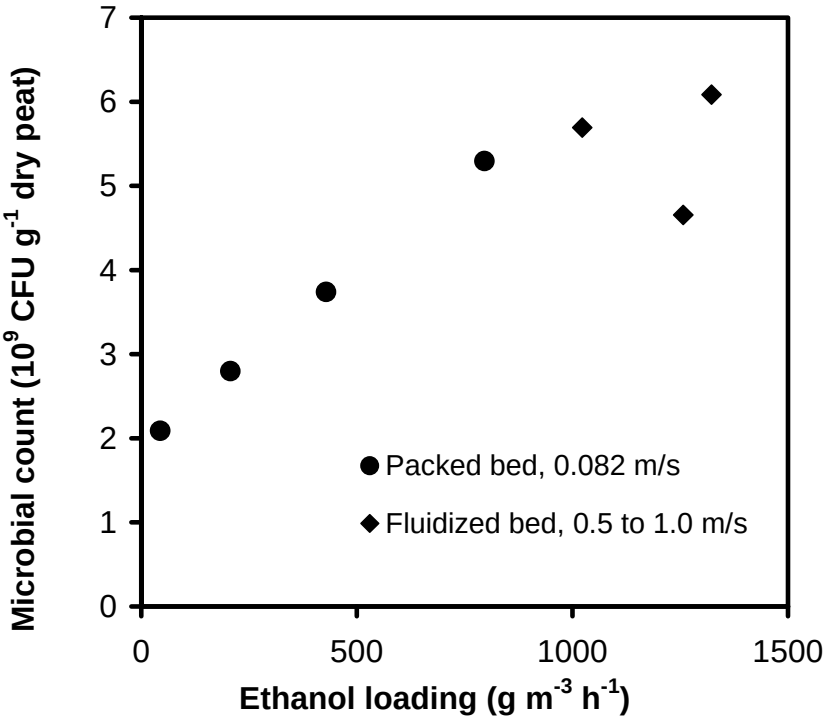

Figure 4.4 Microbial growth on peat granules relative to inlet ethanol loading during packed and fluidized bed bioremediation experiments.

Bioremediation performance was measured in the packed bed mode of the bioreactor at a low velocity (approximately $0.01 \cdot u_{mf}$) and a high velocity ($0.4 \cdot u_{mf}$). Figure 4.5 illustrates the packed bed performance of the bioreactor in terms of elimination capacity (EC) of the ethanol. The dashed line represents the EC if there was complete ethanol removal. In the packed bed

mode at both velocities, the maximum EC was approximately 530 g m^{-3} h^{-1}. The removal efficiency (analogous to percentage conversion) is greater than 95% until the maximum EC is reached. In the low velocity packed bed, there is a decrease in EC after maximum EC is reached. Generally in biofilters, EC increases until it reaches a maximum, and then it remains constant or sometimes decreases (Deshusses and Johnson, 2000; Delhoménie and Heitz, 2003). This behaviour has been explained by a shift in the rate controlling mechanism of the overall bioremediation rate. Below maximum EC, bioremediation may be controlled by diffusion of the pollutant, while microbial kinetics are limiting above the maximum EC (Ottengraf et al., 1986; Delhoménie and Heitz, 2003).

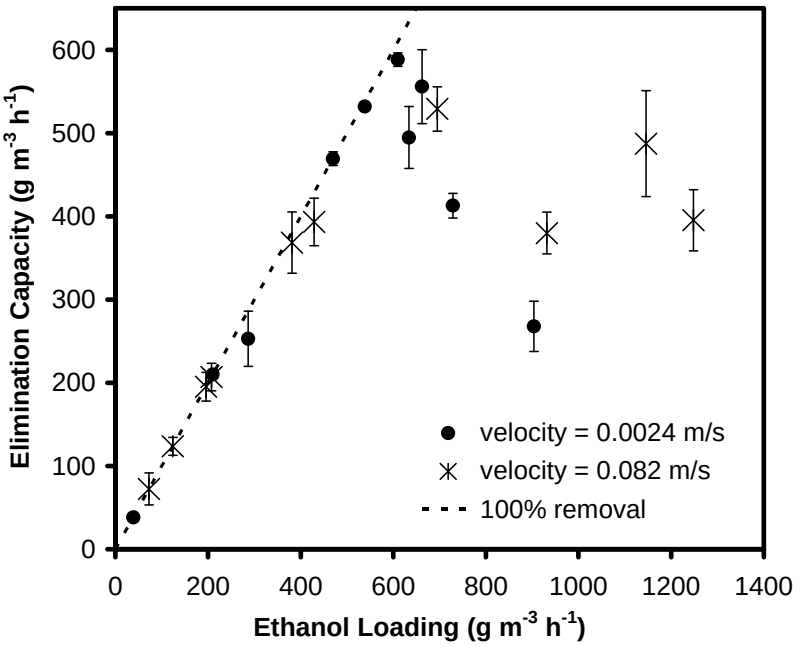

Figure 4.5 Bioremediation rates in packed bed of peat granules at different gas velocities. Error bars represent +/-2 standard deviations of the mean value of elimination capacity.

In the fluidized bed mode, bioremediation performance was measured at three velocities, between approximately $2.5 \cdot u_{mf}$ and $5 \cdot u_{mf}$. The fluidized bioremediation results are summarized in Figure 4.6. Fluidized bed bioremediation performance exceeded that of the packed bed. This is in contrast with our previous study on fluidized bioremediation (Clarke et al., 2007), where the packed bed mode of a sawdust/glass sphere bioreactor outperformed the fluidized mode. An explanation for this dissimilarity is discussed later in this section. Table 4.2 lists results of

ethanol bioremediation experiments in packed and fluidized beds both from the present study and other studies. The maximum EC in the fluidized mode of the peat bed ranges between 1150 and 1520 g m^{-3} h^{-1}, which exceeds that reported by Delebarre et al. (2007) using pure sawdust particles. At a gas velocity of 0.5 m s^{-1}, the maximum EC of ethanol in the fluidized mode was 1150 g m^{-3} h^{-1}. At higher velocities, EC continued to climb as the ethanol loading increased. At a velocity of 0.75 m s^{-1} and a loading of 3400 g m^{-3} h^{-1}, an EC of 1520 g m^{-3} h^{-1} was reached. Although this is a high removal rate, the removal efficiency dropped to 45%.

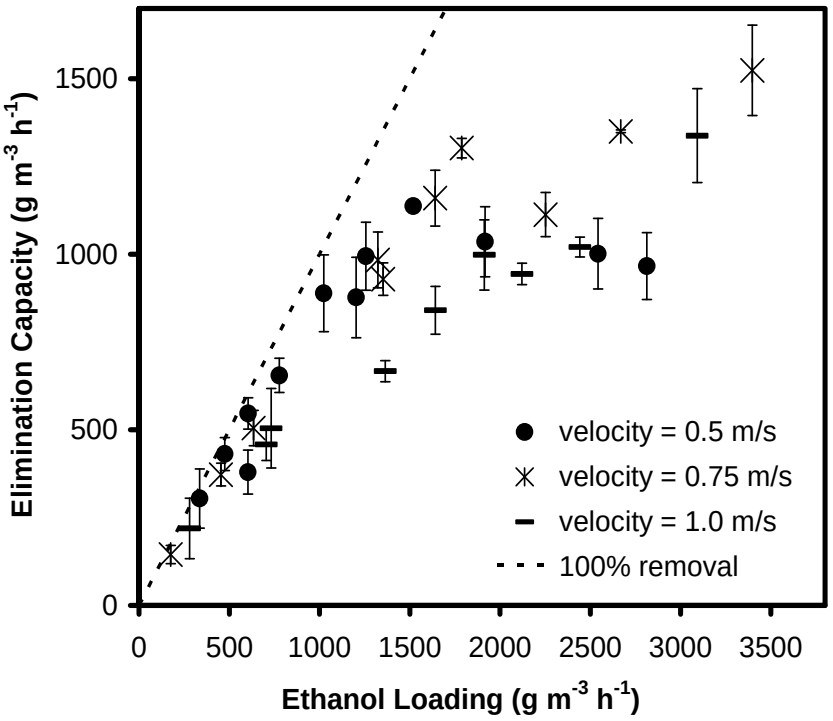

Figure 4.6 Bioremediation rates in fluidized bed of peat granules at different gas velocities. Error bars represent +/-2 standard deviations of the mean value of elimination capacity.

Table 4.2 Bioremediation of ethanol in fluidized and packed bed bioreactors.

Bioreactor	Bed Particles	Superficial gas velocity (m s^{-1})	Maximum EC (g m^{-3} h^{-1})
Packed bed current research	Peat granules	0.0024 and 0.082	530
Fluidized bed current research	Peat granules	0.5	1150
Fluidized bed current research	Peat granules	0.75	1520
Fluidized bed current research	Peat granules	1.0	1340
Packed bed (Clarke et al., 2007)	Sawdust & glass spheres	0.16	225 based on sawdust 59 based on total bed volume
Fluidized bed (Clarke et al., 2007)	Sawdust & glass spheres	0.70	75 sawdust 20 total
Fluidized bed (Delebarre et al., 2007)	Sawdust	0.40	1000 [a]
Packed (Kiared et al., 1996)	Peat granules	0.02	120
Packed bed (Le Cloirec et al., 2001)	Wood chips	0.43	175 [b]
Packed bed (Arulneyam and Swaminathan, 2000)	Compost & polystyrene particles	0.0042, 0.0083 and 0.013	195 total

[a] Estimated from removal efficiency *vs*. ethanol loading data reported in the study of Delebarre et al. (2007).
[b] The highest EC (at 0.43 m s^{-1}) reported by Le Cloirec et al. (2001), while maximum EC was not reported.

Figure 4.7 illustrates that below an EC of 1150 g m^{-3} h^{-1}, removal efficiency ranged between 75% and 100% at the lowest gas velocity of 0.5 m s^{-1}. On the other hand at the higher gas velocities of 0.75 and 1.0 m s^{-1}, removal efficiency is 45 to 100% and 40 to 100%, respectively at ECs below 1520 g m^{-3} h^{-1}. Ottengraf et al. (1986) and Arulneyam and Swaminathan (2000) also report decreased removal efficiency with increased gas velocity in biofilters. At higher velocities, diffusion of the substrate is limited in the biomass (Ottengraf et al., 1986), and the substrate has a reduced ability to reach the gas/biofilm interface due to the shorter residence time (Arulneyam and Swaminathan, 2000). However in their biofilter studies the maximum EC values were the same at different gas velocities, while in the current study, higher fluidization gas velocities resulted in a higher maximum EC.

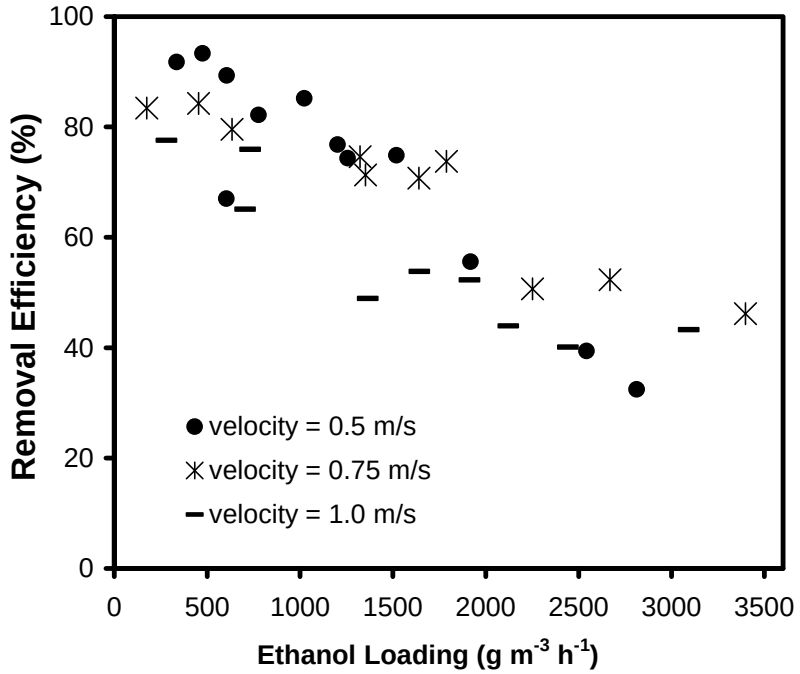

Figure 4.7 Removal efficiency in fluidized bed of peat granules at different gas velocities.

During the fluidization bioremediation experiments, hydrodynamics in the peat bed were found to change with superficial gas velocity. At the lowest velocity, 0.5 m s^{-1}, the bed showed good bubbling fluidization. At 0.75 m s^{-1} some large bubbles (slugs) were observed in the upper layers of the fluidized bed, and at 1.0 m s^{-1}, there were more slugs present at greater depths in the bed. As gas velocity increased, the size and amount of large bubbles (slugs) increased, which appeared to reduce bioremediation efficiency. Levenspiel (1999) suggests that an increase in

bubble size causes a reduction in reaction conversion in bubbling fluidized beds. This may also be the reason why the sawdust/glass sphere packed bed bioreactor outperformed the fluidized bed in our prior study. Sawdust/glass sphere fluidization was in the bubbling/slugging regime and the bubbles were observed to be much larger than those of the peat bed during bioremediation experiments, and the large bubbles were observed throughout the entire sawdust/glass sphere bed.

4.5 Conclusions

This study applies the unique properties of a gas-solid fluidized bed to a bioreactor process for treating air pollution. A fluidized peat granule bioreactor achieved ethanol elimination capacities of 1150 to 1520 g m^3 h^{-1}. The peat bed fluidized bioreactor demonstrated higher bioremediation rates than other packed bed bioreactors (biofilters). Also, the peat fluidized bed outperformed sawdust/glass sphere and sawdust gas-solid fluidized bed bioreactors previously reported in the literature (Clarke et al., 2007; Delebarre et al., 2007).

Further developmental work is warranted to optimize the peat bed gas-solid fluidized bioreactor. For instance, different sizes and size distributions of peat granules should be studied in an effort to obtain bubbles which are as small as possible during fluidization. In the current study, the presence of slugs and larger bubbles likely reduced reaction conversion. If slugging is eliminated in the peat fluidized bed at all fluidization velocities, the next step would be to reassess the effect of fluidization velocity on bioremediation performance.

In industrial settings the operability of a peat gas-solid fluidized bioreactor may be better than a biofilter. It can be difficult to operate biofilters because uneven conditions can develop in the packed bed. Particle mixing during fluidization results in more uniform conditions throughout the fluidized bioreactor. The raw materials of the process are peat granules, nutrient solution and water which are all very low in cost. Costs of a peat fluidized bed could be further reduced by investigating options of on-site production of peat granules from raw peat. As a result, peat fluidized bioreactors are an attractive treatment method for VOC air emissions.

4.6 Nomenclature

d_p Sauter mean particle diameter (μm)

EC Elimination capacity (g m^{-3} h^{-1})

u_{mf} Superficial velocity of gas at minimum fluidization (m s^{-1})

Greek letters

ε_m Fraction of interparticle voids in a packed bed of particles

ε_p Porosity or fraction of pore volume in particles

ϕ_s Sphericity of a particle

ρ_b ,$\rho_{b,max}$ Bulk and maximum bulk density of particles (kg m^{-3})

ρ_p, ρ_s Particle or envelope density (including particle pore volume), skeletal density (excluding particle pore volume) (kg m^{-3})

4.7 References

Arulneyam, D.; Swaminathan, T. Biodegradation of ethanol vapour in a biofilter. *Bioproc. Eng*. **2000**, *22*, 63-67.

Bibeau, L.; Kiared, K.; Brzezinski, R.; Viel, G.; Heitz, M. Treatment of air polluted with xylenes using a biofilter reactor. *Water Air Soil Pollut*. **2000**, *118*, 377-393.

Chan, W.C.; Lu, M.C. A new type synthetic filter material for biofilter: poly(vinyl alcohol)/peat composite bead. *J. Appl. Polym. Sci*. **2003**, *88*(14), 3248-3255.

Clarke, K.L.; Pugsley, T.; Hill, G.A. Fluidization of moist sawdust in binary particle systems in a gas-solid fluidized bed. *Chem. Eng. Sci*, **2005**, *60*, 6909-6918.

Clarke, K.L.; Hill, G.A.; Pugsley, T. Direct comparison of fluidized and packed bed bioreactors for bioremediation of an air pollutant. *Int. J. Chem. Reactor Eng*. **2007**, *5*(Article A11), 1-12.

Delebarre, A.; Andres, Y.; Pellerano, M.; Pero, P.; Garcia Munzer, D.G. Biofiltration of volatile organic compounds by a fluidized bed of sawdust. *Int. J. Chem. Reactor Eng*. **2007**, *5*(Article A22), 1-11.

Delhoménie, M.; Heitz, M. Elimination of chlorobenzene vapors from air in a compost-based biofilter. *J. Chem. Technol. Biotechnol*. **2003**, *78*, 588-595.

Deshusses, M.; Johnson, C. Development and validation of a simple protocol to rapidly determine the performance of biofilters for VOC treatment. *Environ. Sci. Technol*. **2000**, *34*(3), 461-467.

Environment Canada website, Criteria Air Contaminants (CAC) Emission summaries, VOCs: **www.ec.gc.ca/pdb/cac/Emissions1990-2015/EmissionsSummaries/VOC**, 2007.

Groenestijn, J.W.; van Kraakman, N.J.R. Recent developments in biological waste gas purification in Europe. *Chem. Eng. J*. **2005**, *113*, 85-91.

Jorio, H.; Heitz, M. Traitement de l'air par biofiltration. *Can. J. Civ. Eng*. **1999**, *26*, 402-424.

Kennes, C.; Thalasso, F. Waste Gas Biotreatment Technology. *J. Chem. Technol. Biotechnol*. **1998**, *72*, 303-319.

Kiared, K.; Bibeau, L.; Brzezinski, R.; Viel, G.; Heitz, M., 1996, Biological elimination of VOCs in biofilter. *Environ. Prog*. **1996**, *15*, 148-152.

Kunii, D.; Levenspiel, O. Fluidization Engineering, Second Ed.; Butterworth-Heinemann: Newton, MA, 1991, pp 1-12; 64-68; 71-80; 95-108.

Le Cloirec, P.; Humeau, P.; Ramirez-Lopez, E. Biotreatments of odours: control and performances of a biofilter and a bioscrubber. *Wat. Sci. Tech*. **2001**, *44*(9), 219-226.

Leslous, A.; Delebarre, A.; Pre, P.; Warlus, S.; Zhang, N. Characterization and selection of materials for air biofiltration in fluidized beds. *Int. J. Chem. Reactor Eng*. **2004**, *2*(Article A20), 1-19.

Levenspiel, O. Chemical Reaction Engineering, Third Ed.; John Wiley and Sons: New York, 1999, pp 447-465.

National Energy Board, Canada's Oil Sands, a supply and market outlook to 2015, NEB, Calgary, Alberta, 2000, pp 89.

Ottengraf, S.; Meesters, J.; van den Oever, A.; Rozema, H. Biological elimination of volatile xenobiotic compounds in biofilters. *Bioproc. Eng*. **1986**, *1*, 61-69.

CHAPTER 5 – The Use of Peat Granules in a Fluidized Bed Bioreactor

This manuscript is being prepared for submission to the publication ***Canadian Journal of Chemical Engineering***.

Clarke, K.L.; Pugsley, T.; Hill, G.A. The use of peat granules in a fluidized bed bioreactor. *Can. J. Chem. Eng.*, prepared for submission, **2008**.

Contribution of Ph.D. candidate

Experiments were planned by Kyla Clarke, Todd Pugsley and Gordon Hill, and were performed by Kyla Clarke. The submitted manuscript was written by Kyla Clarke, while Todd Pugsley and Gordon Hill provided editorial guidance.

Contribution of this paper to the overall study

This chapter investigates the fundamental fluidization characteristics of moist peat granules. The purpose of fluidizing peat granules is to use them in a bioreactor for treating VOC emissions. Bench-scale experiments using a peat fluidized bioreactor for treating a waste gas are presented in Chapter 4. In order to scale up this bioremediation technology, a greater understanding of the fluidization of peat granules is needed. In this paper, properties of different sizes of peat are characterized, fluidization hydrodynamics are observed, and minimum fluidization velocity is measured and compared to correlations. As described in Chapter 2, it is generally difficult to fluidize moist biomass particles. Therefore this work also investigates the effect of particle moisture content on the fluidization of peat granules. Below certain moisture

contents, peat granules fluidize well in a bubbling bed fluidization regime without the addition of another type of particle as a fluidization aid.

Additional experimental details not in the manuscript

For this study, the apparatus was identical to that used in Chapter 4. Three different sizes/size distributions of peat granules were made from BioAPT peat (10 to 42 mesh). The peat was sieved with Tyler Series equivalent sieves on a Ro-Tap sieve shaker. Additional amounts of smaller peat granules were created by grinding large peat granules in a #1 Wiley mill, fitted with a 1 mm screen, manufactured by Arthur H. Thomas Co., Philadelphia, PA. The ground material was then re-sieved to obtain more Materials 1, 2, and 3 peat granules.

Manuscript

5.1 Abstract

Peat granules are a potential packing material in a gas-solid fluidized bed bioreactor used for treating air pollution. Using abiotic experiments, three sizes of peat granules have been fluidized with air. Relative to other biomass particles, peat granules have a high particle density (1120 to 1240 kg m^{-3}) and sphericity (0.77 to 0.87) which contribute to favourable fluidization behaviour, without gas channelling. Peat granules can retain a high amount of water (more than 200 kg m^{-3} of packed bed volume) without particle agglomeration. As a result, they are suitable as a support for microbial cells in a gas-solid fluidized bioreactor. The fluidization behaviour of the peat granules at different superficial gas velocities was observed, and minimum fluidization velocity (u_{mf}) was found to range between 0.18 to 0.49 m s^{-1}. As the mean size of particles increased, u_{mf} increased. Increasing the moisture content of the peat granules resulted in a transition from bubbling bed fluidization to poor fluidization behaviour. Based on these experiments, peat granules with a Sauter mean diameter of 680 μm and a moisture content of 40 wt% (dry basis) were selected as bed material for a gas-solid fluidized bioreactor. Other types of moist biomass particles such as sawdust are considered to be difficult to fluidize and typically exhibit Geldart group C behaviour. In contrast, it was observed that the 680 μm peat granules fluidized in a bubbling bed regime, typical of group B particles. For this size of peat granule, u_{mf} was 0.21 m s^{-1}, which agreed well with the correlations of Wen and Yu (1966) and Chitester et al. (1984) which predicted values of 0.17 and 0.22 m s^{-1}, respectively.

5.2 Introduction

Biomass particles are used in several gas-solid fluidization processes, particularly as fuels for pyrolysis and gasification (Cui and Grace, 2007). Biomass, which is organic material such as wood chips and straw, is often a waste by-product of the forestry and agriculture industries, and is therefore an inexpensive raw material. A new fluidized bed application involving biomass

particles is bioremediation of contaminated air. Clarke et al. (2007) and Delebarre et al. (2007) proposed using a gas-solid fluidized bed bioreactor for treating air containing low concentrations of volatile organic compounds (VOCs). In a gas-solid fluidized bioreactor, a stream of polluted air fluidizes a bed of particles, in a low velocity fluidization regime. The particles support microorganisms which consume VOCs in the air stream. The microorganisms derive their carbon and energy requirements from breaking down VOCs into water and carbon dioxide. A fluidized bioreactor process may have advantages over packed bed bioreactors such as biofilters. For instance rapid mixing of the particles during fluidization promotes homogeneous conditions (Kunii and Levenspiel, 1991), and may enhance gas/microbial contact (Wright and Raper, 1998).

In a gas-solid fluidized bioreactor, selection of the type of particle is one of the most critical design considerations. The particles must remain very moist in order to sustain microbial cells on the particles. For three-phase spouted and fluidized bioreactors where a waste gas stream was the fluidization stream, Wright and Raper (1998) considered both inorganic and biomass particles including expanded clay beads, plastic discs, vermiculite, and rice hulls. The biomass and inorganic particles which had good wetting properties tended to agglomerate and fluidize poorly. Non-wetting inorganic particles exhibited undesirable properties such as poor water retention, high particle attrition, and high bed pressure drops. Biomass packing material is often used in biofilters. Packing such as compost, peat and wood chips is advantageous because it is able to hold high amounts of moisture and often has a large surface area available as a support for microorganisms (Kennes and Thalasso, 1998). However, even when dry, biomass particles including sawdust, straw and rice hulls are difficult to fluidize because they often have a low density and irregular shape (Clarke et al., 2005; Aznar et al., 1992; Wright and Raper, 1998). In fluidized processes involving biomass, a second inert solid such as sand is often added in order to achieve good fluidization (Clarke et al., 2005; Cui and Grace, 2007). The fluidized state is influenced by the particle properties of size and size distribution, density, shape, and moisture content. During fluidization, bubble size and velocity as well as particle mixing patterns will vary with these properties, which in turn will influence the mass and heat transfer characteristics and the conversion in the fluidized reactor. In a fluidized bioreactor for treating waste gases, poor fluidization behaviour such as gas channelling would lead to ineffective air treatment.

Moist biomass particles are difficult to fluidize with a gas stream, because particles agglomerate together and channelling occurs (Clarke et al. 2005, Wright and Raper, 1998). They

are often typical of Geldart group C particles (Geldart, 1973) which are cohesive and tend to fluidize poorly. Generally for moist particles in gas-fluidized beds, moisture affects fluidization behaviour by introducing interparticle forces (Seville et al., 2000). The addition of liquid to a fluidized bed can shift the fluidization behaviour of the particles from Geldart group A or B to group C (Seville et al., 2000).

Sawdust particles were employed in gas-solid fluidized bioreactors of previous studies (Clarke et al., 2007 and Delebarre et al., *2007*). Delebarre et al. (2007) used a gas-solid fluidized bed of pure sawdust to treat ethanol and toluene emissions. Moisture content in the sawdust bed was difficult to control which led to variability in the microbial cells on the sawdust and bioreactor performance (Delebarre et al., 2007). A mixture of sawdust (d_p of 0.625 mm) and glass spheres (d_p of 0.516 mm) was used in a gas-solid fluidized bioreactor to treat VOC contaminated air (Clarke et al., 2007). The glass spheres prevented agglomeration of sawdust particles during fluidization (Clarke et al., 2005). The sawdust and glass sphere mixture was maintained in a state of bubbling/slugging fluidization in which large bubbles would periodically grow to form slugs that were nearly as large as the column diameter. Poor bioremediation rates suggested that there were few microbial cells on the glass spheres and that the majority of the bioremediation activity took place on the sawdust particles. In a subsequent study, moist peat granules were tested in a fluidized bed bioreactor (Clarke et al., 2008). A bed of peat granules was capable of supporting more microorganisms and producing superior bioremediation rates, while also exhibiting good fluidization behaviour even when the particles were moist. A fundamental understanding of fluidization properties of moist peat granules is needed in order to move forward with design and scale-up of this promising technology.

Various forms of peat particles have been used successfully in biofilters as a packing material for the treatment of VOCs; Chan and Lu (2003) prepared a packing of 2.4 to 6 mm composite particles of polyvinyl alcohol and peat, and Bibeau et al. (2000) used 5 to 10 mm diameter peat balls. In addition, non-granulated peat fuel has been used in fluidized drying and gasification processes for producing power and ammonia (Fagernas, 1993 and Koljonen et al., 1993). In the literature there is a deficiency of reports on the fundamental fluidization properties of moist peat granules including minimum fluidization velocity (u_{mf}) and pressure drop *versus* superficial gas velocity profiles. In general for biomass particles, methods of predicting fluidization properties such as u_{mf} are needed (Cui and Grace, 2007). Relative to other biomass

particles such as sawdust and straw, peat granules are denser and more spherical. Thus, conventional correlations of u_{mf} may work better for peat granules than for other biomass. For non-biomass particles greater than 100 μm in a single component fluidized bed, the most widely used empirical correlation for u_{mf} is by Wen and Yu (1966), valid when $0.001 < Re_{p,mf} < 4000$:

$$\mathrm{Re}_{p,mf} = \left(33.7^2 + 0.0408Ar\right)^{1/2} - 33.7 \tag{5.1}$$

Chitester et al. (1984) propose a variation of this correlation for fluidized systems at pressures above atmospheric, which worked well for coarse particles as large as 688 μm, when $0.01 < Re_{p,mf} < 100$:

$$\mathrm{Re}_{p,mf} = \left(28.7^2 + 0.0494Ar\right)^{1/2} - 28.7 \tag{5.2}$$

For biomass particles when Equations 5.1 and 5.2 have failed, correlations for specific types of biomass particles have been proposed. For instance, Suarez and Beaton (2003) suggest the following correlation for predicting u_{mf} of Cuban coffee husks:

$$\mathrm{u}_{\mathrm{mf}} = 0.19\mathrm{e}^{305\mathrm{d}_{\mathrm{p}}} \tag{5.3}$$

In the present work, a bed of peat granules was used in a gas-solid fluidized vessel. In a series of fluidization experiments, several size distributions and sizes of peat granules, with varying moisture contents and bed heights were assessed for their fluidization properties. Experimental u_{mf} was compared to existing correlations.

5.3 Materials and Methods

5.3.1 Apparatus

Peat granules were fluidized in an acrylic, cylindrical, bench-scale vessel, with an inside diameter of 0.14 m (Figure 5.1). The vessel height above the distributor plate is 1.81 m, and below the distributor there is a windbox, 0.162 m in height. The perforated-plate distributor has 1 mm holes on a square pitch, with a 5.1% open area. A 100 mesh size wire screen over the distributor prevents bed particles from plugging the distributor holes. Ambient air was supplied with a blower, and air velocity was measured using an orifice plate.

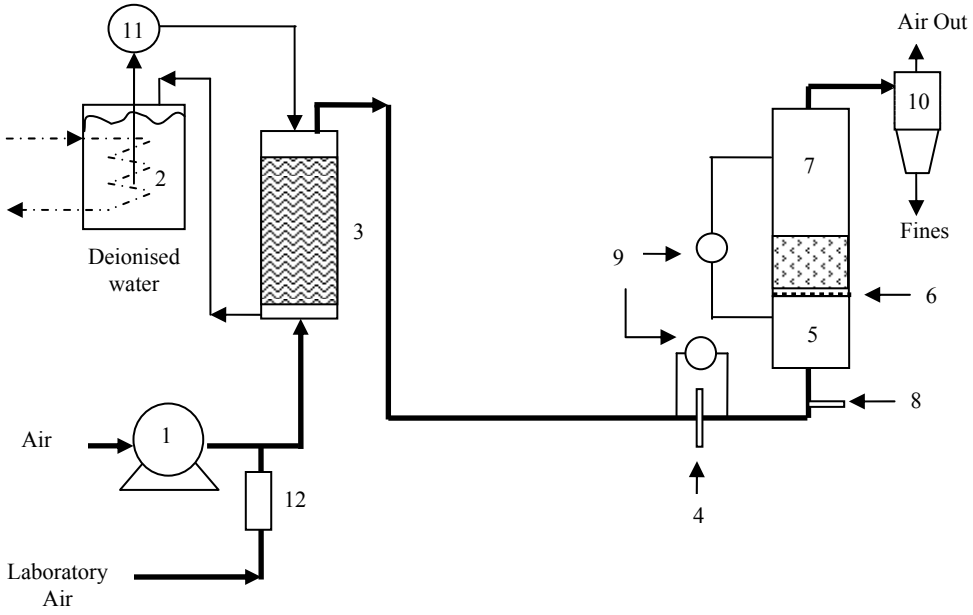

Figure 5.1 Experimental apparatus: (1) blower; (2) water storage (3) humidifier; (4) orifice plate; (5) wind-box; (6) distributor and wire screen; (7) bioreactor vessel; (8) humidity and temperature probe; (9) differential pressure transducers; (10) cyclone; (11) pump (12) rotameter.

During experiments involving moist peat granules, the air entering the bioreactor was saturated with water to prevent the particles from drying out. The air was humidified by passing it through a 0.24 m diameter counter-current humidification column containing a packed bed of PVC rings. Humidity and temperature of the inlet air to the fluidized bed were continuously measured with a HMP 230 series probe by Vaisala (Helsinki, Finland). The pressure drop across the orifice plate and the combined pressure drop across the distributor and fluidized bed were measured with differential pressure transducers. A model MC1-333 data acquisition board by Validyne Engineering (Northridge, CA) was used for data collection from the differential pressure transducers and the humidity and temperature probe. Continuous data logging was carried out using LabVIEW^{TM} software (National Instruments. Austin, TX).

5.3.2 Particle Characterization

BioAPT peat granules (10 to 42 mesh), manufactured from low-ash reed sedge peat were obtained from American Peat Technology LLC (Aitkin, MN). Three narrower particle size distributions were created by sieving with Tyler Series equivalent sieves. Material 1 contained

particles that passed through 12 mesh (1.41 mm) and were retained on 42 mesh (354 μm), material 2 passed through 16 mesh (1.00 mm) and was retained on 32 mesh (500 μm), and material 3 passed through 24 mesh (710 μm) and was retained on 32 mesh (500 μm).

The physical properties of mean size, size distribution, and density were determined for materials 1, 2, and 3. A Mastersizer S-Series Long Bench particle size analyzer by Malvern Instruments Inc. (Malvern, Worcestershire, UK) was used to find the number volume mean diameter and the particle size distribution. The Sauter mean diameter is calculated from the number volume mean by the Malvern software. Helium intrusion, with an Ultrapycnometer 1000, by Quantachrome Instruments (Boynton Beach, FL) was used to measure skeletal density. Skeletal density was determined for material 3 and assumed to be the same for materials 1 and 2. Bulk density was determined by measuring the mass of a known volume of particles placed inside a graduated cylinder, and maximum bulk density was found by tapping the graduated cylinder until a minimum volume was reached. Particle density of the porous peat granules was estimated from the particle density ($\rho_{p,Non\text{-}porous}$) and maximum bulk density ($\rho_{b,max,Non\text{-}porous}$) of non-porous, 0.52 mm glass sphere particles by the method of Abrahamsen and Geldart (1980). This method assumes that the minimum fraction of interparticle voids (voids at $\rho_{b,max}$) for non-porous and porous particles is the same as long as the particles are of similar shape within a narrow size range. Particle density is calculated by:

$$\rho_{p,Porous} = \frac{\rho_{b,\max,Porous}}{\rho_{b,\max,Non-porous}} \rho_{p,Non-porous} K \tag{5.4}$$

where K is assumed to be 1 and the particle density and maximum bulk density of glass spheres are 2481 and 1460 kg m^{-3} respectively.

The fraction of interparticle voids in a packed bed of peat granules is found from Equation 5.5:

$$\varepsilon_m = 1 - \frac{\rho_B}{\rho_p} \tag{5.5}$$

Also, porosity of peat granules is calculated as follows:

$$\varepsilon_p = 1 - \frac{\rho_P}{\rho_s} \tag{5.6}$$

The sphericity, ϕ_s, was established from packed bed data of pressure drop *versus* velocity, by the method outlined in Kunii and Levenspiel (1991), using Equation 5.7:

$$\Delta p_{bed} = L_m \left[\frac{150\mu(u_o)(1-\varepsilon_m)^2}{\varepsilon_m^3 (\phi_{s,eff} d_p)^2} + 1.75 \frac{1-\varepsilon_m}{\varepsilon_m^3} \frac{\rho_g u_o^2}{\phi_{s,eff} d_p} \right] \quad (5.7)$$

where $\phi_{s,eff} \sim \phi_s$

.

Moisture content in peat particles was measured with a Mettler Toledo (Columbus, OH) HB43 halogen moisture analyzer.

5.3.3 Fluidization of Peat Granules

Materials 1, 2 and 3 peat granules were fluidized in the apparatus under different experimental conditions. The moisture content of the peat was varied between 14 and 63 wt% (dry basis) and static bed height was varied between 7 and 14 cm. The particle bed pressure drop and superficial gas velocity were recorded as flowrate to the vessel was gradually increased from the packed bed state. The minimum fluidization velocity was measured, and at the same time the quality of fluidization behaviour was assessed by observation. The minimum fluidization velocity was determined as the point of intersection of the fixed bed pressure drop versus velocity line (at increasing velocity) and the initial bed weight per bed cross-sectional area (horizontal line), similar to the approach of Kunii and Levenspiel (1991).

5.4 Results and Discussion

A bed of peat granules exhibited favourable fluidization behaviour unlike the earlier results with sawdust. It was possible to fluidize peat in a bubbling regime without gas channelling or particle agglomeration, depending on the moisture content, particle size and particle size distribution. Particle characterization of three sizes of peat granules is presented in Table 5.1, and particle size distributions are shown in Figure 5.2. For comparison purposes, Table 5.1 also shows characteristics of sawdust particles reported in a previous study (Clarke et al., 2005). Particle density of peat particles is notably much greater than that of sawdust, and peat granules are more spherical. The porosity of peat granules is much lower than sawdust, while interparticle bed voidage is similar.

Table 5.1 Particle characterization of peat granules and sawdust at selected moisture levels.

Particles	Moisture content (% dry basis)	Particle size[a] d_p (μm)	Bulk density ρ_b (kg m^{-3})	Maximum bulk density $\rho_{b,max}$ (kg m^{-3})	Skeletal density[a] ρ_s (kg m^{-3})	Particle density ρ_p (kg m^{-3})	Packed bed voidage ε_m	Porosity ε_p	Sphericity ϕ_s
Material 1	38	1189	620	660	1581	1120	0.45	0.29	0.82
Material 2	53	895	581	685	1581	1160	0.5	0.26	0.77
Material 3	40	680	680	740	1581	1240	0.45	0.22	0.87
Sawdust[b]	54	625	195		1543	469	0.58[c]	0.7[c]	0.44

[a] Determined using dry particles
[b] Reported in Clarke et al. (2005)
[c] Calculated from Equations 5.5 and 5.6

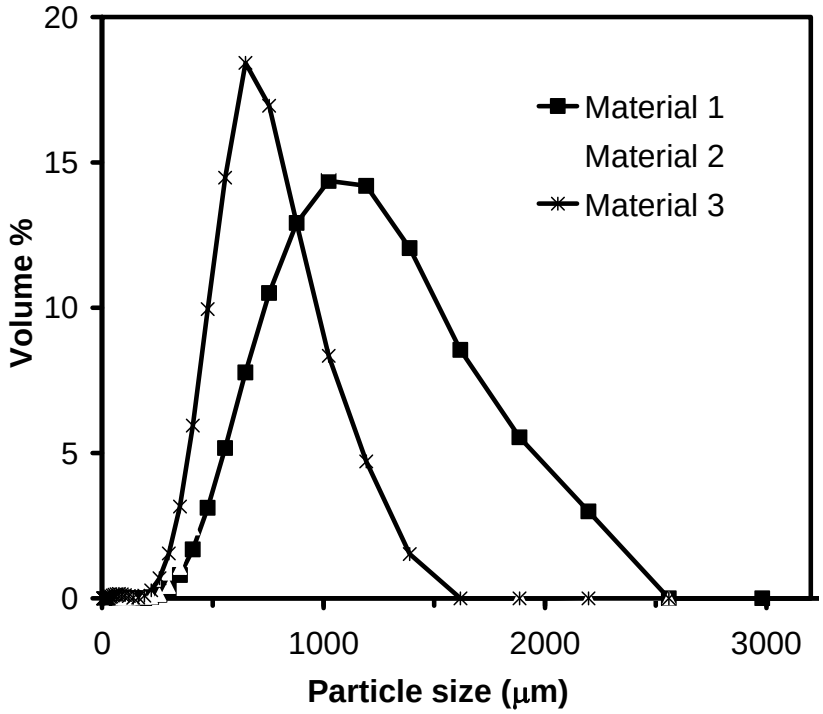

Figure 5.2 Particle size distribution of material 1 (38 wt% moisture), material 2 (53 wt% moisture) and material 3 (40 wt% moisture).

Materials 1, 2 and 3 with varying moisture contents were fluidized and the results are summarized in Table 5.2. Figure 5.3 illustrates bed pressure drop versus superficial gas velocity profiles for materials 1, 2, and 3 at selected moisture contents. Although solid plug formation was not observed with material 2, Figure 5.3 indicates that pressure drop increases greater than the bed weight per unit area at velocities just above minimum fluidization velocity (u_{mf}). This pressure overshoot is likely due to friction between the particle bed, and the distributor plate and the walls of the vessel. Material 1, which has a wider particle size distribution and contains the largest particles, has the highest u_{mf}. The observed bubble size during fluidization of material 1 was large compared to the other peat. There is evidence that narrower particle distribution and smaller particles helps to reduce the size of the bubbles. This is an important feature; Levenspiel (1999) suggests that larger bubbles reduce reaction conversion in bubbling fluidized beds. Overall, material 3 had the most superior fluidization properties. It fluidized in a bubbling regime without plug formation or gas channelling at moisture contents of 40 wt% (dry basis) or lower. In addition, u_{mf} is lowest for material 3 at moistures of 53 wt% or lower.

Figure 5.4 indicates that at static bed heights between one half and one times the bed diameter, bed height had very little effect on fluidization behaviour of material 3 at a moisture content of 15 wt%. Material 3 with a moisture content of 53 wt% was also fluidized at bed heights between 0.67 and 1 times the bed diameter, and no change in fluidization behaviour was observed at the different heights.

Table 5.2 Fluidization of peat granules.

Peat granules[a]	Moisture content, wt% dry basis	u_{mf} (m s^{-1})	Observed fluidization quality
Material 1	14	0.49	Good bubbling at all velocities
	38	0.48	Solid plug formation above u_{mf} when bed is initially fluidized; bubbling with large bubbles
	46	0.47	Solid plug formation; bubbling with large bubbles
Material 2	53	0.34	Good bubbling; bubbling/slugging above 0.6 m s^{-1}
Material 3	15	0.20	Bubbling bed at all velocities
	26	0.20	Bubbling bed at all velocities
	40	0.21	Bubbling bed; bubbling/ slugging above 0.55 m s^{-1}
	53	0.18	Solid plug formation above u_{mf} when bed is initially fluidized; bubbling; bubbling/slugging above 0.55 m s^{-1}
	63	0.29-0.41	Plug formation; bed channelling; bubbling/ slugging at higher velocities

[a]Sieve sizes: material 1 = 354 to 1410 μm; material 2 = 500 to 1000 μm; material 3 = 500 to 710 μm.

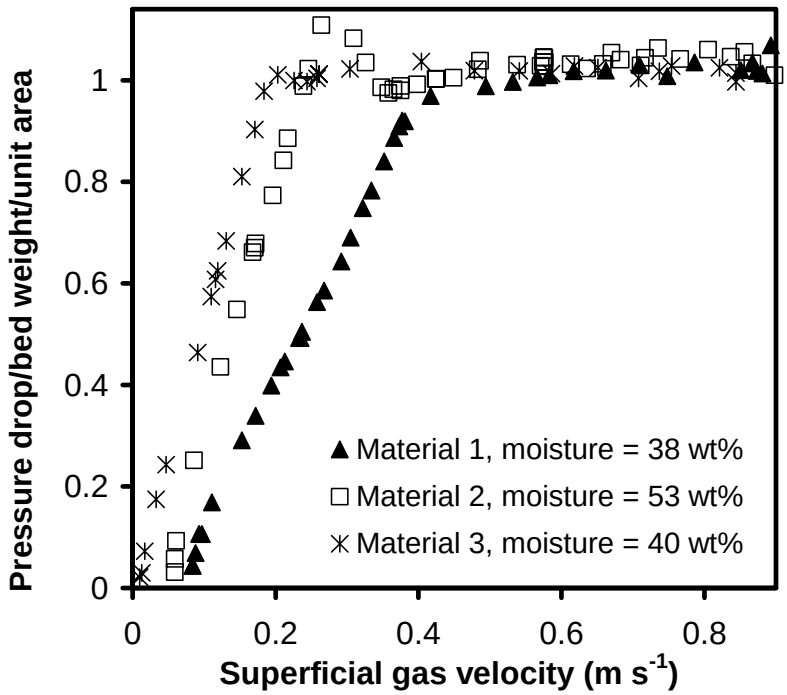

Figure 5.3 Pressure profiles of peat granules at increasing superficial gas velocity (static bed height is 9 cm for material 1, and 14 cm for materials 2 and 3).

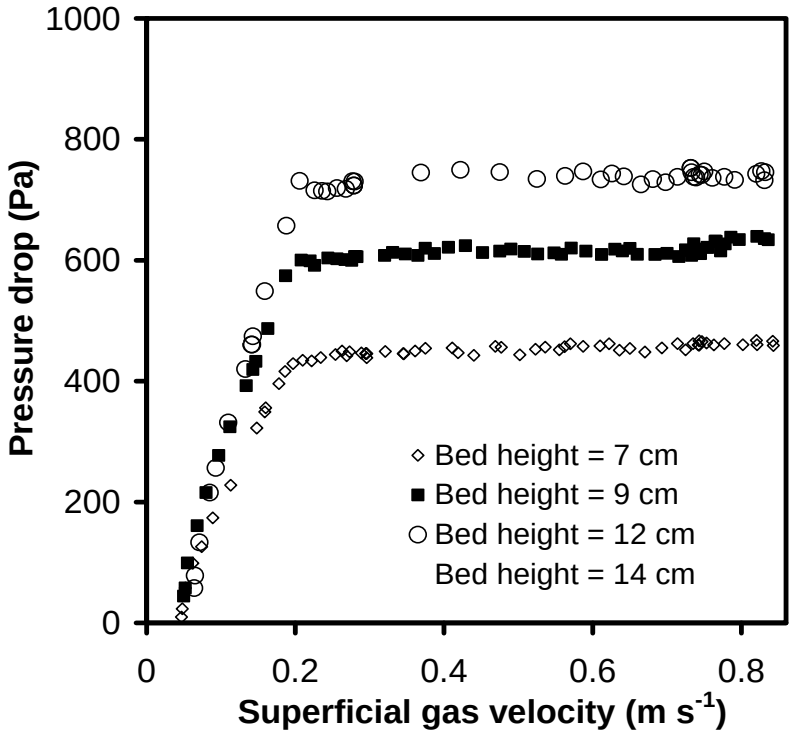

Figure 5.4 Pressure profiles of material 3 at increasing superficial gas velocity at different static bed heights (moisture content = 15 wt%).

At moisture contents of 53 wt% or less, based on particle size and density, material 1 is Geldart group D, while materials 2, and 3 fall into Geldart group B. Increasing the moisture content of material 3 resulted in a transition from good bubbling behaviour at all velocities to bubbling at lower velocities and slugging at velocities more than three times the u_{mf}. At 63 wt% moisture, material 3 particles agglomerated, and poor fluidization characteristics were observed such as the formation of channels in the bed, typical of Geldart group C particles. A likely explanation is that when moisture content reaches a value between 53 and 63 wt%, no more water can be absorbed within the peat granules, and the excess exists as free water on the surface of the particles. The surface moisture leads to liquid bridging and a tendency for the particles to agglomerate. Figure 5.5 shows bed pressure drop versus velocity profiles of material 3 at different moisture levels. Material 3 with a moisture content of approximately 40 wt% was selected for use in the bioremediation experiments because these particles fluidized well in a bubbling regime at velocities above u_{mf}. It is important to remain in the bubbling regime since solid plug flow and channelling in a fluidized reactor will tend to reduce reaction conversion in a gas fluidized bed bioreactor

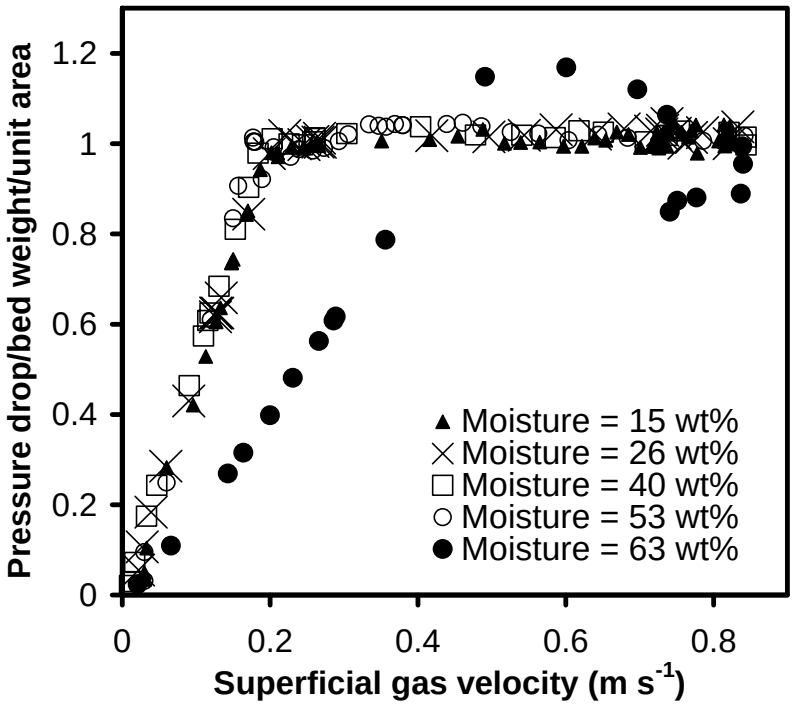

Figure 5.5 Pressure profiles of material 3 peat granules at increasing superficial gas velocity, at different moisture contents (static bed height = 14 cm).

In a fluidized bioreactor, peat granules have several advantages over the sawdust/glass sphere mixture used in our previous study (Clarke et al., 2007). Peat granules fluidize well in a bubbling bed regime without the addition of a second inert particle. The peat granules hold more moisture which helps to sustain microorganisms in the bioreactor, but can still be more effectively fluidized. The peat, with a moisture content of 40 wt% (dry basis), actually holds 200 kg m^{-3} moisture per packed bed volume *versus* 20 kg m^{-3} in the sawdust/glass sphere packing. Also, the u_{mf} of material 3 peat (0.21 m s^{-1} at 40 wt% moisture) was much lower than that of the moist sawdust/glass sphere mixture (0.39 to 0.48 m s^{-1}) (Clarke et al., 2007). A lower u_{mf} is an advantage in a fluidized bioreactor because it allows a wider range of inlet gas flowrates and contaminant concentrations to be treated. Note that the capacity of a biofilter for bioremediation, per unit packed bed volume, generally depends on the loading of the pollutant and not on the pollutant concentration in the waste gas stream (Deshusses and Johnson, 2000). Loading is defined as the pollutant feed rate per packed bed volume. Thus if the particles of a fluidized bioreactor can be fluidized at lower velocities, higher concentrations of pollutants can be treated per unit packed bed volume.

In order to predict u_{mf}, the correlations of Wen and Yu and Chitester et al. (Equations 5.1 and 5.2) and Equation 5.3 were applied to material 3 peat and to sawdust particles used in our previous study (Clarke et al., 2005). The results are summarized in Table 5.3. Experimental u_{mf} of peat granules was found to fall between the values predicted with Equations 5.1 and 5.2, while the u_{mf} of the sawdust particles was severely underestimated. Therefore, unlike the case with other biomass particles such as sawdust, traditional correlations are reasonable predictors of u_{mf} for peat granules. Equation 5.3 which was derived from experimental data specific to the fluidization coffee husk particles is clearly inadequate when applied to either material 3 or sawdust.

Table 5.3 Predicted minimum fluidization velocity of material 3 peat and sawdust.

Correlation	Peat granules (40 wt% moisture) u_{mf} (m s^{-1})	Sawdust (54 wt% moisture) u_{mf} (m s^{-1})
Wen and Yu (1966)	0.17	0.06
Chitester *et al*., (1984)	0.22	0.08
Suarez and Beaton (2003)	0.23	0.23
Experimental results	0.21	0.43[a]

[a]Reported in Clarke *et al*. (2005).

5.5 Conclusions

Peat granules are an ideal candidate as packing material for a gas-solid fluidized bed bioreactor. Peat with a particle diameter of 680 μm and a moisture content of 40 wt%, exhibited group B bubbling fluidization behaviour. High moisture contents around 63 wt% result in gas channelling. The fluidization of larger peat granules leads to plug flow of the particle bed, or the formation of large bubble sizes which may reduce reaction conversion. It is observed that the particle density of peat granules (1120 to 1240 kg m^{-3}) is high compared to other biomass particles such as sawdust (469 kg m^{-3}) and the shape of the peat granules is much more spherical than sawdust. These property characteristics contribute to effective bubbling fluidization behaviour even when the peat granules are moist. Furthermore, the peat granules are able to absorb a high amount of moisture compared to sawdust, such that they can more readily support microbial cells. Finally, it has been found that traditional correlations for gas-solid fluidization can be used to predict u_{mf} of the peat granules, rather than having to use an experimental correlation specific for peat granules. The reason for this finding is likely because the shape and density of 680 μm peat granules differs from that of other types of biomass particles, and similar

to a representative Geldart group B particles such as sand, peat fluidizes well in a bubbling regime.

5.6 Nomenclature

Ar Archimedes number, $\frac{d_p^3 \rho_g (\rho_p - \rho_g) g}{\mu^2}$

d_p Sauter mean particle diameter (μm)

K Experimentally determined factor

L_m Packed bed height (m)

$Re_{p,mf}$ Particle Reynolds number at minimum fluidization, $\frac{d_p u_{mf} \rho_g}{\mu}$

u_o Superficial gas velocity (m s^{-1})

u_{mf} Superficial gas velocity at minimum fluidization (m s^{-1})

Greek letters

Δp_{bed} Pressure drop across a bed of particles (Pa)

ε_m Fraction of interparticle voids in a packed bed of particles

ε_p Porosity or fraction of pore volume in particles

$\phi_s, \phi_{s,eff}$ Sphericity and effective sphericity of a particle

μ Gas viscosity (kg $m^{-1}s^{-1}$)

$\rho_b, \rho_{b,max}$ Bulk and maximum bulk density of particles (kg m^{-3})

ρ_g Gas density (kg m^{-3})

ρ_p, ρ_s Particle or envelope density (including particle pore volume), skeletal density (excluding particle pore volume) (kg m^{-3})

5.7 References

Abrahamsen, A.R.; Geldart, D. Behaviour of gas-fluidized beds of fine powders part I. Homogeneous expansion. *Powder Tech*. **1980**, *26*, 35-46.

Aznar, M.P.; Gracia-Gorria, F.A.; Corella, J. Minimum and maximum velocities for fluidization for mixtures of agricultural and forest residues with a second fluidized solid. I. Preliminary data and results with sand-sawdust mixtures. *Int. Chem. Eng.* **1992**, *32* (1), 95-102.

Bibeau, L.; Kiared, K.; Brzezinski, R.; Viel, G.; Heitz, M. Treatment of air polluted with xylenes using a biofilter reactor. *Water Air Soil Pollut*. **2000**, *118*, 377-393.

Chan, W.C.; Lu, M.C. A new type synthetic filter material for biofilter: poly(vinyl alcohol)/peat composite bead. *J. Appl. Polym. Sci*. **2003**, *88*(14), 3248-3255.

Chitester, D.C.; Kornosky, R.M.; Fan, L.S.; Danko, J.P. Characteristics of fluidization at high pressure. *Chem. Eng. Sci*. **1984**, *39*, 253-261.

Clarke, K.L.; Pugsley, T.; Hill, G.A. Fluidization of moist sawdust in binary particle systems in a gas-solid fluidized bed. *Chem. Eng. Sci*. **2005**, *60*, 6909-6918.

Clarke, K.L.; Hill, G.A.; Pugsley, T. Direct comparison of fluidized and packed bed bioreactors for bioremediation of an air pollutant. *Int. J. Chem. Reactor Eng*. **2007**, *5*(Article A11), 1-12.

Clarke, K.L.; Hill, G.A.; Pugsley, T. Improved VOC bioremediation using a fluidized bed peat bioreactor. *Trans. I. Chem. E., Part B Process Saf. Environ. Protect*. **2008**, *86*, 283-290.

Cui, H.; Grace, J.R. Fluidization of biomass particles: A review of experimental multiphase flow aspects. *Chem. Eng. Sci*. **2007**, *62*, 45-55.

Delebarre, A.; Andres, Y.; Pellerano, M.; Pero, P.; Garcia Munzer, D.G., 2007, Biofiltration of volatile organic compounds by a fluidized bed of sawdust. *Int. J. Chem. Reactor Eng*. **2007**, *5*(Article A22), 1-11.

Deshusses, M.; Johnson, C. Development and validation of a simple protocol to rapidly determine the performance of biofilters for VOC treatment. *Environ. Sci. Technol*. **2000**, *34*(3), 461-467.

Fagernas, L. Formation and behaviour of organic compounds in biomass dryers. *Bioresour. Tech.* **1993**, *46*, 71-76.

Geldart, D. Types of gas fluidization. *Powder Tech.* **1973**, *7*, 285-292.

Kennes, C.; Thalasso, F. Waste Gas Biotreatment Technology. *J. Chem. Technol. Biotechnol.* **1998**, *72*, 303-319.

Koljonen, J.; Kurkela, E.; Wilen, C. Peat-based HTW-plant at Oulu. *Bioresour. Tech.* **1993**, *46*, 95-101.

Kunii, D.; Levenspiel, O. Fluidization Engineering, Second Ed.; Butterworth-Heinemann: Newton, MA, 1991, pp 1-12; 64-80.

Levenspiel, O. Chemical Reaction Engineering, Third Ed.; John Wiley and Sons: New York, 1999, pp 447-465.

Seville, J.P.K.; Willet, C.D.; Knight, P.C. Interparticle forces in fluidisation: a review. *Powder Tech.* **2000**, *113*, 261-268.

Suarez, J.A.; Beaton, P.A. Physical properties of Cuban coffee husk for use as an energy source. *Energ. Source*. **2003**, *25*, 953-959.

Wen, C.Y.; Yu, Y.H. A generalized method for predicting the minimum fluidization velocity. *AIChE Journal.* **1966**, *12*, 610-612.

Wright, P.C.; Raper, J.A. Investigation into the viability of a liquid-film three-phase spouted bed biofilter. *J. Chem. Technol. Biotechnol.* **1998**, *73*, 281-291.

CHAPTER 6 – Modelling Biodegradation in a Fluidized Bed Bioreactor

This manuscript is being prepared for submission to the ***Biochemical Engineering Journal***.

Clarke, K.L.; Hill, G.A., and Pugsley, T.; Modelling biodegradation in a fluidized bed bioreactor. *Biochem. Eng. J.*, prepared for submission, **2008**.

Contribution of Ph.D. candidate

Experiments were planned by Kyla Clarke, Gordon Hill and Todd Pugsley, and were performed by Kyla Clarke. The submitted manuscript was written by Kyla Clarke, while Gordon Hill and Todd Pugsley provided editorial guidance.

Contribution of this paper to the overall study

This chapter presents a modelling study of a fluidized bioreactor. This Ph.D. research set out to design a gas-solid fluidized bioreactor for treating air emissions. Chapters 2 to 4 dealt with the design and testing of a bench-scale fluidized bioreactor. Chapter 5 investigated detailed fluidization information which is required for the scale-up of this technology. In addition, for the design of an industrial-scale fluidized bioreactor, it is important to be able to predict bioremediation performance. In the following work, a model is developed which predicts the outlet concentration from the bioreactor. The model shows the effect of different operating parameters and types of packing on the removal efficiency and bioremediation rates in a fluidized bioreactor.

Additional experimental details not in the manuscript

In this chapter, bubbling and packed bed bioreactors are modelled. In these models, the particulate region gas is assumed to be in non-dispersed, plug flow, following the approach of Kunii and Levenspiel (1990) for bubbling reactors and most authors for packed bed biofilters (Devinny and Ramesh, 2005). Further experimentation is required to determine whether the limiting case of non-dispersed plug flow or completely mixed gas phase is more applicable. The following is a model derivation of the limiting case of a completely mixed particulate region gas phase for the bubbling and packed bed bioreactors which should be read after reading the manuscript material.

Bubbling bed fluidized bed model, completely mixed case

In this case, the concentration of ethanol in the gas phase of the particulate region at any height is equal to the ethanol concentration in the gas leaving the particulate region, as illustrated by Figure 6.01. A steady-state material balance of ethanol in the gas phase of the particulate region is completed over the entire bed height during fluidization (H). The material balance includes the advective flow of gas in and out of the gas phase of the particulate region, bulk flow exchange of gas between the bubbles and the particulate region, and finally the overall rate of disappearance of ethanol ($-r_c$) from the gas phase of the particulate region by absorption into the biofilm. The mass balance in units of mass of ethanol per unit time per volume of bioreactor bed during fluidization is:

$$\frac{u_{mf}}{H}(C_o - C_p) + \frac{Nq}{H}\int_0^H C_b dz - C_p qN - r_c = 0 \tag{6.01}$$

Equation 6.21 is substituted for C_b:

$$\frac{NV_b u_b}{H}(C_o - C_p)\left[1 - \exp\left(-\frac{qH}{u_b V_b}\right)\right] + \frac{u_{mf}}{H}(C_o - C_p) - r_C = 0 \tag{6.02}$$

Let:

$$\gamma = \frac{NV_b u_b}{H}\left[1 - \exp(-\alpha)\right] + \frac{u_{mf}}{H} \tag{6.03}$$

where α is defined by Equation 6.23.

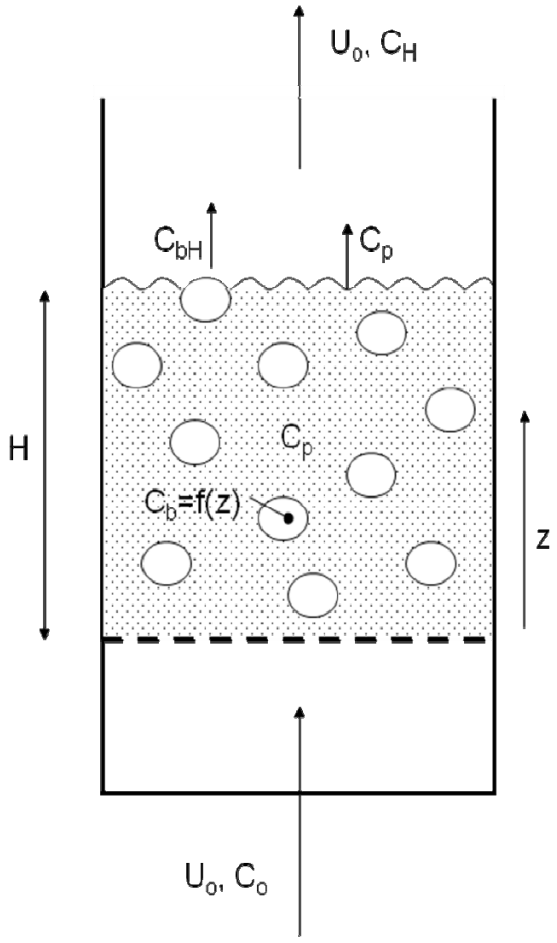

Figure 6.01 Bubbling fluidized bed model, with completely-mixed gas phase.

With first order kinetics, C_p is isolated, and Equation 6.02 becomes:

$$C_p = \frac{C_o}{1 + K/\gamma} \tag{6.04a}$$

C_{bH} is calculated from Equation 6.21 for the top of the bed ($z=H$) and the concentration of ethanol in the gas exiting the bioreactor (C_H) is calculate from Equation 6.31, where $C_p=C_{pH.}$

Conversion of ethanol (X_e) with first order kinetics is equal to:

$$X_e = 1 - \frac{C_H}{C_o} = 1 - \left[\beta \exp(-\alpha) + \frac{1 - \beta \exp(-\alpha)}{1 + K/\gamma} \right] \tag{6.05a}$$

Where:

$$\beta = 1 - \frac{u_{mf}}{u_o} \tag{6.06}$$

For zero order kinetics, the expressions for C_p and X_e are:

$$C_p = C_o - \frac{K_0 f_l}{\gamma} \tag{6.04b}$$

$$X_e = 1 - \left[\beta \exp(-\alpha) + \frac{\left(1 - \beta e^{-\alpha}\right)\left(C_o - \frac{K_0 f_l}{\gamma}\right)}{C_o} \right] \tag{6.05b}$$

Packed bed model, completely mixed case

For complete mixing and first order kinetics, the outlet gas phase ethanol concentration is equal to the concentration throughout the bioreactor:

$$C_p = \frac{C_o}{1 + \frac{KH_m}{u_o}} \tag{6.07}$$

where H_m is the packed bed height.

For zero order kinetics the concentration of ethanol in the gas exiting the bioreactor is given by Equation 6.46:

Biokinetic parameters:

Biokinetic parameters were estimated for the peat bed bioremediation experiments by the same method as in Chapter 3. A biomass calibration was obtained for the predominant cell line (*Pichia* spp.) and is presented in Figure A.11, Appendix A. Batch, shake flask culture experiments were completed. Cells of *Pichia* spp. were removed from an agar plate and used to make an inoculant culture. A 4 mL aliquot of inoculant culture was added to a shake flask containing initially 1900 g m^{-3} of ethanol in 125 mL of nutrient medium. Experimental

measurements of ethanol and biomass were not taken between 28 and 48 hours after inoculation (the college was closed due inclement weather). However, there is sufficient experimental data for estimating kinetic parameters. Yield was calculated from Equation 1.13, and the remaining biokinetic parameters were determined by fitting the experimental growth data to the Monod and Haldane models (Equations 1.8, 1.9, 1.10, and 1.11). These differential equations were solved numerically with a fourth-order Runge-Kutta method. Then K_s, K_I, and μ_m are adjusted with a forward derivative, Newton method in the software Microsoft Excel, while using a sum of least squares method to fit the experimental data to the Monod and Haldane growth models. The growth parameters are summarized in Table 6.01. A more accurate determination of the saturation constant (K_s) requires many data points on the growth curve, at the transition from the exponential growth phase to the stationary phase. However, it is unlikely that for microbial growth on the same substrate (ethanol) as in Chapter 3 that K_s would be significantly different. Therefore, the same K_s which was reported in Chapter 3 for the Monod model was chosen when finding the best fit of the experimental data. Other values of K_s were also tested, but they produced poorer growth curves. Figures 6.02 and 6.03 compare the experimental results to the Monod and Haldane growth models. For the prediction of biomass concentration, the standard error of the estimate was +/- 12.3 and 14.2 g m^{-3} for the Monod and Haldane models respectively.

Table 6.01: Biokinetic growth parameters

Kinetic Parameter	Monod model	Haldane model
Initial biomass X_o (g m^{-3})	50	50
Initial substrate S_o (g m^{-3})	1750	1750
μ_m (h^{-1})	0.098	0.111
K_s (g m^{-3})	0.5	0.5
K_I (g m^{-3})	N/A	11,900
Y_{xs}	0.54	0.54

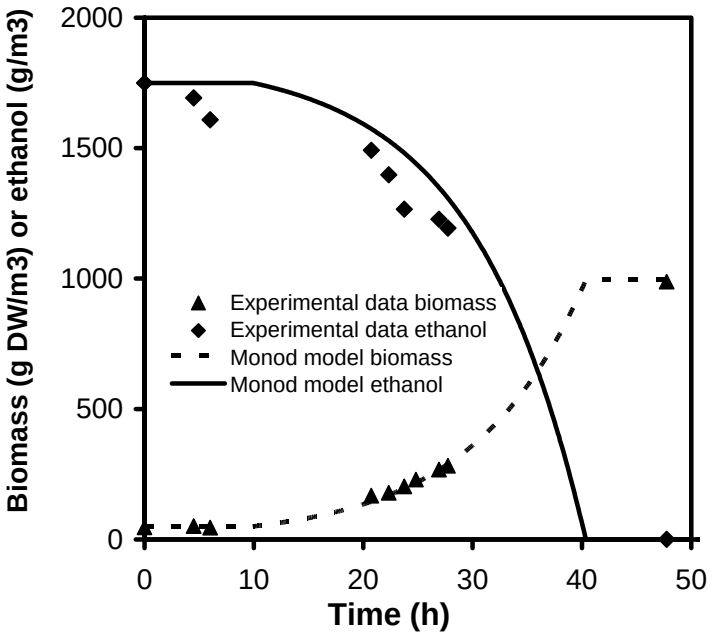

Figure 6.02 Experimental growth curve fitted to the Monod model.

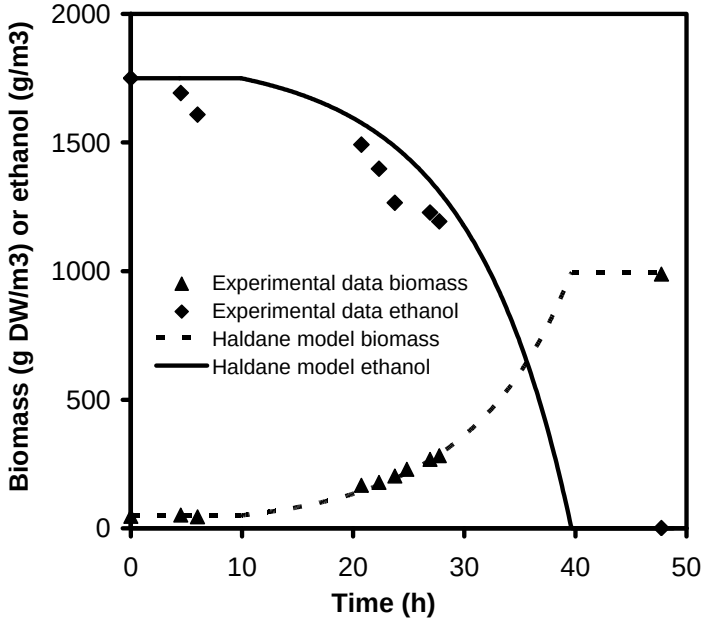

Figure 6.03 Experimental growth curve fitted to the Haldane model.

Manuscript

6.1 Abstract

A steady state, one-dimensional model is developed to describe biodegradation of a volatile organic compound (VOC) in a gas-solid fluidized bioreactor. For comparison purposes, biodegradation in a packed bed bioreactor is also modelled. The models are used to predict outlet concentrations of a VOC substrate (ethanol) and the estimates are compared to experimental data. The fluidized bioreactor model includes properties of the bubbles such as rise velocity, size and gas exchange rate with the particulate region surrounding the bubbles. The overall rate of biodegradation is modelled with the two limiting cases of zero and first order kinetics with respect to the substrate, which depend on whether the overall resistance is limited by microbial growth or mass transport. The models highlight how maximum elimination capacity and removal efficiency are influenced by bubble properties, residence time, maximum specific growth rate of the microorganisms, and microbial population.

6.2 Introduction

A gas-solid fluidized bioreactor (GSFB) has recently been proposed as a novel method for treating air contaminated with volatile organic compounds (VOCs) (Clarke et al., 2007; Clarke et al., 2008; Delebarre et al., 2007). Emissions of VOCs such as benzene and toluene can be damaging to the environment and human health. In the United States, VOC emissions totalled 19.4 million tons in 2002 (EPA, 2008). Therefore there is a need for low-cost, efficient methods for treating VOC emissions.

The GSFB contains a bed of particles which serve as a support for microbial cells. Microorganisms biodegrade VOCs that enter the bioreactor in the polluted air. The polluted air stream has a sufficiently high velocity to fluidize the particle bed in a bubbling or another type of dense phase fluidization regime. Compared to a packed bed, the advantages of fluidization include homogeneous conditions in the bed due to the rapid and uniform mixing of the solids,

and high heat and mass transfer between the fluid and the particles (Kunii and Levenspiel, 1991). These are important features for capturing and bidegrading air pollutants on microbial carrier particles. The GSFB is a departure from commercial, packed bed bioreactors (biofilters) for treating air emissions. The essential difference between the GSFB and biofilters is that in the GSFB the air stream is fast enough to fluidize the bed so it is no longer in the packed bed state. Goals behind the development of the GSFB include improving the efficiency of biofiltration and eliminating the bed clogging problems of biofilters. The GSFB has been used in biodegradation studies to treat ethanol emissions, and has achieved high biodegradation rates (Clarke et al., 2008). In a GSFB, 1520 g m^{-3} h^{-1} of ethanol was biodegraded (based on packed bed bioreactor volume) with removal efficiencies ranging between 45 to 100%, at inlet ethanol loadings up to 3400 g m^{-3} h^{-1} (Clarke et al., 2008).

In order to scale up the GSFB for industrial use, an improved understanding of the important design parameters of biodegradation can be obtained by modelling the bioreactor. Numerous approaches have been used to model biofilters (Devinny and Ramesh, 2005), however the topic of modelling biodegradation in gas-solid fluidization is new.

Biofiltration models often depict contaminated air passing through a bed of particles, governed by advection and dispersion, while contaminants transfer from the gas phase to a liquid biofilm phase on the particles (Devinny and Ramesh, 2005). Additionally, the contaminants diffuse in the biofilm where microbes absorb the contaminant and utilize it for energy. Concurrently, oxygen and other nutrients dissolve into the biofilm liquid and diffuse to the microbes. The liquid biofilm layer may grow in size, and deep sections of it may become stagnant and have no microbial activity. The gas phase flow is usually modelled as dispersed or non-dispersed plug flow in the axial direction, without radial advection.

Hodge and Devinny (1995) modelled a biofilter used for treating ethanol-contaminated air, with a one-dimensional plug flow model. The biofilter is reduced to a two-phase system consisting of a gas phase and water/biofilm/solids phase which includes the particles surrounded by a moist biofilm layer. Later work indicated that axial gas dispersion was negligible except at high flowrates (Hodge and Devinny, 1997). Their model includes the concentration profile of carbon dioxide which evolves from the biodegradation of ethanol. The overall rate of biodegradation is modelled as first order with respect to ethanol concentration. The individual resistances of mass transport and microbial growth kinetics in the overall rate constant were not

assessed. The rate constant was calculated using the model from experimental data of steady-state biodegradation in a biofilter.

Baquerizo et al. (2005) developed a dynamic model of a biofilter for ammonia treatment, which included a Haldane substrate-inhibition model to describe the microbial kinetics. Their model accounts for the fact there is a concentration gradient of substrate in the biofilm, and that, according to Haldane kinetics, the rate of biodegradation changes with substrate concentration in the biofilm. Wisecarver and Fan (1989) modelled a three-phase fluidized bed bioreactor for treatment of phenol in wastewater. Wastewater was the fluidization stream, which flowed upwards through a particle bed. There was also a continuous stream of air injected into the base of the bioreactor. They likewise modelled substrate concentration gradients throughout the thickness of the biofilm, but applied Monod kinetics in the biofilm. Calculation of concentration gradients within the biofilm requires parameters which were very difficult to determine, including biofilm thickness, biofilm boundary conditions, and substrate diffusion coefficient in the biofilm. This modelling approach becomes even more complicated if biofilm properties are not assumed to be constant throughout the biofilter bed.

Ottengraff and van den Oever (1983) modelled microbial kinetics in a biofilter with zero order kinetics with respect to the substrate. Microbial growth was assumed to take place in a biolayer on the particles, in direct contact with the gas phase. For the transport of the substrate from the gas to the biolayer, mass transfer resistance in the gas at the gas/biolayer interface was assumed to be negligible compared to diffusional resistance in the biolayer. The diffusion in the biolayer was shown to be a first order process with respect to the substrate. The researchers found that at high substrate concentrations, microbial growth was limiting, but at lower concentrations, the process was limited by either diffusion or both diffusion and microbial kinetics. Streese et al. (2005) proposed a biofilter model which includes an overall rate equation that approaches zero order kinetics at high concentrations and first order kinetics at low concentrations. The rate equation is analogous in form to the Monod growth model, and the constants in the rate equation were determined directly from biodegradation performance of the biofilter. Their model did not account for the individual contributions of growth kinetics and mass transport to the overall rate of biodegradation.

The simplest method of modelling a bubbling bed gas-solid fluidized reactor is to treat the gas, in both the bubbles and between the particles, as a single region which is completely

mixed (CSTR), or is in non-dispersed, plug flow. Another approach is to use a "two-region" model, where the bubble gas and the remainder of the gas between the particles are treated as two separate regions. Kunii and Levenspiel (1990) point out that unless the two-region model considers the physical properties of the bubbles, these models are generally over-simplified and inadequate at predicting the performance of bubbling bed fluidized reactors. Often in such models, several parameters must be correlated to experimental data. Fluidized bed models which include the mechanics of the bubbles are more accurate (Kunii and Levenspiel, 1990). Intuitively, bubble properties are important in a fluidized bed model because the movement of the bubbles in the fluidized bed contributes to agitation and mixing of the particles which affects concentration profiles within the bed.

The objective of the current study is to model both a gas-solid fluidized bed bioreactor and a comparable packed bed bioreactor (biofilter). Biodegradation of a single contaminant, ethanol, from an air stream is modelled. The model is used to predict steady state bioreactor performance at different operating conditions and the model predictions are compared to experimental bioreactor data.

6.3 Model Development

6.3.1 Preliminary considerations

Figures 6.1 and 6.2 present an overview of the processes involved in the fluidized and packed bed bioreactors, respectively. The fluidized bioreactor consists of two regions: the bubble region and the particulate (emulsion) region. In the former region, gas bubbles of contaminated air travel upwards in the fluidized bed and break at the surface of the bed. The particulate region includes the particles of the fluidized bed and the gas phase which occupies the interparticle space which is not otherwise occupied by gas bubbles. In addition, a liquid/biofilm phase covers the outer surface of the particles and microbial cells inhabit this layer. The biodegradation reactions take place within the microbial cells. The packed bed bioreactor consists of a bed of particles with a liquid/biofilm phase on the surface of the particles, and a gas

phase of contaminated air which entirely fills the interparticle space. Unlike the fluidized bed, there are no gas bubbles in the packed bed.

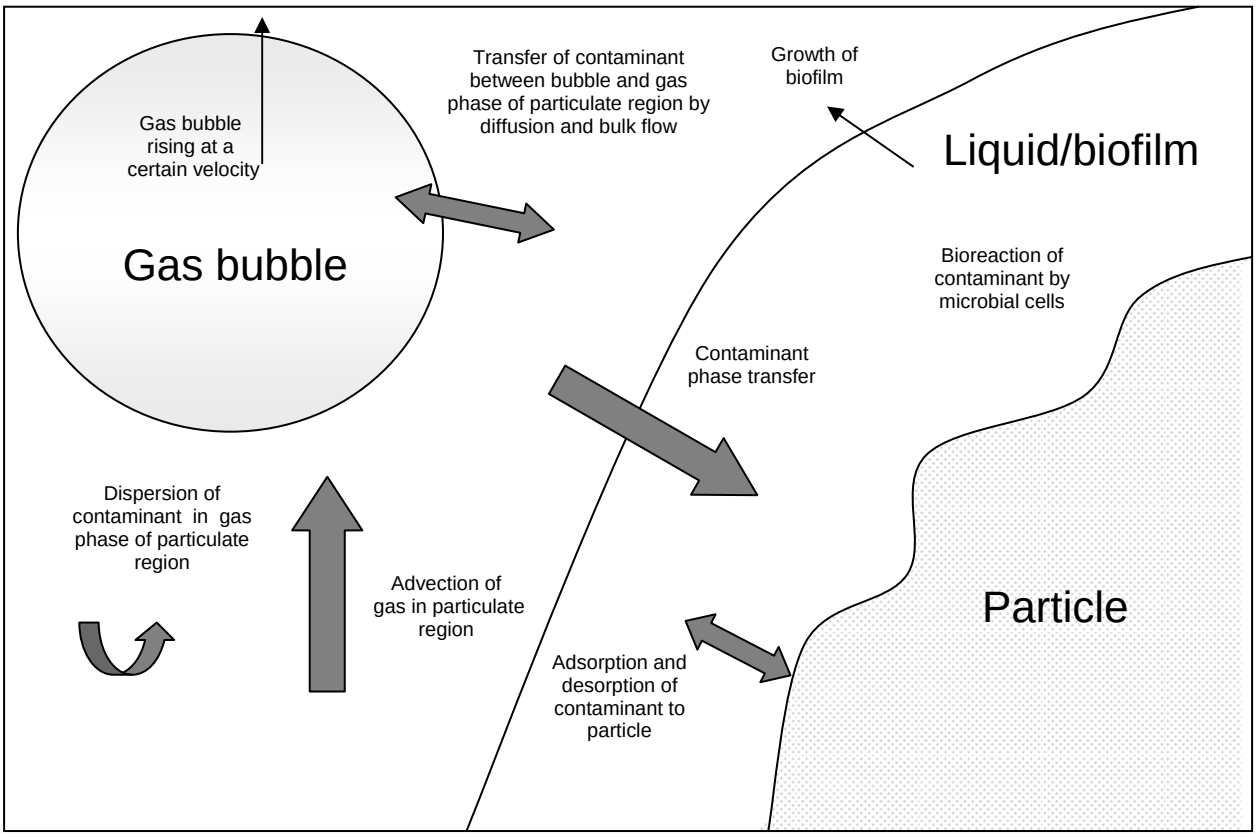

Figure 6.1 Overview of process in a fluidized bed bioreactor.

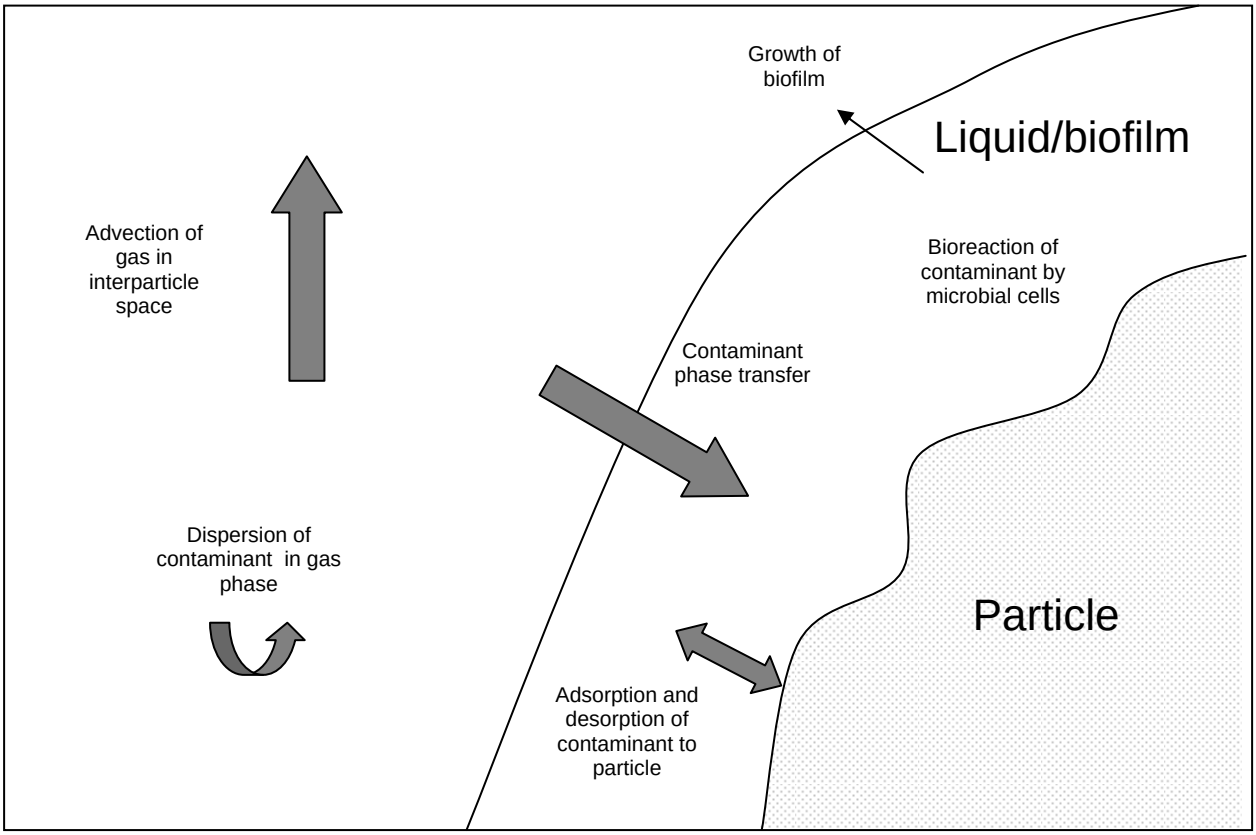

Figure 6.2 Overview of process in a packed bed bioreactor.

Key assumptions of the model development are:

1. Bioreactors are at steady state.
2. Bioreaction occurs only in the liquid/biofilm phase.
3. Because ethanol is highly soluble in water, mass transfer resistance between the gas phase of the particulate region and the liquid/biofilm is dominated by the resistance in the gas film at the interface between the gas and the liquid/biofilm.
4. The saturation constant (K_s) is very low. Thus, microbial kinetics are essentially zero order with respect to substrate concentration. Deshusses and Johnson (2000) suggest that microbial growth in biofilters follows zero order kinetics at inlet concentrations greater than 0.01 to 0.05 g m^{-3} for substrates with high solubility in water.

5. The liquid/biofilm phase is a layer covering the outer surface of particles and not within the pores. As a result, there is always an interface between the liquid/biofilm phase and the gas phase of the particulate region and there is no interface between the solid particles and the gas phase.
6. Solid particle composition is homogeneous throughout the bed.
7. Distribution of the biofilm/liquid on the particles is homogeneous on each particle, and throughout the bed.
8. The equilibrium relationship between the contaminant (ethanol) in the gas phase and the liquid/biofilm phase can be described by the Henrys Law constant for ethanol in water.
9. The properties of the liquid/biofilm phase are identical to those of water.
10. Advection in the bulk liquid/biofilm is negligible.
11. Conditions are isothermal throughout the bioreactor, and there is negligible heat transfer into or out of the vessel.
12. Net adsorption of ethanol onto the solid particles is zero. Because the model is steady state, the rates of adsorption and desorption of contaminant to and from the particles do not need to be included in the model.
13. The rate of evaporation of liquid from the liquid biofilm layer equals the rate of condensation of liquid to the biofilm because the bioreactors are at steady state. Experimentally this was true since the air was saturated with water.
14. There is no advection or diffusion in the radial direction in either the gas or liquid/biofilm phase; thus the model is one-dimensional.
15. All bubbles throughout the fluidized bed are spheres of the same size.
16. The velocity of the gas in the particulate phase of the fluidized bed is at minimum fluidization velocity (u_{mf}) and all gas in excess of u_{mf} travels through the bed in bubbles.
17. In the fluidized bed, there are no particles in the bubbles and no wake of particles dragged upwards by the bubbles.

6.3.2 Biodegradation Kinetics

In biodegradation, microorganisms utilize a contaminant (substrate) which is a carbon and energy source for growth. In aerobic biodegradation processes, substrates are broken down

in the presence of oxygen (and other nutrients), to produce new cells, carbon dioxide, and water. The model proposed in this paper will not include material balances for oxygen, carbon dioxide, or nutrients. Typically, microbial growth rate is assumed to be first order in terms of biomass concentration (X), and zero order in terms of substrate concentration (S):

$$r_x = \left[\frac{dX}{dt}\right] = \mu X \tag{6.1}$$

where biomass is the dry mass of microbial cells, which is directly proportional to cell number. The specific growth rate (μ) depends upon the concentration of the substrate or substrates supplying the energy and nutrient requirements of the microorganisms. The Monod model assumes that there is only one substrate which limits microbial growth, which in this study is ethanol:

$$\mu = \frac{\mu_m S}{K_s + S} \tag{6.2}$$

In biodegradation processes, biomass yield Y_{xs} is defined as the mass of cells produced per the mass of substrate consumed:

$$-r_s = -\left[\frac{dS}{dt}\right] = (r_x)\frac{1}{Y_{xs}} \tag{6.3}$$

Thus, the biodegradation rate with Monod kinetics is:

$$-r_s = \left(\frac{\mu_m S X}{K_s + S}\right)\frac{1}{Y_{xs}} \tag{6.4}$$

According to Equation 6.4, the biodegradation reaction rate approaches first order kinetics in terms of substrate concentration at low substrate concentrations ($S \ll K_s$) and zero order kinetics at high substrate concentrations ($S \gg K_s$).

6.3.3 Fluidized Bed Bioreactor Model

The gas phase in the fluidized bed bioreactor is modelled as two regions as discussed in section 6.3.1. The model calculates the concentration of gas in both the bubble and the particulate regions, following an approach similar to that of Davidson and Harrison (1963) for bubbling, fluidized bed reactors. Unlike other two-region models which ignore the physical

nature of the bubble, the bubble mechanics are considered. The current study expands on previous bubbling bed reactor models by considering a liquid/biofilm phase on the particles, in which bioreaction occurs. The gas phase concentration of ethanol in the bubbles varies with bed height and time. The gas phase of the particulate region is modelled as non-dispersed plug flow (Figure 6.3), very similar to the Kunii and Levenspiel (1990) bubbling bed model for intermediate-sized particles. Unlike the Kunii and Levenspiel model, in this study there is assumed to be no reaction occurring in the gas phase. In a GSFB, biodegradation takes place in the cells which reside only in the liquid/biofilm phase.

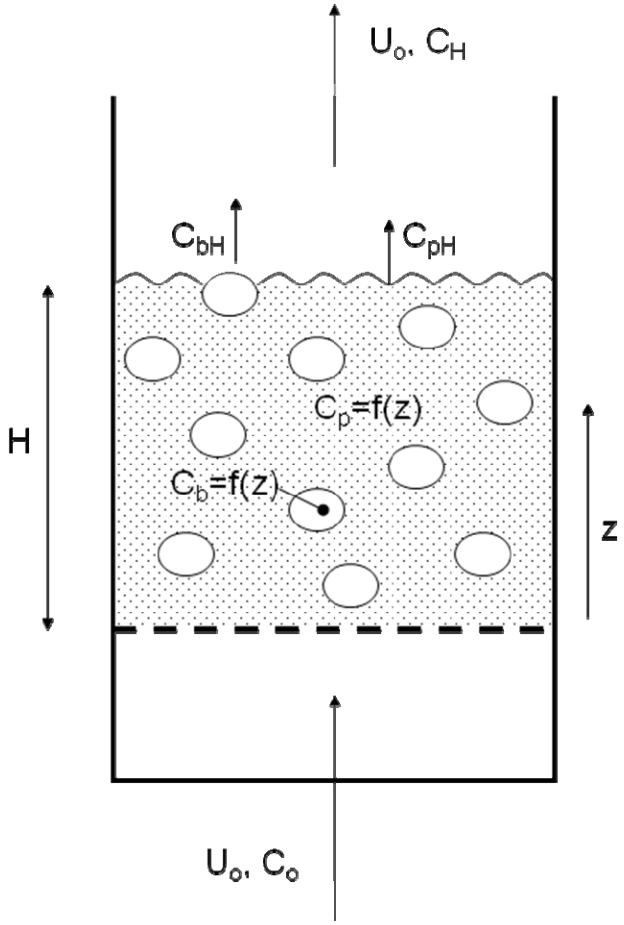

Figure 6.3 Bubbling, fluidized bed modeled with plug flow of the particulate phase.

Davidson and Harrison (1963) show that there are distinctive flow patterns of gas and particles in the vicinity of the bubbles which are a function of particle size. In intermediate-sized

particle bubbling beds, there is no particle wake beneath the bubble. The cloud region surrounding each bubble is so large that they overlap and essentially comprise the entire particulate region (Kunii and Levenspiel, 1990). A bubbling bed of intermediate-particles is defined as meeting the condition (Kunii and Levenspiel, 1990):

$$\frac{u_{mf}}{\varepsilon_{mf}} \le u_b \le 5\frac{u_{mf}}{\varepsilon_{mf}} \tag{6.5}$$

where bubble rise velocity (u_b) is defined below. The types of particles considered in this paper meet this criteria.

Davidson and Harrison (1963) show that bubble rise velocity (u_b) is finite in a bubbling bed, and u_b is determined by first finding the rise velocity of a single bubble (u_{br}):

$$u_{br} = 0.711\left(gd_b\right)^{1/2} \tag{6.6}$$

In a fluidized bed, the bubble rise velocity is greater than u_{br} by:

$$u_b = u_o - u_{mf} + u_{br} \tag{6.7}$$

From assumption 16 for the bubbling bed model, a material balance of the gas phase results in:

$$NV_b u_b = u_o - u_{mf} \tag{6.8}$$

Thus the fraction of bubbles in the fluidized bed during fluidization is:

$$f_b = NV_b = \frac{u_o - u_{mf}}{u_b} \tag{6.9a}$$

Equation 6.9a applies when u_b is approximately equal to $5u_{mf}/\varepsilon_{mf}$. When u_b approximates u_{mf}/ε_{mf}, f_b for intermediate-sized particles is calculated as follows (Kunii and Levenspiel, 1991):

$$f_b = NV_b = \frac{u_o - u_{mf}}{u_b + u_{mf}} \tag{6.9b}$$

The volume of gas in the bubbles causes a change in height of the bubbling bed after u_{mf}. Bed height during fluidization (H) is also calculated from a material balance:

$$f_b H = H - H_{mf} \tag{6.10}$$

Davidson and Harrison (1963) show that the bulk flow of fluid exchanging between a bubble and the particulate region of a fluidized bed is the same as it is for a fixed bubble (Davidson and Harrison, 1963):

$$q = \frac{3\pi u_{mf} d_b^2}{4} \tag{6.11}$$

Generally, in bubbling beds, there is also molecular diffusion between the bubble and the gas phase of the particulate region which is driven by the concentration difference between the gas in the bubble and at the bubble wall. For intermediate-sized particles in gas bubbling beds, molecular diffusion can be neglected (Kunii and Levenspiel, 1990) because q is usually relatively large in magnitude due to bubble diameter.

6.3.4 Rate Equation

The overall rate of disappearance of ethanol from the gas phase of the particulate region ($-r_c$) is a function of mass transfer and biokinetics. The maximum concentration of ethanol in the liquid/biofilm phase is limited by the equilibrium between ethanol in the gas phase of the particulate region and ethanol dissolved in the liquid/biofilm phase. According to Henrys Law, at equilibrium:

$$C_p = H_e S \tag{6.12}$$

In this study, ethanol concentration in the liquid/biofilm is modelled as constant at a given bed height. As per assumption 4 and the Monod model, the bioreaction is zero order with respect to substrate concentration:

$$-r_S = \frac{\mu_m X}{Y_{xs}} \tag{6.13}$$

For simplification, let the zero order rate constant K_0 be defined as:

$$K_0 = \frac{\mu_m X}{Y_{xs}} \tag{6.14}$$

When the overall rate of disappearance of ethanol from the gas phase of the particulate region is controlled by biokinetics, it will also be zero order with respect to ethanol concentration as follows:

$$-r_c = K_0 f_l \tag{6.15}$$

Alternatively, the overall rate of disappearance of ethanol from the gas phase of the particulate region may be controlled by mass transfer. Applying the two-film theory of mass transfer to the gas film:

$$-r_c = k_g a \left(C_p - C_{p,i}\right) \tag{6.16a}$$

where k_g is the gas phase mass transfer coefficient, a is the specific surface area of the particles covered with the liquid/biofilm layer, and $C_{p,i}$ is the ethanol concentration in the particulate region gas at the gas and liquid/biofilm interface. Assuming that the overall mass transfer resistance is dominated by resistance in the gas film (assumption 3), the overall mass transfer coefficient is defined as follows:

$$-r_c = K\left(C_p - H_e S\right) \tag{6.16b}$$

where K is the overall mass transfer coefficient. When the overall rate of disappearance of ethanol ($-r_c$) is controlled by mass transfer, S is negligible because the rates of mass transfer through the liquid film at the interface and microbial consumption of ethanol are very rapid in comparison to the gas film mass transport. Equation 6.16b reduces to:

$$-r_c = KC_p \tag{6.17}$$

Consequently, the overall rate is first order, with K as the first order rate constant.

6.3.5 Material balance for bubbling bed model

In this model, ethanol in the gas phase of the particulate region varies with height. The bubbles rise up through the bed and exchange ethanol with the particulate region. As a result, the concentration of ethanol in an individual bubble (C_b) changes with position in the bed. C_b varies from C_0 at the bottom of the bed to C_{bH} when the bubble breaks at the surface of the bed.

The material balance for ethanol in a single rising bubble is:

$$\frac{q}{V_b}(C_p - C_b) = \frac{\partial C_b}{\partial t} \tag{6.18}$$

The superficial velocity of a single bubble (u_b) is defined as:

$$u_b = \frac{\partial z}{\partial t} \tag{6.19}$$

Assuming negligible molecular diffusion between the bubbles and the particulate region gas, and substituting Equation 6.19 into Equation 6.18 gives:

$$\frac{\partial C_b}{\partial z} = \frac{q}{u_b V_b}(C_p - C_b) \tag{6.20}$$

At the bottom of the bed (z=0), $C_b = C_o$. Equation 6.20 is integrated to find C_b as a function of bed height:

$$C_b = C_p + (C_o - C_p)\exp\left(-\frac{qz}{u_b V_b}\right) \tag{6.21}$$

A steady-state material balance of ethanol over the gas phase in both bubble and particulate regions is completed over a thin section of the fluidized bed of thickness *dz*. The balance includes advective flow of gas in and out of the gas phase of both the bubble and particulate regions and the overall rate of disappearance of ethanol ($-r_c$) due to absorption into the biofilm. The mass balance in units of mass of ethanol per unit time per volume of bioreactor bed during fluidization is:

$$u_{mf}\frac{dC_p}{dz} + \left(u_o - u_{mf}\right)\frac{dC_b}{dz} + r_C = 0 \tag{6.22}$$

Define:

$$\alpha = \frac{qH}{u_b V_b} \tag{6.23}$$

$$\beta = 1 - \frac{u_{mf}}{u_o} \tag{6.24}$$

6.3.5.1 First order kinetics

When the overall rate Equation is first order, Equation 6.20 is substituted into Equation 6.22 to eliminate C_p, and simplified with Equations 6.23 and 6.24:

$$(1-\beta)\frac{H}{\alpha}\frac{d^2C_b}{dz^2} + \left(1 + \frac{KH}{\alpha u_o}\right)\frac{dC_b}{dz} + \frac{K}{u_o}C_b = 0 \tag{6.25}$$

This linear, homogeneous, second order differential equation is converted into its characteristic quadratic equation in the form:

$$ar^2 + br + c = 0 \tag{6.26}$$

where the coefficients *a*, *b*, and *c* are:

$$a = \frac{(1-\beta)H}{\alpha} \tag{6.27a}$$

$$b = 1 + \frac{KH}{\alpha u_o} \tag{6.27b}$$

$$c = \frac{K}{u_o} \tag{6.27c}$$

Also, *r* is equal to either r_1 or r_2, the two real roots of the quadratic equation, which are determined from the quadratic formula. The solution to Equation 6.25 is:

$$C_b = C_1 e^{r_1 z} + C_2 e^{r_2 z} \tag{6.28}$$

where C_1 and C_2 are constants. Differentiating Equation 6.28:

$$\frac{dC_b}{dz} = r_1 C_1 e^{r_1 z} + r_2 C_2 e^{r_2 z} \tag{6.29}$$

C_1 and C_2 are found from the boundary conditions that at z=0, $C_b = C_o$ and $dC_b/dz = 0$. Equations 6.28 and 6.29 are substituted into Equation 6.20 to solve for C_p:

$$C_p = C_1 e^{r_1 z}\left(1 + \frac{z r_1}{\alpha}\right) + C_2 e^{r_2 z}\left(1 + \frac{z r_2}{\alpha}\right) \tag{6.30}$$

Then Equations 6.21 and 6.30 are used to calculate C_{bH} and C_{pH} where z=H. The concentration of ethanol in the gas exiting the bioreactor (C_H) includes both the ethanol from the bubbles and the particulate region:

$$u_o C_H = (u_o - u_{mf}) C_{bH} + u_{mf} C_{pH} \tag{6.31}$$

The net conversion of ethanol (X_e) is then equal to:

$$X_e = 1 - \frac{C_H}{C_o} \tag{6.32}$$

6.3.5.2 Zero order kinetics

For zero order kinetics, Equation 6.22 becomes:

$$\frac{d^2 C_b}{dz^2} + \frac{\alpha}{(1-\beta)H}\frac{dC_b}{dz} = -\frac{K_0 f_l \alpha}{(1-\beta) u_o H} \tag{6.33}$$

The method of variation of parameters is used to solve this linear, non-homogenous second order differential equation. The solution is a sum of the solution of the homogeneous part of the equation, *H(z),* and the function *P(z)* which is a particular integral of the differential equation:

$$C_b = H(z) + P(z) \tag{6.34}$$

H(z) is found by the same method which was used to derive Equation 6.28:

$$H(z) = C_1 + C_2 e^{r_2 z} \tag{6.35a}$$

The following equation satisfies the differential equation:

$$P(z) = -\frac{R}{r_2} z - \frac{R}{(r_2)^2} \tag{6.35b}$$

where *R* is the non-homogeneous term of the differential equation:

$$R = -\frac{K_0 f_l \alpha}{(1-\beta) u_o H} \tag{6.36}$$

Equations 6.35a and 6.35b are substituted into Equation 6.34:

$$C_b = C_1 + C_2 e^{r_2 z} - \frac{R}{r_2} z - \frac{R}{(r_2)^2} \tag{6.37}$$

Differentiating Equation 6.37:

$$\frac{dC_b}{dz} = r_2 C_2 e^{r_2 z} - \frac{R}{r_2} \tag{6.38}$$

C_1 and C_2 are found from the boundary conditions that at z=0, $C_b = C_o$ and $dC_b/dz = 0$.
Upon substitution of Equations 6.37 and 6.38 into Equation 6.20:

$$C_p = C_1 + C_2 e^{r_2 z}\left(\frac{r_2 H}{\alpha} + 1\right) - \frac{R}{r_2}\left(\frac{H}{\alpha} + z\right) - \frac{R}{r_2^2} \tag{6.39}$$

In bioreactors, biodegradation performance is often measured with elimination capacity (*EC*). In this study for both the fluidized and packed bed bioreactors, *EC* is defined as grams of ethanol biodegraded per hour per cubic metre of packed bed volume:

$$EC = 3600(C_o - C_H)\frac{u_o}{H_m} \tag{6.40}$$

Ethanol loading (*L*) to the bioreactor is defined as grams of ethanol entering the bioreactor per hour per cubic metre of packed bed volume:

$$L = 3600(C_o)\frac{u_o}{H_m} \tag{6.41}$$

where H_m is the packed bed height.

6.3.6 Packed Bed Bioreactor Model

For comparison purposes, a packed bed bioreactor is modelled with non-dispersed plug flow which is chosen by most authors (Devinny and Ramesh, 2005). Both zero and first order kinetics are used. In packed bed operation there are no gas bubbles, so all of the gas phase is in the interparticle space. A material balance on the ethanol in the gas phase is:

$$u_o \frac{dC_p}{dz} + r_C = 0 \tag{6.42}$$

6.3.6.1 First order kinetics

For first order kinetics Equation 6.42 becomes:

$$u_o \frac{dC_p}{dz} + KC_p = 0 \tag{6.43}$$

Integrating with the initial condition that C_p=C_o at z=0, results in an expression for C_p as a function of bed height:

$$C_p = C_o \exp\left(\frac{-Kz}{u_o}\right) \tag{6.44}$$

6.3.6.2 Zero order kinetics

For zero order kinetics, the ethanol mass balance in the gas phase is:

$$u_o \frac{dC_p}{dz} + K_0 f_l = 0 \tag{6.45}$$

The concentration of ethanol in the gas exiting the bioreactor is:

$$C_{pH} = C_o + \frac{-K_0 f_l H_m}{u_o} \tag{6.46}$$

6.4 Materials and Methods

Two sets of fluidized and packed bed biodegradation experiments were conducted. In the first set, the bed packing consisted of a 74:26 v/v mixture of 0.52 mm glass spheres and wet sawdust particles. This mixture fluidized in a bubbling/slugging regime. In the second set of biodegradation experiments, wet peat granules were used, which fluidized in a bubbling regime at a superficial gas velocity of 0.5 m s^{-1}. At 0.75 m s^{-1} some large bubbles (slugs) were observed in the upper layers of the fluidized bed, and at 1.0 m s^{-1}, there were more slugs present at greater depths in the bed. Complete details of the experimental set-up and biodegradation results are presented elsewhere (Clarke et al., 2007; Clarke et al., 2008). Table 6.1 highlights properties of the two types of packing and conditions of the biodegradation experiments.

The apparatus (Figure 6.4) was an acrylic, cylindrical, bench-scale vessel, with an inside diameter of 0.14 m, and the vessel height above the distributor plate was 1.81 m. The inlet air stream to the vessel was saturated with moisture before it entered the vessel. Ethanol contamination was introduced by directing a slip stream of the inlet air into an ethanol bubbler. The flowrate of the inlet air to the bioreactor was measured using a rotameter or a flow orifice. The inlet air to the ethanol bubbler was metered using a rotameter.

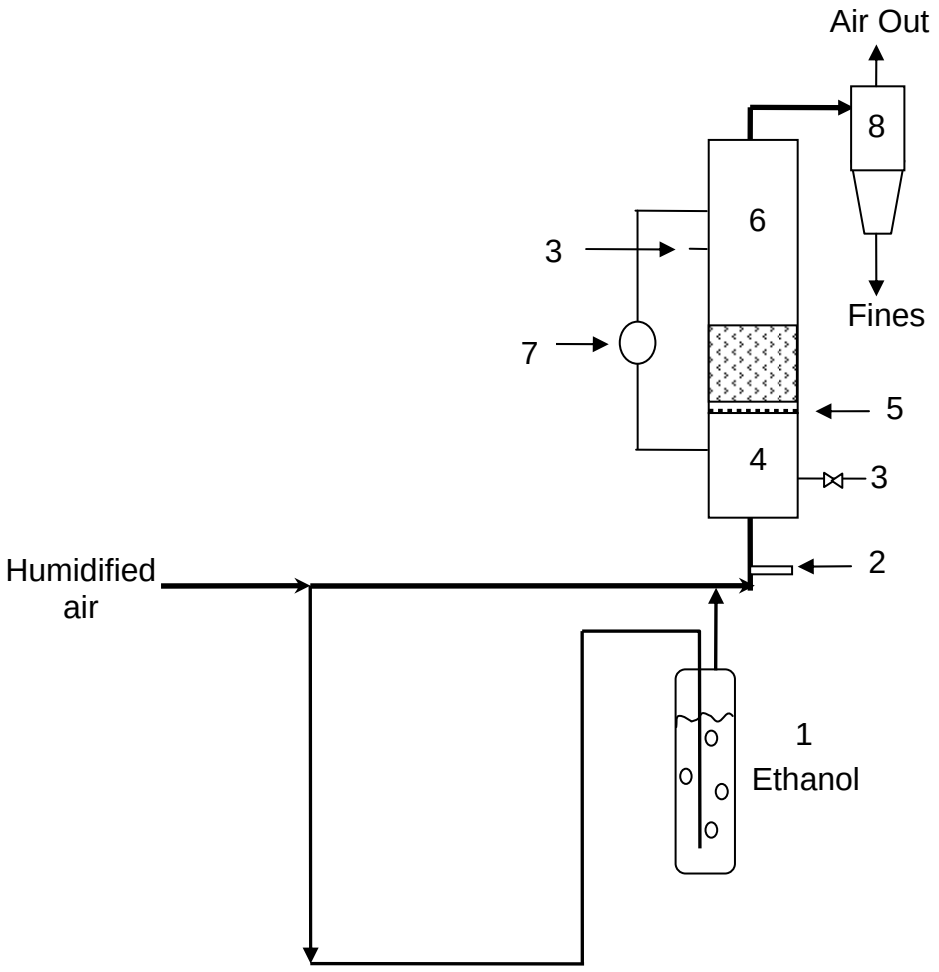

Figure 6.4 Experimental apparatus: (1) bubbler (2) humidity and temperature probe; (3) sampling port; (4) wind-box; (5) distributor and wire screen; (6) bioreactor; (7) differential pressure transducer; (8) cyclone.

Both types of particles were seeded with an active microbial culture and placed in the bioreactor vessel. Ethanol-contaminated air was then fed to the vessel continuously, while the bioreactor was operated in either packed or fluidized bed mode. The most abundant microbial species in the bed material (shown in Table 6.1) were characterized after four and nine weeks of bioreactor operation by the MIDI, Inc. (Newark, DE) Sherlock microbial identification system, for the sawdust/sphere and peat granule beds respectively. Throughout biodegradation experiments, a nutrient solution was periodically mixed into the packing, and it adsorbed into the liquid/biofilm phase. The nutrient solution consisted of 0.84 g KH_2PO_4, 0.75 g K_2HPO_4, 0.50 g $(NH_4)_2SO_4$, 0.06 g NaCl, 0.06 g $CaCl_2$, 0.06 g $MgSO_4$, 0.02g $Fe(NH_4)_2(SO_4)_2*6H_2O$, and 1 mL of trace mineral solution (per litre of deionised water: 0.20 g $ZnSO_4*7H_2O$, 0.06 g $MnCl_2*4H_2O$,

0.60 g H_3BO_3, 0.40 g $CoCl_2*6H_2O$, 0.02 g $CuCl_2*2H_2O$, 0.04 g $NiCl_2*6H_2O$, and 0.06 g $Na_2MoO_4*2H_2O$) in 1 litre deionised water.

The sawdust/sphere and peat granules beds were operated in both fluidized and packed bed modes for biodegradation of ethanol-contaminated air. A set of biodegradation trials was conducted at each of several superficial gas velocities (Table 6.1). The inlet ethanol concentration to the bioreactor was different for each trial. The bioreactor was allowed to reach stable conditions (constant EC) at a given inlet ethanol concentration, before collecting biodegradation data.

Table 6.1 Properties of bioreactor packing and biodegradation experimental conditions

Packing	Sawdust/spheres	Peat granules
Packed bed height, H_m (m)	0.2	0.14
Packed bed voidage, ε_m	0.58	0.45
Minimum fluidization velocity, u_{mf} (m s^{-1})	0.45[a]	0.21
Sauter mean diameter (mm)	0.625	0.680
Moisture content (wt % dry basis)	67	40
Most abundant microbial species	*Pichia anomala*	*Pichia* spp
Superficial gas velocities, packed bed mode (m s^{-1})	0.0024, 0.155	0.0024, 0.0824
Superficial gas velocities, fluidized bed mode (m s^{-1})	0.7	0.5, 0.75, 1.0

(a) Approximated from a pressure profile of a mixture of 79:21 v/v spheres and sawdust at increasing gas velocity, reported in Clarke et al. (2007).

Ethanol concentrations in the air entering and exiting the bioreactor were determined using a Hewlett Packard 5890 series (Agilent Technologies, Palo Alto, CA) gas chromatograph fitted

with a flame ionization detector and a Supelco (Bellefonte, PA) non-polar PTE-5™ column. The injector and detector temperatures were 200 °C, oven temperature was held at 40 °C, column inlet pressure was 90 kPa, and helium was used as the carrier gas at a linear velocity of 30 cm s^{-1}. Air samples were collected in glass sampling bulbs from ports on the bioreactor vessel, using vacuum to draw the contaminated air into the bulbs. A gas-tight syringe was used to withdraw 0.1 to 0.5 mL sub-samples from the bulbs which were manually injected into the GC.

6.5 Results and Discussion

The steady-state, non-dispersed, plug flow fluidized and packed bed bioreactor models described above are applied to experimental biodegradation data for sawdust/sphere and peat granule bioreactors. Experimental elimination capacities (EC) *versus* ethanol loadings (L) have been measured and reported earlier (Clarke et al., 2007, Clarke et al., 2008). Zero and first order rate constants are determined from these experiments for both the packed and fluidized bed operating modes, at various superficial gas velocities. The rate constants are then used to predict EC *versus* inlet ethanol concentration for sawdust/sphere and peat bioreactors and they are compared to experimental data in Figures 6.5 and 6.6.

The first order rate constant, K, is estimated from the linear portion of the EC curve, before the maximum EC value is reached. Here EC is a function of the inlet ethanol concentration in the gas which indicates that the overall rate of disappearance of ethanol ($-r_c$) from the gas phase follows first order kinetics. As a result, the overall rate is assumed to be controlled by mass transfer resistance. As inlet ethanol concentration increases, the overall rate transitions from first to zero order. At this point, EC reaches a maximum, constant value at high ethanol loadings. At maximum EC, the overall rate of biodegradation of ethanol is zero order with respect to ethanol concentration. It is most likely that at maximum EC, the overall rate of disappearance of ethanol from the gas phase is limited by microbial growth which is a zero order process at high ethanol concentrations. The zero order rate constant (K_0) is estimated from the constant EC (maximum EC) region at high ethanol concentrations. K and K_0 were varied by trial and error to obtain a best fit of the models to the experimental EC data by a sum of least squares method.

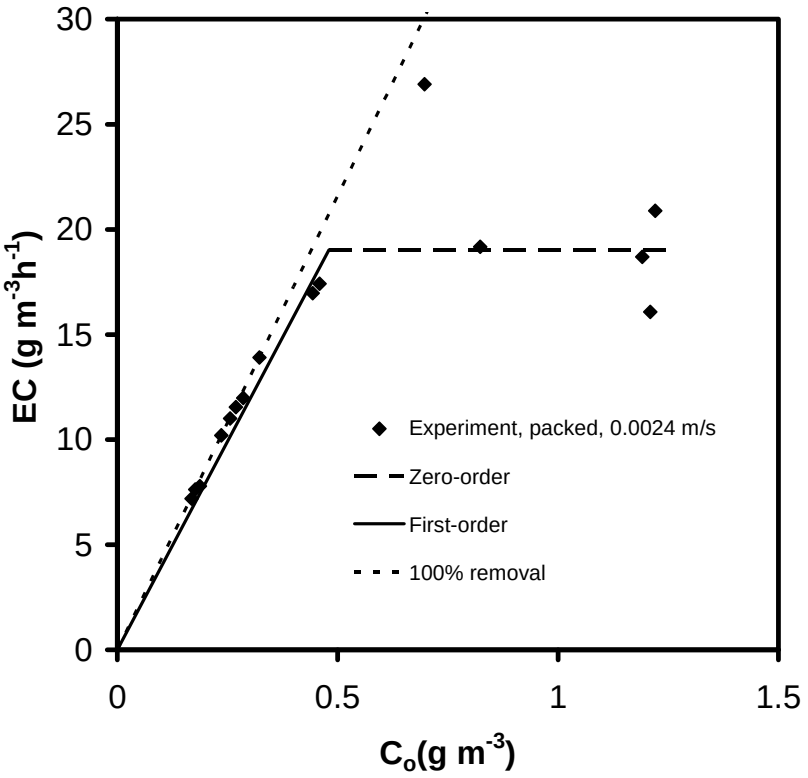
30
25
20
15
10
5
0
EC (g m-3h-1)
0
0.5
1
1.5
Co(g m-3)
Experiment, packed, 0.0024 m/s
Zero-order
First-order
100% removal

(a)

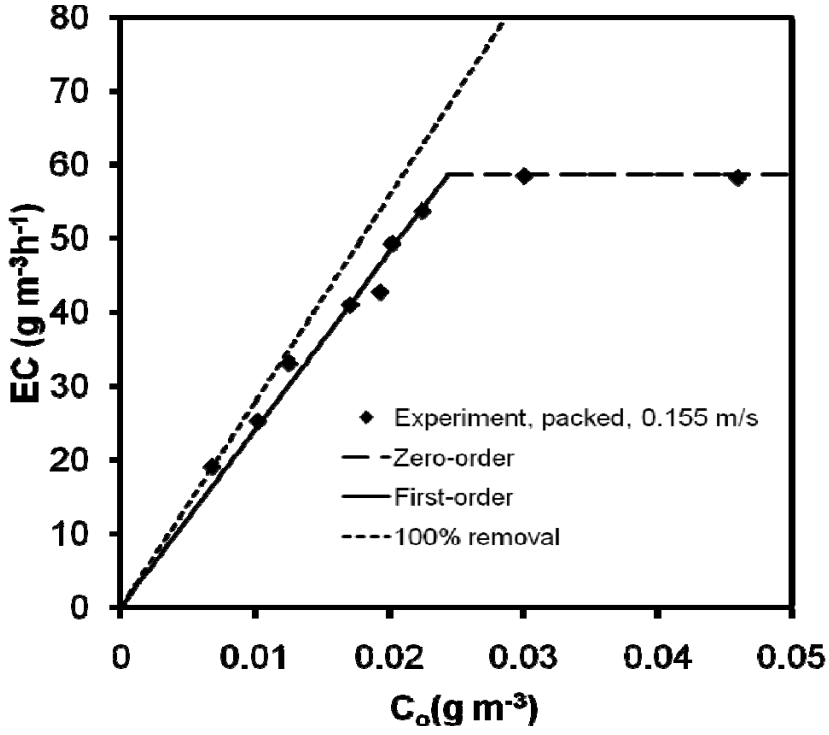
80
70
60
50
40
30
20
10
0
EC (g m-3h-1)
0
0.01
0.02
0.03
0.04
0.05
Co(g m-3)
Experiment, packed, 0.155 m/s
Zero-order
First-order
100% removal

(b)

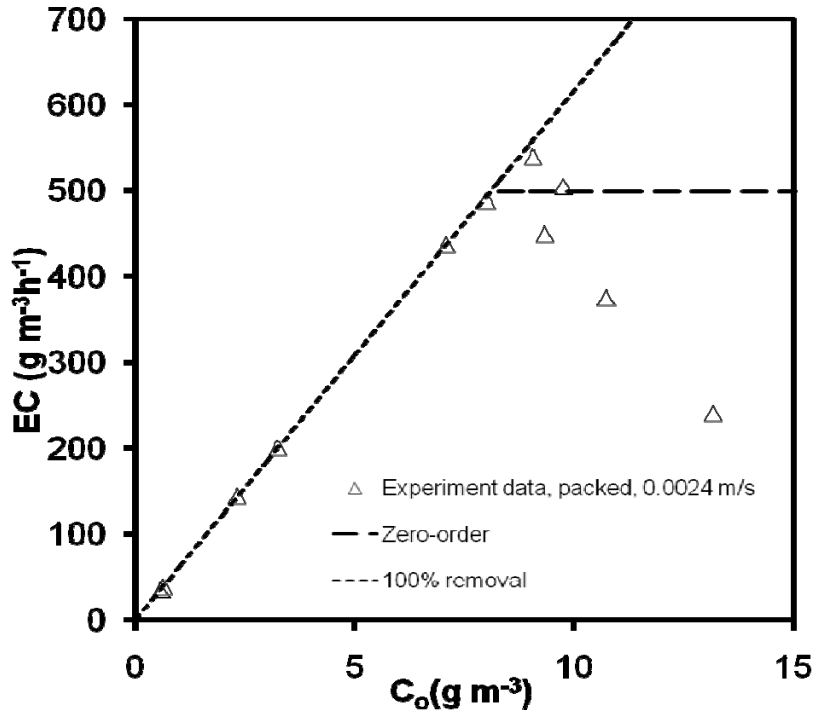

(c)

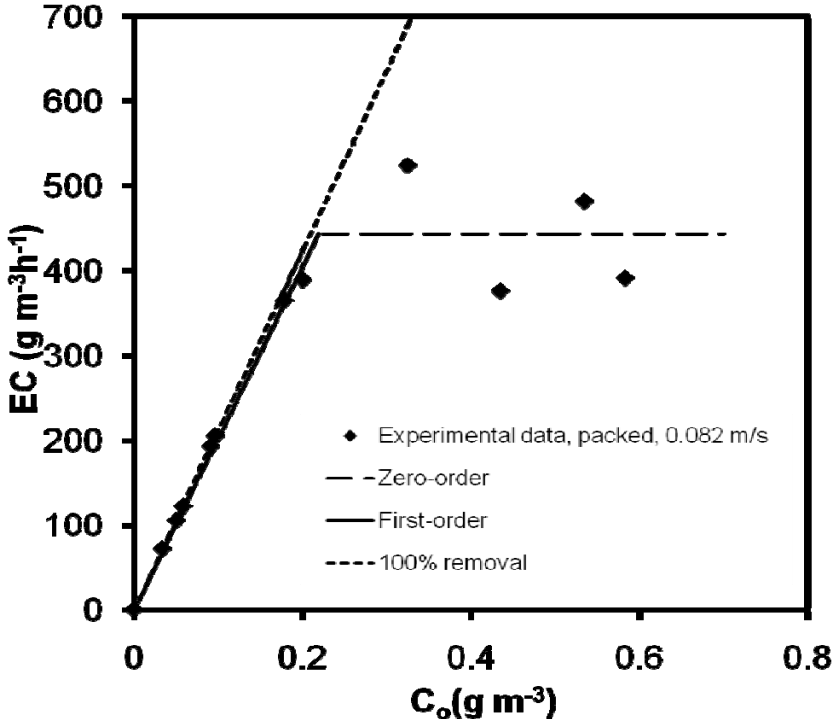

(d)

Figure 6.5 Comparison of plug flow, packed bed model to bioreactor experiments (a) Sawdust/sphere packing, u_o=0.0024 m s^{-1}; (b) Sawdust/sphere packing, u_o =0.155 m s^{-1}; (c) Peat packing, u_o=0.0024 m s^{-1}; (d) Peat packing, u_o=0.082 m s^{-1}.

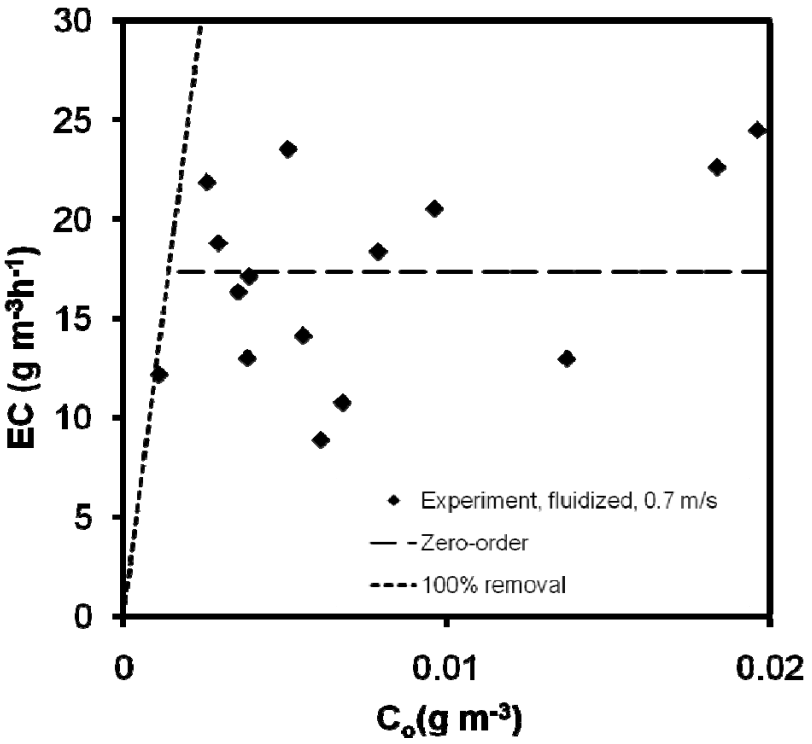
30
25
20
15
10
5
0
EC (g m-3h-1)
0
0.01
0.02
Co(g m-3)
Experiment, fluidized, 0.7 m/s
Zero-order
100% removal

(a)

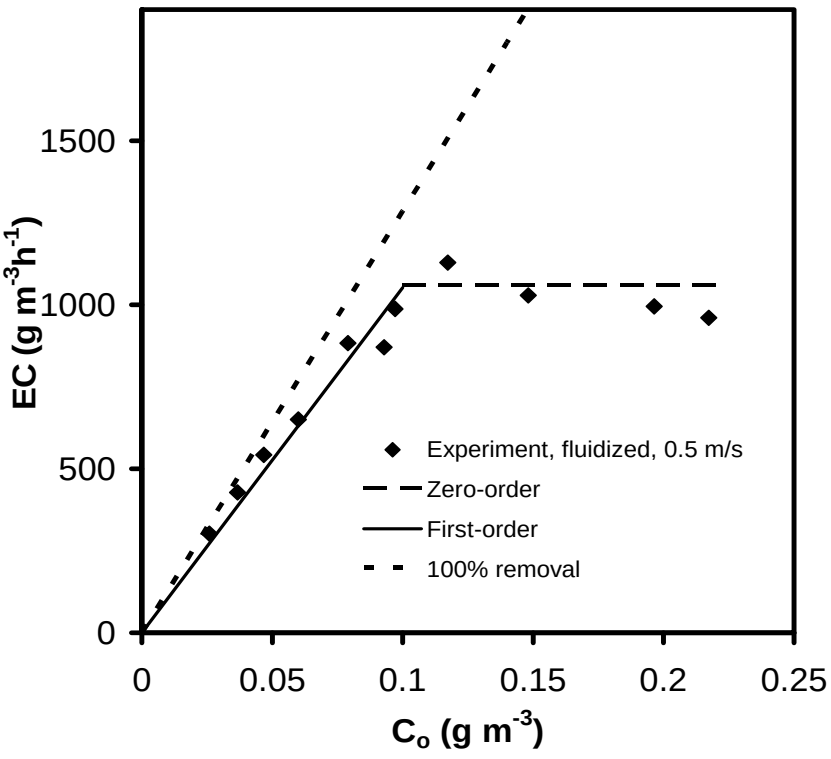
1500
1000
500
0
EC (g m-3h-1)
0
0.05
0.1
0.15
0.2
0.25
Co (g m-3)
Experiment, fluidized, 0.5 m/s
Zero-order
First-order
100% removal

(b)

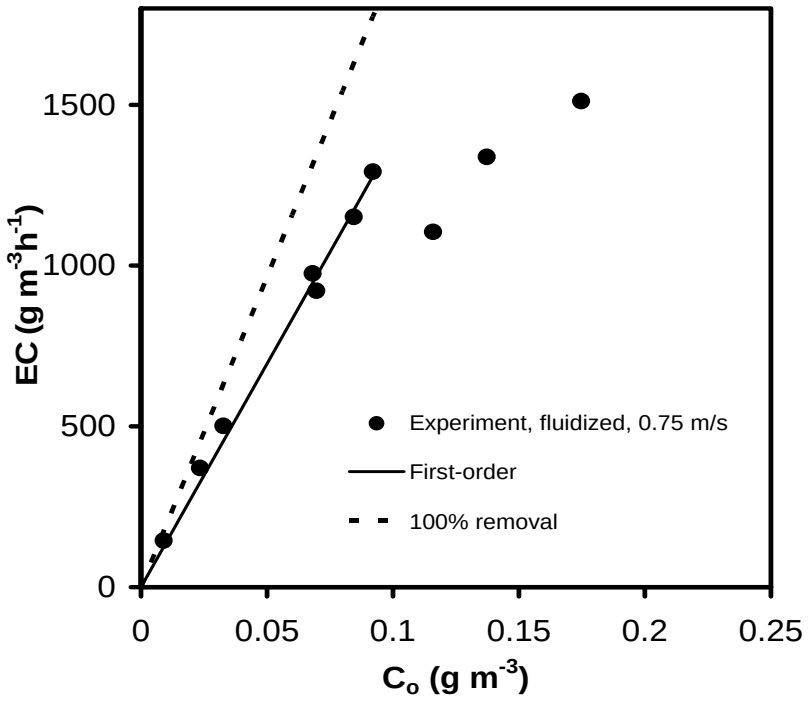

(c)

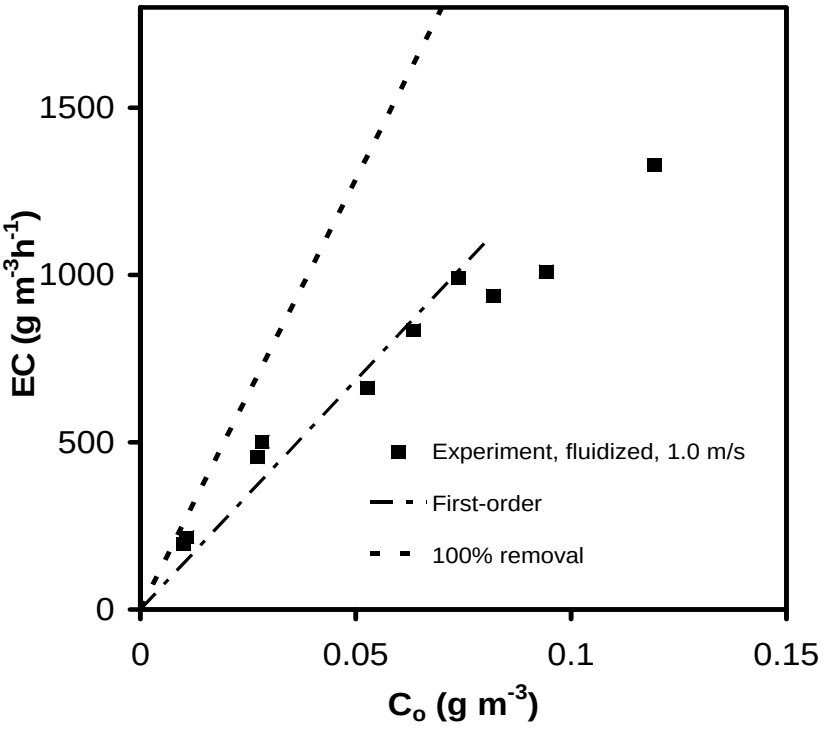

(d)

Figure 6.6 Comparison of bubbling fluidized bed, plug flow model to bioreactor experiments (a) Sawdust/sphere packing, u_o=0.7 m s^{-1}; (b) Peat packing, u_o =0.5 m s^{-1}; (c) Peat packing, u_o=0.75 m s^{-1}; (d) Peat packing, u_o=1.0 m s^{-1}.

The input parameters for the models are presented in Table 6.2, while Table 6.3 summarizes the estimated rate constants. The volume fraction of liquid/biofilm in the bioreactor bed (f_l) is based on moisture content of the peat and sawdust particles, where it is assumed that the volume of moisture constitutes the entire liquid/biofilm phase. Bubble diameters in the fluidized beds were not measured, but by visual observations, bubbles in the sawdust/sphere fluidized bioreactor were approximated as being half of the vessel diameter, and the bubbles in the peat fluidized bioreactor were in the range of 10 to 50 mm. For modelling purposes, bubble sizes of 70 and 30 mm were chosen for the sawdust/sphere and peat beds, respectively, to highlight this size difference.

Table 6.2 Input parameters for packed and bubbling fluidized bed models

Packing	Sawdust/spheres		Peat Granules	
Operating mode	Packed bed	Fluidized bed	Packed bed	Fluidized bed
u_o (m s^{-1})	0.0024 , 0.155	0.7	0.0024 , 0.0824	0.5, 0.75, 1.0
H_{mf} [a] (m)	0.22	0.22	0.16	0.16
f_l	0.02	0.016	0.19	0.13, 0.11, 0.08
d_b (mm)	N/A	70	N/A	30
Q (m^3 s^{-1})	N/A	0.0052	N/A	0.00045
f_b	N/A	0.19	N/A	0.33, 0.48, 0.57
Maximum EC[b] (g m^{-3} h^{-1})	59 [c] , 19[c]	20[c]	530 , 530	1150, ≥1520, ≥1340

(a) Estimated from observations of fluidized bed at u_{mf}.
(b) Reported in Clarke et al. (2008).
(c) Based on packed volume of sawdust and glass spheres.

Table 6.3 Rate constants

	Packed bed	Fluidized bed	Packed bed	Fluidized bed
Model	Packed bed plug flow	Plug flow, bubbling bed	Plug flow	Plug flow, bubbling bed
Packing	Sawdust/spheres	Sawdust/spheres	Peat	Peat
u_o (m s^{-1})	0.0024, 0.155	0.7	0.0024, 0.0824	0.5, 0.75, 1.0
K_0 (g $m^{-3}s^{-1}$)	0.26, 0.81	0.22	0.71, 0.64	1.3, >1.3, >1.3
K (m^3 m^{-3} s^{-1})	0.03, 1.5	----[a]	----[a], 1.8	3.9, 3.4, 2.2

(a) Insufficient data to calculate K.

Both the 0.0024 and 0.0824 m s^{-1} peat packed beds have the same maximum EC values as shown in Table 6.2. After substituting Equation 6.46 into 6.40, it can be observed that the maximum EC is a function of K_0, but not superficial gas velocity:

$$EC = 3600(K_0 f_l) \tag{6.47}$$

Thus, K_0 is identical at both of these velocities. However, as seen in Figure 6.5, after maximum EC is reached, EC of the low velocity peat packed bed begins to decrease as the inlet ethanol loading increases. It is believed that at higher inlet ethanol concentrations, microbial growth slows down due to substrate inhibition effects or the accumulation of toxic intermediates in the bed.

The 0.75 m s^{-1} peat fluidized bed attains the highest EC value, and outperforms the packed bed mode and the sawdust/sphere bioreactor. The 0.75 and 1.0 m s^{-1} peat fluidized beds do not attain a maximum EC at the experimental loadings, as shown in Figure 6.6, indicating that they have higher maximum EC and K_0 values than that of the 0.5 m s^{-1} fluidized bed. These observations suggest that microbial biodegradation is enhanced by fluidization, and that increasing the gas velocity further boosts biodegradation rates. Possibly, fluidization aids in the

absorption of oxygen into the liquid/biofilm layer or increases contact between microbial cells and contaminated gas.

Maximum EC and K_0 values are lowest for the sawdust/sphere bioreactors. Most of the microbial growth occurs on the sawdust particles, with very little growth on the spheres, which unfortunately made up the largest fraction of the bed (Clarke et al., 2007). In addition, peat granules contain more moisture (higher f_l) and possibly support more microorganisms. Lower concentrations of microorganisms in the sawdust/sphere *versus* peat bed would result in lower maximum EC values, as K_0 is directly proportional to biomass concentration (Equation 6.14).

The zero order rate constant is also a direct function of the microbial growth rate (μ_m). Growth rate can be altered by changing environmental operating conditions or by finding superior strains of microorganisms. Figure 6.7 presents predicted EC *versus* loading curves for a peat, fluidized bioreactor at increasing values of μ_m. The model predictions use the properties and rate constants in Tables 6.2 and 6.3 for the peat, fluidized bed at u_o = 0.5 m s^{-1}. Prior to maximum EC, the EC curves at varying growth rates remain unchanged, while the maximum EC increases in proportion to the growth rate.

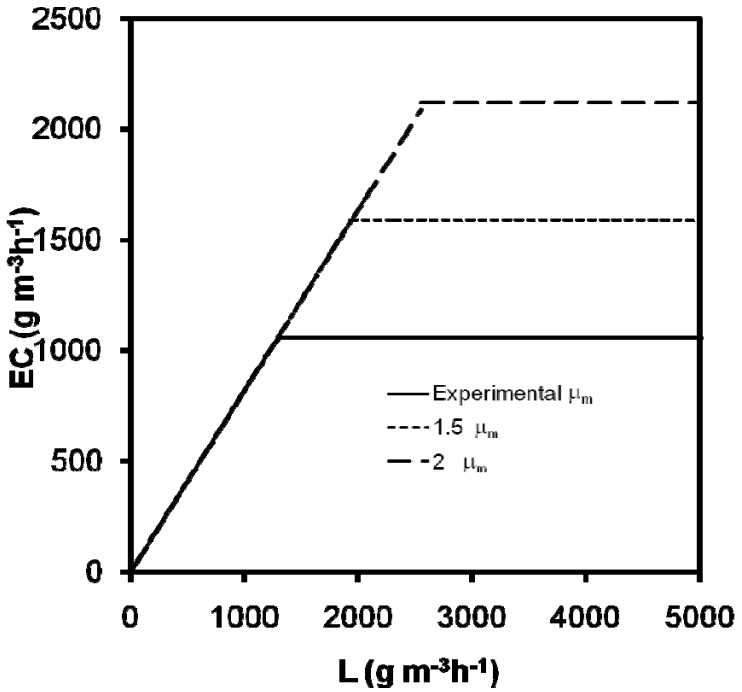

Figure 6.7 Predicted EC *versus* inlet ethanol loading at increasing microbial growth rates in a peat, fluidized bioreactor bed, u_o =0.5 m s^{-1}.

It is of great interest to determine if the zero order rate constant calculated in this study for the fluidized sawdust/sphere bioreactor is reasonable. In Clarke et al. (2007), growth parameters μ_m and Y_{xs} were reported for the microbial culture in the sawdust/sphere bioreactor as 0.065 h^{-1} and 0.48, respectively. Cell density was measured to be 63 to 420 million cells/g dry sawdust and the dry mass of a single cell was estimated as 2 $*10^{-10}$ g. If these cells uniformly occupy the liquid volume of the bioreactor packing, the biomass concentration (X) in the liquid in terms of dry mass of cells is 19,000 to 126,000 g m^{-3}. Applying Equation 6.14 to these biomass concentrations, K_0 ranges between 0.7 to 4.7 g m^{-3} s^{-1}. K_0 based on the bubbling bed model in the sawdust/sphere bioreactor was determined to be 0.22 g m^{-3} s^{-1} (Table 6.3), and it is logical that the modelling value would be lower than the experimental data. During bioreactor operation, many cells may be within the pores of the packing or buried deep in the biofilm, not in contact with contaminated gas, and not participating in biodegradation.

Removal efficiency (conversion), at the point where maximum EC is just attained, is another key performance measure of waste gas biodegradation. Figures 6.5 and 6.6 show that EC generally follows the 100% removal line at extremely low ethanol concentrations. Then at higher ethanol concentrations, elimination capacity deviates from the 100% removal line. Figure 6.8 further emphasizes that first order elimination kinetics exist experimentally at low inlet ethanol concentrations. At low values of C_o, when the overall rate is first order, conversion is approximately constant for a packed and fluidized bed peat bioreactor.

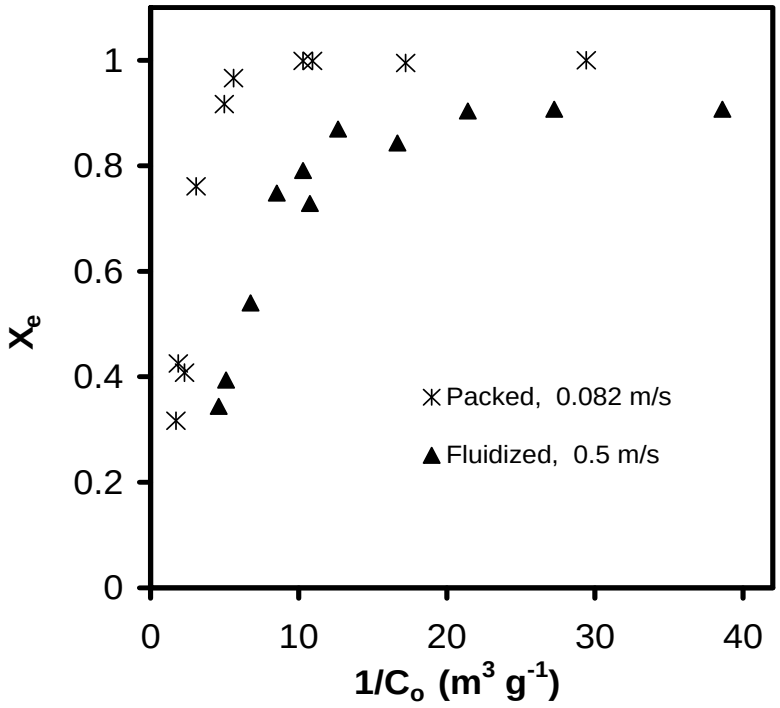

Figure 6.8 Experimental relationship between ethanol conversion and inlet ethanol concentration for a peat packed and fluidized bed.

Removal efficiency is a function of the first order rate constant, when elimination kinetics are first order. The outlet concentration of ethanol from the packed and fluidized bioreactors decreases, and in turn removal efficiency increases, with increased first order rate constant (Equations 6.30 and 6.44). Microbial growth in the sawdust/sphere high velocity packed bed (0.155 m s^{-1}) and fluidized bed (0.7 m s^{-1}) may follow first order instead of zero order kinetics before maximum EC is reached, because the inlet ethanol concentrations are very low (in order to maintain similar ethanol loadings, ethanol concentrations were decreased as superficial gas velocity increased). In these cases, the overall first order rate constant may be dominated by mass transfer, microbial kinetics, or a combination of both.

In the region prior to maximum EC, when the overall rate of biodegradation is first order, removal efficiency is also a function of residence time in the bioreactor. Removal efficiency changes with superficial gas velocity and bed height during operation. For the low velocity (0.0024 m s^{-1}) peat packed bed trials, removal efficiency appears to be 100% until maximum EC is reached. Residence time ($H_m\varepsilon_m/u_o$) is very high for the low velocity packed bed trials. As a result, when the overall rate constant is first order, C_{pH} is low (Equation 6.44) and conversion is

high. Although the peat fluidized beds show excellent performance with high elimination capacities, removal efficiencies prior to maximum EC are clearly lower than those of the packed beds. Figure 6.6 shows that deviations from the 100% removal line increase with increasing gas velocity for the peat fluidized beds. Note that for a packed and a fluidized bed bioreactor containing equal masses of packing material, residence time is calculated using the packed bed height and interparticle voidage (H_m and ε_m) and the fluidized bed height and interparticle voidage (H and ε_f), respectively. As a result, if a fluidized bed bioreactor is designed with particles which fluidize at low velocities, fluidization will not cause a significant decrease in residence time or conversion, compared to packed bed operation. Figure 6.9 compares predicted EC *versus* ethanol loading curves for a fluidized bed at increasing bed heights. The model predictions use the properties and rate constants in Tables 6.2 and 6.3 for the peat, fluidized bed at u_o = 0.5 m s^{-1}. Prior to maximum EC, the slope of the EC curve is proportional to removal efficiency and removal efficiency increases with bed height. It is observed that maximum EC in unaffected by bed height.

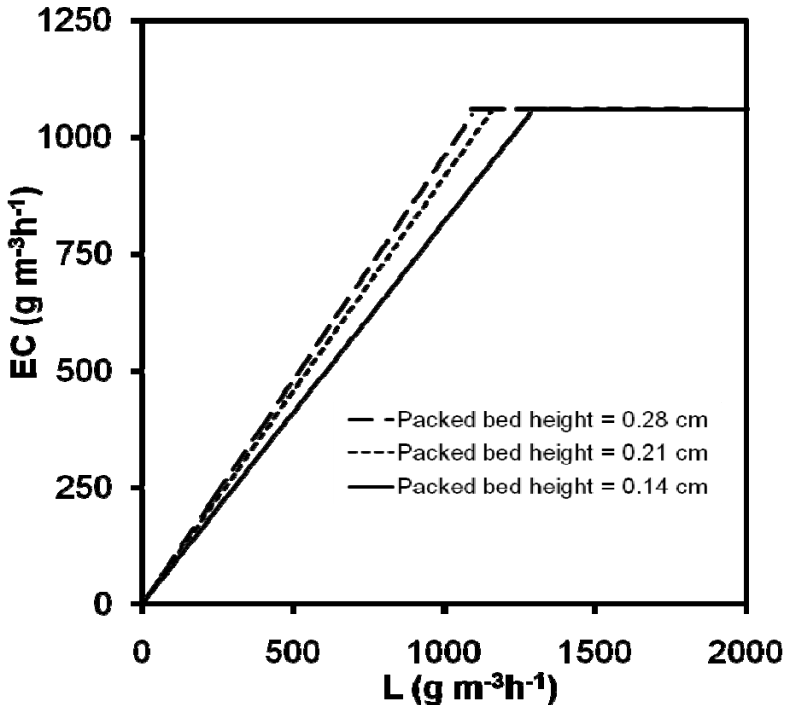

Figure 6.9 Predicted EC *versus* inlet ethanol loading at increasing packed bed heights in a peat, fluidized bioreactor bed, u_o =0.5 m s^{-1}.

For fluidized bioreactors, in addition to the first order rate constant and residence time, the removal efficiency is a function of bubble properties when first order kinetics are present. In Figure 6.6 and Table 6.2, a constant bubble diameter (30 mm) is used for predicting rate constants for the peat fluidized beds. The predicted first order rate constant *K* is found to decrease with increasing gas velocity. However, a decreasing first order rate constant is unlikely the only reason for the decrease in removal efficiency at higher velocity. During experiments, it was observed that bubble diameter increased with the higher gas velocities in the peat fluidized bioreactors. If for instance, *K* actually remains constant even when gas velocity increases, the following analysis shows that increasing bubble diameter may cause a loss in removal efficiency. The bubbling bed model was re-applied to the 0.75 and 1.0 m s^{-1} fluidized bed. By trial and error, bubble diameter of the higher velocity beds is iteratively changed until the predicted *K* is equal to that of the 0.5 m s^{-1} bed (3.9 s^{-1}). The resulting bubble diameters of the 0.75 and 1.0 m s^{-1} beds are 44 and 109 mm, respectively. The predicted first order biodegradation curves for the peat fluidized bioreactors with these larger bubble diameters are presented in Figure 6.10. The effect of bubble size on removal efficiency in a fluidized bioreactor is illustrated again in Figure 6.11. As discussed previously, it is clear that removal efficiency decreases as bubble size increases.

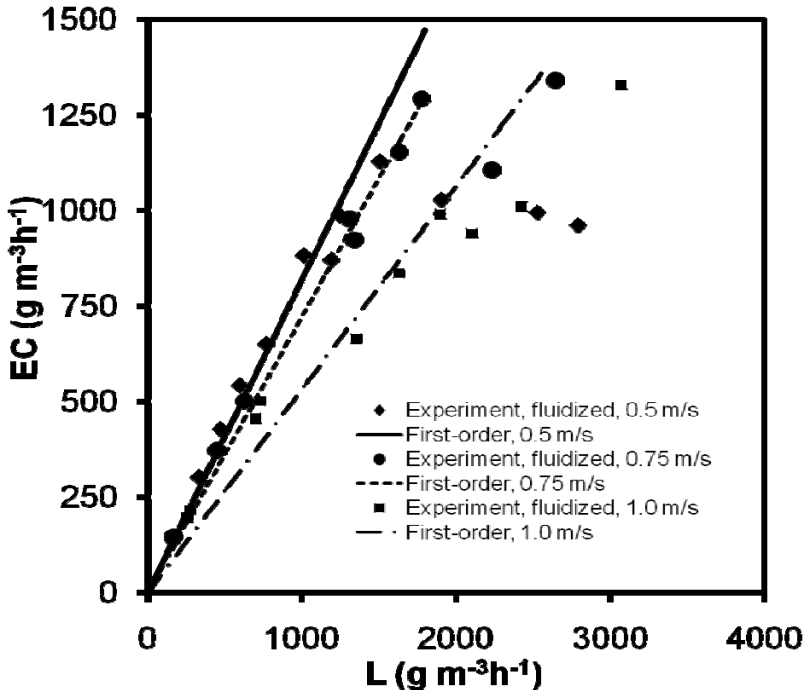

Figure 6.10 Comparison of bubbling bed, plug flow model to fluidized peat bed bioreactor experiments, calculated with a first order K = 3.9 s^{-1}, and bubble diameters of d_b =30 mm, u_o =0.5 m s^{-1}; d_b =44 mm, u_o =0.75 m s^{-1}; d_b = 107 mm, u_o = 1.0 m s^{-1}.

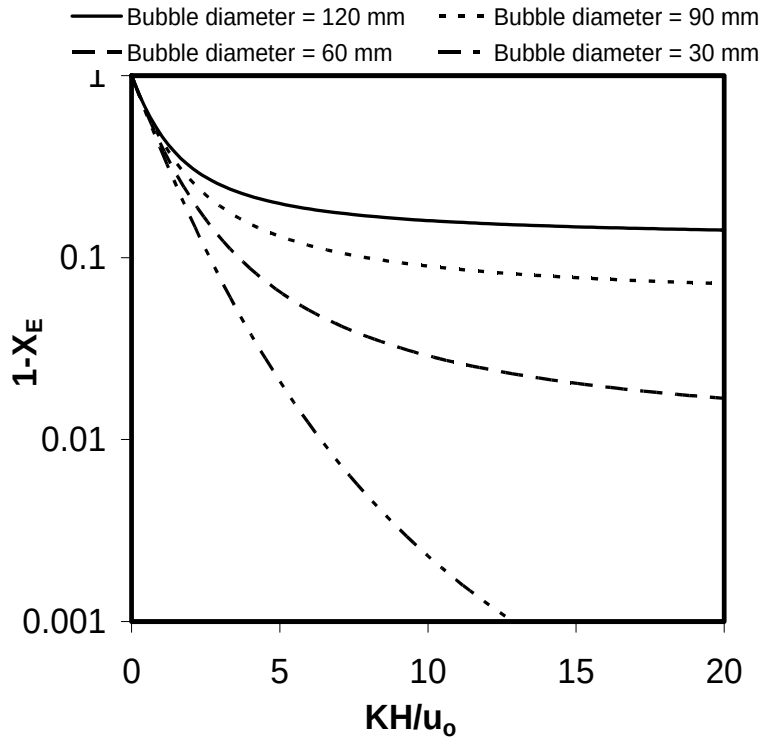

Figure 6.11 Predicted conversion versus the dimensionless first order reaction rate grouping, using the bubbling bed, plug flow model at different bubble diameters, u_o = 0.5 m s^{-1}.

Figure 6.12 compares the plug flow bubbling model to the non-bubbling, plug flow model, when the overall rate of ethanol elimination follows first order kinetics. The non-bubbling plug flow model is determined from Equation 6.44 using the same gas velocity, interparticle voidage and bed height as for the bubbling model. As expected, Figure 6.12 illustrates that the bubbling fluidized bed has lower conversion than a comparable non-bubbling bioreactor. Thus, the hydrodynamic conditions of fluidization cause a loss in removal efficiency and so it beneficial to design the fluid bed to operate at hydrodynamic conditions that optimize biodegradation performance.

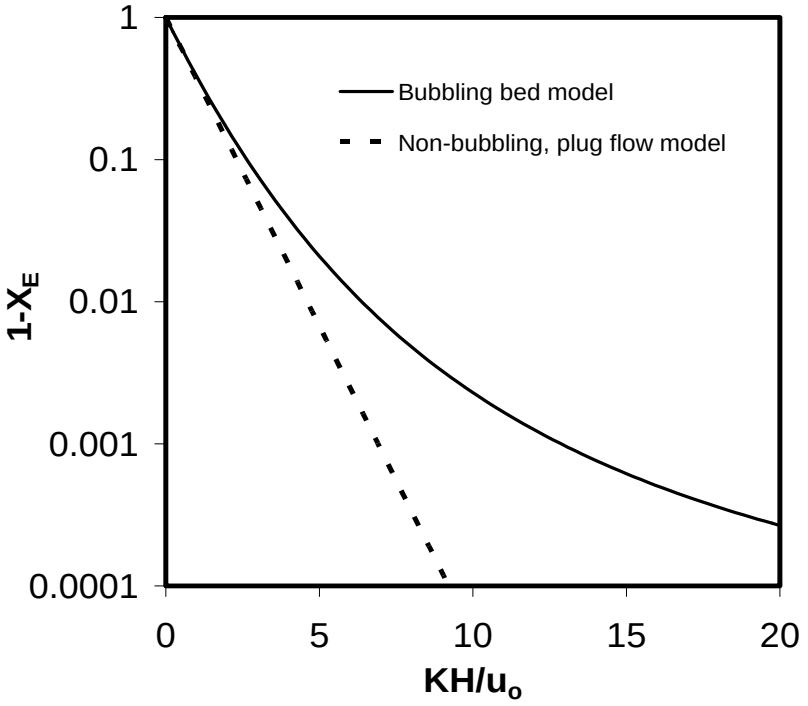

Figure 6.12 Comparison of non-bubbling and bubbling bed models for conversion as a function of the dimensionless first order reaction rate group for a bioreactor; u_o = 0.5 m s^{-1}, ε_f = 0.68, H = 0.24 m.

The absolute values predicted by the models in this study should be used with caution. Bubble properties have a significant effect on model predictions, especially the exchange of gas between bubbles and the particulate region (q). In this study, the calculated value of q (Equation 6.11) is high because the particles used in this study have high minimum fluidization velocities compared to the particles used by Kunii and Levenspiel for modelling intermediate bubbling beds (1990) and those reported in Davidson and Harrison (1963). This bubbling bed model for a

GSFB could be further fine-tuned by determining experimental values of q for the actual peat granules and sawdust/sphere packings used in the GSFB.

Further research could also help to improve the GSFB models. In this study, simplified microbial growth kinetics were assumed, neglecting concentration gradients throughout the depth of the liquid/biofilm layer. Future experimental studies of GSFBs could investigate biofilm thickness at different bed heights and determine diffusion rates in the biofilm layer. A GSFB biodegradation study conducted with varying bed heights would demonstrate whether the non-dispersed plug flow model accurately describes the gas phase of the particulate region or perhaps indicate that a well-mixed gas phase is a better approximation. The accuracy of this bubbling bed model depends on the many assumptions listed above, including a constant bubble diameter, and of spherical bubbles of the same size throughout the bioreactor. In reality, it is known that bubbles grow as they rise through bubbling beds because they coalesce with neighbouring bubbles and their shapes are not spherical.

6.6 Conclusions

A bubbling bed model has been developed and used to model waste gas treatment in a GSFB. Maximum elimination capacity and removal efficiency are two main measures of bioreactor performance. The model emphasizes that maximum EC is limited by microbial growth rate and microbial population, and the overall elimination of a substrate in the bioreactor is a zero order process at maximum EC. The zero order rate constant, K_0 is high for the peat GSFB. Removal efficiency is important at ECs prior to or at the point where maximum EC is reached, when the overall biodegradation rate is first order or a combination of first and zero order. A high first order rate constant results in high removal efficiencies. Packed beds and low velocity fluidized beds with lower residence times have higher removal efficiencies. In fluidized beds, increasing bubble size causes a loss of removal efficiency prior to the maximum EC. Overall, fluidization results in lower removal efficiencies, but significantly higher maximum EC values are obtained, as fluidization appears to enhance microbial biodegradation.

6.7 Nomenclature

a	Specific surface area of the particles covered with a liquid/biofilm layer (m^2 m^{-3} reactor bed during operation).
C_o,C_H	Ethanol concentration in gas entering and exiting bioreactor (g m^{-3}).
C_b,C_{bH}	Ethanol concentration in gas of bubble at any height and at bed surface (g m^{-3}).
C_p, C_{pH}	Ethanol concentration in gas phase of particulate region at any height and at bed surface (g m^{-3}).
d_b	Diameter of bubble (m).
EC	Elimination capacity per packed bed volume (g m^{-3} h^{-1}).
f_b	Volume fraction of bubbles in the bed volume during fluidization.
f_l	Volume fraction of liquid/biofilm phase in the bed volume during fluidization or packed bed operation.
H_m, H_{mf}, H	Bed height packed, at minimum fluidization, during fluidization (m).
H_e	Henry's constant for the equilibrium between ethanol in gas phase and liquid/biofilm phase (m^3 gas m^{-3} liquid).
k_g	Mass transfer coefficient for diffusion of ethanol through gas film from gas phase of particulate region to liquid/biofilm (m^3 gas m^2 area s^{-1}).
K	Overall rate coefficient for disappearance of ethanol from the gas phase of the particulate region, for first order kinetics (m^3 gas m^{-3} reactor s^{-1}).
K_0	Zero order bioreaction rate coefficient in the liquid/biofilm phase (g m^{-3} liquid s^{-1})
K_S	Saturation constant in Monod growth model (g m^{-3}).
L	Contaminant loading per packed bed volume (g m^{-3} h^{-1}).
N	Number of bubbles in a fluidized bed per bioreactor bed volume during fluidization (m^{-3}).
q	Bulk gas exchange between a single bubble and gas phase of particulate region (m^3 s^{-1}).
$-r_c$	Overall rate of disappearance of ethanol from gas phase of particulate region to microbial cells where it is biodegraded in terms of volume of bioreactor bed during operation (kg m^{-3} s^{-1}).
r_s	Rate of consumption of ethanol in liquid/biofilm phase (g m^{-3} s^{-1}).

r_x	Rate of formation of biomass (dry weight) in liquid/biofilm phase (g m^{-3} s^{-1}).
S	Concentration of substrate in liquid/biofilm phase (g m^{-3}).
t	Time (s)
u_o	Superficial gas velocity of contaminated air in bioreactor (m s^{-1}).
u_{mf}	Superficial gas velocity at minimum fluidization (m s^{-1}).
u_{br}, u_b	Rise velocity of a single bubble in stagnant liquid, and rise velocity of bubbles in a bubbling fluidized bed (m s^{-1}).
V_b	Volume of a single bubble (m^3).
Y_{xs}	Yield of biomass (dry weight) per mass of substrate.
X	Concentration of biomass (dry weight) in liquid/biofilm phase (g m^{-3} liquid)
X_e	Conversion of ethanol
z	Axial coordinate in vessel (m).

Greek letters

ε_m, ε_{mf} , ε_f	Volume fraction of voids in a packed bed, fluidized bed at minimum fluidization, and during fluidization.
μ, μ_m	Specific growth rate, maximum specific growth rate of microorganisms, s^{-1}.

6.8 References

Baquerizo, G.; Maestre, J.P.; Sakuma, T.; Deshusses, M.A.; Gamisans, X.; Gabriel, D.; Lafuente, J. A detailed model of a biofilter for ammonia removal: model parameters analysis and model validation. *Chem. Eng. J.* **2005**, *113*, 205-214.

Clarke, K.L.; Pugsley, T.; Hill, G.A. Fluidization of moist sawdust in binary particle systems in a gas-solid fluidized bed. *Chem. Eng. Sci*. **2005**, *60*, 6909-6918.

Clarke, K.L.; Hill, G.A.; Pugsley, T. Direct comparison of fluidized and packed bed bioreactors for bioremediation of an air pollutant. *Int. J. Chem. Reactor Eng*. **2007**, *5*(Article A11), 1-12.

Clarke, K.L.; Hill, G.A.; Pugsley, T. Improved VOC bioremediation using a fluidized bed peat bioreactor. *Trans. I. Chem. E., Part B Process Saf. Environ. Protect*. **2008**, *86*, 283-290.

Davidson, J.F.; Harrison, D. Fluidised Particles; Cambridge University Press: Cambridge, United Kingdom, 1963, pp 21-42, 63-74, 97-122.

Delebarre, A.; Andres, Y.; Pellerano, M.; Pero, P.; Garcia Munzer, D.G. Biofiltration of volatile organic compounds by a fluidized bed of sawdust. *Int. J. Chem. Reactor Eng*. **2007**, *5*(Article A22), 1-11.

Deshusses, M.A.; Johnson, C.T. Development and validation of a simple protocol to rapidly determine the performance of biofilters for VOC treatment. *Environ. Sci. Technol.* **2000**, *34*(3), 461-467.

Devinny, J.S.; Ramesh, J. A phenomenological review of biofilter models. *Chem. Eng. J.* **2005**, *113*, 187-196.

Environmental Protection Agency website: **www.epa.gov/air/emissions/voc.htm,** 2008**.**

Hodge, D.S.; Devinny, J.S. Modeling removal of air contaminants by biofiltration. *J. Environ. Eng*. **1995**, *121*, 21-32.

Hodge, D.S.; Devinny, J.S. Determination of transfer rate constants and partition coefficients for air phase biofilters. *J. Environ. Eng*. **1997**, *123*, 577-585.

Kunii, D.; Levenspiel, O. Fluidized reactor models. 1. For bubbling beds of fine, intermediate, and large particles. 2. For the lean phase. Freeboard and fast fluidization. *Ind. Eng. Chem. Res.* **1990**, *29*, 1226-1234.

Kunii, D.; Levenspiel, O. Fluidization Engineering, Second Ed.; Butterworth-Heinemann: Newton, MA, 1991, pp 1-13, 71-75, 137-162, 277-303.

Ottengraf, S.P.P.; van den Oever, A.H.C. Kinetics of organic compound removal from waste gases with a biological filter. *Biotechnol. Bioeng.* **1983**, *25*, 3089-3102.

Streese, J.; Schlegelmilch, M.; Heining, K.; Stegmann, R. A macrokinetic model for dimensioning of biofilters for VOC and odour treatment. *Waste Manage.* **2005**, *25*, 965-974.

Wisecarver, K.D.; Fan, L.S. Biological phenol degradation in a gas-liquid-solid fluidized bed reactor. *Biotechnol. Bioeng.* **1989**, *33*, 1029-1038.

CHAPTER 7 – Conclusions and Recommendations

7.1 Conclusions

This study involved the design and testing of a novel, gas-solid fluidized bioreactor for the treatment of waste gases. One of the most important design steps was to select suitable particles for the fluidized bed. Initially, 0.625 mm sawdust particles were chosen. While moist sawdust by itself fluidized poorly, the addition of 0.322 and 0.516 mm inert glass spheres was shown to improve the fluidization characteristics of sawdust. The mixture fluidized in a bubbling/slugging regime. In these binary mixtures of sawdust and glass spheres, there was an upper limit of the moisture content of the sawdust at which fluidization could be achieved, above which there was significant particle agglomeration and defluidization of the bed. For instance, the maximum sawdust moisture was 33 wt% (dry basis) and 54% with 0.322 mm and 0.516 mm spheres, respectively, when the mass fraction of glass spheres in the mixtures were above 0.70 and 0.88 respectively.

There was no particle agglomeration in mixtures of larger glass spheres (0.777 and 1.042 mm) and sawdust (at moistures of up to 82 wt%). However, the considerable differences in density and size of the sawdust and spheres resulted in the complete segregation of these two components during fluidization. The binary mixtures of the larger glass spheres and sawdust are likely less cohesive as a result of their lower ratio of liquid interparticle forces to buoyant weight of the particles. Thus, for binary mixtures of moist sawdust there is a very narrow range of sphere sizes for which bubbling fluidization is possible. The minimum size of the spheres is limited by the ratio of interparticle liquid bridging forces to particle weight, and the maximum size is limited by the degree of segregation of the binary mixture.

Existing correlations are unsuccessful at predicting the minimum fluidization velocity (u_{mf}) of the binary mixtures of glass spheres and sawdust. In general, these correlations are

strongly dependent on the types of particles. Furthermore, in the literature there are different definitions of u_{mf} for a binary mixture.

A binary mixture of moist sawdust and 0.516 mm glass spheres was successfully used in packed and fluidized bed bioreactors for the treatment of ethanol-contaminated air. Compared to a packed bed, fluidized bed operation was shown to double the mass transfer rate of the pollutant from the gas phase to the solid particles. Classic bioremediation elimination capacity (EC) curves are obtained in both packed and fluidized modes which confirm that the particle bed is capable of supporting microorganisms, even when fluidized. The maximum EC was 75 g m^{-3} sawdust h^{-1} for the fluidized bed compared to 225 g m^{-3} h^{-1} in the packed bed, even though the fluidized bed had a higher bulk mass transfer coefficient. At the maximum EC, it appears that the overall biotreatment rate is controlled by microbial growth kinetics. Because the packed bed is operated under higher ethanol concentrations, it has higher growth rates, resulting in higher EC values for packed bed operation. For both packed and fluidized beds, the glass spheres in the packing offered very little microbial growth support, which reduced the rate of bioremediation.

In a second bioremediation study, peat granules by themselves with a Sauter mean diameter of 0.680 mm were used as bioreactor packing. The peat bioreactor was operated in both fluidized and packed bed modes. For the treatment of ethanol, the fluidized bed demonstrated higher bioremediation rates than a comparable packed bed. In addition the bioremediation rate was much higher than that of a sawdust/glass sphere fluidized bioreactor and of other packed bed bioreactors reported in the literature. The peat fluidized bioreactor achieved EC values ranging from 1150 to 1520 g m^3 h^{-1}. Removal efficiencies in the peat fluidized bioreactor decreased as gas velocity increased. Larger bubbles (slugs) were observed at higher gas velocities. The increase in bubble size may account for a reduction in bioreactor conversion.

Peat granules were very successful as packing material for a fluidized bioreactor. Peat (0.680 mm) with a moisture content of 40 wt% (dry basis), exhibited bubbling fluidization behaviour. As with the fluidization of wet sawdust/glass sphere packing, there was an upper limit of the moisture content of the peat for which adequate fluidization could be achieved. Moisture contents of equal to or more than 63 wt% resulted in gas channelling through the bed. The fluidization of larger peat granules leads to plug flow of the particle bed, or the formation of large bubble sizes which may reduce reaction conversion. It is observed that the particle density of peat granules is high compared to other biomass particles such as sawdust and the shape of the

peat granules is much more spherical than sawdust. These property characteristics contribute to effective bubbling fluidization behaviour even when the peat granules are moist. Furthermore, the peat granules are able to absorb a high amount of moisture compared to sawdust, such that they can more readily support microbial cells. Finally, it has been found that traditional correlations for gas-solid fluidization can be used to predict u_{mf} of the peat granules, rather than having to use an experimental correlation specific for peat granules.

A bubbling bed model has been developed and used to model waste gas treatment in a GSFB. Maximum elimination capacity and removal efficiency are two main measures of bioreactor performance. The model emphasizes that maximum EC is limited by microbial growth rate and microbial population, and the overall elimination of a substrate in the bioreactor is a zero order process at maximum EC. The zero order rate constant, K_0 are high for the peat GSFB. Removal efficiency is important at ECs prior to or at the point where maximum EC is reached, when the overall biodegradation rate is first order or a combination of first and zero order. A high first order rate constant results in high removal efficiencies. Packed beds and low velocity fluidized beds with lower residence times have higher removal efficiencies. In fluidized beds, increasing bubble size causes a loss of removal efficiency prior to the maximum EC. Overall, fluidization results in lower removal efficiencies, but high maximum EC values are obtained, as fluidization appears to enhance microbial growth rates.

In industrial settings it can be difficult to operate biofilters (packed bed bioreactors) because uneven conditions can develop in the packing. Visually, the fluidized bioreactor was found to achieve a greater amount of particle mixing than the packed bed bioreactor. It could be inferred that more mixing results in more uniform bed conditions in the fluidized bioreactor, and thus improved operability. Fluidized bioreactors containing a bed of peat granules are an attractive treatment method for VOC-contaminated air. They have application for treating high volume emissions with low VOC concentrations, similar to those concentrations which were tested in the bioremediation experiments of this Ph.D. research.

7.2 Recommendations

The addition of glass spheres as a second inert particle to a bed of sawdust particles resulted in adequate fluidization. The glass spheres prevented problems with gas channelling and defluidization. Studies published to date using binary mixtures of sand and sawdust have presented only experimental results without a discussion of what the nature of interaction between the two types of particles may be. More research is needed to improve the fundamental understanding of the mechanisms which cause the improvement in fluidization quality in binary mixtures.

A potential means to enhance fluidized bioremediation performance is to recycle the outlet air from the fluidized bioreactor back to the inlet stream. Although elimination capacities have been found to be higher in a fluidized peat bed bioreactor versus a packed bed, removal efficiencies in the fluidized bed are lower. A recycle stream would boost the overall removal efficiency in the bioreactor.

The raw materials for a fluidized peat bioreactor process are peat granules, nutrient solution and water which are all very low in cost. Costs could be further reduced by investigating options of on-site production of peat granules from raw peat for use in the fluidized bioreactor. Thus, inexpensive raw peat available from local sources could be used. It is proposed that prior to putting the fluidized bioreactor into operation, the commercial operator would prepare peat granules in the bioreactor vessel. Conceivably, fluidization of raw peat in the bioreactor using a hot air stream would be sufficient to granulate the raw peat. Research is required to fine-tune a method of transforming raw peat to peat granules by a fluidization process.

A potential disadvantage of using a fluidized versus a packed bed system for bioremediation is that fluidization involves higher gas velocities in the bed. Higher velocities require more energy for boosting the pressure of the contaminated air. However, the added energy cost may be off-set by higher maximum elimination capacities in a fluidized bioreactor. A complete energy study and cost analysis should be completed to compare the capital and operating expenses of a fluidized bioreactor system to a conventional biofilter.

In the experimental work that was completed in the present study, only a single VOC (ethanol) was treated in the fluidized bioreactor. The bioreactor should be tested for the

treatment of other VOCs, including a hydrophobic contaminant such as toluene which is less soluble in water. The transfer of a hydrophobic contaminant to the biofilm on the bed particles may have an effect on the overall bioremediation rate and removal efficiency. In addition, microbial growth kinetics vary with type of contaminant. Another concern to investigate when treating contaminants that are difficult to decompose is that the microbial culture in the bioreactor may start feeding on organic compounds in the packing material. Peat granules are rich in organic compounds that may be preferred as a food source over the air contaminant. Furthermore, the fluidized bioreactor should be tested for the bioremediation of different mixtures of VOCs.

The bench-scale fluidized bioreactor should be operated for longer run-times of at least several months. These experiments would investigate whether the pollutant removal changes with lengthy run-times or with age of the peat bed. The fluidized bioreactor should be operated continuously in fluidized bed mode during this time period. Another opportunity during long-term experiments is to vary the concentration of the air pollutant to assess how the fluidized bioreactor adapts and responds to changing conditions over time.

The presence of larger bubbles at higher operating velocities likely reduced reaction conversion in the peat fluidized bioreactor. Further work is warranted to assess bioremediation performance with smaller bubbles sizes, yet similar operating velocities. For instance, different sizes and size distributions of peat granules should be studied in an effort to obtain bubbles which are as small as possible during fluidization. Other inlet distributor designs should be tested, as well as the use of bed internals at various bed heights to break up bubbles.

There is very little reported in the literature on the fluidization properties of peat. An additional study of peat bubbling bed fluidization could be completed with the use of more sophisticated measurement techniques such as electrical capacitance tomography (ECT) and radioactive particle tracking (RPT). ECT could be used to measure the size, shape, and growth of bubbles. While particle mixing was visually observed in the peat fluidized bioreactor, RPT would allow for quantification of the amount of mixing at different gas velocities and bed depths.

It is difficult to devise an accurate model of a fluidized bioreactor because bioremediation performance is strongly dependent on the concentration gradients of the microbial cells and the substrates in the biofilm on the particles, which in turn depends on the properties of the biofilms. In reality, biofilm thickness, extent of biofilm coverage on the particles, microbial species,

microbial cell concentration, contaminant diffusion rates in the biofilm, contaminant solubility in the biofilm, and biokinetics may vary throughout a single biofilm. Furthermore, these properties may vary widely throughout the entire particle bed. Similar difficulties are currently faced when modelling biofilters. A great deal of study is necessary, before biofilms can be thoroughly represented by models.

The fluidized bioreactor was modelled using non-dispersed plug flow of the gas phase of the particulate region. Experiments are required to assess whether the non-dispersed, plug flow case, completely mixed case or a combination of both cases better describes the actual bioreactor. Bioremediation trials would be completed at different bed heights at a particular superficial gas velocity, to assess the affect of residence time on conversion. The relationship between residence time and conversion would then be compared to predictions of the model cases.

Further research would help to refine the gas fluidized bioreactor model. The accuracy of the bubbling bed models depends on the assumptions that bubble diameter is constant, bubbles are spherical, and bubbles throughout the bioreactor are the same size. In reality it is known that bubbles grow as they rise through bubbling beds because they coalesce with neighbouring bubbles. Also, bubble shape is not spherical. Experiments are required to characterize the properties of the bubbles, which could then be incorporated into a much more complex, fluidized bioreactor model.

APPENDIX A: Additional Experimental Data and Calibration Curves

A.1 Calibrations for ethanol analysis

Table A.1 GC calibration standards for ethanol in air, at laboratory temperature of 22 ºC; an example of the standards for analysis of inlet and outlet air samples, in Chapters 3 and 4.

Concentration of ethanol in solution added to standard vial (mole/m^3 of liquid)	Calculated concentration of ethanol in headspace of standard vial (g/m^3 of air)
0	0.00000
0.17	0.0019
0.34	0.0037
0.86	0.0092
1.20	0.0129
1.37	0.0148
1.71	0.0185

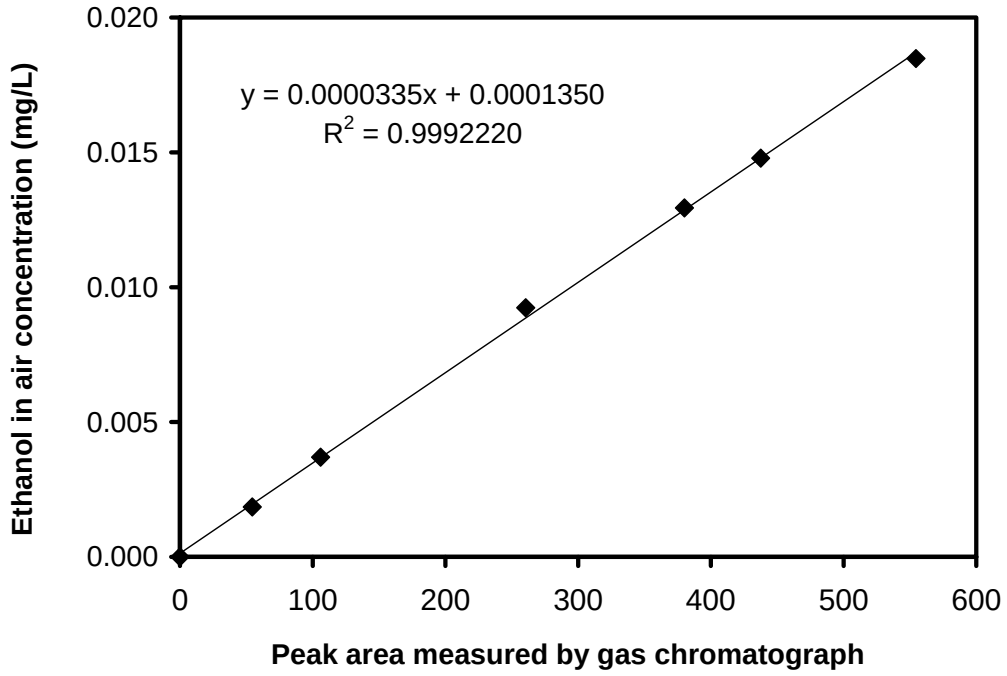

Figure A.1 Gas Chromatograph calibration of ethanol in air using data from Table A.1, laboratory temperature = 22ºC, GC split flow = 24 mL/min, sample size = 0.5 mL; an example of the calibrations used in the analysis of ethanol in inlet and outlet air samples in Chapters 3 and 4.

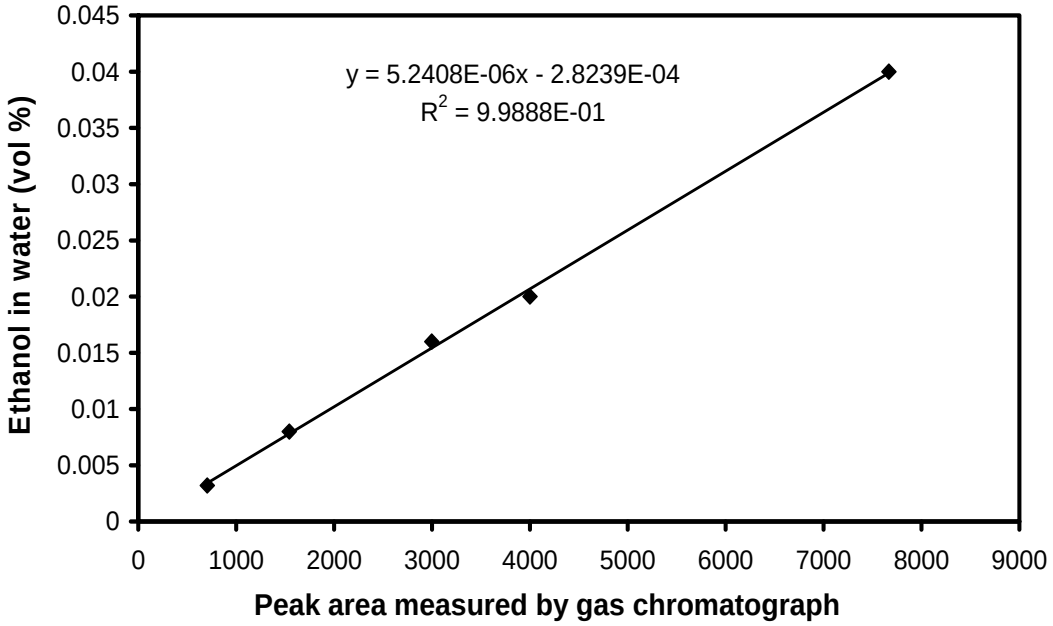

Figure A.2 Gas Chromatograph calibration of liquid ethanol in water, GC split flow = 50 mL/min, sample size = 0.5 μL. An example of the calibrations used for analyzing ethanol in liquid samples from batch growth flask experiments in Chapters 3 and 6.

A.2 Calibrations of rotameters and mass flow meters

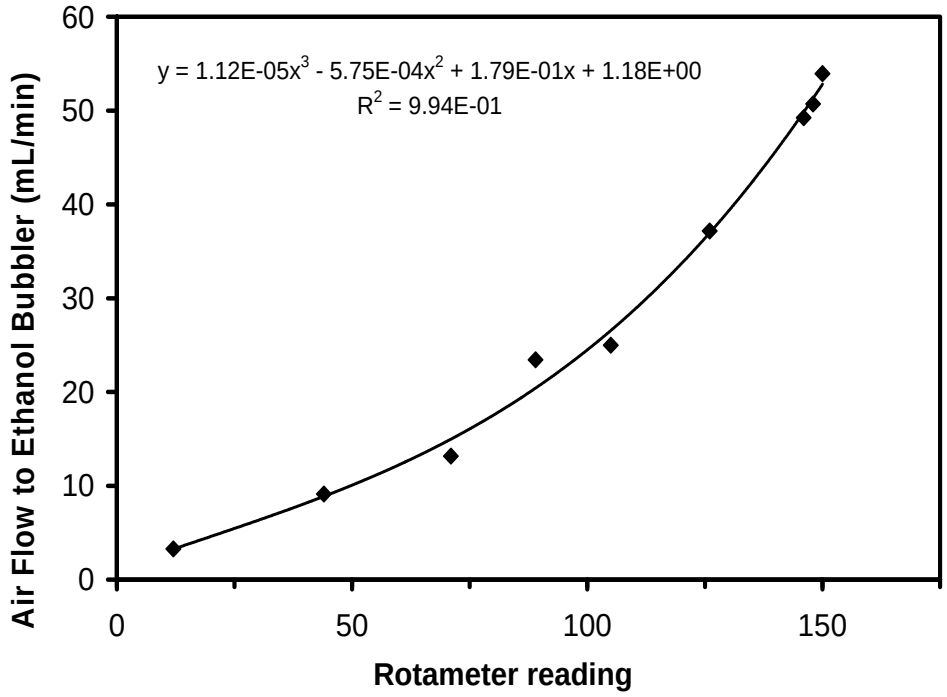

Figure A.3 Calibration curve of rotameter 1 which measured air flowrate to ethanol bubbler.

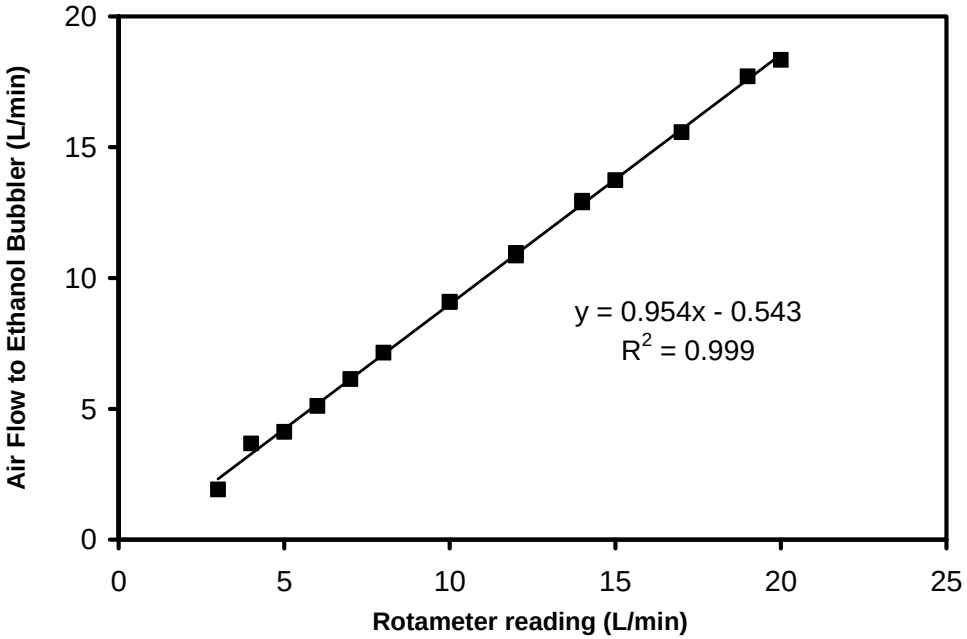

Figure A.4 Calibration curve of rotameter 2 which measured air flowrate to ethanol bubbler.

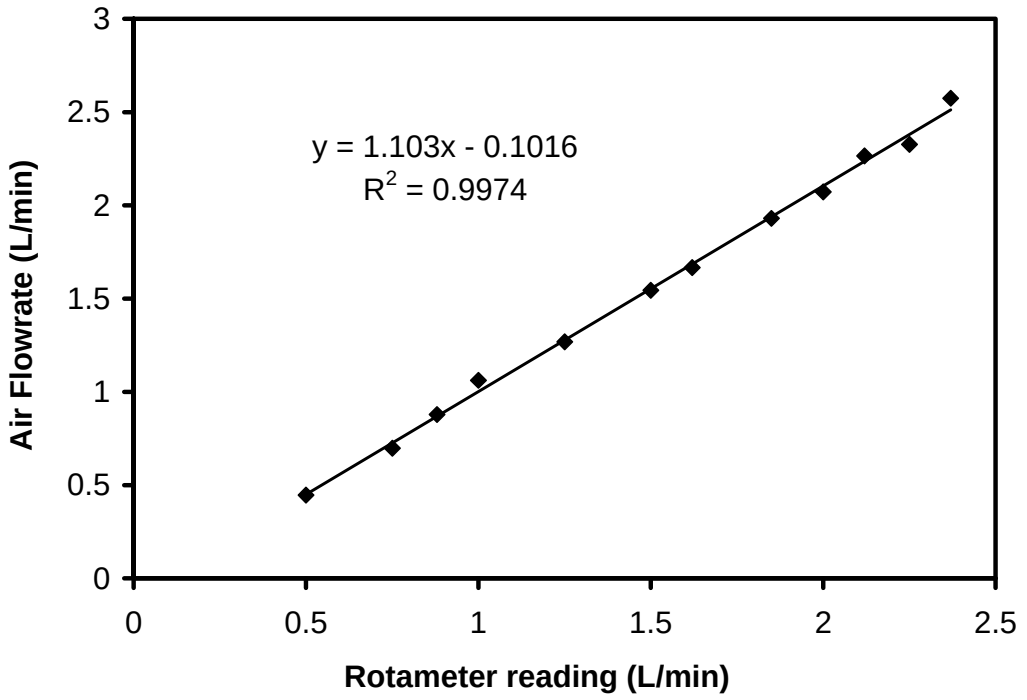

Figure A.5 Calibration curve of rotameter 3 which measured air flowrate to packed bed bioreactor at superficial gas velocities of 0.0024 m s^{-1}.

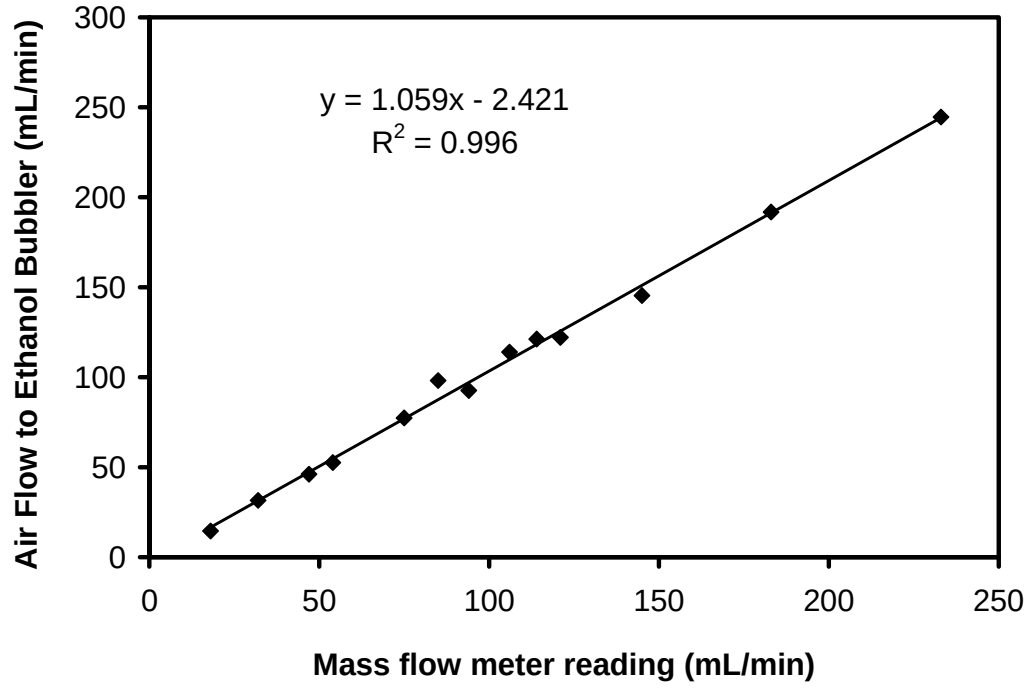

Figure A.6 Calibration curve of mass flow meter 1 which measured air flowrate to ethanol bubbler.

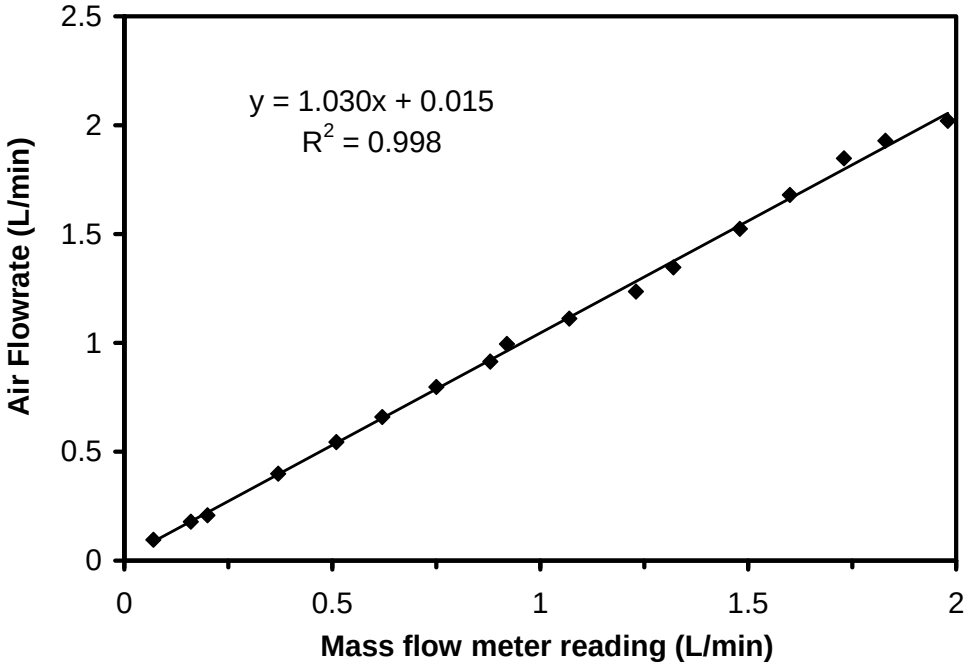

Figure A.7 Calibration curve of mass flow meter 2 which measured air flowrate to ethanol bubbler.

A.3 Flow orifice plate calibrations

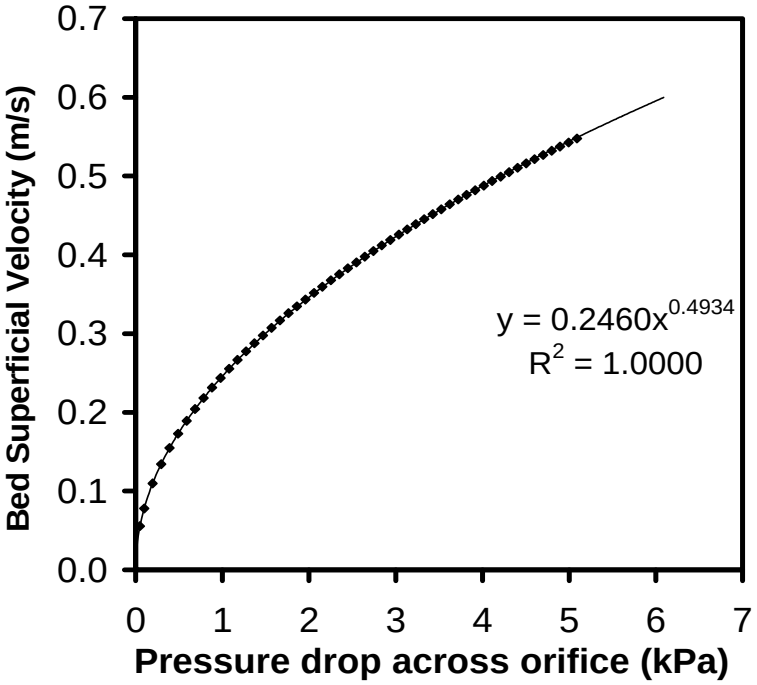

Figure A.8 Calibration curve for 12.7 mm (0.5 inch) flow orifice plate: the superficial velocity in the bioreactor bed is calculated as a function of pressure drop across the orifice plate.

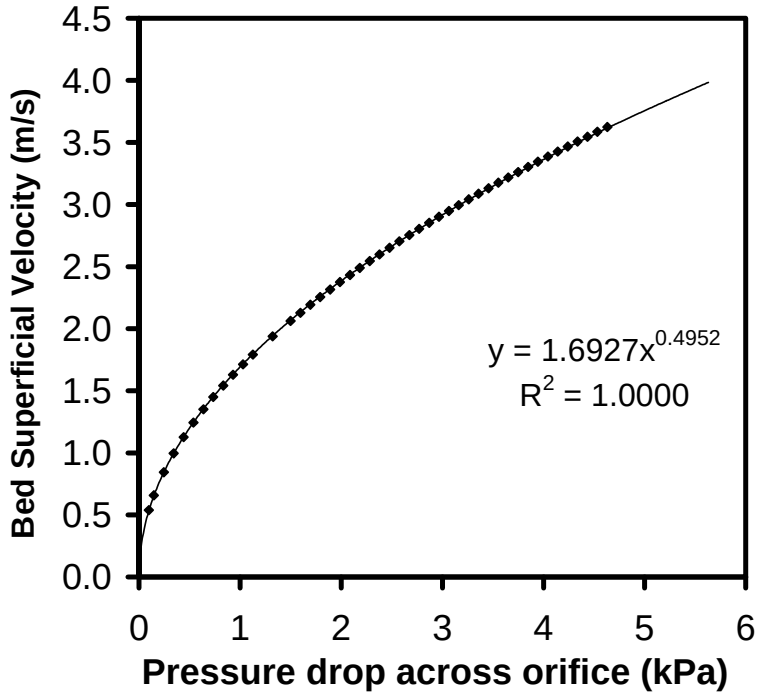

Figure A.9 Calibration curve for 31.8 mm (1.25 inch) flow orifice plate: the superficial velocity in the bioreactor bed is calculated as a function of pressure drop across the orifice plate.

A.4 Biomass calibrations

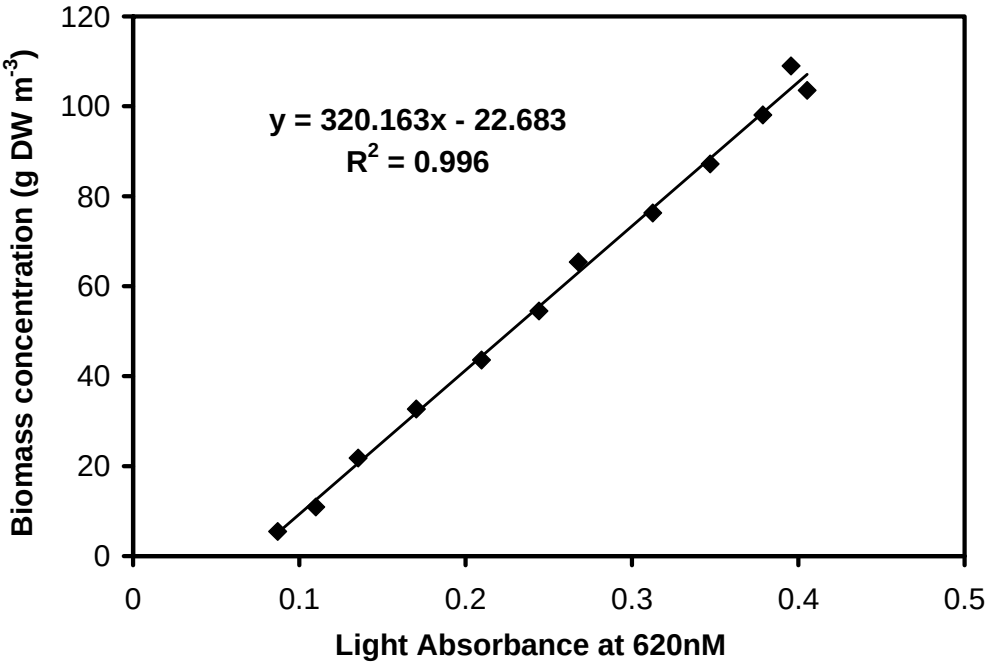

Figure A.10 Calibration curve of biomass concentration versus optical density on spectrophotometer, at a wavelength of 620 nM. Predominant cell line (*Pichia anomala*) during bioremediation experiments using sawdust/glass sphere packing (Chapter 3).

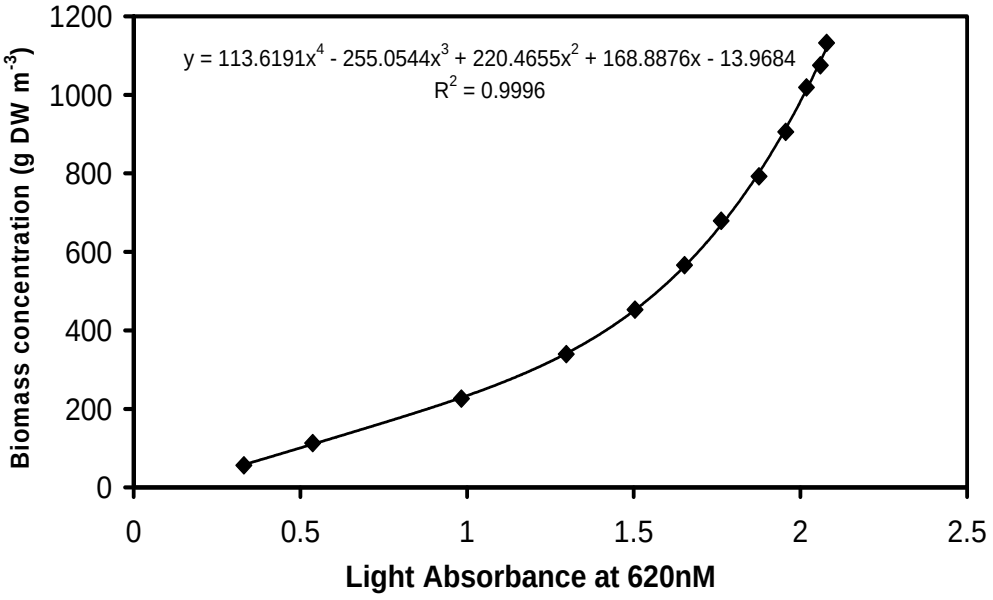

Figure A.11 Calibration curve of biomass concentration versus optical density on spectrophotometer, at a wavelength of 620 nM. Predominant cell line (*Pichia* spp) during bioremediation experiments using peat granule packing (Chapter 6).

A.5 Particle size distributions

Table A.2 Particle size distribution of sawdust particles using sieve analysis.

Tyler Equivalent Sieve Mesh No.	Sieve Opening (mm)	Weight fraction of material collected on sieve
passing through 48	--	0.02
48	0.300	0.02
45	0.354	0.06
35	0.417	0.11
32	0.500	0.26
28	0.589	0.30
24	0.710	0.17
20	0.850	0.06
16	1.000	0.01
12	1.400	0.00

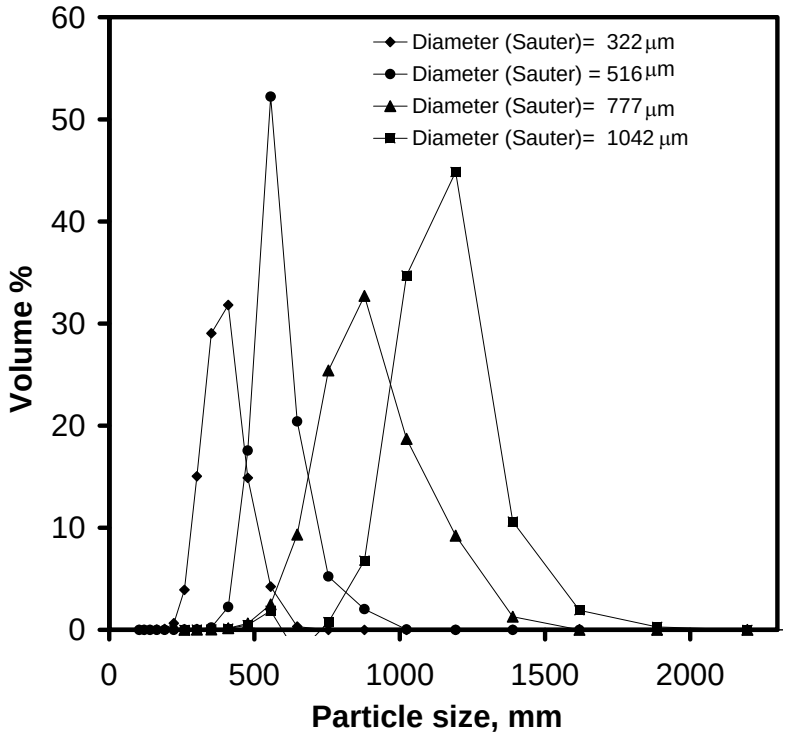

Figure A.12 Particle size distributions of glass spheres measured by Malvern particle size analyzer.

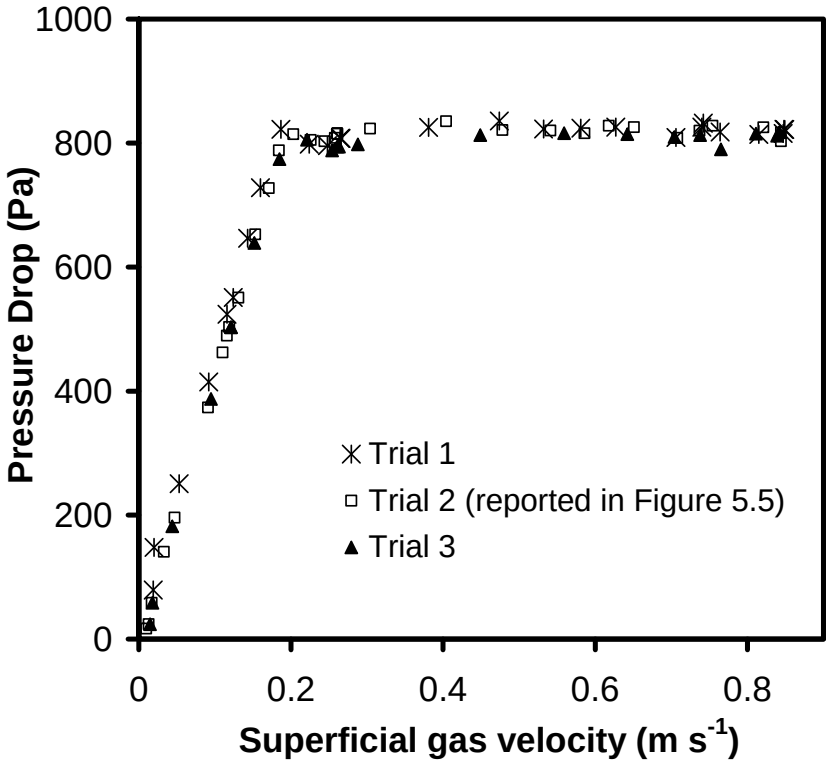

Figure A.13 Triplicate trials showing the reproducibility of pressure drop *versus* velocity profiles of material 3 peat, at increasing velocity (moisture content of 40 wt%, dry basis).

APPENDIX B: Determination of Mass Transfer Coefficients

B.1 Numerical method for calculating mass transfer coefficients

In Chapter 3, Equations 3.1 and 3.2 are used to describe ethanol concentrations in a particle bed, where gas flow is assumed to be non-dispersed, plug flow. The mass transfer coefficient in these equations is determined by first solving differential Equations 3.1 and 3.2 with a fully implicit, finite difference numerical method. From experimental data all variables in these equations are known except for the mass transfer coefficient. The partial differential equations were discretized backwards in time and central in space (Figure B.1).

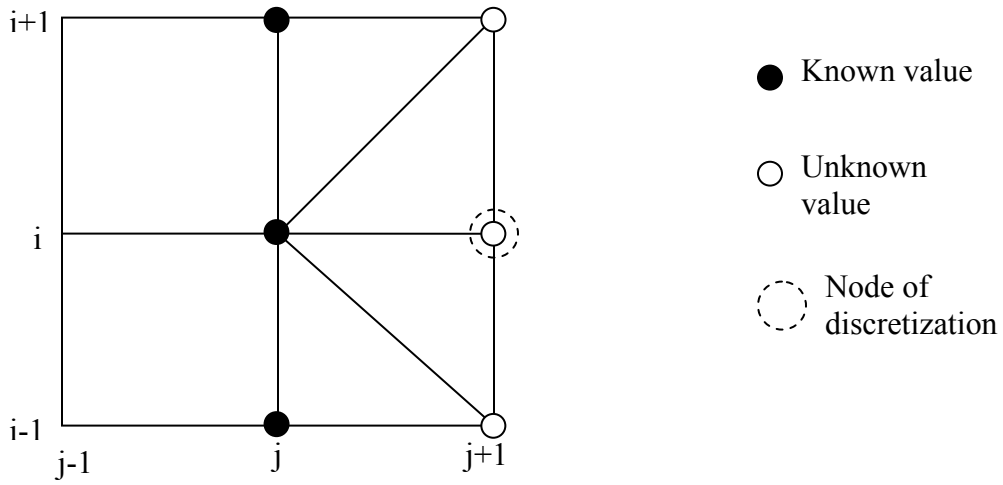

Figure B.1 Discretization scheme of fully implicit method.

For simplification, the non-linear relationship of the adsorption isotherm, Equation 3.3, was approximated by a linear equation. Linear regression was performed with Microsoft Excel software on the data for ethanol concentration in the gas (C) versus ethanol concentration adsorbed in the packing at saturation conditions ($C_{ads,sat}$), to obtain the linear relationship:

$$C_{ads,sat} = k_L C + b \tag{B.1}$$

where k_L = 475 and b = -623. The R^2 value describing the goodness of fit of Equation (B.1) to the experimental data is = 0.98. Figure B.2 compares Equations 3.3 and B.1 to the experimental ethanol adsorption data.

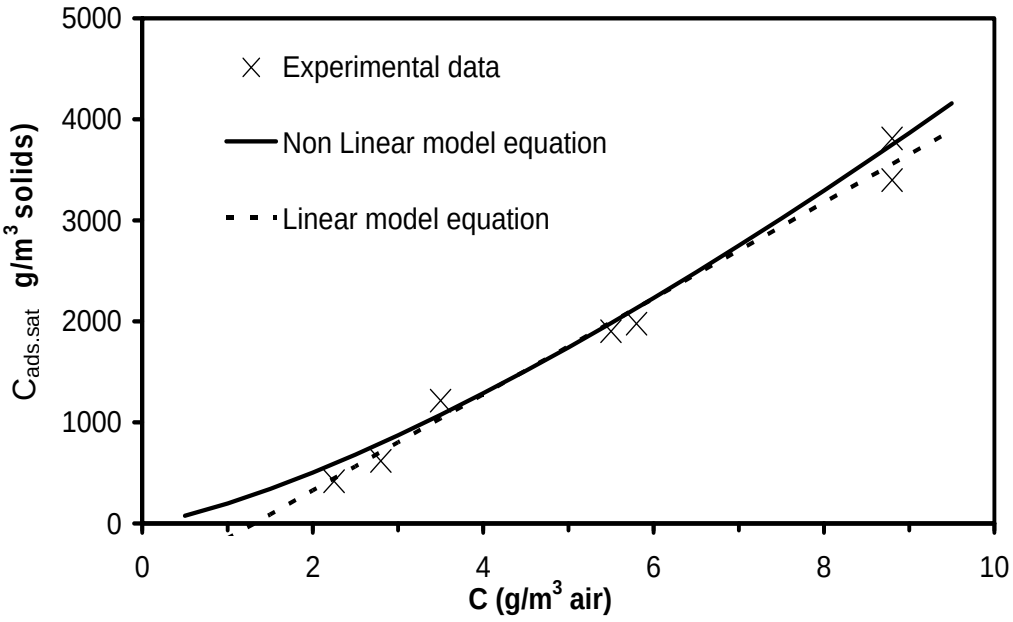

Linear relationship $C_{ads,sat} = 475 \cdot C - 623$

Non-linear relationship $C_{ads,sat} = 189 * C^{1/0.74}$

Figure B.2 Comparison of experimental adsorption of ethanol on sawdust and glass sphere packing by a linear relationship and a non-linear relationship.

Equation B.1 is substituted into differential equations 3.1 and 3.2, and then they are discretized to obtain:

$$\frac{C_{ads,i,j+1} - C_{ads,i,j}}{\Delta t} = K \cdot \left(k_L C_{i,j+1}\right) - K\ C_{ads,i,j+1} + bK \tag{B.2}$$

$$\frac{C_{i,j+1} - C_{i,j}}{\Delta t} = \frac{-V(C_{i+1,j+1} - C_{i-1,j+1})}{2\Delta z} - \left(\frac{1-\theta}{\theta}\right) K\ \left(k_L C_{i,j+1}\ + b - C_{ads,i,j+1}\right) \tag{B.3}$$

where *i* and *j* represent nodes in the axial direction and time respectively, such that:

- At the base of column, *z*=0, *i*=1
- At the top of bed, *i*=n, *z*=*H,* where *H* is the total height of the packed bed.
- At time t=0, *j*=1

Equations B.2 and B.3 are simplified, and known values are isolated to one side of the equation:

$$C_{ads,i,j} - \alpha = \beta C_{ads,i,j+1} + \gamma \cdot C_{i,j+1} \tag{B.4}$$

$$C_{i,j} - E = A \cdot C_{i-1,j+1} + B \cdot C_{i,j+1} - A \cdot C_{i+1,j+1} + D \cdot C_{ads,i,j+1} \tag{B.5}$$

where:

$$\beta = 1 + K\ \Delta t \quad \gamma = -K \cdot\ k_L \Delta t \quad \alpha = -K \cdot b \Delta t$$

$$A = -\frac{V\ \Delta t}{2\Delta z} \quad B = 1 + K \cdot k_L \Delta t \left(\frac{1-\theta}{\theta}\right) \quad D = -K\ \Delta t \left(\frac{1-\theta}{\theta}\right) \quad E = K\ \Delta t \left(\frac{1-\theta}{\theta}\right) \cdot b \tag{B.6}$$

The boundary and initial conditions for the problem are as follows:

- At the base of the column, the inlet concentration of ethanol in the air to the vessel remains constant at all times: $C_{in} = C_{1,j}$ for $t \geq 0$
- At the top of the column (node $i=n$, $z=H$), there is no change in ethanol concentration in the air phase or the particles at all times:

  $\delta C / \delta z = 0$ and $\delta C_{ads} / \delta z = 0$ for $t \geq 0$, $C_{n-1,j} = C_{n,j}$ and $C_{ads,n-1,j} = C_{ads,n,j}$
- Initially, the concentration of ethanol in the particles is zero throughout the bed:

  $C_{ads,i,1} = 0$ for $z \geq 0$ (nodes i=1 to n)
- Initially, the concentration of ethanol in the air within the column is zero, except at the base:

  $C_{i,1} = 0$ for $z > 0$ (nodes i=2 to n)

As a result of the boundary conditions, Equation B.5 is modified for nodes i=2, and i=n-2:

Node i=2:

$$C_{2,j} - A \cdot C_{in} - E = B \cdot C_{2,j+1} - A \cdot C_{3,j+1} + D \cdot C_{ads,2,j+1} \tag{B.7}$$

Node i=n-1:

$$C_{n-1,j} - E = A \cdot C_{n-2,j+1} + (B - A) \cdot C_{n-1,j+1} + D \cdot C_{ads,n-1,j+1} \tag{B.8}$$

At the boundaries, the following equations apply:

Node i=1, j>1

$$C_{ads,1,j} - \alpha = \beta C_{ads,1,j+1} + \gamma \cdot C_{in} \quad \text{(B.9)}$$

Node $i=n$, $j>1$

$$C_{ads,n,j+1} = C_{ads,n-1,j+1} \quad \text{(B.10)}$$

$$C_{n,j+1} = C_{n-1,j+1} \quad \text{(B.11)}$$

The solution scheme for the discretized equations is as follows:

Two tables of values of C and $Cads$ at various times and heights are created. All values for the initial time, at node j=1 are filled in. For time step j+1 the following iteration procedure is followed:

- Boundary condition $C_{ads1,j+1}$ is calculated from Equation B.9
- For nodes $2 \leq i \leq n$-1, $C_{ads,i,j+1}$ and $C_{i,j+1}$ are calculated using Equations B.4 and B.5 entered into a matrix equation (Equation B.12). Equation B.12 is solved for the vector of unknown values (vector $\vec{x}$**),** which contains $C_{ads,i,j+1}$ and $C_{i,j+1}$ for time step j+1**.**
- $C_{ads,n,j+1}$ is calculated from Equation B.10
- $C_{n,j+1}$ is calculated from Equation B.11
- Then all values for $C_{ads,i,j+1}$ and $C_{i,j+1}$ are re-designated as the previous time node (j) as $C_{ads,i,}$ and $C_{i,j}$ and the iteration is repeated for the next time node (j+1).

For nodes $i=2$ to n-1, the difference equations can be summarized by a matrix-vector formulation:

$$[M] \cdot \vec{x} = \vec{b} \quad \text{(B.12)}$$

where $\vec{b}$ is a vector of known values, $\vec{x}$ is vector of unknown values, and *[M]* is the matrix of coefficients multiplied by vector $\vec{x}$ to form the equations for a particular time node:

$$M = \begin{bmatrix} \beta & 0 & . & 0 & \gamma & 0 & . & 0 & 0 & 0 \\ 0 & \beta & . & 0 & 0 & \gamma & . & 0 & 0 & 0 \\ . & . & . & . & . & . & . & . & . & . \\ 0 & 0 & . & \beta & 0 & 0 & . & . & . & \gamma \\ D & 0 & . & 0 & B & -A & 0 & . & . & 0 \\ 0 & D & . & 0 & A & B & -A & . & . & 0 \\ . & . & . & . & . & . & . & . & . & . \\ 0 & 0 & . & D & 0 & 0 & 0 & . & A & (B-A) \end{bmatrix}$$

$$\vec{x} = \begin{bmatrix} C_{ads,2,j+1} & C_{ads,3,j+1}.....C_{ads,n-2,j+1} & C_{ads,n-1,j+1} & C_{2,j+1} & C_{3,j+1}.....C_{n-2,j+1} & C_{n-1,j+1} \end{bmatrix}$$

$$\vec{b} = \begin{bmatrix} C_{ads,2,j} - \alpha & C_{ads,3,j} - \alpha.....C_{ads,n-2,j} - \alpha & C_{ads,n-1,j} - \alpha & C_{2,j} - AC_{in} - E & C_{3,j} - E & .....C_{n-2,j} - E & C_{n-1,j} - E \end{bmatrix}$$

A MatLab program was written to complete the above iteration procedure and to solve the equations. In Matlab, matrix [M] was converted into a sparse matrix $[M]_{sparse}$ to squeeze out all zero entries, and to reduce usage of computer memory. Then an LU factorization was calculated for $[M]_{sparse}$ using the "*luinc*" function to provide preconditioning terms for the function "bicgstab". Using equation B.12, $\vec{b}$ was divided by $[M]_{sparse}$ to solve for $\vec{x}$, with the stabilized biconjugate gradient method, "bicgstab" function. The bicgstab function used the preconditioning terms calculated with the luinc function.

B.2 MatLab program for calculating mass transfer coefficients

```
%Packed bed VOC adsorption Model
%Kyla Clarke
%April 2005
 clear;
close all;
format long g
 [newfile,newpath] = uiputfile('h:\packed.txt',...
   'Save Model Output File');
output_path = strcat(newpath,newfile)
outfile = fopen(output_path,'w');

prompt = {'Simulation Time(min)','Time Step (s)','Height of packed bed
(m)',...
      'Packed bed Nodes'};
title_GUI1 = 'Input Solution Parameters';
lines = 1;
def = {'300','30','0.204','50'};
user_input_matrix = inputdlg(prompt,title_GUI1,lines,def);

t_sim = 60*str2num(user_input_matrix{1}); %sec
del_t = str2num(user_input_matrix{2}); %sec
H_L = str2num(user_input_matrix{3}); %packed bed height in metres
nodes_z = str2num(user_input_matrix{4});
del_z = H_L/nodes_z;

prompt2 = {'Ethanol Concentration of the inlet gas phase (g/m3
air)','Initial ethanol adsorbed Concentration in packing (g/m3
packing)'...
      'Equilibrium coefficient m3 air/m3 packing','Mass Transfer
Coefficient (KLa) (1/s)'...
    'density of packing (kg/L)','equilibrium constant b'};
title_GUI2 = 'Input Model Parameters';
lines2 = 1;
def2 = {'5.8','0.0','475','0.00889','2.13','-623'};
user_input_matrix2 = inputdlg(prompt2,title_GUI2,lines2,def2);
 C_in = str2num(user_input_matrix2{1}); %inlet gas concentration
```

```
Cads_initial = str2num(user_input_matrix2{2}) %g/m3 packing
KH = str2num(user_input_matrix2{3});
KLa = str2num(user_input_matrix2{4});
dens_p = str2num(user_input_matrix2{5}); %kg/L packing
constant_b = str2num(user_input_matrix2{6});

prompt3 = {'packed bed Superfical Gas Velocity (m/s)','Packed bed
Diameter (m)'...
    'Packing Porosity'};
title_GUI3 = 'Flow Parameters';
lines3 = 1;
def3 = {'0.155','0.139','0.433'};
user_input_matrix3 = inputdlg(prompt3,title_GUI3,lines3,def3);

U_GR = str2num(user_input_matrix3{1}); %m/s
d_riser = str2num(user_input_matrix3{2}); %diameter of packed bed
metres
height_packing = H_L %meteres, packing height is height of packed bed
phi_s = str2num(user_input_matrix3{3});

g = 9.81;
 Cads_sat = ((C_in)*(475))-623;%equilibrium concentration of packing
in contact with C_in, g/m3 packing

V_GR = U_GR/phi_s; %interstitial velocity for eqns

alpha1 = -KLa*constant_b*del_t;
beta = 1 + KLa*del_t;
gamma = -del_t*KLa*KH;

A = -V_GR*del_t/2/del_z; %
B = 1+((1-phi_s)/phi_s)*KLa*KH*del_t;
D = -KLa*del_t*(1-phi_s)/phi_s;
E = (constant_b)*KLa*del_t*(1-phi_s)/phi_s;

for i = 1 : nodes_z
   if i==1
      A_mat(i,i) = beta;
```

```
      A_mat(i,i+1) = 0;
      A_mat(i,i+nodes_z) = gamma;
   elseif i == nodes_z
      A_mat(i,i-1) = 0;
      A_mat(i,i) = beta;
      A_mat(i,2*nodes_z) = gamma;
   else
      A_mat(i,i-1) = 0;
      A_mat(i,i) = beta;
      A_mat(i,i+1) = 0;
      A_mat(i,i+nodes_z) = gamma;
   end
end

for i = nodes_z + 1 : 2*nodes_z
   if i == nodes_z + 1
      A_mat(i,i) = B;
      A_mat(i,i+1) = -A;
      A_mat(i,i-nodes_z) = D;
   elseif i == 2 * nodes_z
      A_mat(i,i) = B-A;
      A_mat(i,i-1) = A;
      A_mat(i,i-nodes_z) = D;
   else
      A_mat(i,i-1) = A;
      A_mat(i,i) = B;
      A_mat(i,i+1) = -A;
      A_mat(i,i-nodes_z) = D;
   end
end

%LU decomp
A_mat = sparse(A_mat); %the sparse function condenses matrix to a list
of its non zero values with location
[L U] = luinc(A_mat,'0');
[n m]  = size(A_mat);
b_vectr  = zeros(n,1);
Cads = zeros(1,nodes_z);
```

```
C = zeros(1,nodes_z);
b_vectr([1:nodes_z],1) = Cads_initial;
loop = 0;
total_time = 0;
Cads_in = Cads_initial;

fprintf(outfile,'Packed bed Model Output From ELAB_model.m\r\n\r\n');
fprintf(outfile,'Packed bed Height (m):\t%f\r\n',H_L);
fprintf(outfile,'Delta Z (m):\t%f\r\n',del_z);
fprintf(outfile,'Packed bed Diameter (m):\t%f\r\n',d_riser);
fprintf(outfile,'Height of Packing (m):\t%f\r\n',height_packing);
fprintf(outfile,'Packing Porosity:\t%f\r\n',phi_s);
fprintf(outfile,'Simulation Time (s):\t%f\r\n',t_sim);
fprintf(outfile,'Time Step (s):\t%f\r\n',del_t);
fprintf(outfile,'U_GR (m/s):\t%f\r\n',U_GR);
fprintf(outfile,'KLa (s-1):\t%f\r\n',KLa);
fprintf(outfile,'Equilibrium constant:\t%f\r\n',KH);
fprintf(outfile,'Initial adsorbed solid Concentration (g/m3
packing):\t%f\r\n',Cads_initial);
fprintf(outfile,'Saturation Concentration adsorbed solid
(g/m3):\t%f\r\n',Cads_sat);
fprintf(outfile,'Inlet Gas Phase Concentration (mg/L):\t%f\r\n',C_in);
fprintf(outfile,'Riser Gas Holdup:\t%f\r\n',phi_s);
fprintf(outfile,'alpha1:\t%f\r\n',alpha1);
fprintf(outfile,'Beta:\t%f\r\n',beta);
fprintf(outfile,'gamma:\t%f\r\n',gamma);
fprintf(outfile,'A:\t%f\r\n',A);
fprintf(outfile,'B:\t%f\r\n',B);
fprintf(outfile,'D:\t%f\r\n',D);
fprintf(outfile,'\r\n');

while total_time <= t_sim
   loop = loop + 1;
   total_time = del_t*loop;
   percent_complete = fix(100*total_time/t_sim)
   T_vectr(loop) = total_time;

   b_vectr(1) = b_vectr(1) - 0;
```

```
   b_vectr(nodes_z+1) = b_vectr(nodes_z+1) - A * C_in;

   [X flag(loop)] = bicgstab(A_mat,b_vectr,1e-15,20,L,U);
   Cads(loop,:) = X([1:nodes_z])';
   C(loop,:) = X([nodes_z+1:n])';
   b_vectr([1:nodes_z]) = X([1:nodes_z])-alpha1';
   b_vectr([nodes_z+1:n]) = X([nodes_z+1:n])-E';
   clear X;

end

Cads=Cads
out_node = '%f\t';
out_format = '%f\t';

for ii = 1:nodes_z
   out_format = strcat(out_format,out_node);
end
out_format = strcat(out_format,'\r\n');

fprintf(outfile,'Liquid Phase Concentration\r\n');
fprintf(outfile,'Nodes->');
fprintf(outfile,'\t%f',[1:nodes_z]);
fprintf(outfile,'\r\n');
fprintf(outfile,'Height(m)->');
fprintf(outfile,'\t%f',del_z*[1:nodes_z]);
fprintf(outfile,'\r\n');
fprintf(outfile,out_format,[T_vectr;Cads']);
fprintf(outfile,'\r\n');
fprintf(outfile,'Gas Phase Concentration\r\n');
fprintf(outfile,'Nodes->');
fprintf(outfile,'\t%f',[1:nodes_z]);
fprintf(outfile,'\r\n');
fprintf(outfile,'Height(m)->');
fprintf(outfile,'\t%f',del_z*[1:nodes_z]);
fprintf(outfile,'\r\n');
fprintf(outfile,out_format,[T_vectr;C']);
```

```
fclose (outfile)
figure
surfl(Cads,[65,50])
shading interp
colormap('bone')
ylabel('time');
xlabel('height');
zlabel('solid concentration g/m3');
view(50,20)
figure
surfl(C,[65,50])
shading interp
colormap('bone')
ylabel('time');
xlabel('height');
zlabel('gas concentration g/m3');
view(50,20)

figure
hold
plot(T_vectr(:),Cads(:,nodes_z));
title('Liquid Outlet Concentration');
xlabel('time (sec)');
ylabel('Concentration g/m3 packing(Cads)');

zoom on

figure
hold
plot(T_vectr(:),C(:,nodes_z));
title('Gas Outlet Concentration');
xlabel('time (sec)');
ylabel('Concentration (g/m3 of air)');
zoom on
```